CONTROLLED SYNTHESIS OF TiO_2 NANOPARTICLES AND THEIR APPLICATION IN PHOTOVOLTAICS

Dejan Verhovšek

Doctoral Dissertation
Jožef Stefan International Postgraduate School
Ljubljana, Slovenia, June 2012

Evaluation Board:

Prof. Dr. Miran Gaberšček, National Institute of Chemistry, Hajdrihova 19, 1000 Ljubljana

Assist. Prof. Dr. Goran Dražić, Jožef Stefan Institute, Jamova cesta 39, 1000 Ljubljana

Assist. Prof. Dr. Sašo Šturm, Jožef Stefan Institute, Jamova cesta 39, 1000 Ljubljana

MEDNARODNA PODIPLOMSKA ŠOLA JOŽEFA STEFANA
JOŽEF STEFAN INTERNATIONAL POSTGRADUATE SCHOOL

Dejan Verhovšek

CONTROLLED SYNTHESIS OF TiO_2 NANOPARTICLES AND THEIR APPLICATION IN PHOTOVOLTAICS

Doctoral Dissertation

KONTROLIRANA SINTEZA TiO_2 NANODELCEV IN NJIHOVA UPORABA V FOTOVOLTAIKI

Doktorska disertacija

Supervisor: Prof. Dr. Miran Čeh

Ljubljana, Slovenia, June 2012

Table of Contents

Abstract

Titanium dioxide (TiO_2) in nanoparticle form has recently gained a lot of attention, in both the scientific and industrial communities. This is due to the fact that it exhibits various interesting chemical and physical characteristics, for example, a high photocatalytic activity and the absorption of incident UV light. Many applications have been developed so far, such as UV absorptive coatings, photocatalytically active coatings and dye-sensitized solar cells (DSSCs), which make it possible to produce electrical energy. In particular, the technology of DSSCs and photocatalytic coatings may be of great importance in the field of photovoltaics, which is one of the fastest growing technologies in the world. So far, the most promising photovoltaic technology has been based on silicon semiconductor modules, whose working action is very dependent on the cleanliness of the module surface, which determines the amount of absorbed incident light. Dust and other impurities may lower the efficiency of the silicon module, making the technology more expensive overall due to the required cleaning and maintenance. This also lengthens the overall time for a return on the investment. The use of coatings which would keep the Si module surface clean for a longer period of time could considerably lower the maintenance costs. On the other hand, the relatively new photovoltaic technology, the DSSCs, are based on cheap materials and technology and are a serious candidate for the implementation of low-cost electrical energy acquisition.

The basis of both technologies, photocatalytic coatings and DSSCs, is TiO_2 in nanoparticle form. The TiO_2 nanoparticles were developed using raw materials emanating from the established Sulphate process of pigment production in Cinkarna Celje Inc. The starting material was metatitanic acid. Using the principles of sol-gel and gel-sol chemistry we transformed it into anatase (TiO_2) nanoparticles in polycrystalline form.

The polycrystalline anatase nanoparticles were used in the photocatalytic coating, which was applied to the surface of glass substrates. Then, the coating was analyzed for its photocatalytic activity and the superhydrophilic effect by the use of contact angle measurements and a quantitative method of terephthalic acid sodium salt degradation using a spectrofluorimeter. The coating was also tested on commercially available silicon modules. One module was coated with the photocatalytic coating and compared regarding its efficiency with an uncoated module. The efficiency measurements showed that initially the efficiency of the coated module is not lowered considerably, while long-term tests that are taking place could prove beneficial in keeping the efficiency higher when compared to the uncoated module.

The DSSC technology was based on using a special type of TiO_2 nanoparticles, namely the monocrystalline form. Monocrystalline anatase nanoparticles were synthesized by the hydrothermal method using gel-sol derived polycrystalline anatase nanoparticles as the starting material. Monocrystalline anatase nanoparticles were then used as a raw material in TiO_2 paste production based on the Pechini method. The paste was deposited onto the conductive glass substrate and sintered, forming a photo-anode which was used to construct the final DSSC. We have shown that by changing the initial paste composition and monocrystalline TiO_2 type, various TiO_2 pastes can be formed, effectively influencing the efficiency, which was in our case in the range of 0.5–2.3%.

Povzetek

Titanov dioksid (TiO_2) v obliki nanodelcev je v zadnjem času pritegnil veliko zanimanja tako raziskovalne, kot tudi industrijske sfere, saj izkazuje vrsto zanimivih kemijskih in fizikalnih lastnosti, med katere sodita predvsem visoka fotokatalitska aktivnost in možnost absorpcije UV dela spektra vpadne svetlobe. Temu primerno so že razvili mnoge visoko-tehnološke aplikacije, na primer UV zaščitne premaze, fotokatalitsko aktivne premaze, možno pa je celo pridobivanje električne energije z uporabo fotoelektrokemijskih sončnih celic. Tehnologiji fotoelektrokemijskih sončnih celic in fotokatalitskih premazov sta še posebej zanimivi za področje fotovoltaike, ki je ena izmed najhitreje rastočih globalnih tehnologij. Danes najbolj razširjena oblika fotovoltaike namreč temelji na uporabi Si polprevodnika v obliki modulov, katerih izkoristek je znatno odvisen od čistoče površine, preko katere se zajema vpadna sončna svetloba. Prah in druge nečistoče vpadno površino onesnažijo, kar sčasoma zmanjšuje izkoristek Si modula in posledično zviša ceno tehnologije zaradi dodatne potrebe po vzdrževanju ter zaradi daljšega roka povračila vloženih stroškov. Uporaba premazov, ki bi površino Si modula ohranili dalj časa čisto, bi lahko znatno znižala stroške njihovega vzdrževanja. Po drugi strani pa so fotoelektrokemijske sončne celice sorazmerno nova oblika fotovoltaike, ki temelji na uporabi relativno poceni materialov in tehnologije ter tako predstavlja resnega kandidata za implementacijo nizko-cenovne tehnologije pridobivanja električne energije. Osnova obeh tehnologij, fotokatalitskih premazov in fotoelektrokemijskih sončnih celic, je uporaba nanodelcev TiO_2. Te smo razvili na podlagi uporabe surovin, ki izhajajo iz redne proizvodnje pigmenta TiO_2 po t. i. Sulfatnem postopku, ki je tehnološki proces, kot ga uporablja Cinkarna Celje d.d. V ta namen smo uporabili metatitanovo kislino in jo z uporabo principov sol-gel in gel-sol kemijskih postopkov pretvorili v polikristalinični anatas v obliki nanodelcev.

Polikristalinični nanodelci anatasa so primerni za direktno uporabo v fotokatalitsko aktivnem premazu, ki smo ga nanesli na površino steklenih substratov ter merili njihovo fotokatalitsko aktivnost ter superhidrofilni efekt z metodo kontaktnega kota in kvantitativno metodo meritve razgradnje natrijeve soli tereftalatne kisline s spektrofluorimetrom. Takšen premaz smo preizkusili tudi v realnih razmerah, in sicer na komercialno dosegljivih Si modulih. Eden Si modul smo oslojili s fotokatalitsko aktivnim premazom in merili njegov izkoristek v primerjavi z referenčnim Si modulom, katerega površine nismo oslojili. Meritve so pokazale, da izkoristek oslojenega modula ne upade znatno, predvidevamo pa, da bo dolgoročno testiranje, ki se še izvaja, pokazalo, da se izkoristek ohrani v večji meri kot v primeru neoslojenega Si modula.

Po drugi strani zahteva tehnologija fotoelektrokemijskih sončnih celic posebno obliko TiO_2, in sicer t. i. monokristalinično obliko nanodelcev. Te smo pridobili z uporabo hidrotermalne metode, kjer smo kot izhodni material uporabili suspenzijo z gel-sol postopkom pridobljenih polikristaliničnih nanodelcev anatasa. Monokristalinične nanodelce anatasa smo zatem uporabili za pripravo paste po Pechini metodi in iz paste s sintranjem na prevodnem steklenem substratu izdelali fotoanode. Tem smo zatem določili končen izkoristek. Izkazalo se je, da lahko s spreminjanjem sestave osnovne paste in oblike monokristaliničnih nanodelcev znatno vplivamo na končni izkoristek fotoelektrokemijske sončne celice, ki je v našem primeru znašala od 0,5 do 2,3 %.

Abbreviations

SEM	=	Scanning electron microscopy
TEM	=	Transmission electron microscopy
TS	=	Titanyl sulphate
TTIP	=	Titanium tetraisopropoxide
DSSC	=	Dye-sensitized solar cell
TCO	=	Transparent conductive oxide
ITO	=	Indium tin oxide
WF	=	Work function
MLCT	=	Metal-to-ligand charge transfer
IPCE	=	Incident-Photon-to-Electron Conversion Efficiency (Quantum efficiency)
LHE	=	Light-harvesting efficiency
HOMO	=	Highest occupied molecular orbital
LUMO	=	Lowest unoccupied molecular orbital
VB	=	Valence band
CB	=	Conduction band
PSH	=	Photoinduced superhydrophilic effect
CA	=	Contact angle
UV	=	Ultraviolet
HTS	=	Hydrothermal synthesis
IEP	=	Isoelectric point
TPA	=	Terephthalic acid
HTPA	=	Hydroxyterephthalic acid

1 Introduction

Renewable and environmentally sound energy production technologies are necessary for the replacement of fossil fuels. Currently, most of the world's energy derives from fossil fuels, whose global supplies are dwindling and becoming ever more scarce. The scarcity of fossil fuels has led to an increase in research in the field of renewable and sustainable energy production. Besides wind and geothermal energy, one of the most successful approaches for providing renewable energy is photovoltaics, which is one of the fastest growing industries in the world, with an increase of 40 % per year [1].

Solar cells are an alternative energy source and have been utilized in various forms for many years, converting the incident solar radiation into usable electricity. The most common type of solar cells is based on doped silicon semiconductors with a p-n junction, where a depletion region is formed leading to an electric field that separates the charges. This charge separation produces an electric flow. The silicon-based photovoltaics are commercially available and have so far been the most successful type of technology, but they still lack economic competitiveness when compared to fossil fuels, since current photovoltaic module cost is about $2/watt [1]. Although research and optimization of the silicon-based photovoltaic technology is promising a reduction of price, it is still not clear whether it will take over from the fossil-fuel-based technologies.

The advent of nanotechnology has provided alternative solutions. Nanotechnology exploits the often dramatic differences between nanoscale materials and their bulk counterparts. The differences arise primarily due to the fact that a large percentage of the atoms in a nanomaterial occupy the surface, which alters the physical and chemical properties significantly when compared to its bulk counterpart.

Titanium dioxide, TiO_2, a material that can readily be made in nanomaterial form, exhibits some unique physical and chemical characteristics that may prove useful in the field of photovoltaics. Firstly, TiO_2 is already recognized as being one of the most effective photocatalysts known today, being able to decompose organic pollutants and also remove inorganic dirt due to its superhydrophilic effect. Therefore, it may be of considerable importance to develop a photoactive coating that can be applied on the already commercially available solar modules and thus providing a means to maximize their long-term operational effectiveness.

On the other hand, third-generation-type solar cells show great promise in lowering the price and at the same time increasing the efficiency of the photovoltaic technologies that are yet to come (Figure 1).

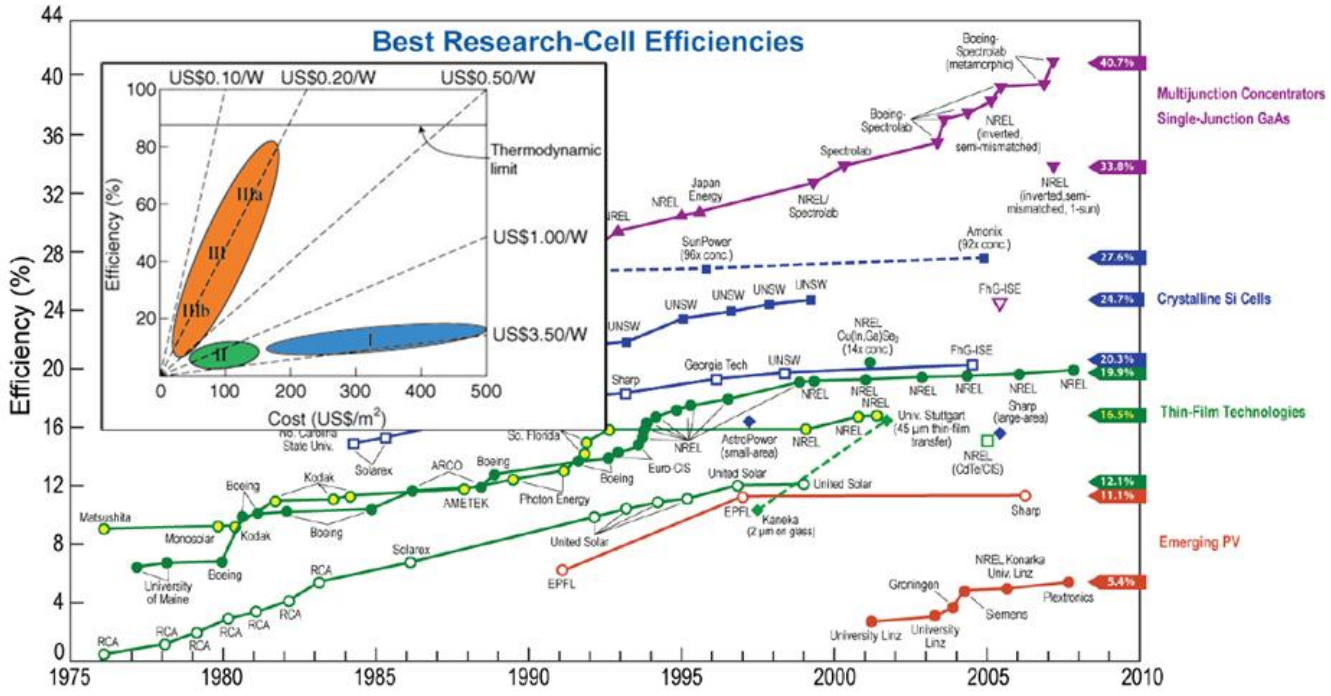

Figure 1: *The efficiencies of different photovoltaic technologies [2]*. The inset illustrates the aim towards third generation solar cells: (I) low efficiency, high cost; (II) low efficiency, low cost; (III) high efficiency, low cost.

One of the third-generation solar-cell technologies is based on using TiO_2 in nano form. These solar cells are the so-called dye-sensitized solar cells (DSSCs), also known as photoelectrochemical solar cells or Gräetzel cells. The research in these cells surged in 1991 when efficiencies of 7.1–7.9 % were reported by Michael Gräetzel [3]. Today, the efficiencies of the best prepared DSSCs have reached 11 % [4, 5]. One of the major advantages of DSSCs is the fact that they consist of low-cost materials and a relatively simple technology. They consist of a layered system with two electrodes, a photo-anode with an active layer of dye chemisorbed TiO_2 nanoparticles and a counter electrode which, in its most common form, is a platinum layer. Both the photo-anode and the counter electrode are coated on a transparent conductive oxide layer on glass or some other substrate. Between the two electrodes, an electrolyte is present which replenishes the electrons in the active dye layer. Hence, besides developing a photoactive coating that could be used to promote the long-term highly-efficient work action of conventional solar cells, one major motivation for the work described was also the development of a suitable type of TiO_2 nanoparticles that could be used to prepare a photo-anode for a DSSC.

To address both problems, we performed various synthesis methods to obtain nano-TiO_2, using materials emanating from the already established Sulphate process of the pigment TiO_2 production set-up in Cinkarna Celje Inc. In particular, metatitanic acid in various forms has proven to be the material of choice, which allowed us to synthesize different types of nano-TiO_2 and was suitable for both photocatalysis and DSSC application. Furthermore, in order to keep nanoparticles dispersed, all of the synthesis methods were focused on producing only a water-based colloidal form of TiO_2. Hence, we have avoided the need to apply energy-consuming procedures of calcinations, which inherently leads to nanoparticle agglomeration and also produces dust that may be environmentally hazardous and thus raise health issues. The as-prepared TiO_2 nanoparticles were used to develop the photocatalytic coatings and photo-anodes for DSSCs and were tested and analyzed in order to optimize the nanoparticles into the best possible form for both applications.

1.1 TiO_2 polymorphs: structure and thermodynamic stability

Titanium dioxide (TiO_2) occurs naturally in three major crystal structures, i.e., rutile, anatase and brookite. While rutile and anatase exhibit tetragonal crystal structures, brookite has an orthorhombic crystal structure. There are also a few other forms of TiO_2, the monoclinic TiO_2 (B) which also occurs naturally, and a few other laboratory-made TiO_2 forms which were synthesized under high-pressure conditions starting from rutile, TiO_2 (II) (srilankite) [6] with a PbO_2 structure and TiO_2 (H) [7] with a hollandite crystal structure.

The crystal structures of the three major TiO_2 polymorphs, rutile, anatase and brookite, can be compared in terms of how the [TiO_6] octahedra, the primary material building blocks, are spatially arranged and distorted. The octahedra are linked entirely by edge sharing in anatase, while the arrangements of [TiO_6] octahedra in rutile and brookite result from different combinations of corner and edge sharing [8–10]. The degree of distortion of the [TiO_6] octahedra differs slightly among the crystal structures. In bulk rutile the respective apical and equatorial Ti-O bond length is 1.98 and 1.95 Å, while in anatase the two values are 1.98 and 1.93 Å, respectively [8].

The three major TiO_2 polymorphs are illustrated in Figure 2.

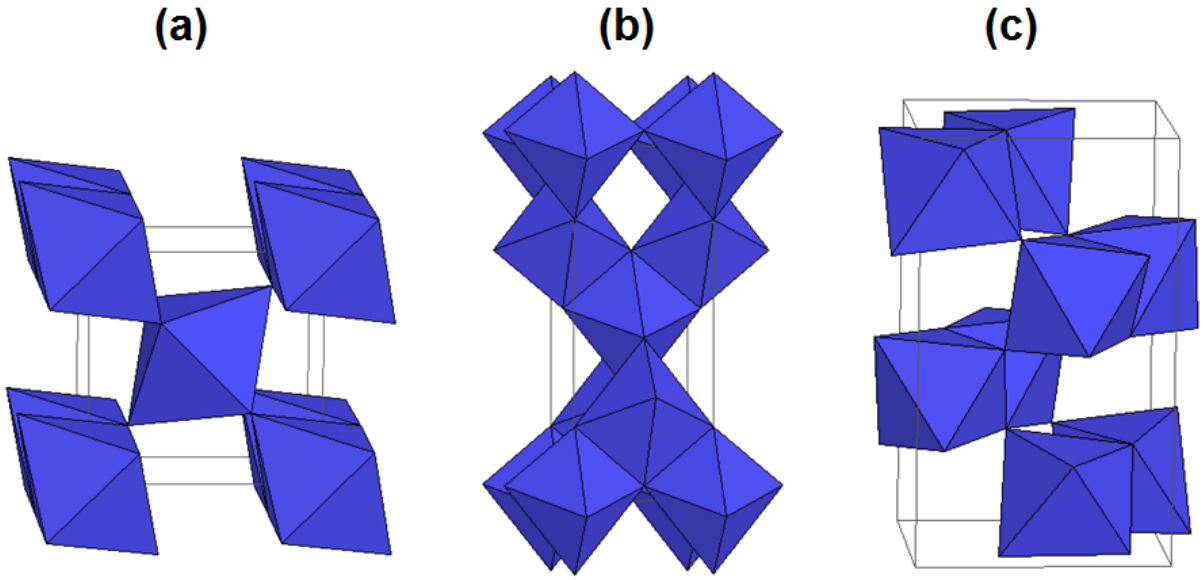

Figure 2: *Crystal structures of rutile (a), anatase (b) and brookite (c).* The crystal structures of the three polymorphs differ in how the [TiO_6] octahedra connect to form the final structure.

The most important structural parameters of the three TiO_2 polymorphs are summarized in Table 1 below:

Table 1: *Structural parameters of anatase, rutile and brookite.*

Phase	Crystal system	a (Å)	b (Å)	c (Å)	Atomic coordinates	Space group
anatase	tetragonal	3.7845	3.7845	9.5143	Ti (0, 0, 0); O (0, 0, 0.208)	$I4_1/amd$
rutile	tetragonal	4.5937	4.5937	2.9587	Ti (0, 0, 0); O (0.305, 0.305, 0)	$P4_2/mnm$
brookite	orthorhombic	9.1840	5.4470	5.1450	Ti (0.128, 0.098, 0.863); O1 (0.008, 0.147, 0.182); O2 (0.229, 0.110, 0.530)	Pbca

As a bulk material, rutile is thermodynamically the most stable phase. Thermodynamic calculations based on calorimetric data suggest that rutile is predominantly stable at all temperatures and pressures up to 60 kbar, where TiO_2 (II) becomes thermodynamically favorable. Therefore, anatase and brookite are only metastable, but the small difference in the Gibbs free energy (4–20 kJ/mole) between the three phases results in anatase and brookite being as stable as rutile at ambient pressures and temperatures [10]. However, it has been shown that the thermodynamic phase stability of TiO_2 is size-dependent. At sufficiently low particle size values of the relative phase stability is reversed due to surface-energy effects. It was demonstrated that rutile is stable for grain sizes larger than 35 nm, brookite is the stable phase for grain sizes ranging from 11 – 35 nm, while anatase is the stable phase at grain sizes below about 11 nm [11]. This is in agreement with the observation that anatase is the common product of the industrial scale Sulphate process, where grain sizes for anatase range from 5 to 10 nm. But, in the case of the Sulphate process, one must also keep in mind that the sulphate ionic species play a crucial role in determining the crystal structure of the final product, since they influence the hydrolysis and polycondensation reactions [12–15].

The stability of a specific polymorph is size-dependent. The reason for this observation is that although the interior of a rutile crystal, thermodynamically the most stable phase when in bulk size, is more energetically stable than that of either of the two other phases. The calculated average surface enthalpy of rutile (1.93 J/m^2) is actually higher than that of brookite (1.66 J/m^2) or anatase (1.34 J/m^2) [11, 16]. Therefore, on the nanometer scale, where a particle's surface energy begins to dominate the total energy of formation, it becomes more energetically costly to form the rutile phase. Consequently, one of the other two polymorphs is favored, depending on the TiO_2 grain size.

1.2 TiO_2 characteristics at the nanoscale

TiO_2 is known for its many important physical and chemical characteristics that make it one of the most versatile and widely used metal oxides. However, its importance only grew when some striking applications became possible due to its enhanced properties at the nano scale. One TiO_2 characteristic that makes it especially well-suited for photocatalytic and similar applications is the ability to generate hydroxyl (OH•) and hydroperoxy (HO_2•) radicals [17, 18]. The hydroxyl radical serves as a powerful oxidant, while the hydroperoxy radical serves as a powerful reducing agent. Furthermore, from the application point of view, one of the most important properties of all three polymorphs is the fact that they are semiconductors. Their electrons occupy bands rather than discrete energy states and possess an electrical conductivity that increases with increasing temperature. This property, coupled with the previously mentioned photocatalytic behavior, makes nano-TiO_2 an ideal material for photovoltaic application. As will be discussed in more detail in later chapters, the band gap energy, E_g, of nano-TiO_2 has values that enable high photocatalytic properties and, when in photoanode form, is coupled very suitably with the energy states of other components in DSSC. The bandgap energies of bulk rutile (3.0 eV; 4.8 x 10^{-19} J), bulk anatase (3.2 eV; 5.1 x 10^{-19} J) and bulk brookite (3.4 eV; 5.4 x 10^{-19} J) were precisely measured and correspond to the maximum excitation wavelengths of 410, 385 and 365 nm, respectively. It is also well-known that these values are size-dependent. As the size of individual TiO_2 crystals decreases below ~ 10 nm the confinement of the electrons to a very small volume leads to the so-called quantization effects, one of which is also the increase in bandgap energy. Consequently,

the electrical conductivity of nano-TiO_2 is expected to be slightly lower than that of bulk TiO_2 [19].

1.3 TiO_2 nanoparticle synthesis methods

The synthesis of nanosized TiO_2 has been the subject of extensive research over the past few decades. Various methods have so far been developed and product-wise differ a great deal from one another since the final material is inherently dependent on the used reaction parameters. The TiO_2 nanoparticles produced may differ greatly in terms of particle size, morphology, crystallinity and surface chemistry.

Generally speaking, there are two distinctive approaches for nanoparticle preparation, the top-down and bottom-up approaches [20]. The top-down approach is mainly based on the mechanical treatment of bulk materials which transforms them into nanoparticles. The top-down approach includes milling or attrition and lithography. The down side of the top-down approach is the broad size distribution of the final nanoparticles, the presence of impurities emanating from the milling medium, defects in structure, etc. On the other hand, the bottom-up approach is mainly based on designing nanoparticles via chemical reactions, where by controlling the reaction parameters and processes, like nucleation and particle growth, one may easily produce chemically well-defined materials with a narrow size distribution. Overall, the bottom-up approach techniques can be divided into [20]:

- thermodynamic equilibrium approach techniques
- kinetic approach techniques

With the thermodynamic approach, the synthesis process consists of the following steps:

- generation of supersaturation
- nucleation
- particle growth

In the kinetic approach the formation of nanoparticles is achieved by limiting the amount of reaction precursors or by confining the process in a limited space, such as aerosol synthesis and micelle synthesis.

We will discuss only the bottom-up approach to TiO_2 nanoparticle synthesis. Generally, the methods for nano-TiO_2 synthesis can be divided into three categories:

- aerosol pyrolysis [21–39]
- non-hydrolytic solution-phase reactions [40–47]
- hydrolytic solution-phase reactions [48–116]

Since the final TiO_2 nanoparticles differ in their characteristics based on the above-mentioned general methods, it is very crucial to select a synthesis method to produce a material with the most desirable properties for a particular application. Moreover, it is crucial that a synthesis method is devised which would allow a cheap and simple method for TiO_2 nanoparticle production, but also allowing a means of tailoring the material according to a specific application.

The following sections provide an overview of the three general methods for nano-TiO_2 synthesis, the typical characteristics of the material that is produced and the advantages and the disadvantages of each synthesis strategy. At the end of the overview, there will be an assessment of the various synthesis routes.

1.3.1 Aerosol pyrolysis

The preparation of nano-TiO_2 in an aerosol requires thermal or laser-induced pyrolysis of a titanium-containing precursor, usually either $TiCl_4$ or a titanium alkoxide ($Ti(OR)_4$) at temperatures ranging from 200 to 1000 ºC. In the case when $TiCl_4$ is used, it is necessary to conduct the reaction in the presence of either oxygen or water vapor, since oxygen atoms are needed to produce the final TiO_2 material. The (non-stoichiometric) chemical reaction can be written as follows [21]:

$$TiCl_4 + (O_2, O^{\bullet}, H_2O, OH^{\bullet}) \xrightarrow{flame,laser} TiO_2 + (Cl_2, HCl) \quad (1)$$

When an alkoxide is used as the precursor, it is possible to obtain TiO_2 even in a dry atmosphere such as nitrogen, since the alkoxy groups of the alkoxide contain oxygen atoms. A simplified chemical reaction may be written as follows [29]:

$$Ti(OR)_4 \xrightarrow{flame,laser} TiO_2 + organics \quad (2)$$

The pyrolytic apparatus produces TiO_2 nanoparticles via a simple reaction in which firstly droplets of the precursor are formed by an aerosol generator. The droplets are then transported by the carrier gas into the quartz reactor tube placed in a heater that produces the desired reaction temperature. After the TiO_2 nanoparticles are produced inside the furnace, they are collected by electrostatic precipitation, a technique that is based on the electrostatic attraction between a positively charged plate and negatively charged particles [23].

As a synthesis method, aerosol pyrolysis offers four advantages, namely:

- it is environmentally friendly since it produces a significantly smaller amount of waste and byproducts than most wet chemical methods [39]
- high purity materials are produced whose grain size, phase composition and surface area can be tuned easily by the selection of the appropriate parameters (temperature, aerosol flow rate, precursor concentration, carrier gas and feed stream [21, 22, 25, 29, 39]
- the equipment needed to perform the pyrolytic synthesis is simple and inexpensive [23, 34]
- crystalline material is produced in a single-step reaction and therefore post-reaction procedures are not needed

Although aerosol pyrolysis exhibits important advantages, it also has a very significant drawback. That is, the material produced is always highly aggregated and consists of particles with a grain size never smaller than about 15 nm. Both drawbacks are undesirable when one wishes to produce high-surface area nano-TiO_2 for applications such as photocatalysis, since the surface area of the powders prepared is between 10 and 50 m^2/g.

1.3.2 Non-hydrolytic solution-phase reactions

For photocatalytic and DSSC applications, high-surface-area TiO_2 nanoparticles are the material of choice. Since the aerosol pyrolysis technique tends to form large, highly-aggregated materials, the synthesis of a nanoparticulate TiO_2 with a large surface area demands the use of wet chemical methods. Although these wet chemical synthesis methods usually rely on hydrolysis reactions taking place in an aqueous environment,

methods have been devised to synthesize nanocrystalline TiO_2 in the absence of water [40–46]. Such non-hydrolytic methods involve elimination reactions at mildly elevated temperatures ranging from 80–300 ºC, between a titanium (IV) halide (usually $TiCl_4$) and an oxygen donor (titanium (IV) alkoxide, ether or alcohol) [40, 41, 44]. The overall reactions for these three routes known as polycondensation, etherolysis and alcoholysis, respectively, are listed below [44]:

$$TiX_4 + Ti(OR)_4 \rightarrow 2TiO_2 + 4RX \quad \text{(polycondensation)} \quad (3)$$

$$TiX_4 + 2ROR \rightarrow TiO_2 + 4RX \quad \text{(etherolysis)} \quad (4)$$

$$TiX_4 + 2ROH \rightarrow TiO_2 + 2RX + 2HX \quad \text{(alcoholysis)} \quad (5)$$

The above reactions are by no means as simple as it would appear, but involve many steps. With etherolysis and alcoholysis, the ether and alcohol molecules first react with the halide group of some of the precursor molecules to create a Ti-OR functional group in a process called alkoxylation. Afterwards, the alkoxide groups react with the remaining titanium halide molecules, forming the Ti-O-Ti bonds [41]:

$$\equiv Ti - X + R - OR \rightarrow \equiv Ti - OR + R - X \quad (6)$$

$$\equiv Ti - X + \equiv Ti - OR \rightarrow \equiv Ti - O - Ti + R - X \quad (7)$$

Furthermore, it was noted that the reactions (3) through (5) are only productive when the reaction temperature is elevated above 80 ºC. Lower temperatures do not yield large amounts of TiO_2, since the reactions are very slow and because other, competitive reactions take place. In fact, the primary reaction at low temperatures is between the precursor molecules in a ligand-exchange process (redistribution) that results in titanium haloalkoxides [40, 41, 44]:

$$\equiv Ti - X + \equiv Ti' - OR \rightarrow \equiv Ti - OR + \equiv Ti' - X \quad (8)$$

$$\equiv Ti - X + R - OR \rightarrow \equiv Ti - OR + R - X \quad (9)$$

$$\equiv Ti - X + H - OR \rightarrow \equiv Ti - OR + H - X \quad (10)$$

Because of the complexity of the above-presented reactions, one can expect that non-hydrolytic TiO_2 synthesis is quite sensitive to reaction parameters such as precursor concentration, choice of halide and alkoxy substituents as well as the reaction temperature. Furthermore, in the case of etherolysis and alcoholysis, the overall reaction should be dependent on the selection of the ether or alcohol. This sensitivity, on the other hand, exerts considerable control on the final material properties. This is clearly the case, since it was shown that by changing the solvent type (either diethyl ether, ethanol or *t*-butyl alcohol) when reacting $TiCl_4$ at 110 ºC, anatase, rutile and a mixed rutile-brookite nano-TiO_2 were formed, respectively [40]. It was also shown that the reaction between titanium (IV) isopropoxide ($Ti(OPr)_4$) and various titanium (IV) halides in heptadecene solvent yields anatase nanoparticles whose grain size was dependent and decreased both with increasing the size of the halide substituent and with the inclusion of trioctylphosphine oxide (TOPO) as a surfactant [43]. Furthermore, it was found that TOPO influences the phase-pure products, whereas performing the reaction without TOPO yields mixtures of anatase, rutile and brookite.

It is clear that the non-hydrolytic synthesis of TiO_2 nanoparticles is advantageous when it comes to tuning the grain size and crystal structure of the end product. Furthermore, non-hydrolytic reactions are advantageous since short reaction times are required (~5 min), the reaction temperature is relatively mild (80–300 ºC) and very fine particles

exhibiting low agglomeration having grain sizes ranging from 4 – 10 nm are produced [43].

The major disadvantage of these reactions is the fact that they require a dry atmosphere that prevents hydrolytic side reactions and that in some cases an additional thermal treatment of the material is needed [40]. Also, although the use of surfactants such as TOPO tends to promote the synthesis of phase-pure materials, their use inherently leads to a surface covered nano-TiO_2. This can be a major problem for such applications as photocatalysis where the activity can be dramatically lowered if the TiO_2 surface is not active. Application-wise, non-hydrolytic synthesis may be disadvantageous since because performing the reactions in a water-free medium, the nano-TiO_2 produced is completely dehydroxylated. The absence of surface hydroxyl groups greatly influences the photocatalytic effect, since $OH^{\bullet}$ radicals cannot be formed. The $OH^{\bullet}$ radicals are thought to be the active species in the oxidative decomposition of adsorbed contaminants [47].

1.3.3 Hydrolytic solution-phase reactions

To produce nano-TiO_2 in a tailor-made fashion and with a hydroxylated surface, it is necessary to turn to the hydrolytic solution-phase reactions. These reactions are numerous and represent the most common approach for obtaining both bulk and nano-TiO_2. The reactions are very complex and may lead to very versatile materials. It is therefore useful to divide these reactions on the basis of the type of underlying mechanisms that lead to material formation as follows:

- sol-gel and gel-sol synthesis
  - hydrolysis-based materials thermally treated in a post-reaction calcination process
  - acid-based hydrolysis
  - surfactant-based hydrolysis
- hydrothermal synthesis

The hydrolysis reactions can be understood as being only an initial step in the nano-TiO_2 synthesis, which in the case of a water-based solvent, is governed by the processes of sol-gel and gel-sol chemistry. The hydrothermal synthesis, on the other hand, relies on using water as a solvent in a high-temperature, high-pressure crystallization process useful for producing well-crystallized materials.

1.3.3.1 The sol-gel and the gel-sol synthesis of TiO_2 nanoparticles

The sol-gel synthesis method, and the lesser known gel-sol synthesis method, may be regarded as two of the most important procedures known today for the production of heterogeneous metal oxides and mixed oxides in a tailor-made fashion.

The sol-gel process is a wet-chemical technique used to synthesize materials starting from an appropriate chemical solution in which colloidal particles (the sol phase) form. The colloid particles formed in the sol phase are of sizes ranging from 1 nm to 1 μm. The process of sol-gel formation is based on the reactions of hydrolysis and polycondensation of the appropriate molecular precursors occurring sequentially and in parallel [48, 49].

The gel-sol process is based on obtaining monodispersed particles in large quantities if one takes advantage of a condensed, highly viscous hydroxide gel, which acts as a matrix for the growing particles. The gel network prevents particle coagulation during formation and is also a reservoir of metal and hydroxide ions. In addition, at the end of the

dissolution–recrystallization process, the precursor gel is expected to disappear and leave a monodispersed product with a yield of 100 %. Since a monodispersed sol is obtained from a gel through a dissolution–recrystallization process in an inhomogeneous system, it was named the "gel–sol method" [50].

The two processes are highly versatile and complex, which is to a large extent the result of the unique properties of water. To understand the sol-gel and the gel-sol process, one has to understand the underlying mechanisms and interactions between a water molecule and metal ions in an aqueous medium [51].

Water acts as a powerful and effective solvent. This is due to its chemical composition and large differences in the physical properties of hydrogen and oxygen. The oxygen atom is more electronegative than hydrogen ($\chi_O = 3.5$, $\chi_H = 2.1$ on the Pauling scale) and consequently the electron density shifts toward the oxygen in the H_2O molecule. Oxygen therefore acquires a large partial negative charge resulting in a high water dipolar moment ($\mu = 1.84$ Debye) and a high dielectric constant when in liquid phase ($\varepsilon \sim 80$). When dissolved in water, metal salts MX_Z dissociate into ions M^{Z+} and X^-, respectively. Because of the dipolar nature of water molecules, both ions are solvated. In the case of metal ions, this leads to the formation of a $[M(OH_2)_N]^{Z+}$ complex. It is known that water molecules also act as a Lewis base (a Lewis base is able to give away its electrons). Therefore, when $M\text{-}OH_2$ bonds form, the electrons of the bonding molecular orbitals σ ($3a_1$) are drawn towards the empty orbitals of the metal ion. This electron transfer weakens the O-H bond, resulting in water acting as a Brønsted acid:

$$\left[M(OH_2)_N\right]^{Z+} + hH_2O \Leftrightarrow \left[M(OH)_h(OH_2)_{N-h}\right]^{(z-h)+} + hH_3O^+ \qquad (11)$$

The parameter *h* is defined as the hydrolysis ratio and corresponds to the number of protons that have been removed from the solvation sphere of the aqua-cation complex:

$$M^{Z+} - OH_2 \Leftrightarrow M^{Z+} - OH^- + H^+ \Leftrightarrow M^{Z+} - O^{2-} + 2H^+ \qquad (12)$$

This hydrolysis step is crucial in determining the chemical state of an individual cation in a water medium. Depending on the hydrolysis ratio, the cation may form various complexes, ranging from aqua complex $[M(OH_2)_N]^{Z+}$ (h=0) to neutral hydroxides $[M(OH)_Z]^0$ (h=z) and even oxo-anions $[MO_{N'}]^{(2N'-z)-}$ which form when all of the protons have been removed from the coordination sphere of the metal ion. The hydrolysis ratio is increased with the higher pH value and the oxidation state of the cation. This can be represented by the pH-charge diagram as seen in Figure 3 below:

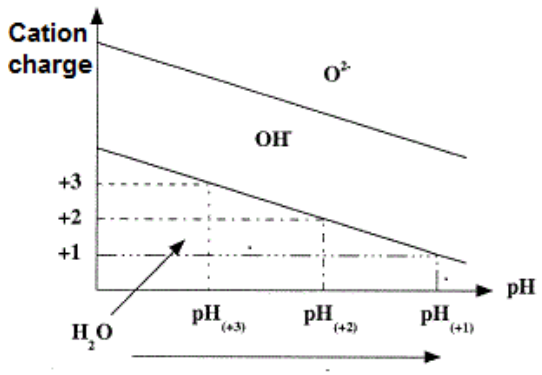

Figure 3: *The pH-charge diagram of a metal cation in a water medium [48]*. Depending on the pH value and the oxidation state, the cation may form various complex types.

As can be seen from the pH-charge diagram the cations having a low positive charge (Na^+, K^+, Cs^+, Ba^{2+},…) exhibit a low polarizing power. Also, their electronegativity and Lewis acidity are weak, resulting in only electrostatic bonding with water molecules. The electrostatic bonds have a short lifetime. Therefore no deprotonation can occur and only aqua-cation-type complexes are possible. On the other hand, small high-valent cations attract electrons strongly and consequently aqua complexes are swiftly transformed into more stable oxo complexes.

The pH-charge diagram is a good tool to predict the type of the complex a metal cation may form in a water medium. The complex formation is the result of hydrolysis reactions and is only the first stage in the process of sol-gel and/or gel-sol formation of the final material. Depending on the type of the hydrolysis complex, sequential reactions take place which are known as polycondensation reactions. These polycondensation reactions are the result of versatile reactions that arise due to the reactivity of a specific complex, as explained by the partial charge model, which will not be discussed here [48, 51]. Nevertheless, the partial charge model is a very useful tool to predict the chemical reactions that take place in the sol-gel process and provides a guide for inorganic polycondensation reactions.

Depending on the type of a specific complex and its reactivity, polycondensation reactions take place. Polycondensation reactions may be explained via two simple mechanisms that occur based on coordination (un)saturation [48]:

- if the preferred coordination of a metal cation is already fulfilled, the condensation proceeds via substitution reactions:

$$M-OX+M-OY \rightarrow M-\overset{X}{O}-M+OY \tag{13}$$

- if the preferred coordination is not fulfilled, the condensation reaction proceeds via addition reactions:

$$M-OX+M-OY \rightarrow M-\overset{X}{O}-M-OY \tag{14}$$

The above reactions are simplistic and provide a general impression about the polycondensation reactions. The principles of substitution and/or addition must be analyzed on specific complexes that occur in an aqueous medium. According to the pH-charge diagram, three types of precursors may be considered:

- oxo-ions $[MO_N]^{(2N-z)-}$- according to the partial charge model, the partial charge of the metal is usually slightly positive, while the partial charge of the oxygen is strongly negative. Consequently, oxo ligands are very good nucleophiles but very poor leaving groups. Polycondensation therefore occurs only via addition when the coordination saturation is not fulfilled.
- aqua-ions $[M(OH_2)_N]^{z+}$ - the partial charge of the metal is usually strongly positive and the charge of the water molecule is only slightly positive. Aqua ligands are therefore not nucleophilic and may act only as leaving groups. Polycondensation reactions do not proceed since there is no entering group.
- other precursors $[MO_NH_{2N-h}]^{(z-h)+}$- with these precursors both nucleophilic ligands (oxo or hydroxo) and leaving ligands (hydroxo or aqua) are present. Polycondensation via substitution may proceed as soon as one hydroxo ligand appears in the coordination sphere. Therefore, in order to get a condensed species (sols, gels, oligomers, precipitates) one has to achieve conditions where the hydroxo domain is possible for a certain metal salt [48, 51]. This can be done either by adding a base or an oxidizer to an aqua precursor, adding an acid or a reducing agent to an oxo precursor or even with thermolysis of an aqua precursor.

Since polycondensation only proceeds with precursors in the hydroxo domain, it is important to identify actual reactions in which the final material is formed.

One mechanism of polycondensation is olation [48, 51]. Olation is a reaction that leads to the formation of a hydroxo or *ol* bridge of the type M-OH-M. Polycondensation reactions of this type are possible with hydroxo-aqua precursors $[M(OH)_x(OH_2)_{N-x}]^{(z-x)+}$, where x is less than N. This is basically a nucleophilic substitution, where M-OH represents a nucleophile and H_2O a leaving group. In the case when zero charged precursors condensate via olation, a solid phase may form. The final type of material produced is the hydroxide $M(OH)_Z$, provided that subsequent oxolation cannot take place.

The other mechanism of condensation is oxolation [48, 51]. Oxolation leads to the formation of an oxo bridge of the type M-O-M. This may occur when the reacting precursor does not contain a water molecule in its coordination sphere. The oxolation reaction is typical for oxo-hydroxo precursors $MO_x(OH)_{N-x}]^{(N+x-z)-}$where x is less than N. The oxolation reaction may be regarded either as a nucleophilic addition reaction or as a nucleophilic substitution reaction. The latter is the result of nucleophilic addition followed by elimination. The difference in the oxolation mechanism type is dependent solely on the coordination saturation. When the coordination is not fulfilled, nucleophilic addition takes place, but when the coordination is fulfilled, the nucleophilic substitution takes place.

Oxolation is also highly dependent on the pH value of the reaction medium. Both acids and bases may strongly catalyze the oxolation reactions, since hydroxide groups and protons promote nucleophilic behavior and the elimination reaction, respectively. This is also, in contrast to olation, the reason why oxolation occurs over a wide range of pH values.

1.3.3.1.1 Hydrolysis-based materials thermally treated in a post-reaction calcination process

This process is used when the sol-gel reactions (hydrolysis + polycondensation) produce non-crystalline materials. Non-crystalline materials form due to specific reaction conditions that promote olation reactions. The amorphous material has to be thermally treated in order to obtain a crystalline TiO_2. To some extent, one can control the grain size of the crystalline product, either by selecting a low or high calcination temperature. Generally, coarser grains are obtained at higher temperatures [52]. Depending on the hydrolysis conditions, anatase is crystallized from the amorphous phase at calcination temperatures between 250 and 400 ºC. Transformation into rutile phase takes place at higher temperatures, usually between 500 and 1000 ºC. The temperature for phase transformation is dependent on the conditions under which the amorphous phase was formed. Above 500 ºC the amount of rutile gradually increases and the amount of anatase decreases [53, 54]. Because the phase transformation from anatase to rutile occurs over a considerable span of temperatures, varying the heating time and temperature provides a means to obtain anatase-rutile mixtures with tunable compositions. This has proven to be useful when preparing a mixed-phase TiO_2 material that has an optimal photocatalytic effect [55].

Although calcination is a relatively simple way of obtaining crystalline TiO_2, it is nevertheless disadvantageous because of severe agglomeration or even aggregation. Also, the grain size increases considerably with high-temperature calcination and only rarely produces grain sizes smaller than 15–20 nm. This reduces the specific surface considerably.

In this thesis we refer to an agglomerate as a particle in which the subunits are connected with each other mainly through physical bonding and can be broken when

subjected to stronger attraction forces or changes in the surface charge. An aggregate, on the other hand, is a consolidated particle in which smaller crystallites are connected mainly with strong ionic bonding. An aggregate cannot be broken down into individual subunits.

1.3.3.1.2 Acid-based hydrolysis

An alternative to calcination is to produce TiO_2 nanoparticles directly during the course of sol-gel/gel-sol reactions by promoting the oxolation reactions that yield crystalline materials. Generally, these reactions proceed in the presence of strong acids (HNO_3, HCl,…) or surfactants at temperatures ranging from 60 to 100 ºC. Acids and surfactants do not only catalyze the formation of crystalline TiO_2 but also act as peptizing agents. Peptizing agents stabilize the individual nanoparticles, which prevents their agglomeration and enables control over particle growth, morphology and also allow the formation of a colloidal sol.

The most common acids encountered with acid-based hydrolysis are of the mineral type, namely HCl, HNO_3 and H_2SO_4. Depending on the reaction conditions, these acids allow the synthesis of TiO_2 nanoparticles with versatile morphologies, specific surface and a predefined crystal structure. The mechanism by which acids exhibit their effect is mainly by directly influencing the Ti (IV) complex type and by altering the pH value of the reaction medium. The acid anions that are introduced into the reaction medium may serve as ligands in the coordination sphere of the Ti (IV) ion and thus directly influence the mechanisms of polycondensation. This is done by influencing how the Ti (IV) octahedra spatially approach one another and condense into oligomers and finally into particles. This is crucial for the determination of the crystal structure of the final material. Furthermore, the protons introduced by the acid strongly influence the hydrolysis ratio and thus the polycondensation reaction type. The influence of both protons and acid anions will be discussed in detail for a particular mineral acid type, as follows.

1.3.3.1.2.1 The effect of the pH value/oxonium ion concentration

The pH value of the reaction medium probably has the most profound effect on the end-material characteristics. As was discussed before, the pH value directly determines:

- the Ti (IV) complex type and thus the mechanism by which it reacts in polycondensation reactions. This is because the pH value directly influences the hydrolysis ratio. The hydrolysis reaction is an equilibrium type protolytic reaction and can be discussed on the basis of the LeChatelier principles. When the proton concentration is changed, i.e., by adding an acid or a base, the hydrolysis ratio changes. The hydrolysis ratio will be higher for basic conditions, and vice-versa. Since the polycondensation reaction is directly dependent on the complex type, namely on the ratio of ligands (oxo, hydroxo and aqua ligands) in the coordination sphere, the control over the pH value has to be strict. This is especially important with TiO_2 nanoparticle synthesis where one has to control the formation of a crystalline product and the final material's crystal structure (determining whether rutile, anatase or brookite will form). In the case of anatase the nuclei form via a polycondensation reaction between complexes having a larger ratio of water and hydroxide ligands. On the other hand, rutile is formed with the growth of nuclei that are formed by the polycondensation reactions between complexes that have a high hydrolysis ratio (no water molecule ligands, few hydroxide ligands) [9, 15, 56]. The effect of the pH value (OH^- molar concentration) on the TiO_2 phase is shown in Figure 4.

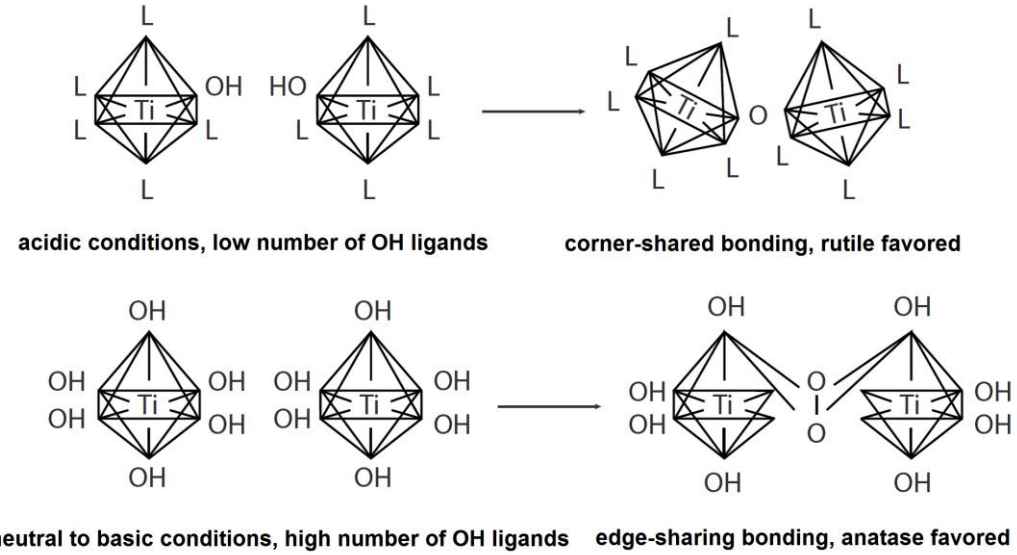

Figure 4: *Influence of the pH value on the crystallization of TiO_2 from hydrolytic reactions [9].* Acidic conditions, under which the number of OH- ligands is small, tend to favor the corner sharing among [TiO_6] octahedra that is characteristic for the rutile crystal structure. The increased number of OH^- ligands under neutral or basic conditions favors edge-shared bonding which is characteristic for the anatase crystal structure. Ligands other than OH^- are simply denoted L.

- the Ti (IV) octahedra polycondensation speed. It was determined that the polycondensation reaction speed is lower when performing the reaction at low pH values and higher when performing it at higher pH values. The reason for this is the fact that protons are able to electrostatically bind directly onto the Ti (IV) complex giving it a positive charge. The positive charge of a complex causes an electrostatic repulsion with other complex species in the nearby reaction medium, thus slowing the polycondensation reaction. The slower polycondensation reaction promotes the formation of TiO_2 with the rutile crystal structure. On the other hand, the polycondensation reactions tend to be faster at higher pH values, which promotes the formation of TiO_2 with the anatase crystal structure [56, 57].
- the course of specific, mainly gel-sol type, reactions where a TiO_2 gel or some other condensed material is used. The protons promote the peptization effect and also deoxolation reactions which inherently leads to [TiO_6] octahedra rearrangement. This promotes the synthesis of either rutile or anatase type TiO_2 [58, 59, 60].
- the nanoparticle size. The protons are able to bind directly onto the surface of the growing TiO_2 particle and in moderately acidic or basic conditions an adsorption-desorption equilibrium is established. This changes the surface chemical composition and consequently the surface energy of the growing particle. When the surface charge density is high (the pH value is different than the point of zero charge (PZC) pH value), the surface energy is strongly decreased. Consequently, the particle size decreases because the energetic penalty to develop a surface is notably reduced [61].

1.3.3.1.2.2 Synthesis of TiO_2 nanoparticles using H_2SO_4

H_2SO_4 is a very strong mineral acid, which acidifies the reaction medium by adding two protons/oxonium ions. The protons exhibit the above-mentioned effects on polycondensation reactions in which the final material is formed. Nevertheless, it is the anions that may play an even more significant role in the material formation process. This is due to the fact that anions, contrary to protons, directly determine the Ti (IV) complex type and its chemical composition, since they act as ligands.

The sulphate anion is one such case. It is well known that the sulphate ion, when present in a sufficiently large amount, promotes the formation of TiO_2 in anatase crystal form. The sulphate anion may be regarded as a phase-specific promoter. This phase-specific promotion arises because the sulphate ion can directly adhere onto the already present Ti (IV) octahedra via two electrostatic bonds with hydrogen atoms on corner-positioned oxygen atoms. When TiO_2 nuclei form in the course of polycondensation reactions, they tend to adopt the anatase crystal structure. This may be due to the fact that doubly bound sulphate anions act as a steric hindrance, which renders it impossible for the $[TiO_6]$ octahedra to nucleate into linear chains, which are specific for rutile crystal structure. On the other hand, the zig-zag nucleation of octahedra is possible, and thus anatase is the only product possible [15, 16].

The phase-specific promotion action of the sulphate anion is demonstrated in Figure 5.

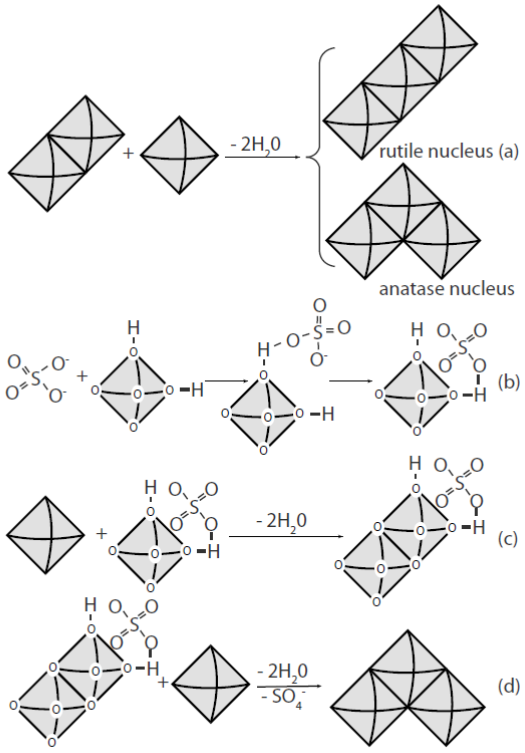

Figure 5: *A scheme of possible precursor transformation into anatase when the sulphate ion is present in the reaction medium.* (a) The TiO_6 octahedra arrangement determines whether a rutile or an anatase nucleus will be formed. (b) The sulphate ion interacts with the $[TiO_6]$ octahedra hydroxyl groups. (c) Two $[TiO_6]$ octahedra share an edge in the presence of the sulphate ion and form a dimer. (d) The third $[TiO_6]$ octahedra can bind to the dimer only on the side edge by which an anatase nuclei forms [15].

On the other hand, the sulphate anion may act directly as a ligand in the coordination sphere of the Ti (IV) ion. It is possible that a specific complex forms, such as $[Ti(OH)_2SO_4(OH_2)_2]^0$, that condenses into anatase nuclei [62].

Although the sulphate anion tends to promote the formation of anatase TiO_2, there are some indications that it is not appropriate for TiO_2 nanoparticle synthesis. Peptization of amorphous TiO_2 with 0.5 M H_2SO_4 produced a well-crystalline anatase material, having a grain size of around 5 nm. But its specific surface was very low, even less than 10 m^2/g. This was attributed to the tendency of the sulphate anion to complex strongly with titanium ions, encouraging the growth of anatase particles in a way that greatly reduced the porosity of the final product [63].

1.3.3.1.2.3 Synthesis of TiO_2 nanoparticles using HCl

The synthesis of TiO_2 nanoparticles with HCl is not well covered. Nevertheless, it is known that hydrochloric acid strongly influences polycondensation reactions by providing protons and chloride anions, which both influence the course of the reaction. In the case of HCl, the reactions tend to produce phase-pure rutile material [59]. The mechanism by which HCl promotes rutile-specific product formation is devised and was, to some extent, already discussed. The phase-specific TiO_2 formation is generally considered based on the formation of a specific Ti (IV) complex. When anions are present, the Ti (IV) complex of the form $[M(OH)_h(OH_2)_{N-h}]^{(z-h)+}$ may be transformed into a $[M(OH)_h(X)(OH_2)_{N-h-1}]^{(z-h-1)+}$ type complex, where X represents an anion [48]. The anions acting as ligands may completely change the initial complex form by changing the ratio of the water and hydroxide ligands. This in turn may change the type of the polycondensation reaction (olation or oxolation) and the geometry by which the Ti (IV) octahedra polycondense into particles. In either case, the anions promote oxolation because when present as ligands they possibly substitute for water molecules, which, as was already mentioned, may not be present in the coordination sphere in order for oxolation to take place.

The complex type responsible for the formation of rutile nanoparticles is considered to be of the $[Ti(OH)Cl_3(OH_2)_2]^0$ type. Interestingly, the brookite-type promoting complex differs only slightly and is considered to be $[Ti(OH)_2Cl_2(OH_2)_2]^0$ [64]. There is yet no clear evidence that HCl is suitable for the synthesis of anatase nanoparticles. Nevertheless, it seems crucial that an appropriate amount of HCl is present in the reaction medium, since this allows the production of a phase-specific product.

The chloride anion also influences the morphology of the nanoparticles. The underlying mechanism for this morphology-dependent effect is probably linked to the specific properties of the TiO_2 crystal structure. The crystal structure of both anatase and rutile is tetragonal, which means that the crystal planes differ in their properties, namely in their surface energies. The surface energies of rutile crystal planes {011}, {110}, {100} and {221} were calculated based on the atomistic simulations and are 1.85, 1.78, 2.08 and 2.02 J/m^2 respectively [65]. The difference in crystal plane surface energies probably results in different adsorption affinities for species in the surrounding reaction medium. Therefore, the ratio of adsorption for chloride ions versus Ti (IV) octahedra is specific for a specific crystal plane and consequently the polycondensation of the octahedra will take place preferentially on the crystal plane having the higher surface energy.

This results in the formation of an anisotropic nanoparticle [66, 67].

1.3.3.1.2.4 Synthesis of TiO_2 nanoparticles using HNO_3

The synthesis of TiO_2 nanoparticles with HNO_3 was studied exhaustively. It seems that HNO_3 was especially well covered when it comes to acid reflux reactions. Many different titanium precursors were tested in reflux reactions, yielding TiO_2 with variable properties. When titanium isopropoxide was refluxed in 0.56 M HNO_3 at temperatures up to 60 ºC, needle-like rutile nanoparticles were formed. The same reaction at a higher temperature (90 ºC) yielded highly agglomerated anatase nanoparticles [68]. Similar, temperature-dependent results were obtained when amorphous TiO_2 was refluxed with 0.1 – 0.5 M HNO_3. At room temperature, the material was a mixture of rutile and anatase, while at higher temperatures the material was mostly anatase containing a small amount of brookite [63].

On the other hand, it was also shown that HNO_3 can also provide phase-pure materials. When refluxing $TiCl_4$ aqueous solutions in concentrated (15 M) HNO_3 one can produce rutile nanoparticles with an anisotropic morphology [68]. The authors did not provide an explanation for the anisotropic morphology of the obtained nanoparticles, but considering the effect that the chloride ion has shown to have, it would be reasonable to assume that the same effect is possible for NO_3^- anions.

However, the temperature seemed to play a significant role in the determination of the TiO_2 nanoparticle crystal structure. This can be understood if one takes into account that the ionic product of water (K_w) is temperature dependent. So when performing a reaction in a mildly acidic medium at a higher temperature the ionic product of water increases significantly and consequently a great number of hydroxide ions form (the concentration of oxonium ions stays relatively unchanged since most of the protons are contributed by the acid). This in turn may affect the polycondensation reactions and to some extent determine the form of the final product [15]. There is also some proof that the nitrate anion could act as a ligand and form Ti (IV) complexes similar to the ones that the chloride anion forms [69]. Therefore, the nitrate anion could act in the same manner as the chloride anion.

It seems that the acid type profoundly affects the final TiO_2 nanomaterial characteristics. This is because the ions present in the acidic medium tend to determine the chemical behavior of the reaction medium, i.e., the type of reactions that will take place, and also determine some other nanoparticle characteristics, such as particle morphology and size. The latter is a consequence of the fact that the particles produced are in colloid form. Therefore, their physical characteristics (zeta-potential, surface charge,…) are determined by the ionic strength of the surrounding medium. When nuclei form and the particle growth phase occurs, the ions determine the colloid particle electrical double layer. Depending on the properties of the electrical double layer, aggregation of crystallites takes place at a specific stage during their growth. Depending on the ionic strength and on the ions present, the aggregation stage may occur sooner or later, the result being polycrystalline nanoparticles of different size [48].

This effect can be observed when performing the sol-gel/gel-sol reactions in the presence of an appropriate water-soluble ionic salt. It was shown that by adding sodium chloride (NaCl) the TiO_2 nanoparticles are smaller in size [62, 66, 67, 70].

1.3.3.1.3 Surfactant-based hydrolysis

Like acids, surfactants possess a threefold purpose:

- they promote the formation of crystalline TiO_2
- they ensure a small particle size
- they stabilize individual particles against agglomeration

Many synthesis methods involving various surfactants were already developed. When performing room-temperature hydrolysis of titanium (IV) *n*-butoxide in *n*-butanol solvent in the presence of para-toluenesulfonic acid (PTSH) and acetylacetone, followed by aging at 60 ºC, monodisperse, non-agglomerated anatase nanoparticles with grains ranging from 1 – 5 nm were obtained [71].

A particularly popular class of surfactants used with nano-TiO_2 synthesis comprises tetra-alkylammonium hydroxides (general formula $NR_4^+OH^-$). These hydroxides have a twofold effect. Since they have a basic pH value, the sol-gel reactions proceed in a way that favors anatase production. Secondly, the NR_4^+ ion associates with the negatively charged TiO_2 nanoparticle surface forming a stable sol [72–75]. Recently, a wet chemical method was developed based on using the tetramethylammonium hydroxide (TMAH) surfactant that by simple variations in its concentration enabled control over particle size, morphology and also organization of TiO_2 crystallites. The process is a simple straightforward reaction involving the formation of amorphous TiO_2 from an alkoxide precursor in a dilute aqueous TMAH solution followed by refluxing under inert gas for 6 h [72]. The results obtained in this experiment indicate that the tetraethylammonium cation ($N(CH_3)_4^+$) adheres preferentially with the (101) crystal plane, thus preventing the addition and polycondensation of new Ti(IV) octahedra to the (101) surface during crystal growth. This results in the formation of anisotropic anatase nanoparticles. Furthermore, it was discovered that size tuning is possible by changing the size of the alkyl substituent on the tetraalkylammonium cation. The synthesis of nano-TiO_2 in the presence of tetramethyl-, tetraethyl- and tetrabutylammonium hydroxide leads to the formation of anatase with a grain size ranging from 40 to 20 nm [74, 75]. A possible explanation for this phenomenon could be that a larger alkyl substituent is more effective in preventing collisions among primary anatase nanoparticles and therefore prevents their growth. Another possible explanation could be that larger alkyl substituents reduce the likelihood of an OH^- ligand being donated to a Ti (IV) d^0 complex ion present in the reaction medium, which in turn reduces the likelihood of condensation reactions between such complexes to create Ti-O-Ti bonds and form solid TiO_2. Either way, it is clear that particle size control is possible to a greater or lesser extent by changing the alkyl substituents.

Some experiments were also made where multiple surfactants were employed. In such cases, one surfactant may act as a catalyst for the formation of crystalline material, while the other might serve to prevent agglomeration. For example, stable dispersions of nano-TiO_2 were made by hydrolyzing titanium (IV) isopropoxide in the presence of both cetyltrimethylammonium bromide (CTAB) and tetramethylammonium hydroxide (TMAH). In this case CTAB was the stabilizer and TMAH the catalyst. It is interesting that as-prepared nano-TiO_2 is reported to have an extra small grain size, among the smallest reported in literature, being around 2 nm in size [76].

As was described with the above provided examples, the surfactant-based hydrolysis methods seem to be very suitable for the preparation of nano-TiO_2 with very small grain size in the form of stable colloids. Yet, despite the extremely high specific surface area of these nanoparticles, their application comes into question since their surfaces are covered with surfactant molecules. This hinders or even eliminates the photocatalytic activity of such materials. Therefore, further purification methods have to be employed in order to prepare an application-wise suitable material. Such purification methods are most commonly salting out, washing, centrifugation and dialysis, which are all labor-intensive and time-consuming. Hence, an additional disadvantage of the surfactant-based hydrolysis reactions is generally a great amount of hazardous aqueous waste.

1.3.3.2 The hydrothermal synthesis

One of the most popular techniques in hydrolysis-based preparation of nano-TiO_2 is the hydrothermal processing. This method is based on using elevated pressures and temperatures in the presence of water to prepare the final well-crystalline product. Properly addressed, this technique is termed solvothermal processing where a liquid other than water is used as the solvent, even if water is present for hydrolysis [77]. Although some researchers use the two terms interchangeably, this presented work will use the term ‘’hydrothermal’’ to describe any high-temperature, high-pressure water-based solution-phase reaction.

Hydrothermal crystallization is carried out in a sealed autoclave, an example of which is shown in Figure 6 below.

Figure 6: *A typical autoclave used for laboratory hydrothermal synthesis experiments.*

Autoclaves are usually made of stainless steel or titanium, but it is also possible to purchase vessels made from corrosion-resistant alloys that allow us to perform reactions under highly acidic or basic conditions. A possible wide-spread alternative is to use a Teflon liner that protects the vessel’s interior during reactions where the reaction medium is corrosive or aggressive in some other way. However, since Teflon melts at around 250 ºC, it cannot be used in reactions above 250 °C.

In a hydrothermal reaction, a heating mantle or an oven is used to raise the temperature above the standard boiling point of the solvent, at which point the evaporating solvent begins to generate an internal pressure. This pressure, which arises exclusively due to the refluxing solvent, is known as autogenous pressure. The temperature needed for crystallization under hydrothermal conditions depends on the material. To produce hydrothermally-prepared nanocrystalline TiO_2, temperatures ranging from 150 to 350 ºC are most commonly used. These temperatures are well below the temperatures encountered with calcination. The corresponding pressures depend on the filling volume of the autoclave. A high filling volume of 85 % corresponds to a pressure of 120 bar at 220 °C or even around 300 bar at 240 °C. Lower filling volumes of about 50 % result in much lower pressures of about 10 – 15 bar at around 200 °C. Hydrothermal reaction times may be short (2 h) but are generally quite long (1 – 2 days).

Hydrothermal processing using either amorphous TiO_2 or a titanium-containing precursor has been shown to be an ideal method for obtaining nano-TiO_2 with small grain sizes and a high specific surface as well as high crystallinity [9, 72–75, 78–114]. Usually,

hydrothermal processing is performed on a suspension or a slurry of amorphous TiO_2 obtained via hydrolysis of $TiCl_4$ or a titanium (IV) alkoxide. It is however possible to combine the hydrolysis and crystallization step in a single-vessel process. This is accomplished by injecting a solution of the precursor into a pre-heated autoclave or by initially placing the precursor (dissolved in an organic medium) and the hydrolysis water in separate regions of the autoclave so that they only come into physical contact when the water boils upon heating. This is a controlled hydrolysis with a limited amount of water in an organic solvent. The final product is a very fine anatase with crystallite size ranging from 10 to 30 nm and a high specific surface (50 – 280 m^2/g). Correspondingly, the photocatalytic performance of such materials is very good as well. This is because of the presence of a large number of surface sites for adsorption [81, 83, 84, 87, 94, 114]. The formation of such small nanoparticles was attributed to the low solubility of TiO_2 in organic solvents, the consequence of which is that anatase nanocrystals, once nucleated, are unlikely to grow to an appreciable size via dissolution and precipitation (Ostwald ripening).

The importance of the amount of water needed for hydrolysis and particularly the molar ratio of water to precursor is nevertheless still undisclosed due to different hydrothermal reactions so far performed and the variety of materials that have been produced. For instance, it has been observed that when performing the hydrothermal reaction using amorphous TiO_2 made from an alkoxide, an increase in the water-to-alkoxide ratio correlates with a decrease in the grain size in the final product. This could be due to the fact that a higher water content results in a more rapid hydrolysis rate, which favors the nucleation of new particles over the growth process of the existing particles [90]. However, this proposed correlation may not be as simple as that. It was reported that when performing the hydrothermal synthesis of anatase in the presence of HNO_3 or HCl, finer particles were formed when the ratio of water to alkoxide was low rather than high [115]. This result was attributed to hydrogen bonding between the freshly formed anatase particles which would be enhanced at higher water-to-alkoxide ratios. This consequently encourages the aggregation of the nuclei into coarse primary particles. Nevertheless, it is clear that under a given set of conditions, one can change the properties of the final material by manipulating the water-to-precursor ratio while simultaneously understanding other reaction parameters that influence the physical characteristics of TiO_2.

As is the case with other hydrolytic-based methods, it is possible to selectively obtain a particular crystalline phase in a hydrothermal reaction by adjusting the pH of the reaction medium. As was already noted, acidic conditions promote the rutile phase, while the neutral or basic conditions promote anatase phase formation. It was also noted that the hydrothermal reaction temperature may, to some extent, determine the phase purity of the final material. The temperature range 210–240 ºC appears to be optimal to obtain anatase, whereas rutile and brookite impurities are observed when performing the synthesis outside the stated temperature range [85, 90, 96, 116].

When the hydrothermal synthesis is performed without a surfactant, the nanoparticles form loose agglomerates, while no aggregation seems to occur. A major setback regarding the hydrothermal synthesis is that the TiO_2 formed rarely exhibits a very large surface area. Also long aging times and sometimes the use of harmful organic solvents are clearly disadvantageous when trying to produce a chemically-wise pure material in large quantities.

1.3.4 Synthesis methods summary

The various types of methods to produce nano-TiO_2 that were described in this section are summarized in Table 2.

Table 2: *Summary of the various synthesis methods used to obtain nanocrystalline TiO_2.*

Synthesis method	***Reaction temperature / °C***	***Crystallite size / nm***	***Advantages***	***Disadvantages***
Aerosol pyrolysis	200 – 1000	> 15	• environmentally friendly • high crystallinity • tunable phase composition	• large particles • severe agglomeration
Non-hydrolytic solution-phase reactions	80 – 300	4 – 10	• short reaction times • fine particles • minimal agglomeration • high surface area	• organic ligands on particle surface
Hydrolytic solution-phase reactions followed by heat treatment	500 – 1000 (during calcination)	> 15	• high crystallinity • tunable phase composition • easy synthesis	• large particles • severe agglomeration
Acid- or surfactant-based hydrolytic solution-phase reactions	60 – 100	2 – 10	• fine particles • minimal agglomeration • high surface area • high crystallinity • tunable morphology and phase composition	• surfactants on surface • may produce large quantities of waste • sometimes long reaction times
Hydrothermal synthesis	150 – 350	8 – 30	• fine particles • high surface area • easy synthesis • high crystallinity	• some agglomeration

It should be noted that although some methods have clear technical advantages (reaction time, the amount of waste,…) over the others, the question of whether a

particular method is advantageous material-wise, often depends primarily on the intended final application. In the case of the present work, two major objectives were set. One was the synthesis of a photocatalytically active TiO_2 intended for photocatalytic coatings, and the other the synthesis of TiO_2 that would best-suit the DSSC application. Both applications are intended in general for photovoltaics. Furthermore, as was already noted, we had to develop TiO_2 for both applications based on raw materials emanating from the established Sulphate process of pigment production in Cinkarna Celje, Inc. in a way that agglomeration, aggregation and possible dusting of the final material would be avoided. Thus, only the water-based colloid formation of TiO_2 suits the above-mentioned limitations.

The synthesis methods that would be appropriate and were used in TiO_2 synthesis experiments throughout the course of the proposed investigations were the sol-gel and the gel-sol acid-based hydrolysis and the hydrothermal processing. With these methods various materials may be produced that differ in their basic characteristics, namely morphology, particle size, crystal structure and crystallinity. This, however, may provide a great deal of possible materials that can be tested for either photocatalysis or DSSCs and consequently enables us to experimentally determine the material-of-choice for a given application.

1.4 TiO_2 in photovoltaics and photocatalysis

One of the aims of the present work was to develop a nano-TiO_2 material that could be used in the field of photovoltaics. The use of nano-TiO_2 for photovoltaics can be understood in terms of two possible applications.

Firstly, nano-TiO_2 has become the material-of-choice for third-generation-type solar cells, so-called dye-sensitized solar cells (DSSCs), whose technology is based on the use of relatively cheap materials.

Secondly, nano-TiO_2 can be used for a photocatalytic coating that could be beneficial when applying it onto the surface of the silicon solar modules. By exerting the ability to degrade organic pollutants and the ability for inorganic pollutants to be rinsed off due to the superhydrophilic effect, the efficiency of the modules could be preserved over a longer period of time.

The two possible applications of nano-TiO_2 in photovoltaics are briefly described in the following section.

1.4.1 Dye-sensitized solar cells (DSSC)

DSSCs have a relatively simple structure shown in Figure 7.

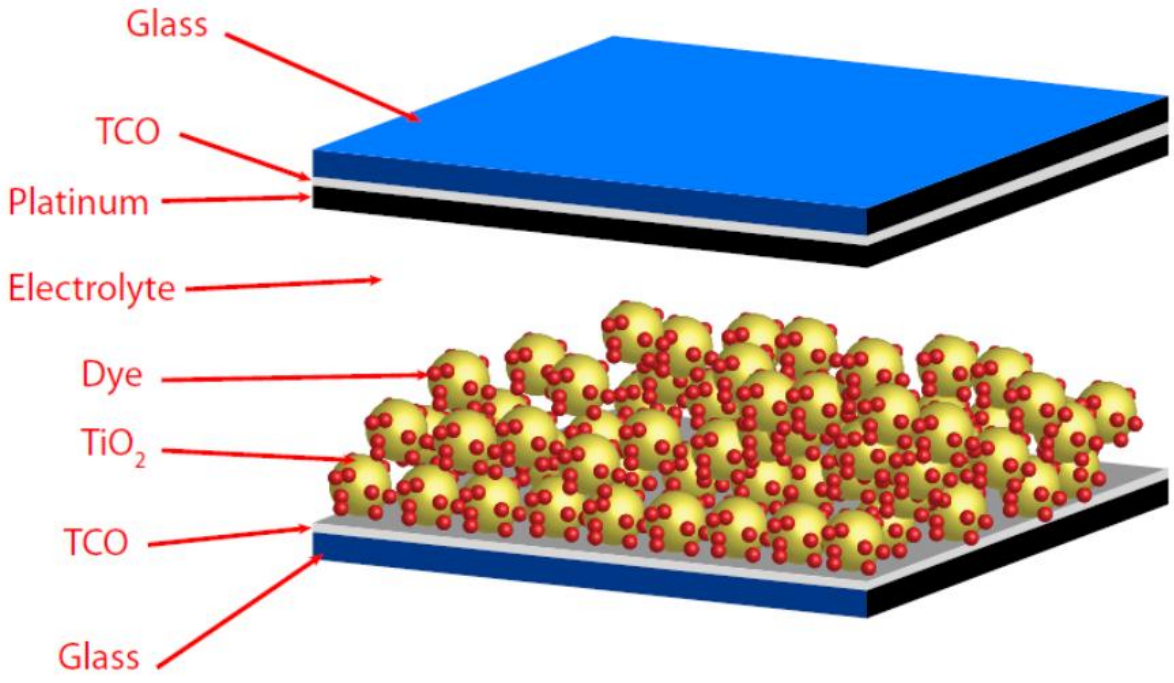

Figure 7: *A schematic representation of the components of the working DSSC.*

The DSSC consists of five layers working together to produce and transfer electrical current. The top electrode is usually a glass substrate coated with a transparent conductive oxide (TCO) and a dense barrier layer that hinders recombination. Dye molecules are adsorbed onto the surface of a wide-bandgap semiconductor film that is deposited or grown on the barrier layer. The semiconductor acts as the electron-transfer material while the dye represents the photoactive layer. An electrolyte fills the interlayer spacing

between the film and the bottom electrode and acts as a reducing agent for the dye and enables the renewable process. The counter electrode consists of a sputtered layer of platinum on a TCO-coated glass substrate. The DSSCs work is similar to the photosynthesis process, with the dye acting in the same manner as chlorophyll. The dye is excited by sunlight so that a high energy conversion may occur [117–119].

Every one of the five layers in the DSSC has a specific role in enabling the cell to function well. The **electrode substrates** are designed for mechanical strength and must have a maximum light transmission, since the amount of light activating the dye molecules determines the cell output. A suitable substrate for DSSC is TCO-coated glass where the TCO most commonly consists of fluorine-doped tin oxide with a thickness of about 0.5 μm and an electrical resistance of about 8-10 Ω/cm^2 [120]. Other doped oxides are also utilized, such as indium-doped tin oxide (ITO) since empirical studies show that the fluorine-doped tin oxide markedly increases efficiency. The work function (the work function, WF, is defined as the energy required to remove an electron from the Fermi energy level of the surface to the vacuum level) of the metal on the counter electrode determines the output voltage. Platinum, which is most commonly used, has a work function of about 5.6 eV and provides a large potential output voltage. If, for example, gold were used instead, a 0.5 V loss in photovoltage would occur since gold has a WF of just 5.1 eV.

The **sensitizer**, a dye monolayer, is the active layer in which an electron is shifted to a higher energy level upon solar irradiation. The dye layer must be very thin, preferably one molecule in thickness. This is because only the dye molecules which are in direct contact with the semiconductor and the electrolyte can transfer charge. Any additional dye layer may actually impede electron transfer from the electrolyte to the dye molecule causing a less than optimal operation of the DSSC [121, 122]. A monolayer coverage on a high-surface semiconductor is ideal as it allows the maximum possible absorption of photons. Also, with a dye monolayer, there are minimal losses which can arise because of a relaxation of the excited state electron, since there is always a semiconductor surface nearby to accept the electron into the conduction band [123].

The dye molecule absorbs the photon causing the electron excitation from the ground state (HOMO orbital) to the carboxylate ligand by metal-to-ligand charge transfer (MLCT). Afterwards, electron injection occurs as the electron is injected from the carboxylate ligand into the semiconductor conduction band. The injection process is very swift as it is carried out in a period of a few picoseconds. This is because the n^* orbital of the carboxylate ligand overlaps with the conduction band of TiO_2 [123, 124]. The electron injection from the ligand to the TiO_2 conduction band is favoured energetically, as the conduction band's energy is lower than the lowest unoccupied molecular orbital (LUMO) energy of the dye. Also, the electron injection is favoured in terms of entropy, since once the electron is injected into the conduction band it is averaged over many states. Because of the two mentioned reasons the back reaction is not favoured. Electron injection is reported to be hindered by impurities in the semiconductor, such as iron or some other dopant. Experiments have shown that this effect may be lessened if a high-purity layer of TiO_2 is deposited on the already existing TiO_2 photoanode, which is most often done by hydrolyzing titanium tetrachloride. This causes the surface area to increase, since if the hydrolysis is done correctly, small TiO_2 particles form and cover the photoanode surface. The increased surface area and the presence of high-purity material promote electron injection [125].

The sensitizer must be designed for maximum absorption across the solar spectrum, must contain ligands that adhere readily to the semiconductor surface, must enable a high efficiency transfer of the excited electrons to the conduction band and must have a high reduction potential so that reduction is rapid compared to relaxation [126].

The energy levels of the sensitizer must be well matched with the energy levels of both the semiconductor and the electrolyte. The excited state of the sensitizer should lie just above the semiconductor conduction band in order for electron injection to be a low energy and rapid process. The ground-state energy level of the sensitizer should be just below that of the electrolyte and should be of sufficient reduction potential to be easily reduced by the redox couple. The sensitizers most commonly used are the N3 dye (Ru(4,4′-dicarboxylic acid-2,2′-bipyridine)$_2$(NCS)$_2$), the black dye (Ru(2,2',2"-(COOH)$_3$-terpy)(NCS)$_3$) and the N719 dye, which are shown in Figure 8.

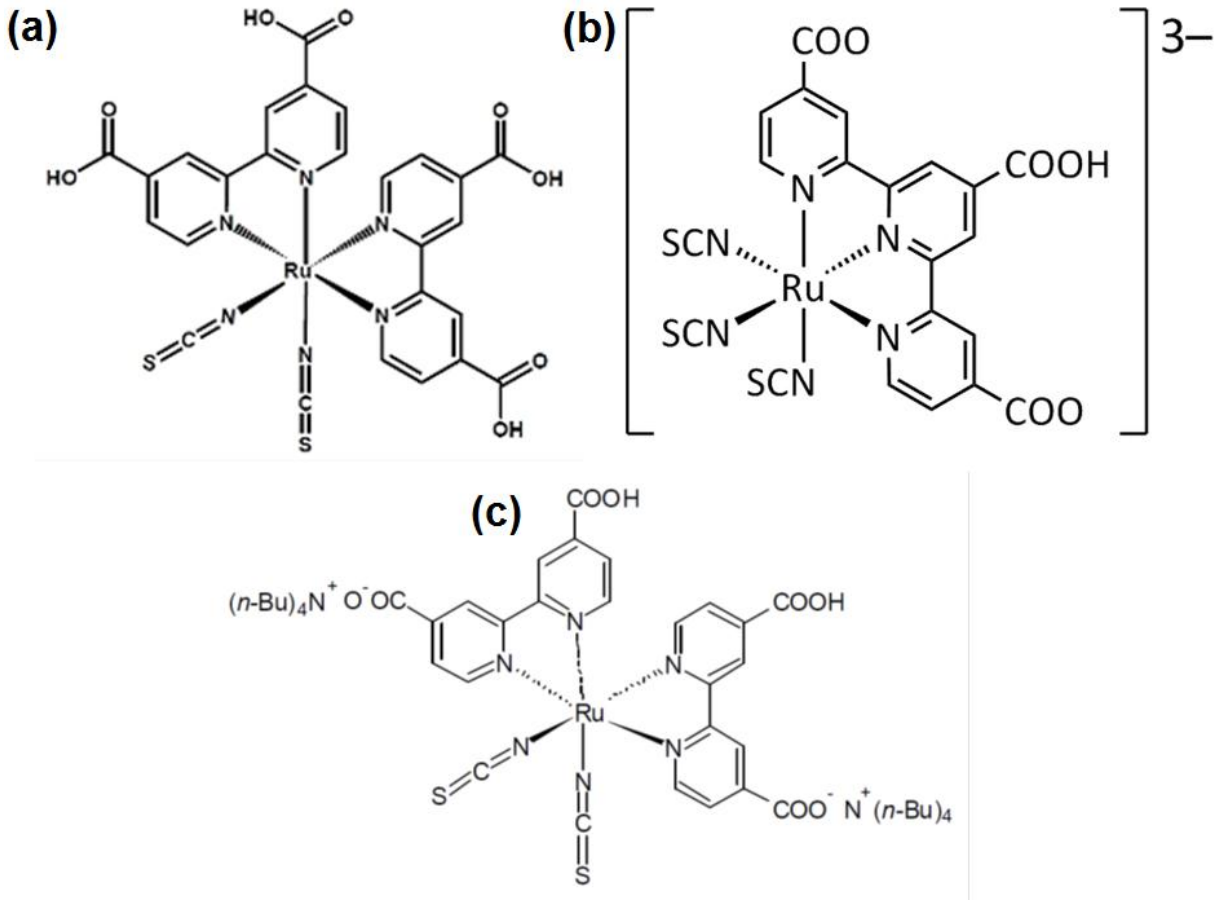

Figure 8: *The chemical structures of the most commonly used dyes for DSSCs [128]*. (a) The N3 dye. (b) The ‘’black dye’’. (c) The N719 dye.

The black dye and the N3 dye have so far given the highest efficiency DSSC that is 10.4 % and 10.6 %, respectively [126, 127]. Figure 9 shows the external spectral response curve of the photocurrent for a nanocrystalline TiO_2 solar cell sensitized by N3 and black dye with the I^-/I_3^- redox mediator, where the incident photon-to-current conversion efficiency (IPCE) is represented as a function of the wavelength. The IPCE is obtained by the following equation:

$$IPCE(\%) = \frac{1240(eVnm) \cdot J_{sc}(\mu A/cm^2)}{\lambda(nm) \cdot \phi(\mu W/cm^2)} \cdot 100 \qquad (15)$$

where J_{sc} is the short-circuit photocurrent density for monochromatic irradiation, λ is the wavelength and Φ is the monochromatic light intensity. The IPCE can be regarded as the number of electrons generated by light in the external circuit divided by the number of incident photons.

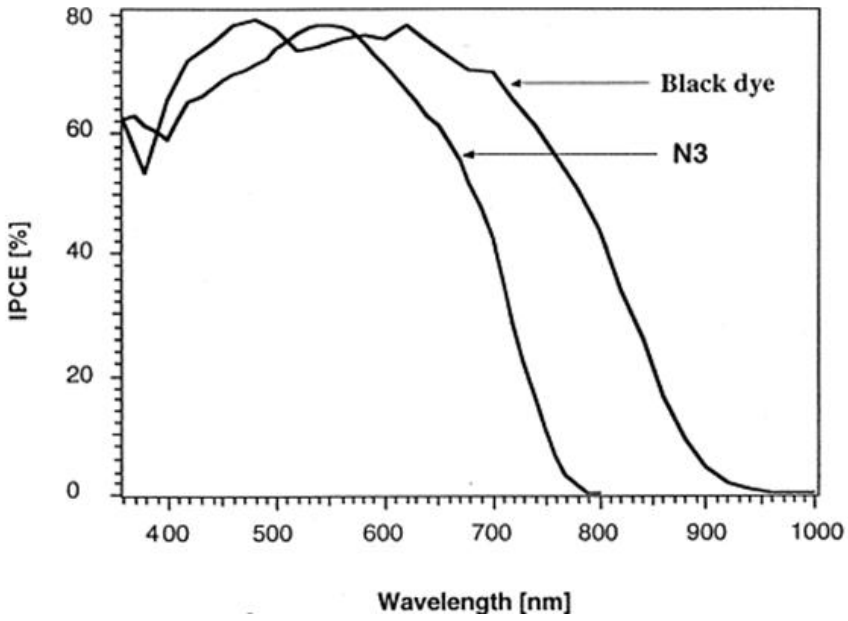

Figure 9: *Spectral responses (IPCE) of N3- and black dye sensitized TiO_2 solar cells [128]*. It can be clearly seen that the IPCE values of the two dyes are very high in the visible light spectra. If we take into account all the losses due to light adsorption, the IPCE value is near unity which means that nearly the entire incident light is transformed into the electron flow.

As shown in the Figure 9, solar cells having N3– or black dye as sensitizers can effectively convert visible light to electrical current.

The N3 dye responds to the light of wavelength between 400 to 800 nm, while the black dye responds to light with a wavelength between the near-IR region and 950 nm. The IPCE of the N3-dye-sensitized solar cell reaches 80% at 550 nm and exceeds 70% in the region from 450 to 650 nm. If we also take into consideration the light loss due to reflection and absorption by the FTO glass substrate, the IPCE is of a value between 90-100% which indicates that the DSSC is highly efficient in solar energy conversion [126, 128]. IPCE can also be defined as:

$$IPCE = LHE \cdot \phi_{inj} \cdot \eta_c \tag{16}$$

$$LHE = 1 - T = 1 - 10^{-A} \tag{17}$$

The LHE is the light-harvesting efficiency, Φ_{inj} is the quantum yield of electron injection and η_c the efficiency of collecting the injected electrons at the back electrode. If the Φ_{inj} and η_c are equal to unity, then the IPCE is determined only by the LHE (1–T) of the dye absorbed on the TiO_2 film, where T is the transmittance of the DSSC.

The **electrolyte** is comprised of reduction-oxidation (redox) molecules that reduce the sensitizer after photoexcitation and are themselves reduced at the counter electrode. The redox couple must have a reduction potential between the platinum work function and the sensitizer reduction potential, which creates a driving force for electron transfer. The most common electrolyte type used ever since the early stages of DSSC development is the iodide/triiodide couple [121]. It is produced simply by mixing iodine with an iodide salt in an appropriate solvent, such as acetonitrile [129]. Adding guanidinium thiocyanate to the electrolyte screens the coulombic interactions between the dye molecules, producing a more dense dye layer that decreases recombination losses [126].

At the platinum electrode, the electrons that have passed through the electrical circuit, are donated to the redox couple. The redox couple than reduces the excited sensitizer molecule which enables continuous operation. The sensitizer must be reduced rapidly

because as soon as it replenishes an electron to the ground state, the excited electron may not relax, which would result in losses. Generally speaking, the relaxation process of the excited electrons does not occur because the electron injection process is very rapid and takes place in a matter of picoseconds ($\tau < 7$ ps) [125]. Furthermore, the metal-to-ligand charge transfer that occurs before electron injection is much more rapid in the forward direction. Some other redox couples such as $(SCN)_2/SCN^-$ and $(SeCN)_2/SeCN^-$ have a higher reduction potential than iodide/triiodide and have also been tested, but the final DSSC efficiencies were drastically lower. This is most likely due to a slower dye regeneration rate [130, 131].

All of the electrolytes discussed above have a common problem. Namely, the final DSSC may eventually degrade because they are all liquid type electrolytes. Although the liquid type electrolyte allows complete filling of all of the pores and small crevices in the photonoade, it often degrades in air and/or under thermal stress making sealing of the cell a very difficult task, which must be done perfectly so that the cell may have a long lifetime. Specifically, degradation occurs after a short period at 80-85 ºC, causing a problem for the DSSC's use in outdoor conditions [126]. The degradation is caused by the crystallization of the iodide salt. Hence, a great deal of research is being focused on solid-state electrolytes that avoid both leakage and degradation. Polymer matrix electrolytes offer fewer leakage problems but still have degradation issues as well as low efficiency because of their slow ionic conductivity [132–134]. Nanocomposite gel electrolytes combine both the solid state and the liquid state of the electrolyte. A typical nanocomposite gel electrolyte encompasses a mixture of inorganic material, such as silica, with its inner pores filled with an organic material that acts as the active ionic conductor [135]. The organic component can be optimized for the speed of ionic conductivity, but percolation conditions are necessary to allow for the greatest conductivity. In this way the liquid is more stable because there is a lesser chance of environmental degradation.

The **semiconductor photoanode** is probably the most important part of the DSSC and is being intensively researched in order to better understand and enhance the final efficiencies. The mesoporous, wide-bandgap semiconductor is adhered on the TCO/glass surface and is responsible for the transfer of the electrons from the dye molecule to the TCO electrode. Experiments have shown that TiO_2 provides the highest efficiencies. In particular, zinc oxide has been utilized as a possible alternative to TiO_2, but experiments have shown that it provides a lower current conversion efficiency and takes much longer to adsorb the dye onto its surface than TiO_2 [136]. The lower efficiency of the ZnO-based DSSC seems to be the consequence of lower dye-to-semiconductor electron injection or a consequence of an increase in recombination losses [136]. Some other materials have been investigated as well, such as SnO_2, Fe_2O_3, Nb_2O_5, CdS and CdSe, but in every case the efficiencies were lower than with TiO_2 [137–140].

The most important properties of the photoanode include mechanical strength, uniform thickness, high surface area and rapid dye adsorption throughout the film. High surface area is one of the main features, since the current output is directly related to the amount of dye molecules adsorbed on the TiO_2 film. A high-surface-area film can be produced by using nanoparticles which increase the roughness factor of the electrode by over 1000-times and consequently the surface area may increase to 100 m^2/g [126]. TiO_2 nanoparticles also promote electron transfer even without being additionally doped to achieve better electrical conductivity. This is because the addition of the injected electron allows the TiO_2 to become an n-type semiconductor (the Fermi level is raised).

A very large number of reports and review papers exist about the production of titanium dioxide in various forms (particles and films), providing detailed information about how to make nano-TiO_2 suitable for a photoanode layer in DSSCs. Sol-gel methods

[141, 142], dispersion methods [125], and hydrothermal growth methods [143] among many others, have all been used and investigated, accentuating the need to control the thickness of the deposited nano-TiO_2 layers with regard to their particle size, surface area, the porosity of the formed photoanode layers, the pore size and their distribution, together with the need to know the activity of the surface sites of the formed nano-TiO_2 particles. Grätzel used mesoporous thin films of spherical titanium dioxide and achieved a DSSC efficiency up to 10.6 %. The corresponding TiO_2 nanoparticles, which were made via the hydrothermal sol-gel synthesis from a titanium isopropoxide precursor [144], are well formed and have a narrow particle size distribution. TiO_2 in nanoparticle form is commercially available in the form of a suspension and dispersion; for example, P25 (Evonik), consists of approximately 80 % anatase and 20 % rutile, while a sol-gel produced nano-TiO_2 usually consists of only anatase, due to a heat-treatment at 450 ºC. Anatase is mostly the material-of-choice for DSSCs.

Although a great deal of work has been centered on providing an optimal solution for the production of a homogenous, well-adhered and highly-porous TiO_2 film, there are still remaining problems to be solved, which are mainly of technological type. Namely, all of the methods presented are complex, time-consuming and labour-intensive. These problems, on the other hand, have so far proven to be critical when it comes to setting-up the DSSC technology for a possible large-scale production. Therefore, new methods must be used that would enable a low-cost, rapid TiO_2 layer production. Among these new methods the TiO_2 paste preparation methods have shown great promise. TiO_2 paste preparation is based on using TiO_2 nanoparticles as a raw material that is mixed into an appropriate solvent, a binder and a dispersing agent. Upon mixing a fine and homogenous TiO_2 paste is formed and can readily be applied onto the substrate and then thermally treated to form the final photoanode. Although some TiO_2 paste preparation methods may be time consuming [145], the ones based on the Pechini method could prove to be efficient and relatively cheap. They also provide easy handling and fast preparation [146]. What is especially important with the sol-gel based Pechini TiO_2 paste preparation method is the fact that it can readily be used for nano-TiO_2 in the form of water suspensions and/or slurries. These advantages were the reason to accommodate this preparation method to produce TiO_2 pastes for DSSC preparation in the course of this thesis.

1.4.1.1 DSSC energetics

The energy diagram and the electron transfer path of the most common type of DSSC is shown in Figure 10. Generally, the working performance of a DSSC is based on the kinetics of the electron-transfer reactions. Electrons are injected from the dye into the TiO_2 and the hole is injected into the electrolyte. Therefore, charge separation and charge transport occur in different media and are spatially separated. A more detailed description of the process is as follows [123, 128]:

- the dye becomes photo-excited which results in the injection of the electrons into the conduction band of the TiO_2
- the electrons diffuse toward the back contact (FTO – SnO_2:F) and consequently reach the counter electrode through the external load and wiring
- the excited state of the dye is short-lived since it is reduced by the electrolyte present and is usually comprised of an organic solvent containing a redox system, such as the iodide/triiodide couple. The regeneration of the dye forbids the electrons injected in the conduction

band from flowing backwards and therefore become lost in the process of sunlight conversion.

- the oxidized redox mediator, the I_3^- ion diffuses to the counter electrode and is re-reduced to the I^- ion over the Pt surface

Therefore, no net chemical reaction occurs because every oxidation reaction at the photoelectrode has a corresponding reduction reaction at the counter electrode. Overall, electric power is generated without any permanent chemical reaction. The performance of the DSSC is predominantly based on four energy levels of the components [128, 147]:

- the excited state (approximately LUMO) and the ground state (HOMO) of the Ru dye photosensitizer (or some other photosensitizer)
- the Fermi level of the photoelectrode which is located near the conduction-band level
- the redox potential of the redox mediator (I^-/I_3^-) in the electrolyte solution

The photocurrent obtained from the DSSC is determined by the energy difference between the HOMO and the LUMO of the photosensitizer (the HOMO-LUMO energy difference corresponds to the band gap for inorganic semiconductor materials). The smaller the HOMO-LUMO energy gap, the larger the photocurrent because of the utilization of the long-wavelength region in the solar spectrum.

The energy gap between the LUMO level and the conduction-band level of the TiO_2 film, ΔE_1, is important and the energy level of the LUMO must be sufficiently negative with respect to the conduction band of the TiO_2 film (must lie higher than the TiO_2 conduction band) in order to inject electrons effectively. In addition, substantial electronic coupling between the LUMO and the conduction band of the TiO_2 film also leads to effective electron injection. The HOMO level of the complex must be sufficiently more positive than the redox potential of the I^-/I_3^- redox mediator to accept electrons effectively (ΔE_2). The energy gaps, ΔE_1 and ΔE_2, must be larger than approximately 200 mV in order for the optimal electron-transfer efficiency to be achieved.

Another characteristic of the DSSC is the photovoltage. It is developed by the energy gap difference between the Fermi level of a TiO_2 electrode and the redox potential of the I^-/I_3^- in the electrolyte solution. The conduction band level of the TiO_2 photoelectrode and the redox potential of I^-/I_3^- are estimated to be -0.5 V versus a saturated calomel electrode (SCE) and 0.4 V versus the SCE, respectively. In the case of DSSC using a TiO_2 photoelectrode and I^-/I_3^- redox mediator, the maximum open-circuit photovoltage upon illumination is expected to be approximately 0.9 V, depending on the components of the electrolyte solution because the Fermi level of the TiO_2 photoelectrode depends on the species and concentrations of the electrolyte components [123, 128, 147].

It should be noted that at least 100-200 mV of the photovoltage is needed as a driving force for the electron-transfer reactions. Another voltage drop (0.4 V) can be accounted to the reduction of the photoexcited dye by iodide. This significant voltage drop directly pinpoints the possible adjustment that could be made to increase the photovoltage above ~ 0.7 V, but so far no other candidate has proven to be as efficient with the kinetics of dye interception and electron uptake as the I^-/I_3^- couple.

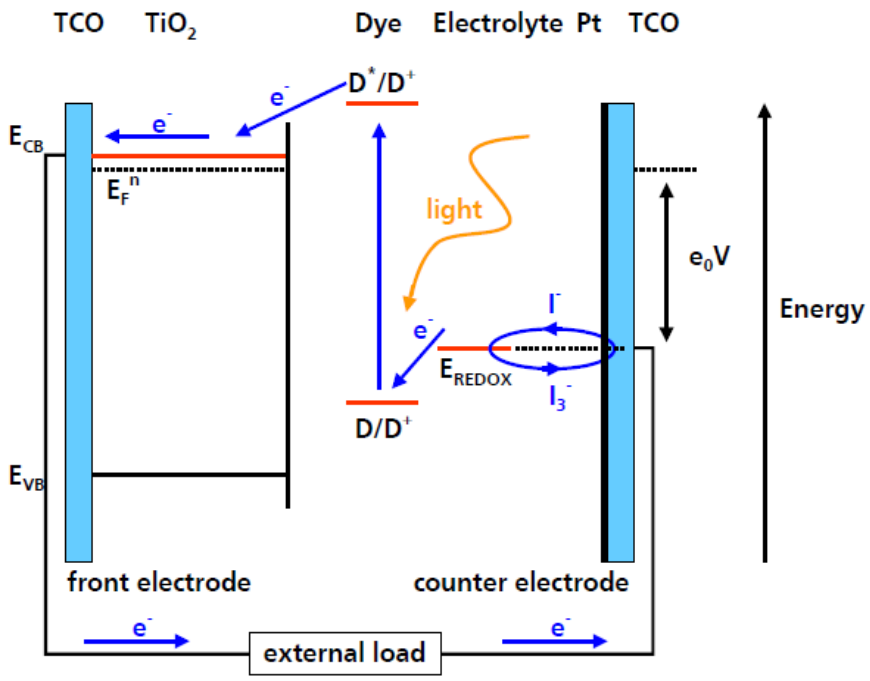

Figure 10: *Energy diagram and operating principle of a DSSC [128].*

Solar energy-to-electricity conversion efficiency (η) under white light irradiation (air mass; AM 1.5) can be obtained from:

$$\eta = \frac{J_{sc} \cdot V_{oc} \cdot ff}{I_0 \cdot 100} \tag{18}$$

I_0 is the photon flux (approximately 100 mW/cm^2 for AM 1.5), J_{sc} is the short-circuit photocurrent density, V_{oc} the maximum photovoltage (open circuit voltage) and *ff* the fill factor. The fill factor is defined as the ratio of the actual maximum obtainable power to the product of the open circuit voltage and short circuit current and is used in evaluating the performance of solar cells. The power, P, produced by the solar cell is determined by the product of the maximum photocurrent density (short-circuit current density, J_{sc}), the maximum photovoltage (open-circuit voltage, V_{oc}), and the fill factor (ff).

$$P_{\max} = J_{sc} \cdot V_{oc} \cdot ff \tag{19}$$

The value of J_{sc} depends on the sensitizer light absorption efficiency and on the electron injection efficiency. The value of V_{oc} is determined by the energetics of the system. The theoretical maximum attainable V_{oc} is determined by the energy difference between the conduction band and the electrochemical potential of the redox couple. Recombination reactions will in effect reduce both V_{oc} and J_{sc}. Therefore, the performance of the DSSCs depends on both the thermodynamic properties of the materials as well as on the kinetics of the reactions occurring in the DSSC.

The nanoporous nature of the TiO_2 allows for migration of the redox couple throughout the metal oxide network, which is crucial for efficient dye regeneration. However, injected electrons near the surface can be captured by the oxidized species in solution (I_3^-) resulting in reverse charge flow. This process can in principle take place not only at the TiO_2 interface, but also at the TCO back contact. This deleterious reaction is often referred to as the dark current and can be estimated by the electrochemical properties of the DSSC in the absence of illumination.

1.4.2 TiO_2-mediated photocatalysis

One of the most studied and environmentally significant applications of nano-TiO_2 is heterogeneous photocatalysis, i.e., light-induced chemical transformation of gas- or pollution-phase species on the surface of a solid catalyst, which is usually a semiconductor. The first indication that TiO_2 may act as a photocatalyst came when experiments were done in which a TiO_2 electrode was used to photochemically split water into producing hydrogen gas [148]. Although hydrogen production using a TiO_2 electrode is interesting due to possible clean-energy production, the most significant photocatalytic application for nano-TiO_2 however is still the photooxidative degradation of organic species in air and in wastewater systems. So far, TiO_2 has been widely recognized as the best semiconductor photocatalyst used for oxidative remediation of water contaminated by various organics [47]. Depending on the organic contaminant, it may be only partially oxidized, forming an innocuous or less harmful species, while in some other cases the photocatalytic oxidation may result in complete mineralization, i.e., the pollutant being completely converted to CO_2 and H_2O and other simple inorganic molecules [149].

1.4.2.1 Basic principles of TiO_2-mediated photooxidation in aqueous solutions

1.4.2.1.1 Steps in photocatalysis

TiO_2 photocatalysis efficiency depends on many physical variables, which include grain size, phase composition, surface area, defect sites, extent of surface hydroxylation and surface modification. These variables are discussed in more detail in this section, but in order to understand how and why TiO_2 physical characteristics influence the photocatalytic efficiency, it is first necessary to understand the underlying mechanisms of photocatalysis on the molecular level. Figure 11 is a schematic illustration of the events taking place on the surface of TiO_2 upon organic pollutant (denoted A) degradation in an aqueous environment.

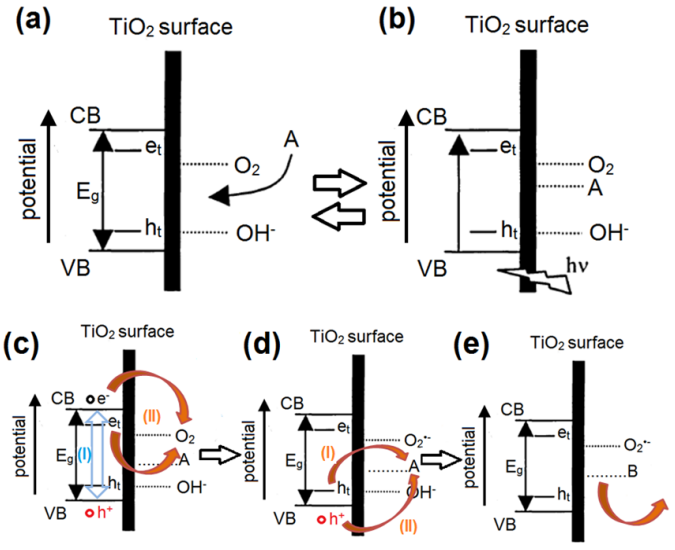

Figure 11: *Schematic representation of the elementary steps in TiO_2-mediated photooxidation.* (a) Adsorption of the pollutant (A). (b) Photoexcitation (exciton formation). (c) (I) Exciton recombination (blue arrow) or (II) reduction of the adsorbed oxygen (red arrow). (d) Oxidation of A to B (final product of A oxidation) by valence band holes (I) or by trapped holes. (II) (e) Desorption of B.

First, the reversible adsorption of the pollutant A on the TiO_2 surface takes place due to electrostatic or chemical bonding:

$$A \rightarrow A(ads) \tag{20}$$

Depending on the nature of the adsorbate and the TiO_2 material, an adsorption equilibrium may be established after an hour or may take several days. This points to the fact that the pollutant adsorption may be an essential step for effective photooxidation, which suggests that TiO_2-mediated photocatalytic reactions are indeed dominated by processes that occur on the semiconductor particle surface rather than between free species in the solution [17, 47, 149, 150].

In the next step, the aqueous TiO_2 + adsorbate suspension is irradiated with ultraviolet light of energy $E_{h\nu}$ which is equal or greater than the TiO_2 material's bandgap energy E_g. This results in the excitation of the valence band (VB) electron to the conduction band (CB). The excitation results in the creation of an electron/hole (e^-/h^+) pair (exciton), the lifetime of which is a critical determinant of a photocatalyst's efficiency:

$$h\nu + TiO_2 \rightarrow TiO_2 + e^- + h^+ \tag{21}$$

The excited electron may either recombine with the hole and heat is generated or can go on to reduce an adsorbed electron acceptor, most likely molecular oxygen [17, 47, 151, 152]:

$$e^- + h^+ \rightarrow heat \tag{22}$$

$$e^- + O_2(ads) \rightarrow O_2^{\bullet -}(ads) \tag{23}$$

In the absence of electron- or hole-trapping species on the TiO_2 surface, the exciton (e^-/h^+ pair) recombination will occur in 10-100 ns. However, the reduction of the surface adsorbed oxygen is a much slower process and requires 1 ms or more [17, 153]. In order for the CB electron to participate in the reduction of oxygen or any other electron acceptor on the surface, exciton recombination must be inhibited.

This may happen via trapping of the electrons and/or holes at thermodynamically favourable states (designated e_t and h_t) between the VB and CB. Charge-carrier trapping can occur either in the presence of a surface adsorbed charge scavenger (hole trapping by surface hydroxyl groups on the time scale of ~ 10 ns) or at a surface defect site (electron trapping at a coordinatively unsaturated Ti^{4+} resulting in Ti^{3+} formation which occurs on the time scale of ~ 10 ns) [149]. In order to compete with the very rapid process of exciton recombination, the charge trapping sites must readily be available, i.e., charge scavengers and/or defect sites must be present either at the surface or within the TiO_2 particle volume.

If the charge-carrier sites are present, then the photogenerated hole will have sufficient time to initiate the oxidative degradation of A to some other species B. This, in principle, may occur via two different mechanisms. One is a direct hole advance in which the untrapped VB hole itself reacts with A to produce B (Equation (24)). The other possibility is that a hydroxyl-mediated attack takes place in which the hole reacts with a surface adsorbed hydroxyl group to produce a reactive radical (most likely $OH^{\bullet}$) which only then oxidizes A to B (Equations 25 and 26):

$$h^+ + A(ads) \rightarrow B(ads) \tag{24}$$

$$h^+ + OH^-(ads) \rightarrow OH^{\bullet}(ads) \tag{25}$$

$$OH^{\bullet}(ads) + A(ads) \rightarrow B(ads) \tag{26}$$

These interfacial charge-transfer reactions, in which the adsorbate degradation occurs, typically require about 100 ns, which is again comparable or slower than charge-carrier recombination. Hence, the trapping of either photogenerated electrons or holes is a prerequisite for efficient photooxidation.

After the photooxidation, when A has been chemically converted to species B, the latter desorbs from the TiO_2 surface and diffuses into the solution:

$$B(ads) \rightarrow B \tag{27}$$

Again, it should be noted, that depending on the chemical nature of A and B, the time scale for adsorption and desorption may vary greatly, which affects the efficiency of degradation considerably. For example, if A adsorbs only weakly, than the probability of the oxidation will be low. Likewise, if species B is adsorbed strongly, than the long time of B desorption will effectively prevent A's adsorption, again causing low oxidation rates.

As was described previously, it is the exciton formation that is primarily responsible for the photooxidation of various adsorbed species. But there is still some debate on the chemical nature of the actual species that causes photooxidation. For now it is believed that the primary oxidation species is the $OH^{\bullet}$ radical, which is the result of a reaction between a photogenerated hole and a surface hydroxyl group [17].

This was confirmed by the identification of various hydroxylated intermediates during various organics' photodegradation [154–158] by transient absorption and emission spectra as well as electron spin resonance (ESR) studies that indicate photogenerated hole trapping by OH groups present on the TiO_2 surface [159–161]. It was also discovered that photocatalytic performance is improved for anatase and rutile when the number of surface hydroxyl groups is large [155, 162, 163]. But still there is a great deal of evidence that species other than the $OH^{\bullet}$ radical may play an important or even dominant role in photocatalysis. One strong candidate that provides photocatalytic action is the superoxide radical, $O_2^{\bullet-}$, formed via a reduction of adsorbed oxygen by a photogenerated electron [164]. Again, the trapping of the electron must first take place in order to avoid recombination, since we have already mentioned that the direct reduction of surface oxygen tends to be too slow. Otherwise, oxygen is an effective trap for CB electrons, since the CB of TiO_2 is almost isoenergetic with the reduction potential of oxygen. In some cases it was even found that the photocatalytic activity was completely suppressed when oxygen was not present [47].

It is recognized that both the hydroxide radical, $OH^{\bullet}$, and the superoxide radical, $O_2^{\bullet-}$, act as photocatalysis-enabling species. A general scheme representing their action in photocatalysis is provided in Figure 12 [47].

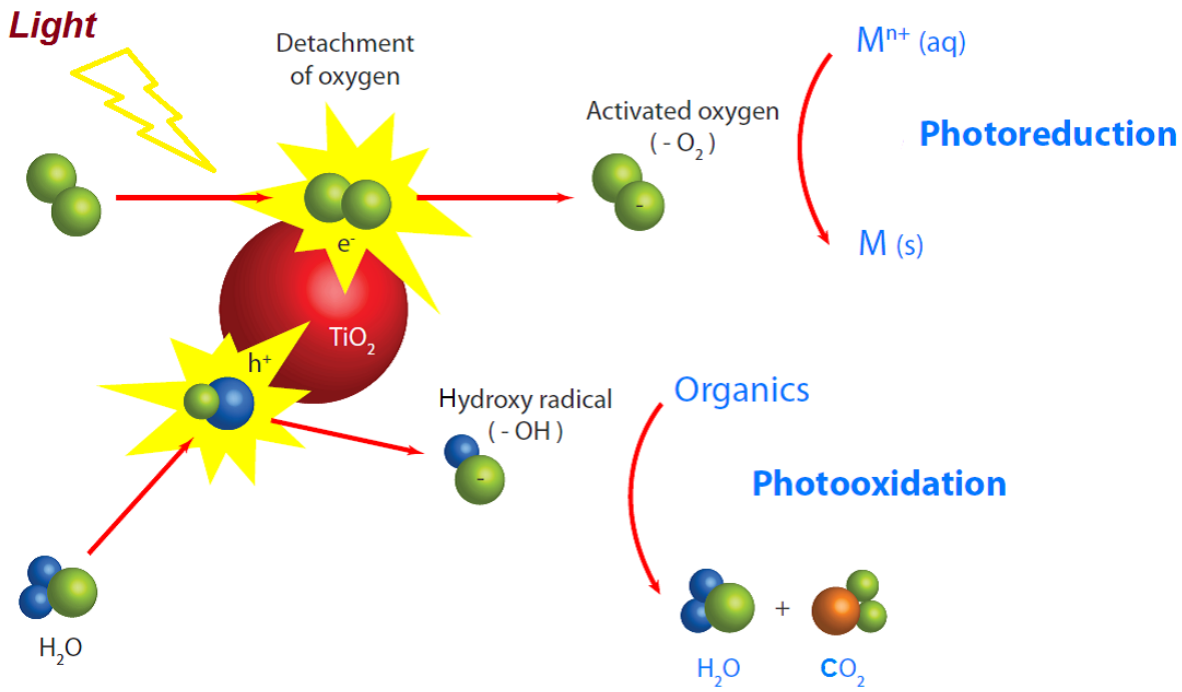

Figure 12: *A general scheme of TiO_2-mediated photocatalytic performance.* Both, the hydroxide radical, $OH^{\bullet}$, and superoxide radical, $O_2^{\bullet-}$, perform in photocatalytic reactions.

But, in order for the TiO_2 material to be as an effective photocatalyst as possible, two conditions must be met. Firstly, the reactant molecule must be adsorbed onto the surface of the catalyst effectively. Secondly, the recombination of the photogenerated holes and electrons must be inhibited so that the charge carriers are available for surface redox reactions. Therefore, the dependence of a photocatalyst's activity on its physical characteristics can be best understood in terms of how such properties influence the two critical phenomena, adsorption and charge separation.

1.4.2.1.2 The effect of crystallite size, surface area and agglomeration on the photocatalytic action

Heterogeneous photocatalysis takes place on solid particle surfaces, which makes the overall efficiency highly dependent on the total surface area available for adsorption. It is reasonable to prepare nano-TiO_2 in non-agglomerated form in which the nanoparticles have a maximum possible surface area. As was mentioned previously, some surfactant-based and acid-based synthesis methods allow the production of nanoparticles in low or even non-agglomerated form. But, producing nano-TiO_2 in non-agglomerated form is not the only goal one has to achieve in order to produce a highly photocatalytic material. Properties that influence charge separation have to be taken into account as well.

In the case of grain size, it is not entirely clear whether a decrease in crystallite size affects charge-carrier dynamics in a way that may increase or decrease the photocatalytic activity. There is some disagreement about whether the size quantization effects (effects arising from the quantum confinement of charge carriers in particles with crystallite size of less than 10 nm in diameter) would promote or inhibit exciton recombination [149]. On the one hand, the exciton charge carriers are confined to a small volume which makes the probability for recombination high because of charge close proximity [165]. On the other hand, the charge carriers can migrate more easily onto the surface and access charge-trapping sites in small particles than in larger ones [166]. What makes things even more

complicated is that site quantization in semiconductors results in an increase in the energy of the CB, which again can either decrease or increase the photocatalytic activity. Since the CB energy increases while the VB energy stays unchanged, the bandgap energy is increased with small particles compared to larger ones. Consequently, a small crystallite sized material absorbs a lesser amount of incident light, resulting in a less effective photocatalyst [165]. The increase in CB energy results in the increase of the redox potential for reactions taking place at the semiconductor surface, namely for the reduction of molecular oxygen by CB electrons. This is why there is a greater energetic driving force for at least one of the elementary reactions essential for efficient photocatalysis [167, 168].

Given the numerous competing and/or complementary effects stated above, it would be reasonable to expect that an optimum dimension (D*) should exist where the photocatalytic activity is at its maximum. Indeed, some of the D* dimensions have been identified but differ in value significantly. A D* value of 11 nm has been reported for the photodegradation of aqueous chloroform by hydrothermally prepared anatase [169]. A D* value of 5-6 nm has been reported for the gas-phase photooxidation of 1-butene over anatase nanoparticles prepared by an acid-based sol-gel reaction [168]. A D* value of 25-40 nm has been reported for phenol decomposition using TiO_2 prepared by flame pyrolysis [165]. Because of the great variations in D* values it is hard to say whether the optimal crystallite size depends more on the reaction or on the preparation method, but nevertheless it is clear that the photocatalytic activity of TiO_2 can be optimized by tuning the crystallite size, which results in the tuning of both the material surface and the electronic properties.

1.4.2.1.3 The effect of crystallinity and phase composition

It is known that in order for TiO_2 to exhibit a photocatalytic effect, it must be highly crystalline and must have no or a negligible amount of amorphous phase. A more intriguing question however is which of the TiO_2 polymorphs, rutile, anatase or brookite, is best suited for photocatalytic reactions. Most researchers consider anatase to be the best photocatalyst of the three polymorphs [17, 47, 150, 167]. But it was also shown that for specific photocatalytic reactions and under specific reaction conditions rutile can compete or even outperform anatase [149, 170–172].

Also, brookite, although seldom studied, has shown itself to be highly photocatalytic for specific aqueous redox reactions, such as the dehydrogenation of isopropanol and silver metal decomposition from silver salt solutions [173].

Clearly, it is impossible to identify a single TiO_2 polymorph that is a superior photocatalyst under all conceivable circumstances. Nevertheless, some insight regarding the advantages and disadvantages each polymorph possesses in photocatalysis can be obtained by examining the electronic, structural and surface properties of each phase.

1.4.2.1.3.1 Anatase versus rutile

Anatase and rutile have different surface, structural and electronic properties which affect their photocatalytic activity and are summarized in Table 3 [174].

Table 3: *Summary of some physical properties that influence the photocatalytic activities of anatase- and rutile-phase TiO_2.*

	Anatase	**Rutile**
Size of some commercially available particles (nm)	< 50	> 200
Bandgap energy (bulk) (eV)	3.2	3.0
Maximum excitation wavelength (nm)	385	410
Adsorptive affinity for organics	high	low
Relative hole trapping rate	10	1

An examination of individual properties listed in Table 3 reveals that there are competing contributions from various physical characteristics to the overall photocatalytic activity for anatase and rutile.

1.4.2.1.3.2 Bandgap energy

Bulk anatase has a bandgap energy, E_g, of 3.2 eV, which corresponds to an excitation wavelength λ of 385 nm. The bandgap energy of bulk rutile is slightly smaller (E_g of 3.0 eV and λ of 410 nm), which means that rutile absorbs more of the incident light because it ranges further towards visible light spectra than bulk anatase.

But, as is known for nanoparticles constituted of very small crystallites, quantization effects may become important. That is, bandgap energies change and become slightly larger than with bulk counterparts. This is also true with very small crystallites of anatase and rutile, respectively, where both exhibit a blue shift (an increase) in bandgap energies. This shift is estimated using the approximation given below [175]:

$$\Delta E_g = \frac{\hbar^2 \pi^2}{2r^2}\left\{\frac{1}{m_e}+\frac{1}{m_h}\right\} - 1.786\frac{e^2}{\varepsilon r} - 0.248E_{RY}^{*} \qquad (28)$$

ΔE_g is the bandgap shift, ħ is the Planck constant (h/2π) of 1.1 x 10^{-34} Js, r is the particle radius (m), m_e and m_h the respective masses of an electron and a hole in a photogenerated exciton, e is the elementary unit of charge (1.6 x 10^{-19} As), ε the dielectric constant of TiO_2 photocatalyst (48 for anatase and 114 for rutile) and E_{RY}^{*} the effective Rydberg energy given by:

$$E_{RY}^{*} = \frac{e^4}{2\varepsilon^2 h^2\left\{\frac{1}{m_e}+\frac{1}{m_h}\right\}} \qquad (29)$$

It has to be noted that equations 28 and 29 may only be used in case that the nanoparticles are spherical and monodisperse. With anisotropic nanoparticles or nanoporous micron sized particles, equations 28 and 29 do not provide an adequate approximation for the bandgap shift.

Although the above equations are not always found to be accurate for experimental studies, they are nevertheless qualitatively accurate in predicting bandgap shifts for spherical and monodisperse nanoparticles. These shifts are of an order of a few tenths of an eV for TiO_2 nanoparticles exhibiting quantization effects [176]. It should be noted

however that even if size quantization effects and the corresponding bandgap shifts are taken into account, rutile is still expected to have a smaller bandgap than anatase.

Therefore, on the basis of bandgap value alone it should be expected that rutile is a more efficient photocatalyst than anatase. But as was already mentioned, this is clearly not the case. It is evident that other factors play a more decisive role for the photocatalytic activity of the two phases.

1.4.2.1.3.3 Charge carrier dynamics and redox potentials

It was already noted that quantization effects not only influence the semiconductor's bandgap but also affect the energetic driving force for the reduction of surface-adsorbed oxygen by CB electrons. It was found that the anatase CB is sufficiently negative for the reduction of oxygen, whereas that of rutile is very close to the oxygen reduction potential. This means that O_2 reduction on a rutile surface may be too slow to compete effectively with exciton recombination.

This eliminates the possibility of holes participating in an oxidative process on the rutile surfaces [167]. Whether or not size quantization must be taken into account, the simultaneous and competing effects of less efficient light absorption and more energetically favorable redox potential (associated with a larger bandgap value) is important in determining the relative photocatalytic efficiency of anatase and rutile. Since anatase was experimentally shown to have a higher photocatalytic activity, it is likely that the larger redox potential arising from a bandgap increase should be more important than anatase's smaller range of UV light absorption.

Furthermore, when it comes to oxygen reduction potential, the rutile phase is less capable of efficient oxygen surface adsorption, which makes exciton recombination even more profound. This is in accordance with the fact that anatase shows a higher hole-trapping ability than rutile, which makes recombination in anatase comparably far less possible. This again helps to explain its general higher photocatalytic activity [47, 174].

1.4.2.1.3.4 Crystallite sizes and surface areas

The typical crystallite sizes and the corresponding surface properties of anatase and rutile are quite different. There are already quite a few commercial nano-TiO_2 types which are either in powder or colloid form, but in any case the average crystallite size for anatase is far less than that for rutile. One reason for this large difference in crystallite size lies in the fact that a thermodynamically stable phase is size-dependent, which makes anatase the most stable phase for crystallite sizes below 11 nm [11]. It is therefore much more difficult to prepare rutile with very small crystallite sizes. Because rutile generally consists of larger particles than anatase, the specific surface area is also usually smaller. The difference in surface area and the fact that anatase shows a higher adsorption efficiency for oxygen and organic components, could partially account for the higher photocatalytic efficiency of anatase.

It should also be noted that the photocatalytic activity is often reported on a per gram basis. It is therefore not always clear whether one TiO_2 phase performs better than the other because of surface area differences or because of some other effect related to their basic structural and electronic properties. It was found that with the degradation of aqueous 2-chlorophenyl the anatase phase was more efficient than rutile when compared on a per gram basis, but has proven to be similar in photocatalytic activity on a per surface area basis [172]. This again does not mean that anatase and rutile will exhibit comparable activities, since activity in general is dependent on both the reaction and physical properties not only on the surface area.

1.4.2.1.3.5 Mixed phase TiO_2 photocatalyst

Since the rutile phase shows a relatively poor photocatalytic activity when compared to anatase, it would be expected that the incorporation of rutile into an anatase sample would have a deleterious effect of the overall photocatalytic activity. However, numerous studies and experiments involving both commercial and research-related nano-TiO_2 have revealed that the opposite is often true. There appears to be a specific synergistic effect between anatase and rutile in a mixed-phase photocatalyst, which most certainly has to arise from the enhancement of charge separation after photo-induced exciton formation [55, 177–179]. The exact mechanism by which this charge separation occurs is on the other hand somewhat controversial. When studies were made using a commercially available P25 powder (Evonik) which is a mixture of 80 % anatase and 20 % rutile, it was postulated that photo-excitation occurs in anatase while rutile acts as an electron sink. This leaves the photogenerated VB holes free to access surface trapping sites [179]. This model is illustrated in Figure 13.

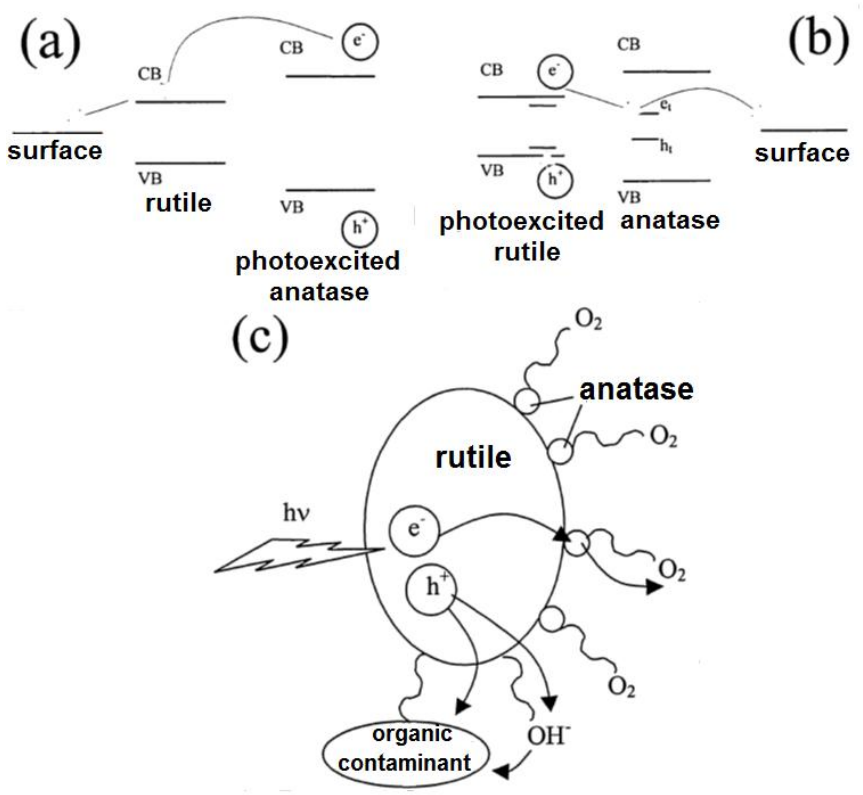

Figure 13: *A proposed mechanism for charge separation in anatase-rutile mixtures [174]*. (a) Anatase absorbs incident light while rutile serves as an electron sink. (b) – (c) Rutile absorbs incident light while anatase serves as an electron sink.

The theoretical basis for such an assumption is that the rutile CB is lower than that of anatase, which makes it energetically favorable for a photogenerated electron to migrate from anatase to rutile CB. But this explanation fails to account for the electron trapping sites either at the surface or within the anatase particle volume. These sites occupy even lower energy levels than the rutile CB and would therefore be more likely to represent possible trapping sites than an adjacent rutile particle [174]. EPR studies on the P25 material were the basis of an alternative explanation regarding rutile-anatase synergy. The EPR data indicate that once an exciton is formed in P25, electrons are transferred from the rutile CB to energetically low trapping sites in anatase. To put it in other words, photoexcitation occurs in rutile, while anatase serves as an electron sink and holes

migrate to the lattice and/or surface trapping sites in the rutile particle where the exciton was first created [174]. The holes can then directly or indirectly oxidize the adsorbed organic molecules. In parallel, the transferred electrons migrate to the anatase surface where they reduce the adsorbed oxygen or some other electron acceptor. Therefore, the presence of both anatase and rutile in P25 tends to have a twofold positive effect. One effect is that rutile, which has a smaller bandgap than anatase, absorbs light over a greater wavelength range. The second effect is that the presence of energetically favorable electron trapping sites in anatase facilitates photogenerated electron transfer from rutile to anatase, effectively inhibiting exciton recombination. However, this effect can only arise when the two phases are in close contact with one another and when rutile crystallites are small enough for the electrons to migrate across the particle volume and access an adjacent anatase particle before recombination occurs. Therefore, not every mixed-phase TiO_2 photocatalyst is superior to phase-pure TiO_2.

1.4.2.1.3.6 Morphology effect on photocatalytic activity

The study of how particle morphology and specifically, the dominant crystallographic facets in anisotropic particles affect the photocatalytic activity is a matter of discussion. Studies on a ZnO photocatalyst have indicated that the morphology may indeed enhance or reduce activity depending on the dominant crystallographic facet.

With ZnO, the photocatalytic decomposition of acetaldehyde proceeds more efficiently on the $(10\bar{1}0)$ surface than on the (0002) surface [180, 181]. Similar studies have not been done for TiO_2. However it should be noted that water adsorption theoretical studies suggest that specific crystallographic facets may be more photocatalytically active than others. This is dependent on whether a water molecule adsorbs to a surface primarily dissociatively (either as H^+ either as OH^-) or non-dissociatively (as a molecule). In particular, it is more energetically favorable for the anatase (101) surface to adsorb water non-dissociatively than dissociatively [182, 183]. The consequence of the latter surface property is that there are fewer OH^- groups available that can form photocatalytically active $OH^\bullet$ radicals. On the contrary, the anatase (001) surface is likely to adsorb water dissociatively. This suggests it is better suited for photocatalysis in which the $OH^\bullet$ radicals play a crucial role [183].

1.4.2.2 Photo-induced superhydrophilicity (PSH) – a helping hand to clean surfaces

It was recently discovered that TiO_2 may exhibit the so-called photo-induced superhydrophilicity (PSH) which was observed during water wettability experiments in which a TiO_2 layer was illuminated with UV light [184]. The surface wettability is generally evaluated by the water contact angle (CA). The CA is defined as the angle between the solid surface and the tangent line of the liquid phase at the solid-liquid-gas interface. A TiO_2 layer that is not exposed to UV light usually shows a CA of about several tens of degrees, which is mainly dependent on surface roughness. When the surface is exposed to UV light, water on the TiO_2 layer begins to show a decrease in CA and finally spreads flat across the surface [185, 186].

After some time the CA drops to almost 0 and the surface is termed superhydrophilic. After UV illumination is removed the CA begins to gradually increase, but the superhydrophilic state can be restored by exposing the surface to UV light once more. The change in CA was explained by surface changes in TiO_2 upon UV illumination that cause the formation of a metastable phase which exhibits a very low CA. The nature of

the metastable phase itself has not been fully explained yet, but it is believed that it is caused by an increase in the number of hydroxyl (OH) groups on the TiO_2 surface [187].

The main species responsible for PSH are the photogenerated holes [187]. It is possible that the photogenerated holes in TiO_2 diffuse to the surface and are trapped at lattice oxygen sites. Most of these photogenerated holes are consumed in reactions with the adsorbed organics directly, or with water molecules which results in $OH^{\bullet}$ radicals. However, a small portion of the trapped photogenerated holes may react with TiO_2 itself by breaking the bond between the lattice titanium and oxygen ion with the coordination of water at the titanium site. The coordinated water molecule releases a proton for charge compensation and consequently a new OH group forms. These OH groups are singly coordinated to the titanium ion and are believed to be less thermodynamically stable compared to doubly coordinated OH groups. Consequently, the surface energy of the TiO_2 layer covered with these less-stable OH groups is higher than that of the TiO_2 surface with its initial OH groups. The water droplet consequently spreads almost instantaneously across such a surface causing the observed CA decrease regarded as the PSH. This effect is of great importance for a possible removal of inorganic dirt and dust particles that would otherwise be unaffected by the TiO_2 photocatalytic effect.

2 Aims and Hypothesis

Titanium dioxide (TiO_2) is one of the most versatile inorganic chemicals in the world. When in nano form it exhibits various interesting chemical and physical characteristics, for example, a high photocatalytic activity and absorption of the incident UV light. This makes it ideal for many technological applications, among others for photocatalytically active coatings and the so-called dye-sensitized solar cells (DSSCs). Both applications are very interesting in the field of photovoltaics, which is one of the fastest growing industries in the world. However, the two applications require a specific nano-TiO_2 type. For photocatalytic coating a nano-TiO_2 with a high specific surface, anatase crystal structure and small non-agglomerated particles is the material of choice. The nano-TiO_2 particles may be either poly- or monocrystalline. On the other hand, with DSSCs, the nano-TiO_2 has to have a high specific surface area, anatase crystal structure and must be in the form of small monocrystalline particles.

In view of this, the primary aim and goals of the conducted research were the synthesis and processing of nano-TiO_2 material that would best suit the two applications, respectively. The synthesis and processing of the nano-TiO_2 material had to be conducted using only raw materials which emanate from the Sulphate process of pigment production set up in Cinkarna Celje, Inc. Also, the synthesis methods used should not lead to the production of powder phase materials. Therefore, any thermal treatment must be avoided, since it can lead to agglomeration, aggregation and dusting of the final material. The final nano-TiO_2 materials should be made in an optimal form and used for the two applications: the photocatalytic coatings and DSSCs.

The main hypothesis was that when using various synthesis methods, nano-TiO_2 with different physical and chemical characteristics can be formed. The synthesis methods we used were the sol-gel method, the gel-sol method and the hydrothermal method, which are all based on the synthesis reaction which takes place in an aqueous medium. These synthesis reactions differ in the nano-TiO_2 type that they produce. The final nano-TiO_2 particles may differ in morphology, particle size, crystal structure and crystallinity. This, however, may provide a great deal of possible materials that could be tested for either photocatalysis or DSSCs and consequently could enable us to experimentally determine the material of choice for a given application.

The more specific aims and goals of the conducted research were as follows:

- To develop water-based synthesis methods for nano-TiO_2 particles that could enable the production of materials that differ in morphology, particle size, crystal structure and crystallinity.
- To determine the possible crystallization and growth mechanisms for nano-TiO_2 for every specific synthesis method that was used.
- To analyse and test the final nano-TiO_2 materials and determine their most important characteristics. A special emphasis was made on the use of electron microscopy techniques. Besides analysing their basic physical properties, also the photocatalytic activity of the raw materials was measured.
- To use the specific nano-TiO_2 type and prepare a photocatalytically active coating that can be used on various substrate surfaces. The coating was used on

commercially available Si solar modules and was tested for the possibility to prolong the surface cleanliness. This would be beneficial in maintaining a higher light-to-electricity conversion efficiency.

- To use the specific nano-TiO_2 type and prepare a TiO_2 paste. The TiO_2 paste was then used to prepare the final DSSC photoanode. The photoanode is one of the main components of the DSSC and was used with other commercially available components to assemble the final DSSCs. The DSSCs were then tested for their final efficiency.

3 Materials and Methods

3.1 TiO_2 nanoparticles synthesis

3.1.1 Precursors for TiO_2 nanoparticles synthesis

The precursors used for the TiO_2 nanoparticles synthesis all originate from the established Sulphate process of the pigment TiO_2 production set-up in Cinkarna Celje, Inc. The following precursors were used: titanyl sulphate ($TiOSO_4$), metatitanic acid and sodium titanate.

Metatitanic acid is produced in the process of ‘’black-liquor’’ hydrolysis, the latter being produced by dissolution of ilmenite ore or a titanium-rich slag by concentrated sulfuric acid. The hydrolysis conditions of the black liquor lead to the production of a highly agglomerated material with the chemical formula $TiO_2 \cdot H_2O$ [18]. The metatitanic acid is crystalline and is composed of very small nanocrystalline particles with a diameter of about 5 nm [188, 189]. The crystallites have an anatase crystal structure and form nanosized aggregates that are 60 to 100 nm in size, which themselves are connected into large agglomerates a few micrometres in diameter. The aggregates are bound in the larger agglomerates by sulphate ionic bridges [188].

Titanyl sulphate ($TiOSO_4$) is the main titanium form in the black liquor solution and is readily hydrolyzed into metatitanic acid during TiO_2 pigment production. On the other hand, a chemically-wise purer form of titanyl sulphate can be produced by dissolution of the already formed metatitanic acid using concentrated sulfuric acid. The latter titanyl sulphate form was used to carry out the experiments of TiO_2 nanoparticles synthesis.

Sodium titanate is produced under specific reaction conditions using the metatitanic acid as the starting material. The chemical formulae of the sodium titanate used in our experiments are not known. Depending on the reaction medium and the reaction conditions the sodium titanate forms may differ significantly in morphology, particle size and crystal structure. In order to carry out the experiments of TiO_2 nanoparticles synthesis, different forms of sodium titanate were used.

3.1.2 TiO_2 nanoparticle synthesis methods

The TiO_2 nanoparticle synthesis was approached using ‘’wet’’ chemical methods in which the final material is produced in colloid form only. No additional thermal treatment was applied and so the nano-TiO_2 was prepared in a form defined by specific reaction parameters and the chemical nature of the precursor used.

The ‘’wet’’ chemical methods used for nanoparticle synthesis were the sol-gel synthesis, the gel-sol synthesis and the hydrothermal synthesis.

3.1.2.1 Sol-gel synthesis of TiO_2 nanoparticles

The sol-gel synthesis of TiO_2 nanoparticles was performed on a laboratory-scale reactor system of the HWS type (1 L and 10 L) equipped with stirrer CAT R100CT, Knick pH meter, thermal regulation Lauda E312 with Pt resistance thermometer, HEIDOLPH pump and automated data acquisition (temperature, pH, mixing speed). The reactor system shown in Figure 14 allowed a controlled synthesis of nanoparticulate material, since all of the main reaction parameters (pH, T, stirring speed) can be adequately monitored and set via a computer interface connection.

The sol-gel synthesis was carried out using the titanyl sulphate solution. The titanyl sulphate solution was produced in the course of pigment TiO_2 production and had a molar concentration of 2.1 M which is equivalent to about 336 g/L $TiOSO_4$. Two approaches were used to carry out the sol-gel synthesis method.

In the first approach, the titanyl sulphate solution was used as-prepared and was subjected to specific reaction conditions during which the hydrolysis and particle formation occurs. The main parameters changed during the course of the sol-gel synthesis using native titanyl sulphate solution was the dilution ratio (the amount of water added) and the reaction temperature.

The second approach was based on transforming the titanyl sulphate solution into a highly-voluminous hydrolyzate by carrying out neutralization with sodium hydroxide (4 – 17.5 M). The neutralization of titanyl sulphate at lower temperature leads to the production of the so-called ortotitanic acid (alpha titanic acid), rather than to the formation of metatitanic acid (beta titanic acid). Ortotitanic acid ($TiO_2 \cdot (H_2O)_2$ or $Ti(OH)_4$) may be prepared in amorphous form by keeping the temperature of the reaction mixture during the course of neutralization relatively low (lower than 50 ºC). The ortotitanic acid was rinsed thoroughly with deionized water in order to remove the ionic salts (sodium sulphate) produced during neutralization and other water-soluble salts that are present in the native titanyl sulphate solution. The amorphous ortotitanic acid was used to prepare a Ti (IV) aqueous solution by dissolving it in a mineral acid. Hydrochloric acid (HCl, 37 % w/w) and sulfuric acid (H_2SO_4, 98 % w/w) were used for the dissolution of ortotitanic acid, producing an acidic aqueous $TiCl_4$ solution and $Ti(SO_4)_2$ solution, respectively. It must be noted, that the chemical formula of the Ti(IV) ion compounds formed in the dissolution step are not accurately known and will rather be regarded as the most probable complex form that may form in this process. The as-prepared Ti (IV) solutions were used for the sol-gel synthesis of nano-TiO_2 by carrying out the experiments in reaction conditions at which the solutions controllably hydrolyzed and formed the final crystalline materials. The main parameter varied in the sol-gel synthesis method was the volume amount of mineral acid added to dissolve a fixed amount of ortotitanic acid. The amount of mineral acid added effectively determines the final Ti(IV) molar concentration and probably also the type of the Ti (IV) complex formed, since the molar ratio of various ligands that form the Ti ion coordination sphere differs significantly depending on the chemical composition of the reaction mixture.

Figure 14: *The reactor system set up in Cinkarna Celje laboratory used to carry out the sol-gel and gel-sol synthesis reactions.*

3.1.2.2 Gel-sol synthesis of TiO_2 nanoparticles

The gel-sol synthesis of TiO_2 nanoparticles was carried out in the same laboratory-scale reactor (Figure 14) using metatitanic acid. Two approaches were used to carry out the experiments. The first approach was based on using the metatitanic acid as the material from which nanoparticles of anatase were produced in a straightforward way via a simple ionic reaction using a barium chloride ($BaCl_2$) aqueous solution. The second approach was based on using the metatitanic acid as the precursor for sodium titanate synthesis. Sodium titanate was then used to produce the final TiO_2 nanoparticles by applying specific reaction conditions.

The first approach, the ionic reaction using barium chloride solution, can hardly be regarded a typical gel-sol reaction, since the reactions taking place are simple precipitation reactions arising due to the fact that barium ions form hardly soluble precipitates with the sulphate ion. Nevertheless, the colloid (sol) form of anatase nanoparticles is formed in this reaction starting from a highly-viscous gel (metatitanic acid), therefore making use of the term gel-sol reaction a little bit less dubious. The basis of this approach is the fact that the sulphate ions, holding the anatase aggregates tightly together in the metatitanic acid agglomerate, are removed when barium ions are added in sufficient amounts. Hence, the metatitanic acid agglomerate breaks apart, releasing the

individual anatase aggregates which due to their high zeta potential form a very stable colloid [188].

The metatitanic acid is formed during the black liquor hydrolysis under specific reaction conditions which inherently determine its final form. The reaction condition that most profoundly influences the metatitanic acid form is the amount of anatase seeds used to inoculate the black liquor [188, 189]. The anatase seeds are prepared separately by hydrolysing a 0.25 M titanyl sulphate solution at 80 ºC and are added into the black liquor prior to its hydrolysis. It is well-known that inoculation seeds exhibit various positive effects on the process of particle formation due to specific mechanisms of secondary nucleation [70]. Therefore, the quantity of anatase seeds added was varied in order to test the influence on the produced metatitanic acid type and consequently on the type of anatase nanoparticles (aggregates) produced in the following ionic reaction. The amount of anatase seeds that was added was varied through 0.1 – 1.8 % (regarding the TiO_2 content in the black liquor) in order to produce different metatitanic acid types. The various forms of metatitanic acid having a mass concentration of about 370 g/L TiO_2, were subjected to ionic reactions using barium chloride solutions with a molar concentration ranging from 0.25 to 1.4 M. It should be noted that the barium chloride molar concentration does not influence the final anatase nanoparticle properties since the latter are determined in the course of metatitanic acid preparation. The various types of anatase nanoparticles produced will be named **type A** anatase nanoparticles throughout the thesis.

The second approach is based on performing a typical gel-sol reaction using sodium titanate as the starting material, which is produced from metatitanic acid in a complex reaction. Two sodium titanate types were used, namely type ST1 and type ST2.

Type ST1 sodium titanate was provided by Cinkarna Celje and it was used without any further purification. A known amount of the precursor was poured into a beaker and then mineral acids were added drop-wise until a specific acid concentration was achieved. The reaction mixture was then heated to temperatures ranging from 50 to 100 °C and stirred slowly for 3 hours. The final product was an aqueous suspension of nanoparticles.

To investigate the effect of temperature on the end product characteristics we carried out the synthesis reactions varying only the temperature of the reaction medium while keeping all other parameters constant (hydrochloric acid concentration 70 g/L, TiO_2 precursor concentration 120 g/L). The temperatures used during the synthesis reactions ranged from 50 to 100 °C.

We investigated the effect of supersaturation by changing the amount of the precursor in the reaction while keeping all the others constant (hydrochloric acid concentration 70 g/L, reaction temperature 80 °C). The precursor concentration was varied between 60 and 180 g/L (calculated as TiO_2).

Most of the experiments were carried out using hydrochloric acid in order to determine its effect on the produced TiO_2 nanoparticles. We prepared different samples varying the hydrochloric acid concentration while keeping other parameters constant (temperature at 80 °C, TiO_2 precursor concentration at 120 g/L). The hydrochloric acid concentrations were set at 40 g/L (1.1. M), 50 g/L (1.35 M), 60 g/L (1.64 M), 70 g/L (1.91 M), 100 g/L (2.7 M), 130 g/L (3.5 M) and 160 g/L (4.4 M).

Also, experiments were carried out using nitric and sulfuric acid instead of hydrochloric acid. Other reaction parameters were kept the same (80 °C, precursor concentration of 120 g/L), only the acid concentration was varied and was set at 70 g/L and 130 g/L with nitric acid which equals 1.15 and 2.1 M, respectively. The sulfuric acid concentration was varied and was set to 50 g/L and 100 g/L, which equals about 0.5 M and 1 M, respectively.

The gel-sol-derived TiO_2 nanoparticles using type ST1 sodium titanate will be named **type B1** nanoparticles throughout the thesis.

Type ST2 sodium titanate was also provided by Cinkarna Celje and it was used without any further purification. Based on the experience gained with the gel-sol reaction using ST1 sodium titanate, the reactions were performed using the hydrochloric acid (HCl, 37 % w/w) and sulfuric acid (98 % w/w). The HCl acid concentration was varied and ranged from 20 to 150 g/L, which equals 0.55 to 4.1 M, respectively. The sulfuric acid concentration was varied and was set to 50 g/L and 100 g/L, which equals about 0.5 M and 1 M, respectively. The TiO_2 concentration was also varied and ranged from 60 to 180 g/L. A known amount of the precursor was poured into a beaker and then HCl was added drop-wise until a specific concentration was achieved. The reaction mixture was then heated to a temperature ranging from 50 to 100 °C and stirred slowly for 3 hours. The final product was an aqueous suspension of nanoparticles showing good dispersion and a bluish haze. The gel-sol derived TiO_2 nanoparticles using type ST2 sodium titanate will be named **type B2** nanoparticles throughout the thesis.

3.1.2.3 Hydrothermal synthesis of TiO_2 nanoparticles

The hydrothermal synthesis was carried out using a laboratory-scale autoclave to produce a highly crystalline nanoparticulate TiO_2 material. The starting material for the hydrothermal synthesis (HTS) was an acidic suspension of TiO_2 nanoparticles (250 g/L) that was, prior to HTS, stabilised with a dispersant (sodium polyfosfate, $Na_5P_3O_{10}$) and neutralised with a NaOH solution (17.5 M) to the pH value ranging from 7 – 11. Stabilization using a dispersing agent was crucial in order to avoid nanoparticle agglomeration during neutralization. This sustains the high specific surface area of the precursor material which is important so it's dissolution in the HTS process is carried out relatively fast. The TiO_2 concentration prior to performing the HTS was varied from 50 – 400 g/L. The parameters of HTS were also varied, namely the temperature ranged from 180 – 240 ºC and the reaction time from 3 – 24 h. The filling volume of the Teflon liner was about 50% which correspond to pressures of about 12 bar at 180 °C and 20 bar at 240 °C. The heating to the desired temperature was done by placing the laboratory autoclave (similar so the one in Figure 6) in an oven that was set to the specific temperature at which the hydrothermal reaction took place. The as-prepared TiO_2 nanoparticles will be named **type C** nanoparticles throughout the thesis.

3.2 Si solar module testing and manufacture of photocatalytic layer

The preparation of a TiO_2 layer on glass was carried out at the University of Nova Gorica (UNG). In order to prepare a stable suspension used for the final coating application that exhibits good adhesion, mechanical stability and also super-hydrophilicity, a soft chemical method was employed. The TiO_2 nanoparticles were used in the form of an acidic suspension that was prepared as described above. To the acidic anatase suspension (5 mL), water (40 mL), ethanol (Fluka) (40 mL) and a silica binder solution (400 μL) (made from either of the two silica sources, i.e., colloidal silica Levasil (200/30%) and TEOS precursor) was added and stirred until a homogenous mixture formed [190]. The molar ratio of Ti to Si in the final suspension is 1.3:1. The as-prepared suspension is very stable and remains so for a period of about six months. The as-prepared suspension was used to prepare self-cleaning coatings using various techniques, such as spraying and dip

coating onto various substrates. No thermal treatment of the resulting coatings at elevated temperatures was required.

The as-prepared coating was also applied onto commercially available Si solar modules (Bisol, Slovenia). The Si solar modules were tested for their light-to-electricity conversion efficiency and the coated module was compared in efficiency to an uncoated module to determine the effect of the TiO_2 coating on the short- and long-term electricity production efficiency.

3.3 DSSC paste preparation and DSSC cell assembly

The TiO_2 pastes were prepared using the sol-gel Pechini method [146]. The basis of the Pechini method is the preparation of a polyester which is formed in a reaction between citric acid, ethylene glycol and a titanium metal alkoxide (most often titanium isopropoxide, TTIP). Polyester was formed by heating the ethylene glycol (Riedel-de-Haen) to about 60 ºC and then adding titanium isopropoxide (Sigma Aldrich). The mixture is stirred and then citric acid (Fluka) is added. The mixture is heated to 90 ºC and stirred until a clear solution forms. This is the polyester that is used for TiO_2 paste preparation. The composition of the polyester was varied. The molar concentrations of metal alkoxide : citric acid : ethylene glycol was 0.5 – 1.5x : 5x : 20x, where X represents a chosen molar amount of any of the components. The variation of the polyester composition was done to determine the influence on the final DSSC efficiency. The variation in metal alkoxide molar ratio is necessary since the amount depends on the specific surface area of the TiO_2 nanoparticles added to the final polyester. Since various TiO_2 nanoparticle types were produced, the variation in polyester composition pin-pointed the appropriate polyester type that gave the best possible efficiencies for the final DSSC.

Since TiO_2 nanoparticles are in the form of a water suspension a small amount of an organic acid (acetic acid) was additionally added to the polyester. The organic acid plays a two-fold role. Firstly, it prevents metal alkoxide hydrolysis, which would otherwise occur because of the presence of water in TiO_2 suspensions. Secondly, the organic acid is also a dispersing agent that changes the surface properties of TiO_2.

Because metal alkoxide hydrolysis must be avoided during paste preparation, a possible substitution compound was also tested. A possible substitute compound that was tried out instead of TTIP was the titanyl sulphate solution. The titanyl sulphate solution was added in the same Ti (IV) molar ratio as was the TTIP.

After polyester formation the final TiO_2 paste was prepared by adding TiO_2 nanoparticles in suspension form. Also P25 TiO_2 (Evonik, Germany) in powder form was used for paste preparation, since P25 is well suited for DSSCs and gives an appreciably good efficiency. P25 was therefore used as a reference material in order to determine the suitability of the synthesized TiO_2 nanoparticles for DSSC application. The molar ratio of the metal alkoxide/titanyl sulphate and TiO_2 nanoparticles added was preferentially 1:7. The paste was mixed in a mortar grinder (RM 200, Retsch, Germany) for a period of about 2 h.

After TiO_2 paste preparation, photoanodes and final DSSCs were made. The task was carried out in Cinkarna Celje, Inc. using commercially available compounds used for DSSC cell assembly. All of the commercially available components were purchased at Solaronix (Switzerland):

- The substrate used for photoanode preparation was TCO30-8, which is a 3-mm-thick sodame glass coated on one side with a fluorine doped tin oxide

(SnO_2:F) layer ("FTO" glass). The sheet resistance of the FTO layer is ~8 ohm/square and its transmission is > 65 % from 500 to 1000 nm.

- The counter electrode was prepared using Platisol T, which is an alcohol-based paint containing a chemical platinum precursor. It is intended for the deposition of a platinum layer by painting with a brush or it may also be sprayed to obtain a suitable platinum coating. After firing at 450°C for 10 minutes, a quasi-transparent activated platinum layer is obtained with Platisol T. Such a layer is suitable for reducing overpotentials of the iodide/tri-iodide redox couple.
- The sensitizer used was the Ruthenizer 535, which sensitizes very efficiently wide band-gap oxide semiconductors, like titanium dioxide, up to a wavelength of 750 nm. Ruthenizer 535 is also known as N3 is the literature, and has been so far one of the most efficient sensitizers in DSSCs.
- The electrolyte used was of the iodide/tri-iodide series, namely either Iodolyte PN-50, which is a low viscosity electrolyte with 50 mM of tri-iodide in propionitrile, or Iodolyte Z-50 Iodide, which is a low viscosity electrolyte with 50 mM of tri-iodide in 3-methoxypropionitrile. The PN-50 electrolyte is intended for high-performance cells, while the Z-50 electrolyte is intended for high-performance and temperature-stable cells.

The TiO_2 photoanode was prepared by the deposition of the TiO_2 paste using the so-called doctor-blade technique (Figure 15). A hard squeegee is used, or doctor-blade, to spread a portion of titania paste onto the substrate. With this technique, the thickness of the titania layer is determined by the thickness of a spacer placed on both sides.

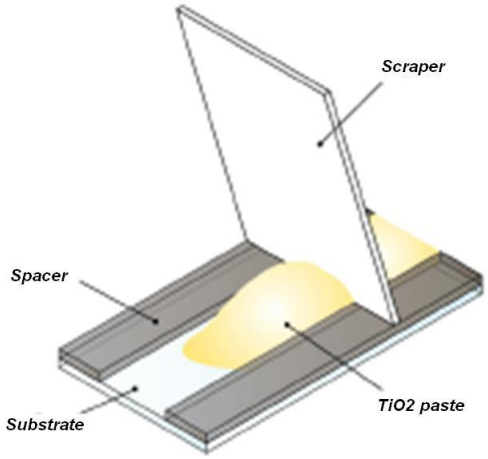

Figure 15: *A scheme of the doctor-blade technique.* The doctor-blade technique was used to spread the TiO_2 paste onto the TCO glass substrate evenly.

Thermal treatment of the paste deposited on TCO glass took place at a temperature up to 450 ^{0}C (high temperature sintering) for a period of about 45 min. The working electrode for DSSC was stained in a sensitizer solution of commercially available dye (Ruthenizer 535 – known also as N3 dye). Staining was carried out by soaking the electrode in an alcohol solution of synthetic dye with a concentration of ~ $3 \cdot 10^{-4}$ g/l for 10 hours. The procedure could be accelerated when heating the sensitizer solution to ~ 80 ^{0}C for 2 hours.

The same substrate with a deposited Pt catalyst was used for the counter electrode. The electrodes were sealed with a sealing film, which serves as a mechanical connection as well as the spacer. Through two previously drilled holes in the counter electrode the electrolyte was filled and the holes were subsequently sealed. Due to better contact and in order to facilitate the implementation of measurements, silver paint was applied on the side contacts of the two electrodes.

3.4 Characterization

The synthesized TiO_2 nanoparticles were analysed using various analytical techniques. For the majority of applied analytical methods (SEM, TEM, photocatalysis measurement,…) the suspension was used as-prepared or was washed. In order to remove the soluble ionic species present in the TiO_2 suspensions, centrifugation was used. The centrifugation of the suspension resulted in the formation of a ‘’cake’’ and supernatant, which was removed by decantation. The ‘’cake’’ was than readily re-dispersed to form the final TiO_2 suspension containing far less of the impurities than the initial suspension.

3.4.1 X-ray powder diffraction

For X-ray powder diffraction (XRD) investigations the suspensions were neutralized after the reaction, filtered, washed with distilled water and dried at 80 °C in order to acquire TiO_2 powder that was used for characterization. The TiO_2 powder was pressed into a pellet and the spectra recorded from 10° to 70° (2-theta angle) with a CuK_α radiation (λ=1.5418 Å) using a CubiX PRO PW 3800 instrument (PANanalytical). The TiO_2 crystal structure was identified using the X’Pert Data Viewer software.

3.4.2 Scanning electron microscopy

Scanning electron microscopy (SEM) was used to determine the basic nanoparticle characteristics, namely particle size, morphology and chemical composition and was also used to analyse the final TiO_2 films as-prepared for DSSCs and photocatalytically active layers.

The TiO_2 nanoparticles were prepared by drying TiO_2 nanoparticle suspension droplets on an adhesive carbon conductive tape. No additional conductive coating was applied. The TiO_2 nanoparticles were analysed using a scanning electron microscope (JEOL JSM-7600 F, Jeol Ltd, Tokyo, Japan) with an in-lens thermal field-emission gun (FEG) equipped with detectors for secondary electrons (SE), backscattered electrons (BSE), energy-dispersive X-ray spectroscopy (EDXS) (X-MAX, Oxford Instruments, Oxfordshire, UK), wave-length-dispersive X-ray spectroscopy (WDXS) (INCA Wave, Oxford Instruments, Oxfordshire, UK), electron backscatter diffraction (EBSD) (EBSD Channel 5, Oxford Instruments, Oxfordshire, UK) and electron lithography (XENOS Semiconductor Technologies GmbH, Kusterdingen, Germany). Electron micrographs were obtained using the in-lens detector at an accelerating voltage of 5 kV and a working distance of 3 mm.

The TiO_2 nanoparticles were also analysed using a scanning electron microscope (Sigma VP, Zeiss, Oberkochen, Germany) with an in-lens thermal field-emission gun (FEG) equipped with detectors for secondary electrons (SE), backscattered electrons (BSE), energy-dispersive X-ray spectroscopy (EDXS) (Oxford Microanalysis System Inca Energy, Oxford Instruments Nanoanalysis, Bucks, England) and a scanning transmission electron microscopy (STEM) (Multimode STEM Detection System, Zeiss, Oberkochen, Germany) detector. Electron micrographs were obtained using the in-lens detector at an accelerating voltage of 2 kV and a working distance of between 2 and 4 mm.

The TiO_2 photoanodes and the photocatalytically active TiO_2 layers were analysed exclusively with the Sigma VP scanning electron microscope. The samples were analysed as final layers on glass substrates or were analysed by first mechanically removing a small portion of the layer with a spatula and transferring the removed material onto the conductive carbon tape. No additional conductive coating was applied. We determined the TiO_2 layer porosity, layer thickness and the occurrence of possible mechanical cracking for the final TiO_2 layers.

3.4.3 Transmission electron microscopy

Transmission electron microscopy (TEM) was used to determine the basic nanoparticle characteristics, namely particle size, morphology and chemical composition and also their crystallinity.

The samples for TEM analysis were prepared by dropping a TiO_2 aqueous suspension onto lacey, carbon-coated nickel grids. The TiO_2 nanoparticles were analysed using a transmission electron microscope (JEOL JEM-2100, Jeol Ltd., Tokyo, Japan) with a LaB_6 filament operating at 200 kV and equipped with an EDXS detector (JED 2300T Jeol Ltd., Tokyo, Japan) and a CCD camera (Orius DC 1000, Gatan Inc., Pleasanton, USA).

3.4.4 Dynamic light scattering measurements

The nanoparticle size and agglomeration state were determined using Dynamic light scattering (DLS) measurements (Zeta PALS, Brookhaven, US). The samples for DLS measurement were made by dispersing a single TiO_2 suspension droplet into 50 mL of distilled water. The final sample was translucent. The sample was poured into a plastic vessel (10 mL) which was transferred to the instrument cell where it was analysed at a fixed angle of 90° using a laser with a wavelength of 660 nm.

3.4.5 Zeta potential measurements

The zeta potential of TiO_2 nanoparticles was determined with a Zeta PALS (Brookhaven). The samples for the zeta potential measurements were prepared by dispersing a single TiO_2 suspension droplet into 50 mL of distilled water and mixing it to form a translucent suspension. The electrophoretic mobility was converted to zeta potential using a PALS Zeta Potential Analyzer software and was based on the Smoluchowski approximation.

3.4.6 Inductively coupled plasma atomic emission spectroscopy analysis (ICP-AES)

The chemical composition of the TiO_2 nanoparticles and precursor materials was determined using Inductively Coupled Plasma Atomic (Optical) Emission Spectrometer (ICP-AES Vista AX Pro, Agilent Technologies, Santa Clara, US) and was performed in the analytical laboratory of Cinkarna Celje, Inc. The emitted spectral lines were analysed in the EM range from 168 to 785 nm by the CCD (Charge Couple Device).

3.4.7 Photocatalytic activity measurements of TiO_2 nanoparticles and coatings

The photocatalytic activity of the synthesized TiO_2 nanoparticles and of the final coatings was performed using three different methods:

- The contact-angle method. The TiO_2 suspension was used to prepare a nanoparticle layer. This was done by dip-coating microscope glass slides (76x26 mm, Menzel-Gläser) into a TiO_2 suspension (100 g/L) (dipping speed of 70 or 100 mm/min) or into the final photocatalytically active coating. Dip-coating of the microscope glass slides was performed only once. The layers were used as-prepared or were additionally thermally treated (400 – 450 ºC, 30 min) in order to achieve better adhesion onto the glass substrate and also to improve the crystallinity of the nanoparticles. Methyl stearate (p.a., Fluka) (0.2 M solution in hexane) was used as a test organic pollutant and was added onto the TiO_2 layers using dip coating (100 mm/min). After the addition of the methyl stearate the contact angle was measured, while the layers were illuminated with UVA (CLEO light source, 20 W, 438 mm x 26 mm, λ 355 nm, Philips). The contact-angle method was carried out at the University of Nova Gorica (UNG).
- Photocatalytic measurement based on the deposition of a UV and visible light transparent solid layer of a sodium salt of terephthalic acid (TPA) onto the TiO_2 surface [191, 192]. The deposition of the TPA was done by dip-coating, as described above. When such a system is irradiated, the organic layer decomposes forming hydroxyterephthalic acid (HTPA), which is highly fluorescent and can easily be detected using HPLC-FLD or spectrofluorimeter. This method gives a quantitative result of TiO_2 photocatalytic action and was carried out at the University of Nova Gorica (UNG).
- Decomposition of the resazurin dye. This is a simple qualitative test to determine the photocatalytic activity based on the decomposition of the resazurin dye. The decomposition of the resazurin dye may be perceived by the change in colour from blue to colourless. The resazurin dye decomposition method was carried out at the University of Nova Gorica (UNG).

3.4.8 Measurement of Si modules output

The testing of the Si modules was carried out after setting up the testing instrumentation in Cinkarna Celje, Inc. and is illustrated in Figure 16.

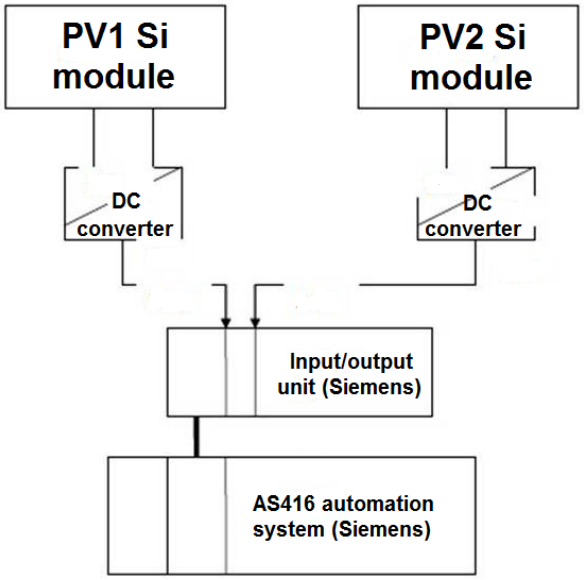

Figure 16: *Testing instrumentation scheme used to determine the difference in light-to-electricity conversion efficiency for PV Si modules (Bisol).*

Both PV modules were polycrystalline Si types provided by Bisol (Slovenia). Every module has a surface area of about 2 m^2, which produces around 245 W. Each module provides 4.5 – 5 A of electrical current and 12 – 50 V of electrical voltage (open circuit). These module characteristics correspond to a 12.5 % efficiency, as declared by the producer (Bisol). Each Si module was connected to two 60 W light bulbs. The produced electrical current was monitored on the basis of the set-up system which converted the PV module signal (electrical current in Amps; 0 A – 10 A) into a standard electrical current signal with values ranging from 4 – 20 mA. The signal was then directed into an analogue input module which transformed the analogue data into digital data (32-bit transformation). The final signal could then be monitored on-line on the computer screen. The electrical current produced by the PV module is based on the following calculation:

$$I[A] = \frac{10A}{16mA \cdot (I[mA] - 4mA)} \qquad (30)$$

I [A] is the current produced by the Si module and I [mA] the current signal as seen on the computer screen.

3.4.9 I-V measurements of DSSC cells

The I–V characteristics of DSSCs cells (Isc, Voc, FF and efficiency) were obtained with the aid of an Oriel class AAA solar simulator model 94023A (2’’x2’’ beam size) (Newport, US).

The tested DSSC cells were illuminated with artificial light (1 sun equivalent, Newport solar simulator, 1000 W/m^2 at room temperature). The Newport solar simulator will be set to AM 1.5 conditions after calibration of the DSSC, using a calibrated reference silicon solar cell. The relaxation time of the devices after processing and before measuring was set to 1 h.

4 Results and Discussion

4.1 Nanoparticle synthesis

4.1.1 Sol-gel synthesis of TiO_2 nanoparticles

The sol-gel synthesis of TiO_2 nanoparticles was carried out using a titanyl sulphate ($TiOSO_4$) solution, which is readily made in Cinkarna Celje, Inc. for the purposes of pigment production. Titanyl sulphate is a water-soluble form of titanium and is thus ideal for the sol-gel synthesis approach, which is based on various complex reactions that begin and proceed on a molecular level.

The appropriate molecular precursor in this case is a specific titanium complex, where the coordination sphere of the central titanium ion is surrounded by various ligands. Because titanyl sulphate forms an acidic solution it would be reasonable to assume that the ligands present are mostly sulphate ligands and water molecules (the hydrolysis reactions are hindered significantly by the acidic environment). Especially the first are important, since it was already mentioned that the sulphate ions promote polycondensation reactions towards the production of particles with an anatase crystal structure [14, 15].

The synthesis reactions where titanyl sulphate was used as the starting material were carried out by varying either the reaction temperature or titanyl sulphate concentration. Both parameters were varied according to the standard theory of nucleation, which states that the precursor concentration and the reaction temperature determine the level of supersaturation and thus the particle size [20, 193]. The standard nucleation theory states that the reduction of the overall Gibbs free energy (ΔG) of the solution is the driving force for the nucleation and growth of the final particle. The change of free energy per unit volume of the solid phase is dependent on the solute concentration:

$$\Delta G_v = -\frac{kT}{\Omega}\ln(c/c_0) = -\frac{kT}{\Omega}\ln(1+\sigma) \tag{31}$$

The parameter k is the Boltzmann constant ($1.38 \cdot 10^{-23}$ J/K), T the absolute temperature (K), Ω the atomic volume, σ the supersaturation, defined as $(c-c_0)/c$ where c is the solute concentration and c_0 its solubility.

With nanoparticle synthesis starting from a supersaturated solution, homogenous nucleation occurs and the particles formed are limited in size with the degree of supersaturation. The bigger the supersaturation, the smaller and more numerous the particles are. The lower limit of nanoparticle size in a supersaturated system governed by homogenous nucleation is given as:

$$\Delta G = \Delta\mu_v + \Delta\mu_s = \frac{4}{3}\pi r^3 \Delta G_v + 4\pi r^2 \gamma \quad (32)$$

$$d\Delta G / dr = 0 \quad (33)$$

$$r^* = -2\frac{\gamma}{\Delta G_v} \quad (34)$$

The parameter $\Delta\mu_v$ is the reduction in the molar free Gibbs energy ascribed to the formation of a solid phase, while $\Delta\mu_s$ is the increase in the Gibbs free energy due to the formation of a solid phase. The parameter γ is the surface energy per unit area and ΔG is the total change in the Gibbs free energy upon nucleus formation.

It has to be noted that equations 32 – 34 are based on a simplified model of nucleus formation. If the nuclei concentration is too great, if the nuclei form in a matrix with a limited space for the growing particles or if there are some other interferences in the medium, the underlying mechanisms of particle formation change. Consequently also the equations that describe the thermodynamics of nuclei formation and growth differ significantly [194].

Temperature influences the particle nucleation and the final particle size by determining the solute solubility at a given temperature. By lowering the temperature, the solubility drops and consequently the supersaturation increases, leading to the formation of more nuclei and consequently to a greater number of smaller particles. Also, the temperature influences the surface tension and the overall surface energy of the system, which again may considerably influence the final nanoparticle size.

Based on the above provided theory of nucleation it was assumed that by controlling the solute ($TiOSO_4$) concentration and the reaction temperature, it would be relatively easy to synthesize anatase nanoparticles with a predefined particle size. However, all of the experiments performed have shown that little or no control could be achieved over the final particle size, as would be expected according to the standard nucleation theory [195]. Very little variation in material properties was observed when the solute concentration was changed considerably and the final material was generally always in the order of a few 100 nm in size with a poorly defined morphology. Still, the XRD analysis confirmed that the material has an anatase crystal structure. A typical product is shown in Figure 17.

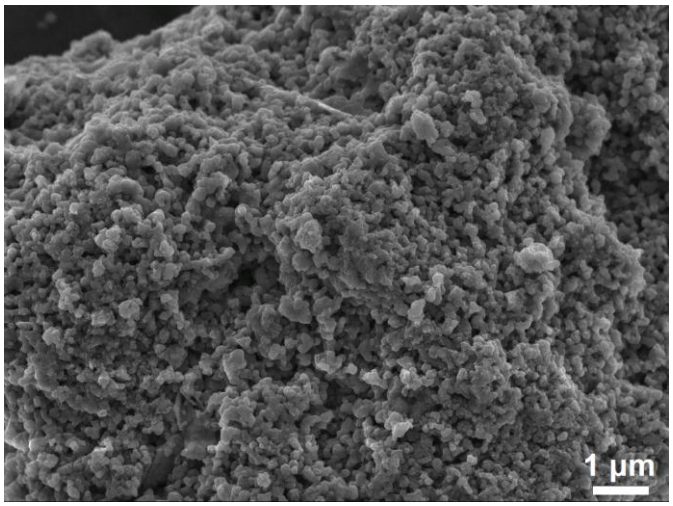

Figure 17: *Sol-gel synthesized TiO_2 particles prepared by using titanyl sulphate solution as the starting material.* The sol-gel synthesis of TiO_2 particles was carried out using a native titanyl sulphate solution of varying concentrations and hydrolyzing it at elevated temperatures.

The observed morphology and the particle size of the synthesized anatase could result because a native titanyl sulphate solution was used which not only contains a high amount of free sulfuric acid, but also various other elements in ionic form. The typical titanyl sulphate composition used in our experiments is given in Table 4.

Table 4: *The chemical composition of titanyl sulphate solution as produced in Cinkarna Celje*. The ICP-AES analysis of titanyl sulphate solutions shows considerable chemical diversity and heterogeneous composition.

parameter	**ICP-AES** λ (nm)	unit	**$TiOSO_4$ (April 2009)**	**$TiOSO_4$ Sept. 2009)**	**$TiOSO_4$ (Nov. 2009)**
SO_4	182.040	g/l	**325.3**	**332.6**	**327.3**
Ti		g/l	**68.09**	**62.47**	**62.6**
Al	167.080	mg/l	3	1	4
Ba	455.403	mg/l	< 1	< 1	< 1
Ca	393.366	mg/l	35	35	37
Co	238.892	mg/l	1	2	1
Cr	283.563	mg/l	< 1	< 1	< 1
Cu	324.754	mg/l	4	4	1
K	766.491	mg/l	10	9	9
Mg	279.553	mg/l	7	8	9
Mn	257.610	mg/l	< 1	< 1	< 1
Na	589.592	mg/l	< 1	< 1	< 1
Ni	231.604	mg/l	< 1	< 1	< 1
Pb	220.353	mg/l	< 1	< 1	< 1
Si	251.611	mg/l	6	7	11
Zn	213.856	mg/l	< 1	< 1	< 1

The highly versatile composition of titanyl sulphate solution and consequently a large solution ionic strength are not favorable for a controllable nano-TiO_2 synthesis. Therefore, we used another approach, namely the formation of ortotitanic acid by way of titanyl sulphate solution neutralization.

The neutralization was carried out using a sodium hydroxide solution (4 – 17.5 M), while titanyl sulphate solution was used in diluted form in order to prevent too intensive heating arising from neutralization enthalpy. When the titanyl sulphate solution was diluted by a ratio 1:4, the temperature during neutralization never rose over 40 ºC which is important since higher temperatures lead to crystallization of the product formed. This is why it was easy to produce an amorphous type ortotitanic acid below this temperature range. The amorphous type of the ortotitanic acid ($TiO_2 \cdot (H_2O)_2$ or $Ti(OH)_4$) may readily be dissolved in mineral acids. But before dissolution, the ortotitanic acid was washed and rinsed considerably with deionized water in order to remove the water-soluble ionic salts. The quality of ion removal was tested using a qualitative test, namely, adding a barium chloride solution drop-wise to the filtrate and observing if any precipitate forms. The latter could form when the sulphate ion is present at a considerable concentration. The washing of the ortotitanic acid was continued until the precipitate test gave a negative result.

At first, only sulfuric acid was used to dissolve the ortotitanic acid. The ortotitanic acid was dissolved with concentrated sulfuric acid (98 % w/w) so as to set-up a final H_2SO_4 concentration between 1 – 3 M and the final Ti (IV) ion concentration from 0.25 – 1 M. Also, the reaction temperature was varied in order to provide a mechanism of control over supersaturation and consequently over the final particle size.

Nevertheless, the final material produced, lacked both the targeted nano size and particle morphology. A typical anatase material synthesized using the described approach is shown in Figure 18.

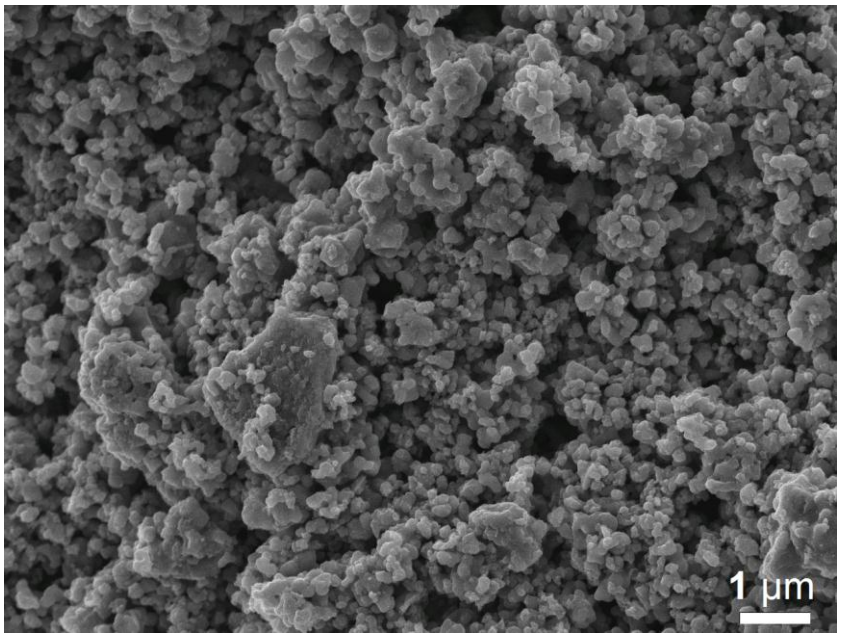

Figure 18: *Sol-gel synthesized TiO_2 particles prepared by using ortotitanic acid as the starting material.* The sol-gel synthesis of TiO_2 particles was carried out using ortotitanic acid derived by neutralizing the native titanyl sulphate solution. The ortotitanic acid was dissolved in sulfuric acid and had variable Ti(IV) concentrations. The solutions were hydrolyzed at elevated temperatures resulting in TiO_2 particle formation.

As seen from Figure 18, the particles exhibit a wide size distribution and are of submicron size at best. It was concluded that the approach using sulfuric acid to dissolve the ortotitanic acid lacks control over the particles' properties and is therefore not suitable for producing nanosized anatase. The inability to produce nanosized anatase is attributed to the sulphate ion, which encourages the growth of anatase particles in a way that greatly reduces the porosity of the final product as was observed in other studies as well [63].

Since sulfuric acid was proved to be inappropriate for the purpose of synthesizing nanosized anatase; hydrochloric acid (37 % w/w) was used instead. The hydrochloric acid was used to dissolve the ortotitanic acid. It is appropriate to assume that a specific Ti (IV) complex forms, whose form is decisive for the formation of the final TiO_2 polymorph. As was already pointed out, the acid concentration in the final solution is crucial since in order to produce a phase-pure product only one complex type should be present [61].

Therefore, the acid concentration was varied between 1 M and 4 M in the final precursor solution, while the Ti (IV) concentration varied from 0.3 to 1.6 M, the latter being the upper concentration limit due to the high voluminosity of the ortotitanic acid. The temperature of the reaction was held constant at 80 ºC. It is assumed that a $TiCl_4$ solution forms upon ortotitanic acid dissolution in HCl [15].

The XRD diffractograms of the formed products differ significantly. Namely, when the sol-gel reactions were performed at lower acid concentrations, a mixed-phase product of anatase and rutile was formed. Increasing the acid concentration increased the rutile/anatase formation ratio. This was already observed and was attributed to the fact that the molar ratio between the protons and the titanium ion ($[H^+]/[Ti^{4+}]$) promotes the formation of the rutile form when increased [59]. This is in agreement with other

experimental results, which showed that protons promote rutile polymorph formation [56–60]. Protons alone do not provide the sole parameter for the type of material that is produced. Based on our experiments, it is clear that chloride anions play a crucial role during the sol-gel reaction. This is a direct result of their ability to act as ligands. The chloride ions are present in the coordination sphere of the Ti (IV) ion. It is appropriate to assume that a Ti (IV) complex of a type $[Ti(OH)Cl_3(OH_2)_2]^0$ may form, which is known to be the starting precursor in rutile particle formation [64]. The complex could react via polycondensation reactions to produce a particle with the rutile crystal structure as presented in Figure 19.

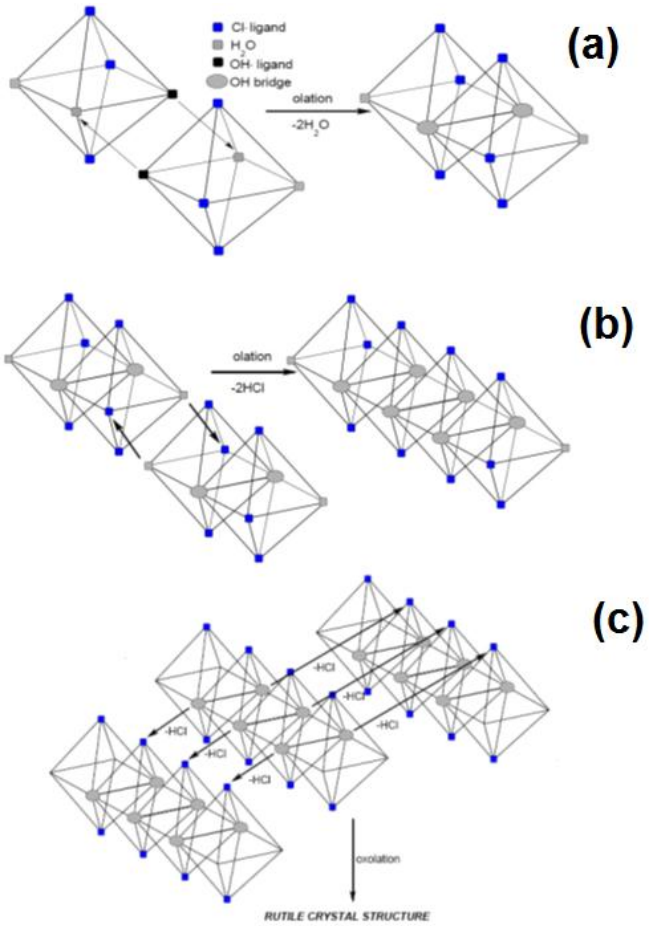

Figure 19: *The formation of TiO_2 particles with the rutile crystal structure starting from the $[Ti(OH)Cl_3(OH_2)_2]^0$ complex.*

The complex $[Ti(OH)Cl_3(OH_2)_2]^0$ may polycondense into final TiO_2 particles as follows:

(a) The initial reaction is olation, which results in the formation of a complex dimer. The olation is crucial and must take place first, since it results in the elimination of water molecules from the coordination sphere of the starting complex.

(b) The complex dimer reacts via olation reactions and forms longer linear chains that are characteristic for rutile crystal structure. Again, it is presumed that water molecules are eliminated from the coordination sphere of the central Ti (IV) ion. OH bridges form and link the dimers together.

(c) The linear chains react via oxolation resulting in the formation of nuclei/particles having the rutile crystal structure. Oxolation leads to the formation of M-O-M oxide bridges.

If the complex precursor would be significantly different than $[Ti(OH)Cl_3(OH_2)_2]^0$, the polycondensation reactions could lead to a different arrangement of the TiO_6 octahedra, forming a product with another crystal structure. It is therefore quite clear that the sol-gel approach may provide a way to produce phase-pure products, but strictly when the reaction parameters and the solution chemical composition are appropriately met. Our experiments show that rutile particles form when the HCl acid concentration is above 3 M and are in agreement with the reported results [59]. In view of this we conclude that the mechanism of formation of the final product is dependent on HCl concentration used to carry out the synthesis reaction.

TEM analysis was used to investigate the particle size and morphology, when the sol-gel synthesis was carried out in a way to produce pure rutile only. The TEM images of the particles produced are shown in Figure 20.

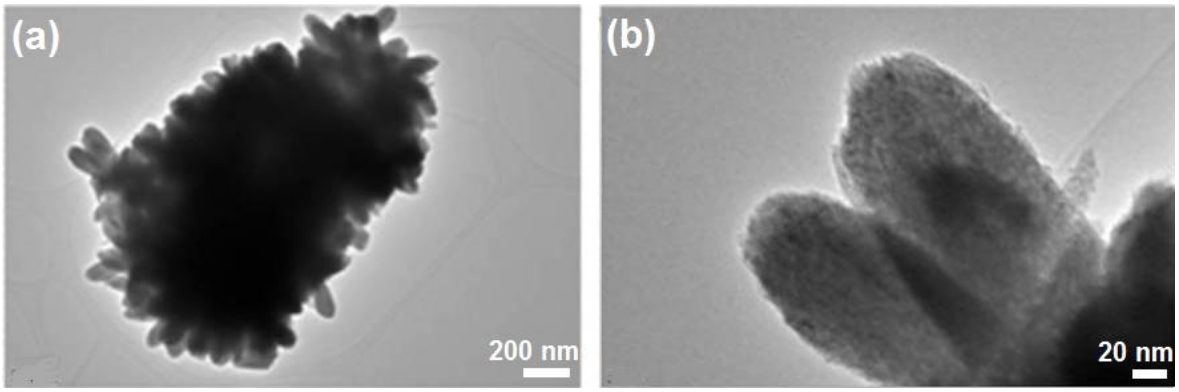

Figure 20: *TEM images of rutile particles produced by the sol-gel synthesis using ortotitanic acid as the starting material.* (a) A large agglomerate of rutile particles. (b) A higher magnification image of rutile particles.

As can be seen from Figure 20 the rutile material produced is an agglomerate which could not be dispersed into individual particles. Also, the particles that constitute the agglomerate in Figure 20 are much larger than 100 nm. Therefore, the sol-gel synthesis that we carried out was not suitable to produce nanoparticles, although the supersaturation (Ti (IV) ion concentration) was quite high. We tried to produce smaller particles using two separate ways:

- by increasing the supersaturation by performing the sol-gel synthesis at a lower temperature
- by performing the sol-gel reaction in the presence of rutile nanoparticles which would act as seeds via mechanisms of secondary nucleation

The first approach was easily carried out. The temperature of the sol-gel reaction was set at 50 ºC with the range of Ti (IV) ion concentrations between 1 – 1.5 M, while the HCl concentration was kept constant at about 3 M. A typical material produced had the rutile crystal structure, as determined with XRD analysis. SEM and TEM analyses of the material were performed in order to determine the particle size and morphology (Figure 21).

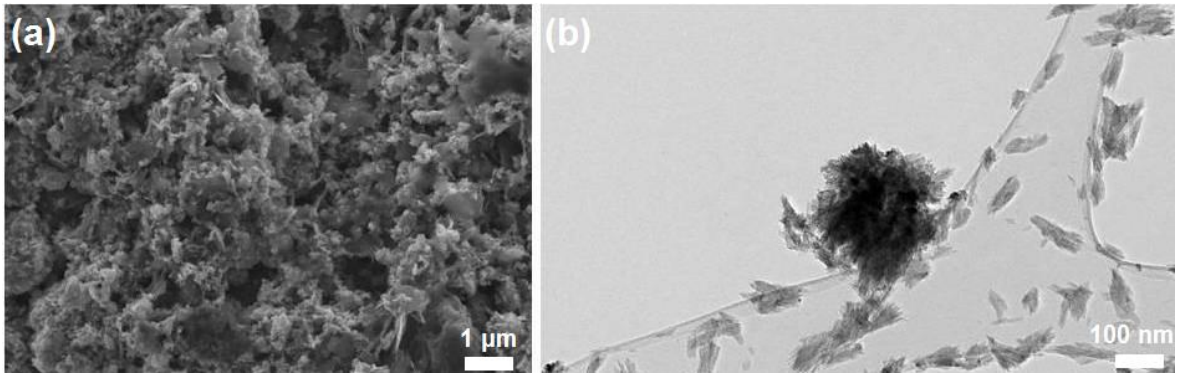

Figure 21: *Rutile nanoparticles synthesized by the sol-gel method at lower temperature to increase supersaturation.* (a) SEM image of rutile nanoparticles. (b) TEM image of rutile nanoparticles.

As can be seen from Figure 21, the rutile particles produced are of nano size, although with a relatively wide size distribution. Also, the morphology of the particles seems poorly defined, with some particles being elongated, while others showing a platelet-like structure. Although lowering the reaction temperature seems to produce a nano form of rutile TiO_2, the differences in the particle properties are too large when considering a possible application. Namely, the goal would be to produce a homogenous nano-TiO_2 whose overall properties (the properties of a large number of particles) could be evaluated by the properties of an individual particle.

Therefore, we tried the sol-gel synthesis approach where additional rutile nanoparticles were added (4 % per TiO_2 in solution phase) into the Ti (IV) solution prior to performing the reaction. Other reaction parameters were kept constant. The rutile nanoparticles were added as a seed material, since it is known that seeds may have a profound effect on the following characteristic of the reaction product [70]:

- end material morphology
- particle size
- rate of crystallization
- material crystal structure
- reaction yield increase

The material produced was analysed using XRD, SEM and TEM analysis. The XRD showed that the material has the rutile crystal structure. The SEM image and the XRD diffractogram of the particles formed are shown in Figure 22.

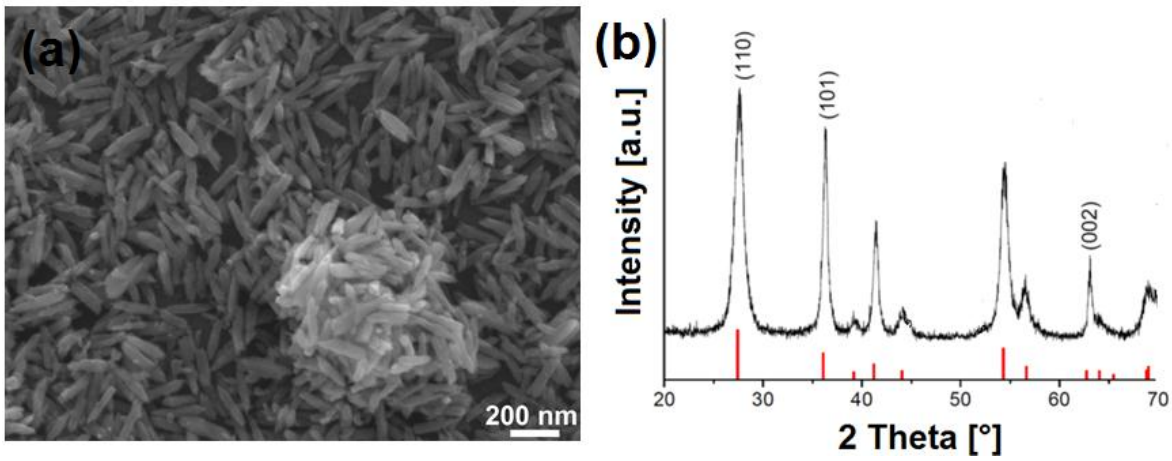

Figure 22: *SEM image and XRD diffractogram of rutile nanoparticles synthesized by the sol-gel method based on seed inoculation.* (a) SEM image of rutile nanoparticles. (b) XRD diffractogram of rutile nanoparticles with inset vertical bars that denote the standard diffraction data for rutile (JCPDS, No. 76-1940).

As can be seen from Figure 22, the formed rutile nanoparticles have a narrow size distribution, are anisotropic in shape and are of nano size. We concluded that the rutile nanoparticles added into the reaction mixture prior to hydrolysis play a crucial role in determining the final material properties. It this case the rutile seed nanoparticles enabled the production of a phase-pure product via mechanisms of secondary nucleation, as follows:

- the seeds increase the surface area of the system and thus promote the process of heterogeneous nucleation, which is thermodynamically favorable when compared to homogenous nucleation. Since rutile seeds were added and the same material was being produced, the critical energy for nucleus formation (ΔG^*) was zero. The nuclei formation may, in this case, be explained by mechanisms of contact nucleation and models such as ECSN ("embryo coagulation secondary nucleation") [188, 193].
- the use of seeds promotes the formation of nuclei and particles having the rutile crystal structure. The latter fact is more evident when comparing the change in the Gibbs free energy for the hydrolysis of the $TiCl_4$ acidic solution, which is -59.32 kJ/mol and -54.29 kJ/mol for rutile and anatase formation, respectively. The small difference in the Gibbs free energy is favorable for rutile formation, but it is nevertheless too small to account for the formation of phase-pure rutile. Therefore, the seeds seem to catalyze and promote the synthesis reaction in which pure rutile forms [70].

What was also an interesting observation is the fact that when performing the reaction in the presence of rutile nanoparticles (seeds) while changing the Ti (IV) concentration, the final particles differ in size. This is understandable since the change in supersaturation influences the number of nuclei produced and consequently the final particle size. The change in particle size based on different supersaturations (Ti (IV) ion concentration) is seen on SEM images in Figure 23.

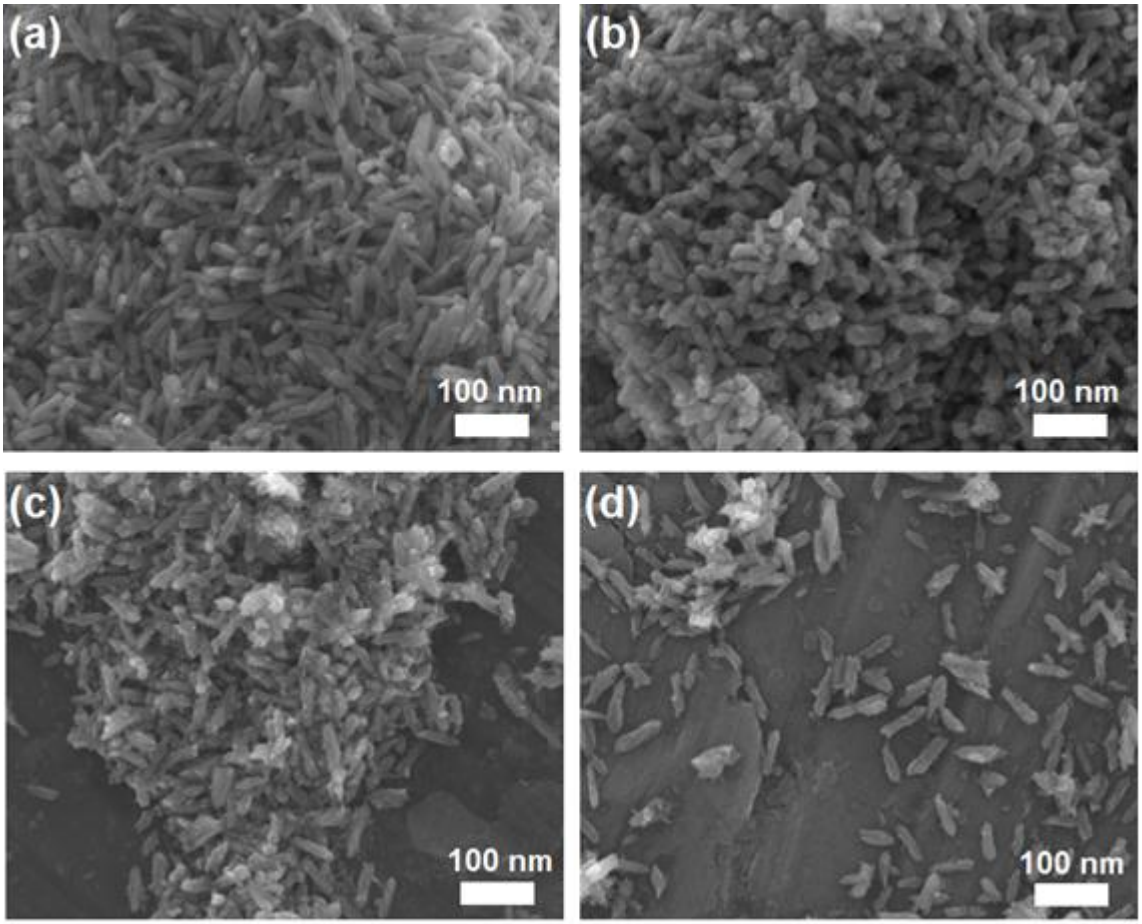

Figure 23: *Rutile nanoparticles synthesized by the sol-gel method based on seed inoculation and by changing the Ti (IV) concentration.* (a) SEM image of rutile nanoparticles synthesized at Ti (IV) concentration 0.3 M, (b) 0.6 M, (c) 0.9 M and (d) 1.2 M.

The SEM images in Figure 23 (a) and (b) show that the size of nanoparticles decreases when the Ti (IV) supersaturation is increased. However, this is not the case when Ti (IV) concentration is increased even more (Figure 23 (c) and (d)). We expected that even smaller nanoparticles would form at a higher Ti (IV) concentration, but quite the opposite was observed. A possible reason for this discrepancy could be the fact that the $TiCl_4$ hydrolysis is also dependent on the water concentration as the corresponding overall chemical reaction may be written as:

$$TiCl_4 + 2H_2O \rightarrow TiO_2 + 4HCl \tag{35}$$

At lower Ti (IV) concentrations, the hydrolysis is rapid and consequently the rate of nucleation increases. The decrease in nanoparticle size is observed at lower Ti (IV) concentrations where the amount of water is sufficient to promote the hydrolysis and nucleation rate. When the Ti (IV) concentration is increased over a specific limit, the H_2O concentration is so low, that the $TiCl_4$ hydrolysis rate decreases. Consequently, the rate of nucleation also decreases and fewer nuclei form which inherently leads to the production of larger particles [70].

TEM analysis was made on TiO_2 rutile sample shown in Figure 23 (a) to determine the particle properties, especially crystallinity and crystallite size which was compared with the XRD Scherrer calculation based on peak broadening. The TEM images and the XRD diffractogram, with the most intensive (110) rutile peak on which the Scherrer calculation

was performed (anisotropic morphology of the particles was not taken into account), are shown in Figure 24.

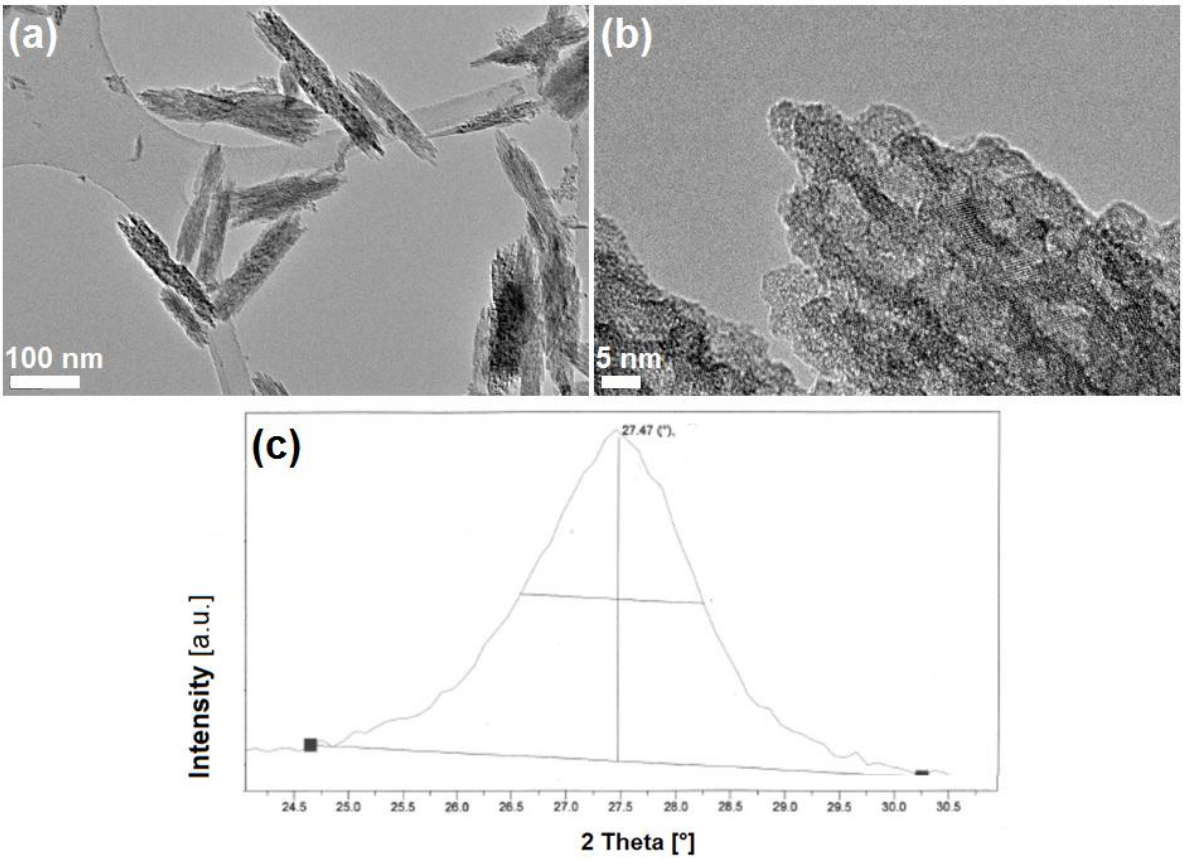

Figure 24: *TEM image and XRD (110) peak diffractogram of rutile nanoparticles synthesized by the sol-gel method based on seed inoculation and by changing the Ti (IV) concentration.* (a) A low magnification TEM image of rutile nanoparticles. (b) A high magnification TEM image of a rutile nanoparticle showing individual crystallites which are about 5 nm in size. (c) The X-ray diffractogram rutile (110) peak. The peak shows considerable broadening which is attributed to the very small crystallite size.

As seen in the lower magnification TEM image, the rutile nanoparticles exhibit anisotropic, rod-like morphology, which could be attributed to selective adsorption-desorption affinities for the chloride ion and the Ti (IV) complexes [66, 67]. A closer inspection of the nanoparticle crystallinity has shown that the particles are polycrystalline, the basic crystallites being about 5 – 10 nm in diameter, which is in accordance with the Scherrer calculation based on the considerable (110) peak broadening observed using XRD analysis. The size of the rutile crystallites (5 – 10 nm) are some of the smallest so far observed.

In the sol-gel method described above, the final product is always rutile, or at the best a mixed-phase material consisting of rutile and anatase, since both chlorine ions and protons clearly favor the rutile phase formation. Since the main goal of the present work was the synthesis of anatase nanoparticles for photocatalytic coatings and DSSCs, no further attempts were made in trying to optimize the sol-gel method for the possible anatase synthesis and preferably other methods were tried out that are described in the following chapters. Nevertheless, the sol-gel method described can be satisfactorily used for applications where the mixture of anatase and rutile nanoparticles is needed.

4.1.2 Gel-sol synthesis of TiO_2 nanoparticles

The gel-sol synthesis of TiO_2 nanoparticles was carried out using metatitanic acid as the starting material. Metatitanic acid is a product of the so-called ‘’black liquor’’ hydrolysis and is one of the most important materials produced in the Sulphate process of TiO_2 pigment production. It can either be used as a precursor for sodium titanate preparation, which due to its properties is very suitable for nanoparticle synthesis, or it can be used for the direct formation of nanoparticle colloids via a simple ionic reaction. The latter approach will be discussed first.

4.1.2.1 Gel-sol synthesis of TiO_2 nanoparticles via ionic reaction precipitate formation

The metatitanic acid is an agglomerate of anatase nanoparticles. Figure 25 shows the typical form of metatitanic acid as formed in the course of the Sulphate process.

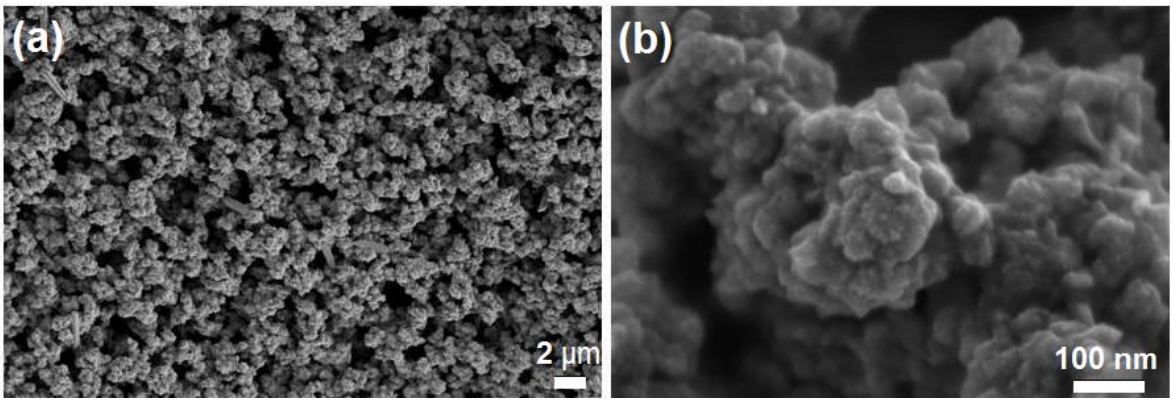

Figure 25: *SEM image of metatitanic acid.* (a) Low-magnification SEM image of metatitanic acid showing large agglomerates. (b) High-magnification SEM image of metatitanic acid showing aggregates which form the agglomerate.

In view of the difference between an agglomerate and an aggregate used in this thesis, we refer to metatitanic acid as an agglomerate, being made up of smaller subunits, aggregates, which themselves are made up of very small anatase crystallites. The crystallite mean size is about 5-6 nm, the aggregate size ranges from 40 to 100 nm, and the agglomerate size is in the order of 1-2 µm [188, 189].

Since the aggregate size is in the nano region, we refer to them as nanoparticles in this thesis. The size of the anatase nanoparticles forming the metatitanic acid agglomerate can easily be adjusted by simply controlling the hydrolysis reactions of dissolved ilmenite (“black liquor”) solution [188]. The aggregates that form the metatitanic acid agglomerate are mainly connected through sulphate bridges. The sulphate bridges are electrostatic bonds which arise due to the negative charge of the sulphate ion [188]. When subjected to water-soluble barium salts, the barium ion, having a greater affinity for the sulphate ion, draws the sulphate ions holding agglomerates together and breaks them apart into individual anatase nanoparticles. Since the final suspension is acidic, the nanoparticles within it are well dispersed. The suspension is, therefore, very stable, which enables the separation of the nanoparticles from the barium sulphate precipitate. Barium sulphate forms in the reaction between the barium ions and the sulphate ions [188].

The metatitanic acid is produced using the Sulphate process in which ilmenite is dissolved with concentrated sulphuric acid and then hydrolysed in the presence of anatase seeds. The anatase seeds are prepared separately by hydrolysing a titanyl sulphate

solution at 80 ºC and are added into the black liquor solution. Anatase seeds are crucial for the hydrolysis of the titanyl sulphate solution, since seeding provides better control over the final hydrolysis product. These seeds can have many distinctive benefits [70, 188, 189], such as:

- they promote the precipitation process
- they control particle formation and ensure a narrow size distribution of the synthesised nanoparticles
- they increase the reaction yield
- they provide an active surface, which can greatly accelerate the crystallization process, since crystallization on a solid-solid interface is much easier than nucleation in a liquid phase
- they decrease the activation energy of a reaction, thus further promoting crystallization

The inoculation of a reaction mixture with suitable seeds provides all the above-stated benefits through a process of heterogeneous nucleation. Since the seeds used in our reactions are of the same crystal structure as the final product, we term such heterogeneous nucleation a secondary nucleation.

In order to better understand the effect of seeding on the morphology and size of the final product, we conducted experiments where we varied the quantity of seeds that was added to the black liquor solution. According to the literature, the variation of the seeding volume should directly affect the size of the primary nanoparticles [189]. The SEM results in Figure 26 (a-e) indeed showed that larger seeding volumes produce smaller anatase nanoparticles, while smaller seeding volumes produce larger anatase nanoparticles. It was concluded that one can effectively control the size of the anatase nanoparticles by changing the amount of added anatase seeds. This result also demonstrates that the seeds directly control the nucleation process via secondary nucleation mechanisms.

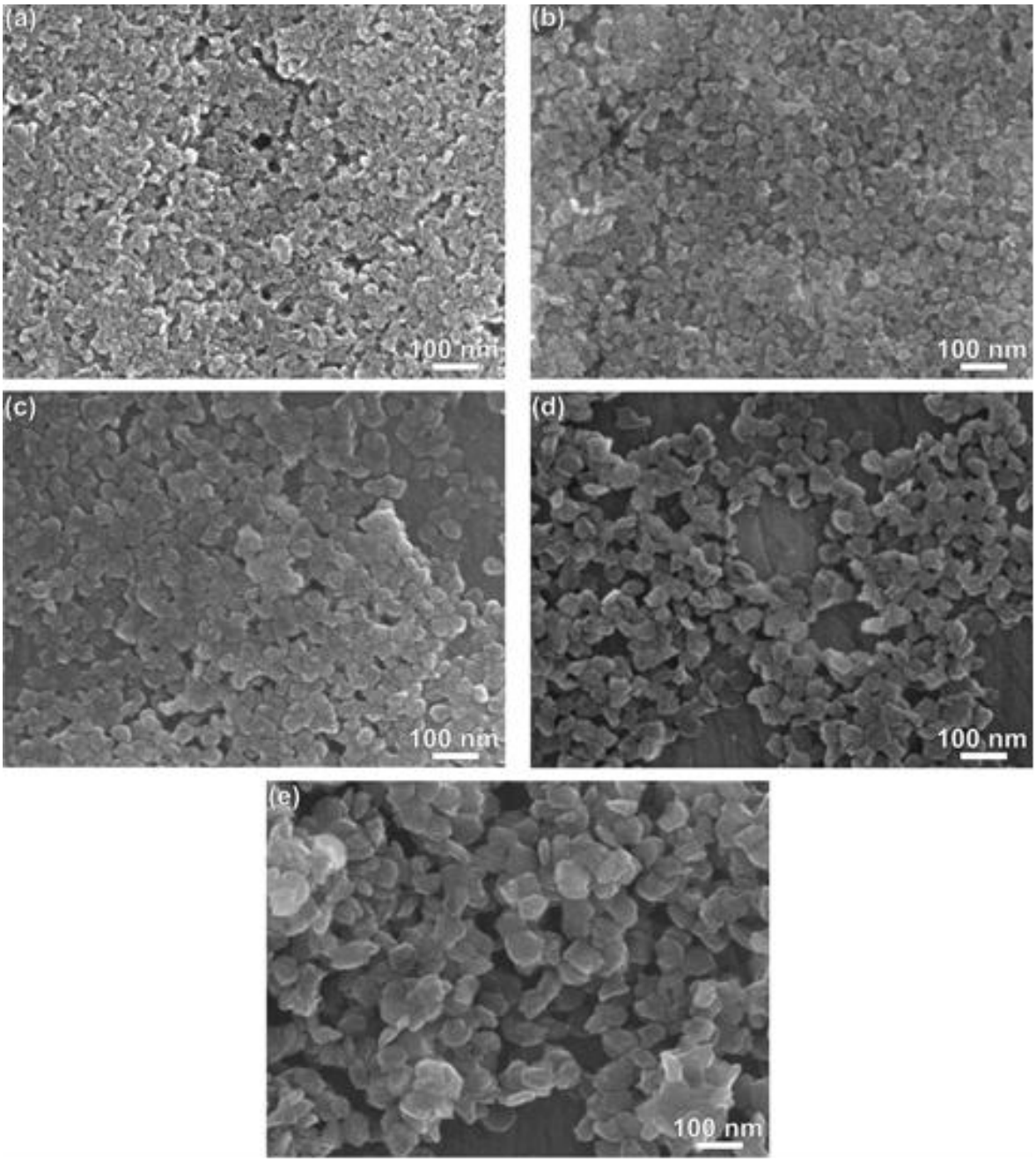

Figure 26: *SEM images of anatase nanoparticles produced by the hydrolysis of a black liquor solution when different seeding volumes were used.* The quantity of seeds (regarding to the TiO_2 content in black liquor in wt %) was (a) 1.8 %, (b) 0.9 %, (c) 0.6 %, (d) 0.3 % and (e) 0.1 %.

The theory of heterogeneous nucleation states that the free-energy change needed for nucleation depends on the wetting angle in a liquid-solid system. In the case of secondary nucleation, the seeds of the same material as the one being crystallized are used. This means that the contact angle becomes zero and that the free energy of nucleation is also zero. In this case no additional nuclei are formed in the supersaturated reaction medium when it is seeded [70]. This is in direct agreement with the observed results of our experiments. Since no additional nuclei were produced after the inoculation with the seeds, they are solely responsible for particle formation and also determine their final size. As stated previously [189] the seeds added could act as centres for nucleation of the newly formed nanoparticles. It was shown that the number of nanoparticles formed is of

the same order of magnitude as the number of crystals inoculated as seeds. This suggests that every nanoparticle arises from a single seed particle, as shown in Figure 27.

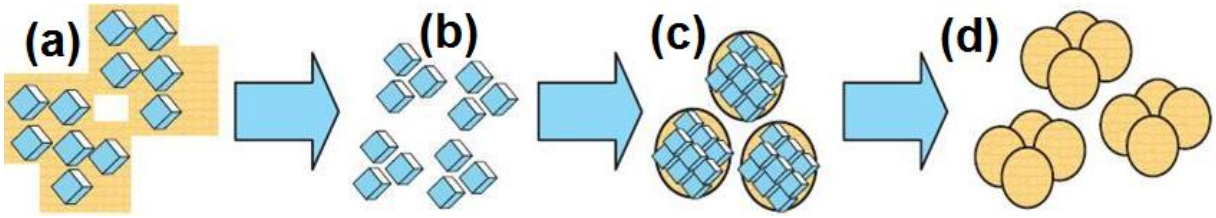

Figure 27: *Scheme representing a possible mechanism of particle formation via secondary nucleation using seed inoculation [189].* (a) Anatase seeds are in agglomerate form when added into the black liquor. (b) The anatase seeds disperse into smaller particles or even individual crystallites. (c) The dispersed anatase seeds act as centres for nucleation of the newly formed nanoparticles. Nanoparticles formed are aggregates of smaller crystallites. (d) The nanoparticles (aggregates) form the metatitanic acid via sulphate ion bridges.

The seeds used in the synthesis are large agglomerates of very small anatase crystallites, as shown in Figure 28 (a). It is very likely that they break up when added to the black liquor solution, since their surface charge changes because of the change in the pH value. Zeta potential measurement of the anatase seeds was performed by using a diluted water suspension (~ 5 g/L) that was titrated with sodium hydroxide solution (1 M). The titration was done starting at an acidic pH value (~ 2.5) and raised to ~ 10.5. As seen in the diagram of zeta-potential measurements in Figure 28 (b), the seeds exhibit the point of zero charge (the isoelectric point, IEP) at a pH around 5, which is very near to the actual pH of the seed suspension that was used. The IEP measured for anatase seeds is lower than expected for anatase, which is around 6 [196]. The observed difference could have arisen because of surface impurities such as anions that were adsorbed onto the TiO_2 surface. Sulphate anions adsorb onto the TiO_2 surface and may reduce the IEP value, as was observed in our measurements [197].

Nevertheless, it is reasonable to assume that the seeds are highly agglomerated under such conditions. But when they are added into the acidic black liquor solution, the pH drops rapidly and consequently their zeta-potential becomes more positive, which may give rise to deagglomeration of the seed particles into smaller particles, or even individual crystallites.

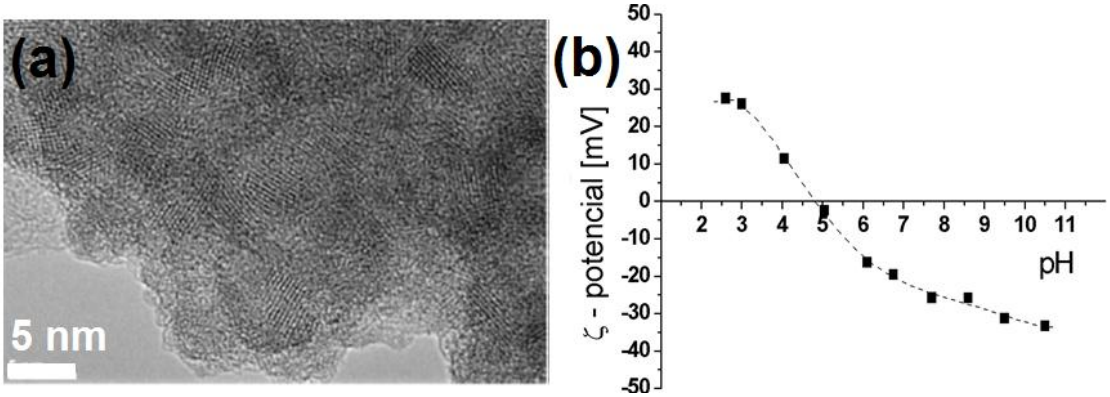

Figure 28: *HRTEM image and zeta potential measurement of anatase seeds used to inoculate the black liquor solution.* (a) Bright-field TEM image of anatase seed agglomerate. Inset shows high-resolution TEM image of anatase seeds in which smaller, approximately 5 nm crystallites of anatase can be clearly distinguished. (b) Zeta-potential measurement of anatase seeds used to inoculate black liquor solution. The isoelectric point (IEP) of the anatase seeds is around a pH value of 5, which is also the pH value of the seed suspension used for inoculation.

The mechanism of particle formation during seeding has been researched extensively [193, 198, 199]. The so-called ‘’embryo coagulation secondary nucleation (ECSN)’’ model was developed, which combines classical nucleation theory with colloid science [199]. The model states that the supersaturated solution already contains a large number of embryos. When the seeds are inoculated the embryos migrate to the surface of seeds, where they gather in large numbers, which then promotes the formation of clusters that are larger than the critical nucleus size. Afterwards, the formed nuclei can be swept away from the surface by shear forces, which are the result of solution mixing and the consequent collisions between particles. The freed nuclei can then initiate secondary nucleation or they can remain attached to the seed and form a polycrystalline aggregate (nanoparticle). In any case, highly consolidated polycrystalline particles are formed with a narrow size distribution (Figure 26 and Figure 29 (a)). A high-resolution TEM image of an individual anatase particle is shown in Figure 29 (a), where individual crystallites of approximately 5 nm in size are clearly visible. From the X-ray diffractogram in Figure 29 (b) it is evident that the produced particles have the anatase crystal structure. It has to be noted that a small amount of rutile TiO_2 is also present. The shoulder on the right-hand side of the (101) anatase peak corresponds to the (110) peak for the rutile TiO_2. A small amount of rutile is present in metatitanic acid and is the consequence of the production procedure.

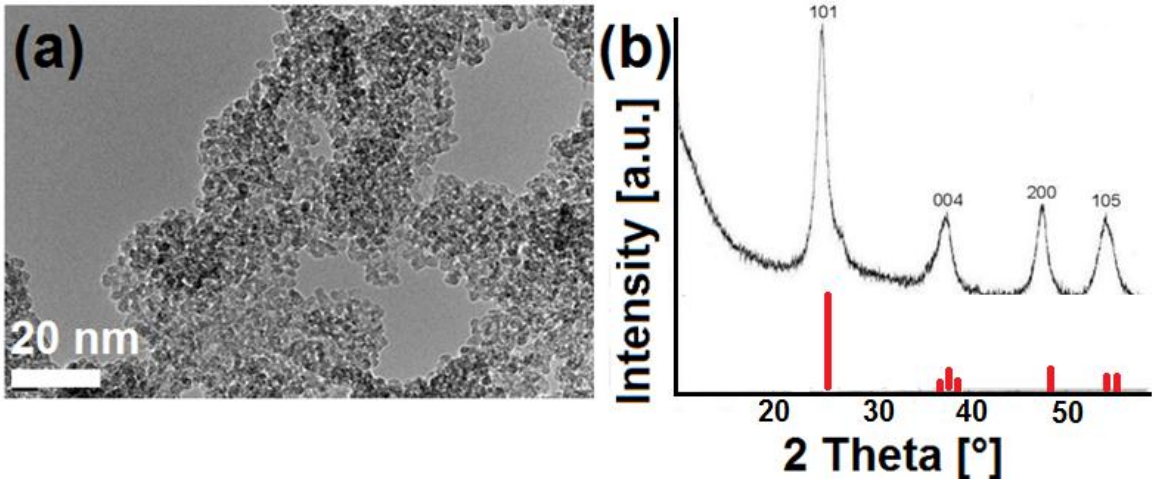

Figure 29: *TEM image and XRD diffractogram of polycrystalline anatase nanoparticles.* (a) TEM image of anatase nanoparticles showing their polycrystalline (aggregated) nature. The individual crystallites are approximately 5 nm in size and they are aggregated into an anatase nanoparticle. (b) X-ray powder diffractogram of the anatase nanoparticles with inset vertical bars that denote the standard diffraction data for anatase (JCPDS, No. 84-1286).

As was already mentioned, the metatitanic acid is made up of the anatase aggregates presented in Figure 29 (a), which are connected into large agglomerates through sulphate ion bridges. In order to produce a stable suspension of anatase nanoparticles, sulphate bridges have to be removed, which is possible with the addition of an appropriate amount of barium chloride. Since the barium ion bonds with the sulphate ion that holds the anatase aggregates together in the metatitanic acid agglomerate, it is very important to add enough of the barium chloride solution in order to remove most of the sulphate ion bridges. This results in the formation of a finely dispersed and stable suspension.

The optimal addition of barium chloride solution was defined by performing DLS measurements as shown in Figure 30. The curves in Figure 30 correspond to DLS measurements of nanoparticle suspensions prepared using different amounts of barium chloride solution that were added to the metatitanic acid. Namely, 400 mL of metatitanic

acid suspension was mixed with 110 mL of 0.5 M solution of barium chloride, 120 mL, 130 mL and 140 mL, respectively.

If the volume added is too low (110 mL barium chloride solution added to 400 mL of metatitanic acid), the metatitanic acid agglomerate breakage is not sufficient and the average particle size is around 110 nm (red curve). By increasing the volume addition (at least 120 mL $BaCl_2$(aq) added to 400 mL of metatitanic acid) the agglomerates break apart and the average size attained is around 50 nm, which coincides very well with the actual particle size observed by SEM (Figure 26).

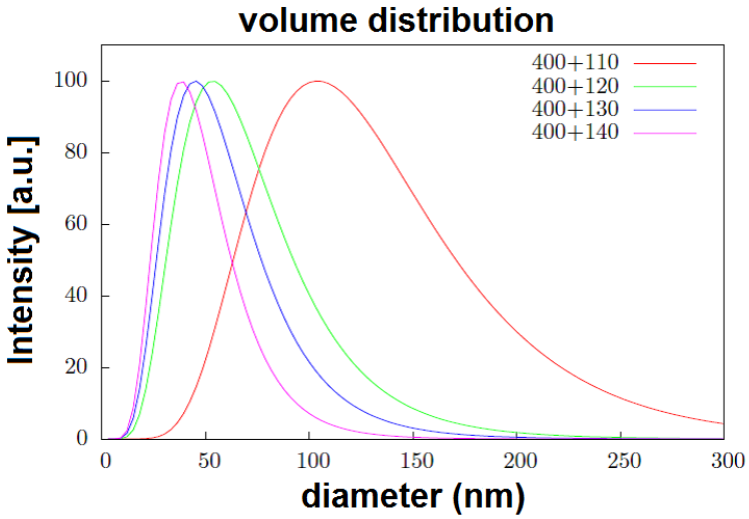

Figure 30: *DLS measurements of nanoparticle suspensions that were made from metatitanic acid and the subsequent addition of a barium chloride solution.*

From the obtained results it can be concluded that the optimal amount of barium chloride is in the molar ratio TiO_2:$Ba(II)_{(aq)}$ of approximately 30:1 ($BaCl_2$ volume addition shown as a blue curve in Figure 30). This ratio enables the production of very stable anatase nanoparticle suspensions, which can be effectively separated from barium sulphate via various separation procedures such as centrifugation or filtration.

The separation of barium sulphate and TiO_2 nanoparticles is quantitative since TiO_2 nanoparticles exhibit a high zeta potential at acidic pH values, which prevents their sedimentation. The zeta potential of the TiO_2 nanoparticles is shown in Figure 31.

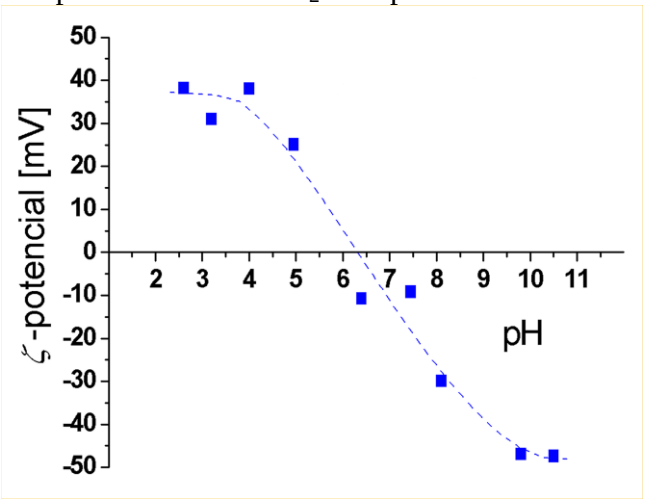

Figure 31: *The change in zeta potential for anatase nanoparticles when titrating the acidic suspension with sodium hydroxide solution.* The zeta potential is large for the acidic suspension but drops when sodium hydroxide is added. The IEP seems to be at the pH value of about 6 which is in accordance with the results found in the literature [196].

On the other hand, the barium sulphate particles are larger and settle when centrifugation is applied. This was also confirmed with an XRD (Figure 32) analysis of the settled material which is pure barium sulphate.

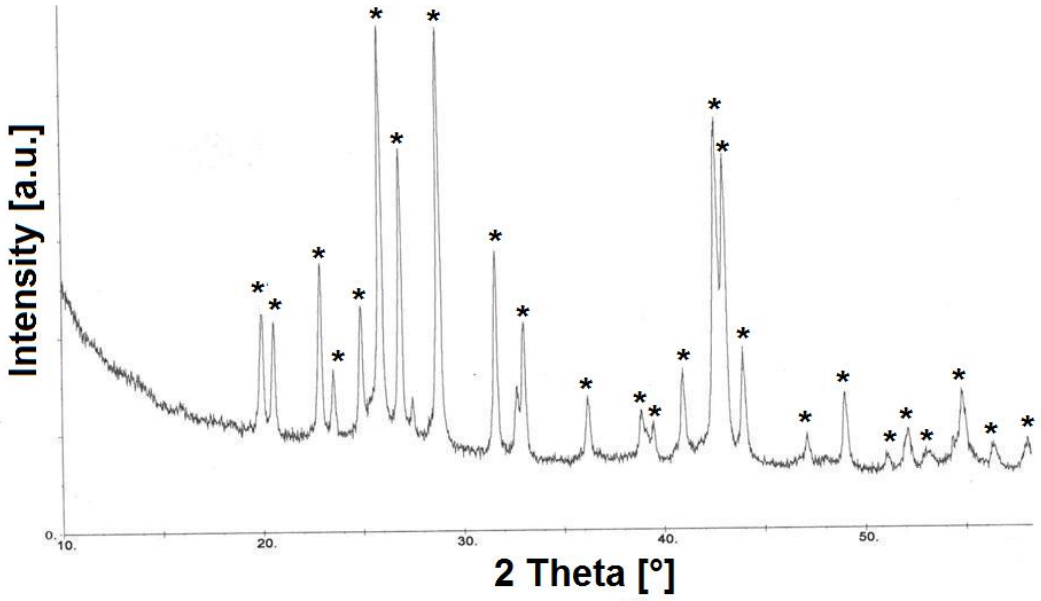

Figure 32: *The X-ray powder diffractogram of the material collected after the centrifugation cycle was finished.* The diffractogram exhibits all the peaks (labeled with *) for barium sulphate while no observable peaks for anatase are evident. The diffractogram peaks were identified using the ‘’Database of Raman spectroscopy, X-ray diffraction and chemistry data for minerals’’ [200].

This is important since the method allows the production of a very stable TiO_2 acidic suspension without a by-product being present. The concentration of TiO_2 in the final suspension is dependent only on the amount of metatitanic acid that is used. The transformation of the metatitanic acid into TiO_2 nanoparticle suspension has a very high yield (~ 100 %) since only a sufficient amount of barium chloride has to be added in order to remove the sulphate ions holding the anatase nanoparticles together in the metatitanic acid agglomerate.

It is also interesting to note that by the slow addition of a barium chloride solution almost monodispersed particles of barium sulphate are formed (Figure 33). They are in the size range from 0.5 μm to 1 μm, which depends on the concentration of barium chloride used. As expected, the barium sulphate particles are formed according to the classical theory of nucleation, where control over the particle size can be easily achieved by controlling the solute concentration (supersaturation). If a concentrated barium chloride solution was used (Figure 33 (a)), smaller particles formed since supersaturation was larger. On the other hand, if a diluted barium chloride solution was used (Figure 33 (b)), then the particles were bigger since supersaturation was lower.

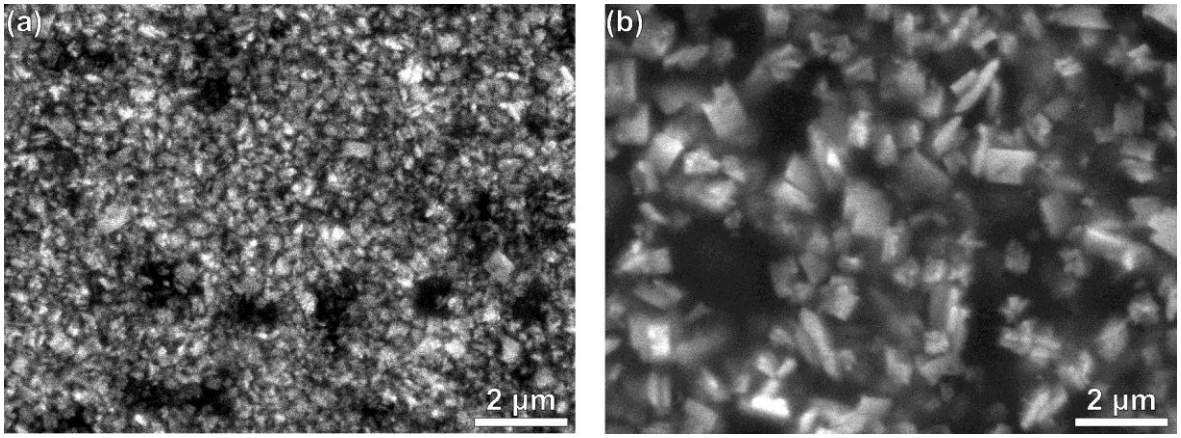

Figure 33: *SEM image of barium sulphate particles.* (a) Barium sulphate particles formed by use of a concentrated solution of barium chloride. (b) Barium sulphate particles formed with the use of a diluted solution of barium chloride.

This approach clearly demonstrates that a phase-pure TiO_2 in anatase crystal form may be prepared via a simple reaction using a barium chloride solution. The nanoparticles produced are in the form of a stable acidic colloid, which is suitable for the preparation of a photocatalytic coating [190]. The nanoparticles produced by this method are named type A nanoparticles to distinguish them from TiO_2 types that were synthesized by other methods.

4.1.2.2 Gel-sol synthesis of TiO_2 nanoparticles using sodium titanate as the precursor

Another approach in which metatitanic acid is used as the starting material for the synthesis of TiO_2 nanoparticles is the gel-sol reaction with the use of so-called sodium titanate. In this approach the metatitanic acid is only a precursor to prepare the sodium titanate material in a complex reaction. The process of sodium titanate preparation is versatile and allows the production of various sodium titanate forms. In our experiments two forms of sodium titanate were used to synthesize TiO_2 nanoparticles, namely ST1 and ST2 which are shown in SEM images in Figure 34.

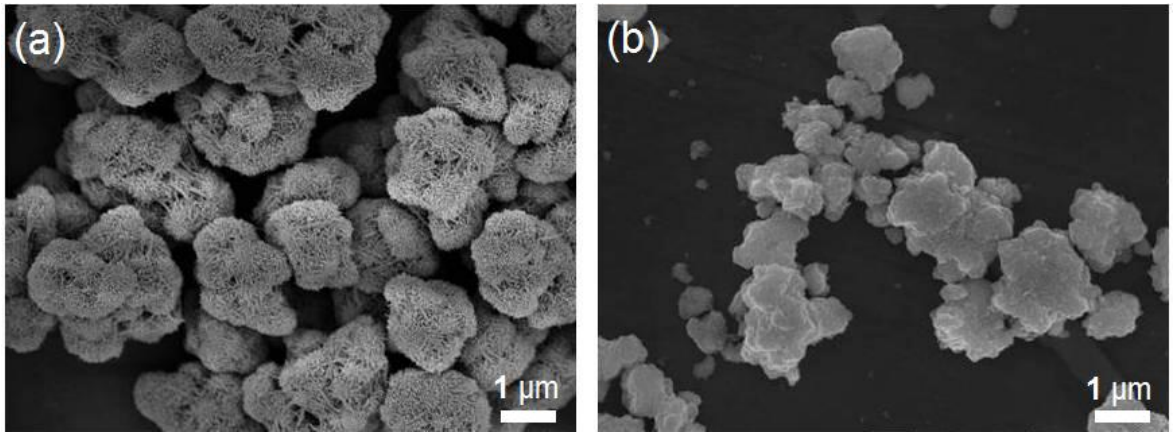

Figure 34: *SEM images of sodium titanate types used for the gel-sol synthesis of TiO_2 nanoparticles.* (a) SEM image of type ST1 sodium titanate. (b) SEM image of type ST2 sodium titanate.

As can be seen from Figure 34, the ST1 and ST2 sodium titanate types differ significantly in particle size and morphology. Both sodium titanates were developed in particular for the purpose of TiO_2 nanoparticle synthesis via the gel-sol reaction.

4.1.2.2.1 Gel-sol synthesis of TiO_2 nanoparticles using type ST1 sodium titanate

4.1.2.2.1.1 The effect of temperature on TiO_2 nanoparticle formation

The effect of temperature was determined by performing the gel-sol reaction at different temperatures. The XRD results of the products showed that all the samples exhibit a rutile crystal structure. Since XRD did not show any distinctive differences between the samples, the SEM analysis was additionally performed. The SEM analysis was used to compare the characteristics of the nanoparticles, especially the particle sizes and their morphology.

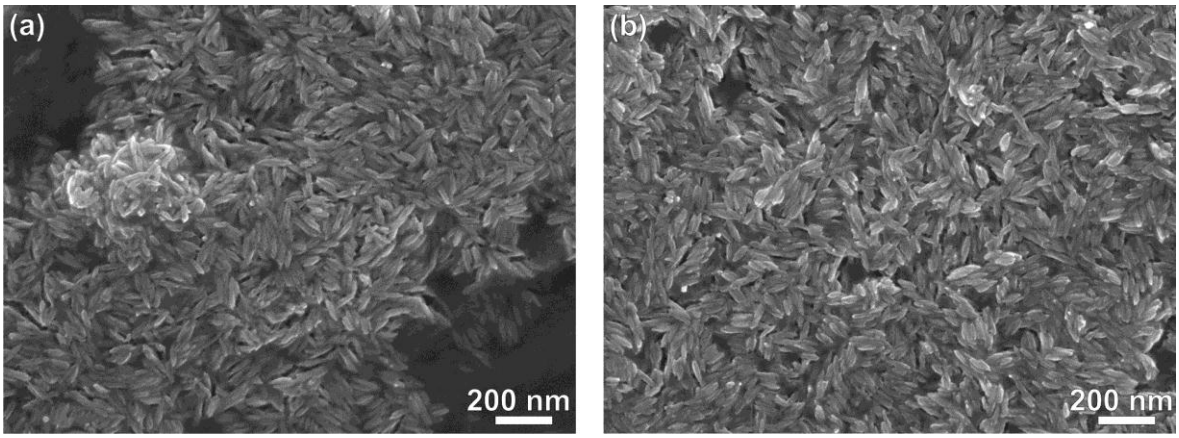

Figure 35: *SEM image of rutile nanoparticles synthesized at 50 °C (a) and at 100 °C (b).*

As can be seen in Figure 35 the temperature variation of the reaction medium does not have any significant effect on either the particle size or morphology. It is possible that the reaction temperature mostly influences the reaction kinetics since it is well known that higher reaction temperature accelerates the reaction progress because the activation energy of the molecules in the reaction medium is attained more rapidly.

4.1.2.2.1.2 The effect of precursor concentration on TiO_2 nanoparticle formation and nucleation mechanism

The precursor concentration in the reaction medium is one of the most important reaction parameters since it determines the supersaturation and therefore the final product particle size as stated by the Becher-Döring nucleation model [195]. Supersaturation is a well-known thermodynamic parameter which determines the change in the Gibbs free energy of the system when particles begin to form. Depending on the change in the Gibbs free energy the critical size of the nucleus of the growing particle is determined. The bigger the change in the Gibbs free energy, the critical size of a stable nucleus becomes smaller. Consequently more nuclei are formed and the final particles are smaller. Therefore, with a substantial supersaturation of the precursor, a large number of nuclei form. Since the amount of the precursor during particle growth is limited, the number of nuclei present directly determines the size of the particles at the end of the reaction. This is one of the most important mechanisms that enables a direct influence on product characteristics, namely particle size, simply by setting and changing the precursor concentration. Exact

knowledge of the nucleation theory also enables us to perform reactions in a way that mostly monodisperse particles are acquired as proposed by the Lamer-Dinegar diagram which provides a correlation between nucleation and subsequent nuclei growth [20].

Although we expected that by varying the precursor concentration would directly affect the final rutile particle size, it was later determined that almost no change in size occurred. The particles exhibited the same morphology and very similar size as shown in Figure 36.

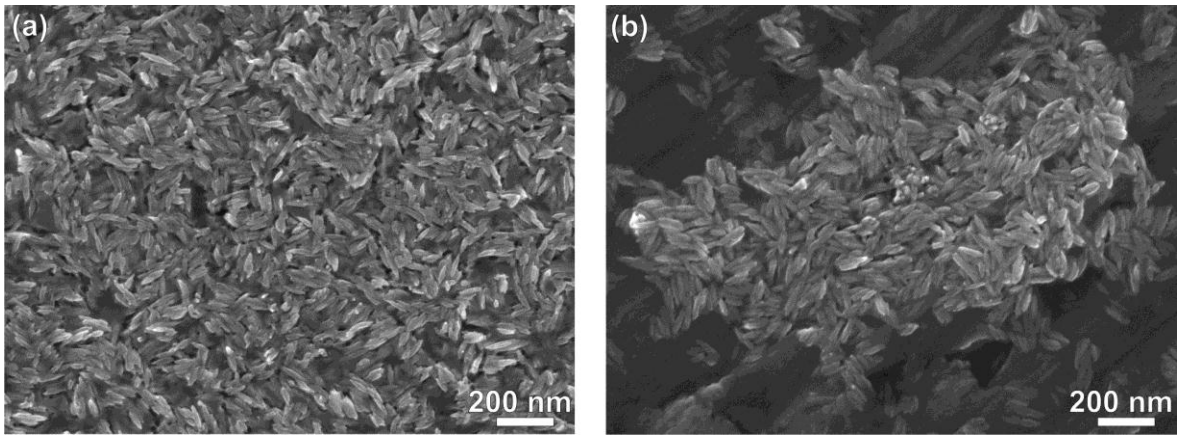

Figure 36: *SEM image of rutile nanoparticles prepared at different precursor concentrations.* SEM image of rutile nanoparticles prepared at precursor concentration of 60 g/L (a) and 180 g/L (b).

The result clearly contradicts the expected difference in particle size which would be expected based on the difference in precursor concentrations. It seems that the underlying mechanism of nucleation is different from the predictions of the Becher-Döring model. The classical nucleation model is based on three assumptions, which are described in detail elsewhere [201]. One of the assumptions is that the supply rate of the solute is independent of nucleation and growth events. This means that the amount of solute and its consumption during the reaction are not in equilibrium. In this case a monodisperse system is only possible when both the nucleation stage and the growth stage are separated as proposed by Lamer-Dinegar model [201].

With the gel-sol system the above stated assumption is not true. As was already mentioned the gel-sol synthesis of monodisperse nanoparticles is based on the phase transformation of a highly condensed metal hydroxide gel or some other gel-like precursor into a sol. The gel acts as a reservoir for the growing particles during its dissolution, which is normally fast enough to be virtually in equilibrium with the consumption rate of the metal ion within the gel throughout the phase-transformation process. Therefore, the supersaturation is not lowered below the nucleation level. Consequently, the nuclei continue to generate and grow. The nuclei form in parallel with the growth process until the precursor gel is dissolved completely. However, it is difficult to explain why the final rutile nanoparticles exhibit such a narrow size distribution. According to Sugimoto [201] the explanation for the observed state is assigned to a possible reduction of supersaturation with the stabilization of the gel network which leads to the separation between nucleation and growth. This leads to the formation of a monodispersed system of rutile nanoparticles. Since this explanation is based on aging experiments of the $Ti(OH)_4$ hydroxide gel, the same assumption may not be strictly applicable in our case. As was already stated, the rutile nanoparticles form in the reaction between the precursor gel and an appropriate acid. The reactions are therefore different to those that occur during the aging of the gel. A reasonable explanation could be that the

particles become monodisperse via two interconnected processes, namely the formation of primary particles (singlets) that aggregate into secondary particles with narrow size distribution [202].

It is possible that at first primary particles form via burst nucleation, but because of the conditions in the reaction medium they aggregate irreversibly and form the final rutile particles. The conditions that lead to the formation of secondary (final) particles are determined by the composition of the reaction medium and have a direct impact on the physical characteristics of primary particles such as zeta potential. It is possible that after burst nucleation in which primary (monocrystalline) particles form they aggregate into secondary (polycrystalline) nanoparticles due to changes in their zeta potential that approaches the isoelectric point when primary particles achieve sufficient size. This is in accordance with the observed results. We observed that the underlying structure of rutile nanoparticles consists of rod-like monocrystalline particles that are irreversibly connected into rutile polycrystalline particles.

Since the isoelectric point is directly dependent on the pH and/or ionic strength of the reaction medium the model was tested by changing the medium's chemical composition.

4.1.2.2.1.3 The effect of the mineral acid type used in the synthesis reaction

The synthesis conditions and the characteristics of the synthesized TiO_2 nanoparticles (particle size, morphology, crystal structure) are given in the Table 5.

Table 5: *Summary of the results for the gel-sol synthesis of TiO_2 nanoparticles using type ST1 sodium titanate as the precursor.* The results provided in Table 5 are based on synthesis reactions where the mineral acid type and acid concentration have been changed.

Mineral Acid / Ionic Salt	***Crystal Structure***	***Particle Size (Length/Width) / nm***	***Particle Morphology***
HCl – 40 g/L	A + R	ND* (* - not determined)	Poorly defined
HCl – 50 g/L	A + R	ND	Poorly defined
HCl – 60 g/L	A + R	ND	Poorly defined
HCl – 70 g/L	R	~ 80 / ~ 20 – 30	Anisotropic
HCl – 100 g/L	R	~ 80 – 90 / ~ 25 – 30	Anisotropic
HCl – 130 g/L	R	~ 110 – 130 / ~ 25 – 30	Anisotropic
HCl – 160 g/L	R	~ 150 – 160/ ~ 30 – 40	Anisotropic
HCl – 70 g/L + NaCl	R	~ 65 – 75 / ~ 15 – 20	Anisotropic
HNO_3 – 70 g/L	A + R	ND	Poorly defined
HNO_3 – 130 g/L	R	~ 80 / ~ 15 – 20	Anisotropic
H_2SO_4 – 100 g/L	A	ND	Poorly defined
H_2SO_4 – 200 g/L	A	ND	Poorly defined
H_2SO_4 – 300 g/L	A	ND	Poorly defined
H_2SO_4 – 400 g/L	A	ND	Poorly defined

The gel-sol synthesis was first conducted with hydrochloric acid. The X-ray diffraction analysis revealed that the hydrochloric acid concentration directly influences the crystal structure of the TiO_2 product. But only when the acid concentration was high enough pure rutile phase was obtained. When the acid concentration was kept under a certain level, a mixed product of both anatase and rutile was obtained (Figure 37).

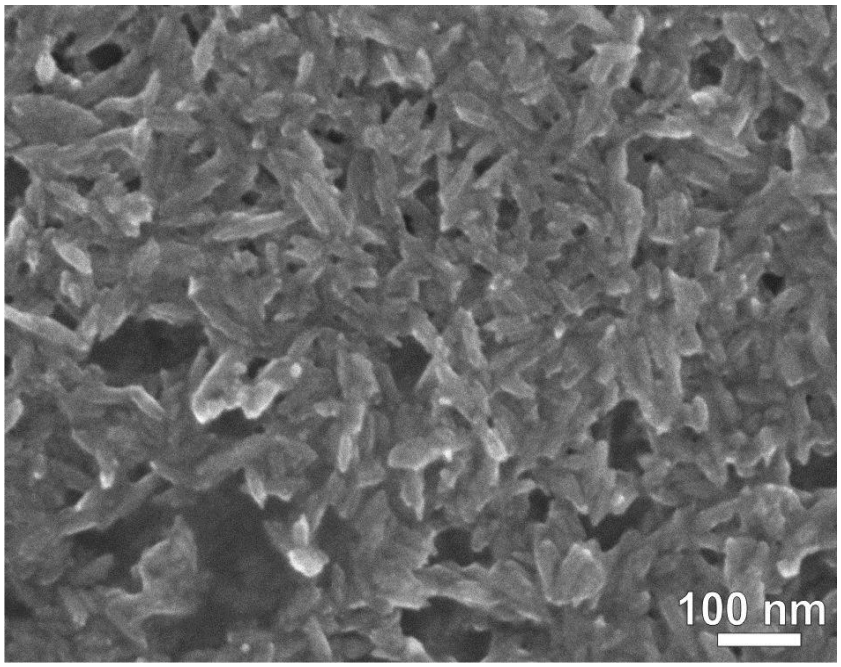

Figure 37: *SEM image of a mixed product (R+A) prepared when HCl acid concentration was lower than needed for total conversion of precursor gel into rutile nanoparticles.*

This effect could be the consequence of the precursor sodium titanate structure in which the [TiO_6] octahedra arrangement resembles very closely the arrangement of [TiO_6] octahedra in anatase [60]. The acid leads to the rearrangement of the [TiO_6] octahedra present in the sodium titanate structure. Depending on the HCl acid concentration the rearrangement of the octahedra can result either in the anatase or rutile phase or a mixture of both. The rearrangement mechanism must clearly be different for the two TiO_2 polymorphs since they differ in crystal structure and since in our experiments pure TiO_2 as well as mixed TiO_2 products were produced.

The anatase crystal structure can be viewed as a zig-zag chain of octahedra, linked to each other through shared edges. The rutile crystal structure, on the other hand, is formed by sharing two opposing octahedra edges creating linear chains along [001] [58].

Some anatase phase was produced only when the HCl acid concentration used during the gel-sol synthesis was much lower than 70 g/L. In this case the acid could act only to remove the interlayer ions present in the titanate precursor, which would lead to the merging of the octahedra layers. Since the octahedra arrangement within the titanate layers is similar to the octahedra arrangement in the anatase crystal structure, the merging of the layers leads to anatase formation. When the acid concentration was equal or more than 70 g/L, only rutile particles were produced.

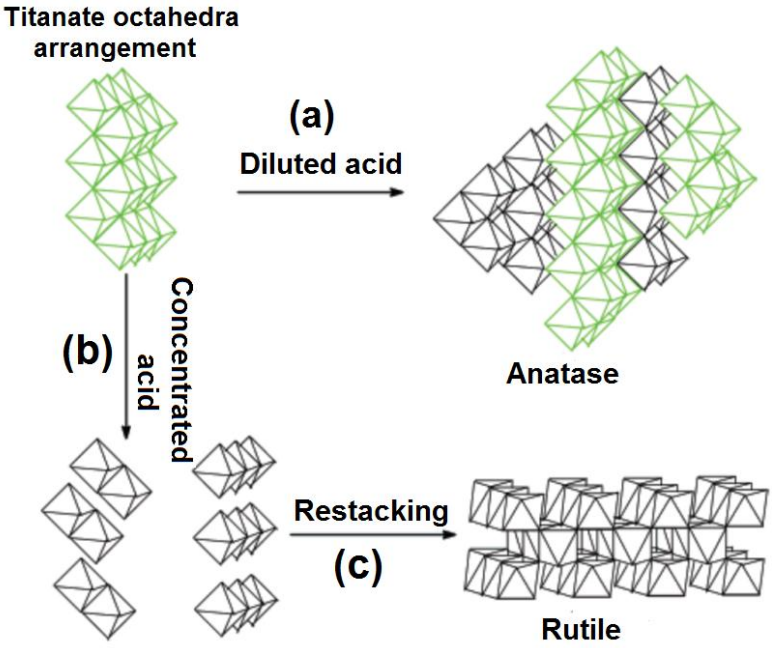

Figure 38: *A schematic presentation of a possible phase transition between titanate material and anatase and rutile TiO_2 crystal structures [60]*. (a) If a diluted HCl is used, the [TiO_6] octahedra layers of the titanate merge and form particles with the anatase crystal structure. (b) – (c) If concentrated HCl is used, the titanate dissolves and the [TiO_6] octahedra restack into particles with rutile crystal structure.

Since the rutile crystal structure differs in [TiO_6] octahedra arrangement compared to titanate, the rearrangement mechanism should begin with deoxolation reactions that lead to the detachment of the octahedra in the titanate precursor [59]. Deoxolation could start with the advance of the electrophilic protons on the oxygen bridges between titanium ions. This results in a lowered electron density on the latter and makes it more electrophilic. This leads to the attraction of the titanium ions with the chloride anions and consequently to the breaking of the oxolation bond. The reduced number of Ti-O-Ti bonds leads to structural rearrangements of the [TiO_6] octahedra and consequently very small rutile particles form. This is in accordance with the fact that very acidic environments preferably lead to the formation of the rutile phase [56]. Our experiments confirmed that when hydrochloric acid was used in a high concentration only rutile particles were formed. When the acid concentration was lowered the mixture of both, anatase and rutile was produced due to the fact that octahedra rearrangement occurred via both mechanisms which are competitive.

The distinction between the two [TiO_6] rearrangement mechanisms becomes even more evident when analysing the morphology of the produced particles. When the HCl acid concentration was low, both phases, anatase and rutile, formed. TEM analysis revealed that rutile was produced in the form of very small anisotropic nanoparticles consisting of rod-like crystallites. On the other hand, anatase was produced in the form of larger aggregates consisting of very small crystallites about 5 nm in size.

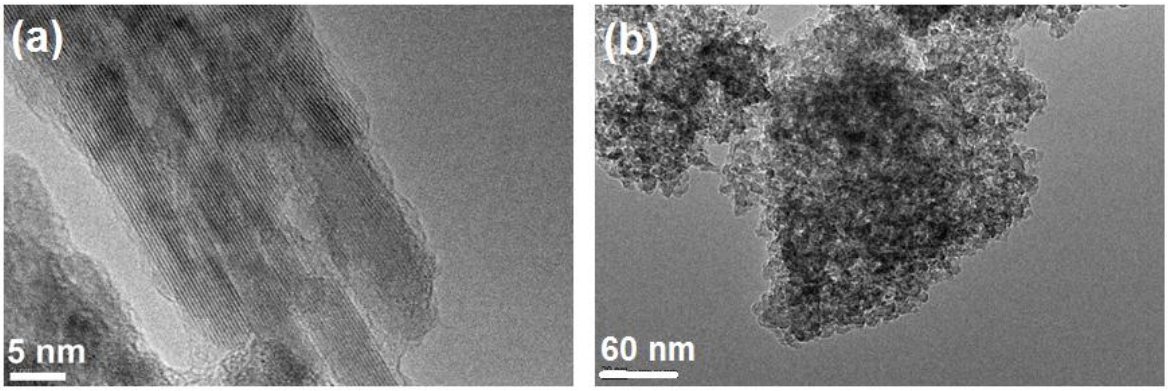

Figure 39: *TEM image of a polycrystalline TiO_2 particles produced using different HCl concentrations.* (a) HRTEM image of anisotropic rutile nanoparticles produced when HCl concentration was high. (b) TEM image of anatase particles that were produced alongside rutile nanoparticles when HCl concentration was lower.

The difference in constituent crystallite size and particle morphology between the rutile and anatase phase can only be possible when particle formation mechanisms differ. Anatase is present in the form of large aggregates which is consistent with the fact that the deoxolation reaction does not occur (Figure 38) and therefore the initial titanate precursor is not broken down. In order that rutile particles form, deoxolation must occur, since only then the [TiO_6] octahedra within the titanate precursor split and can rearrange into the rutile crystal structure. The morphology of the crystallites that form the rutile nanoparticles are a clear evidence of this. The crystallites that form the rutile nanoparticles are depicted in Figure 39 (a).

As can be seen in Figure 39 the crystallites that form the rutile nanoparticles exhibit rod-like anisotropic morphology and have a well-defined structure. Their morphology and crystallinity can be explained via polycondensation reactions starting from the [TiO_6] octahedra that form in a highly acidic environment. The [TiO_6] octahedra form because of the deoxolation reactions and breaking of the Ti-O-Ti bonds. The [TiO_6] octahedra act as building blocks for the newly formed rutile particles. The anisotropic morphology of the rutile nanoparticles is a direct result of specific [TiO_6] octahedra rearrangement and polycondensation reactions that take place on a newly formed rutile nuclei. The rutile crystal structure is tetragonal. Therefore, the surface energies of individual rutile crystal facets differ [66]. The difference in surface energies can lead to selective adsorption of the species present in the reaction medium. The [TiO_6] octahedra and chloride anions can both adsorb on the surface of the growing rutile crystal. Since the crystal facets of rutile differ in their energies the adsorption of the two species is different for a specific facet. Depending on the adsorption ratio of the [TiO_6] octahedra and chloride anions on a specific rutile facet the propagation speed of crystal growth becomes different. Consequently, the rutile crystal grows faster in the {101} direction since a higher ratio of [TiO_6] octahedra is adsorbed [66]. This leads to anisotropic crystal morphology as seen on HRTEM image in Figure 39. Eventually, the crystallites aggregate and form the final rutile nanoparticles.

This is probably because of the specific conditions present in the reaction medium. We propose that during the growth of the crystallites their properties (i.e. zeta potential) changes. At a certain crystallite size the isoelectric point is attained and at this point irreversible aggregation of the crystallites occurs and the final rutile nanoparticles form. This was tested by performing the synthesis reactions with higher HCl acid concentrations. In such conditions the zeta potential of the growing particles is different compared to the zeta potential at lower HCl acid concentrations because the particle electrical double layer is directly affected by the chemical composition of the reaction

medium. The consequence is that the crystallites and rutile nanoparticles become different in size since the isoelectric point during crystallite growth is attained at different stages. This is supported by SEM analysis of the rutile nanoparticles that were synthesized with various HCl acid concentrations (Figure 40).

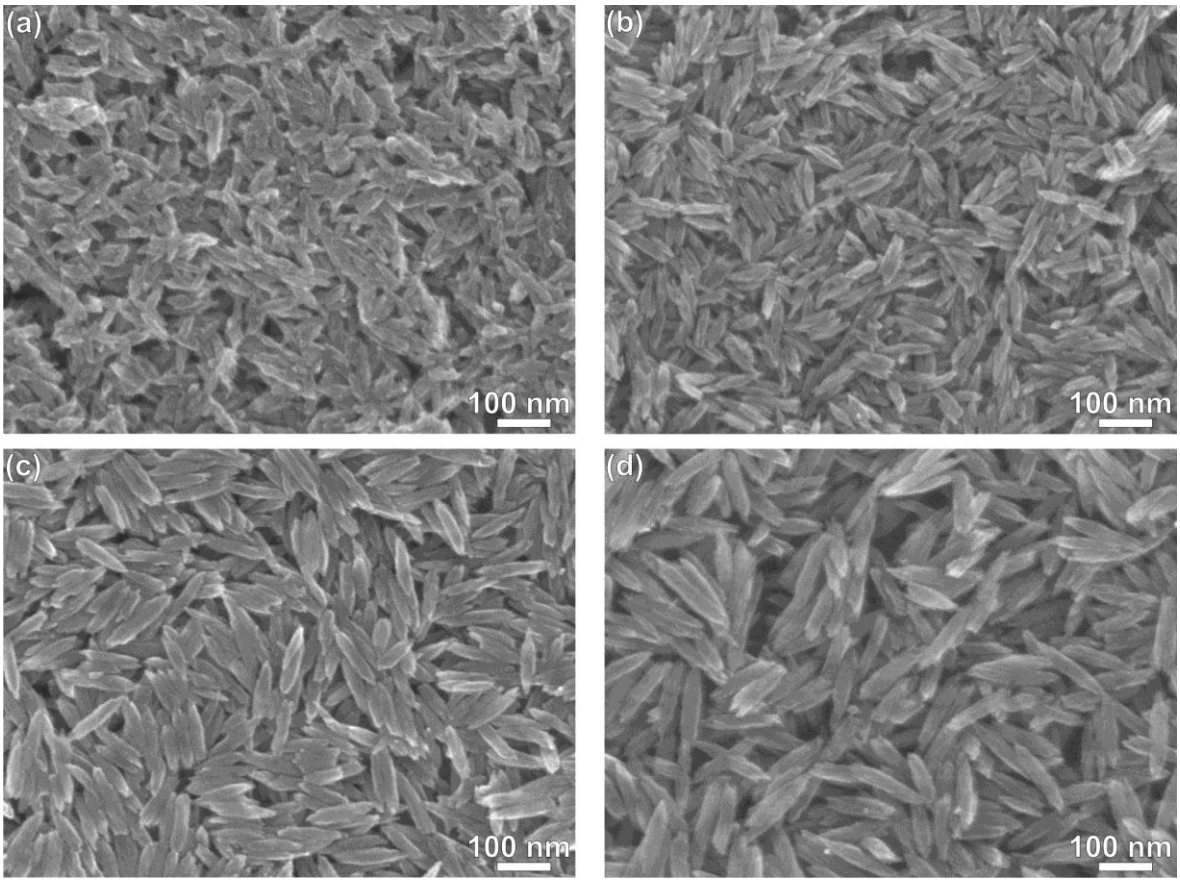

Figure 40: *SEM images of rutile nanoparticles that were synthesized using varying hydrochloric acid concentrations.* The rutile nanoparticles were synthesized with the following HCl concentrations: 70 g/L (a), 100 g/L (b), 130 g/L (c) and 160 g/L (d).

From the SEM micrographs in Figure 40 it can be seen that when performing the gel-sol reaction with a higher hydrochloric acid concentration, the rutile nanoparticles become larger. This can mainly be attributed to the difference in reaction medium chemical composition, which differs mostly in the ionic strength. Ions present in the medium constitute the electrical double layer of the colloid particles and in a large extent determine their physical properties, such as stability, zeta potential, etc. Changing the ionic strength of the medium directly changes the electrical double layer of the growing colloid rutile particle which consequently affects the isoelectric point. Consequently, the irreversible aggregation of rod-like crystallites into the final rutile particles happens at different stages. This leads to the formation of rutile nanoparticles with different sizes.

In order to additionally elucidate the effect of the reaction medium’s composition on the structure and size of rod-like crystallites that aggregate into final rutile nanoparticles, HRTEM analysis was employed (Figure 41).

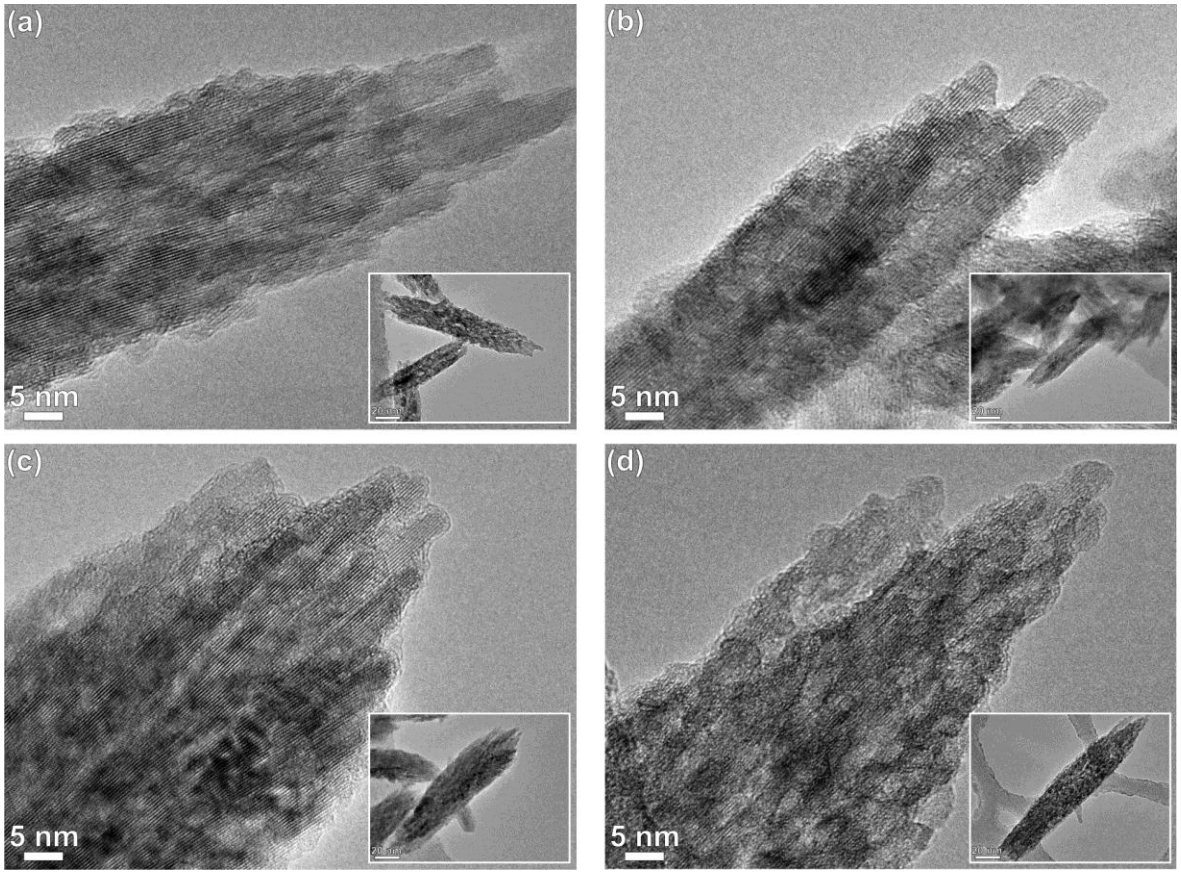

Figure 41: *TEM images of rutile nanoparticles prepared with gel-sol synthesis using varying HCl concentration.* The HCl acid concentration was (a) 70 g/L, (b) 100 g/L, (c) 130 g/L and, (d) 160 g/L. The nanoparticles exhibit a structure with constituent crystallites having rod-like morphology. The crystallites are anisotropic and differ slightly in length while their width is about the same (~4-5 nm).

As seen from TEM images, the increased acid concentration directly affects the size of the rod-like crystallites and nanoparticle as a whole. The rod-like crystallites grow in length when the acid concentration is increased, while the width stays about the same. This is in accordance with the above proposed crystallite aggregation model that is directly dependent on the ionic strength of the reaction medium. The ionic strength of the reaction medium is mainly affected by the HCl acid concentration used during the synthesis. Therefore, when the HCl acid concentration is increased, the aggregation of the crystallites occurs at a different stage than when the HCl concentration is lower. The rod-like crystallites can therefore grow for a longer period of time at a higher HCl concentration, which increases their length and the length of the rutile nanoparticle as a whole.

The effect of chemical composition (ionic strength) of the reaction medium on the nanoparticle size was tested by performing experiments in which an ionic salt was added. The ionic salt added was sodium chloride, since it has already been established that a sodium cation may affect the size of TiO_2 particles during their formation [62, 66, 67].

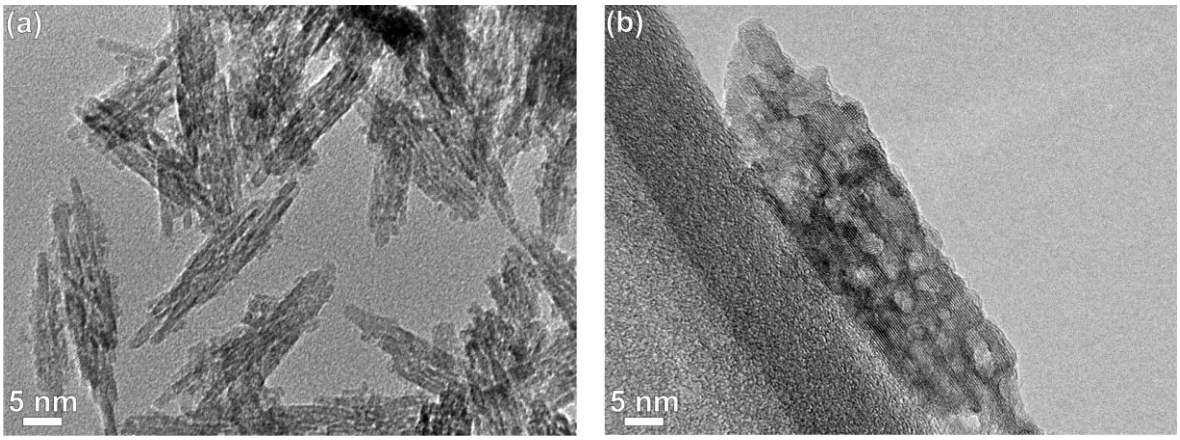

Figure 42: *Low-magnification and HRTEM of rutile nanoparticles prepared at 70 g/L HCl concentration and NaCl.* (a) TEM images of rutile nanoparticles acquired by adding sodium chloride into the reaction medium. (b) HRTEM of a rutile nanoparticle prepared with gel-sol synthesis where the acid concentration was 70 g/L and the reaction medium also contained NaCl.

As can be seen from Figure 42, the rutile nanoparticles synthesized in the presence of sodium chloride are smaller from those obtained in a reaction performed only with HCl.

It seems that HCl, its concentration and also the presence of other ionic species exhibit the most profound effect on the produced TiO_2 nanoparticles. Based on these results it was reasonable to carry out the same experiments with other mineral acids, such as nitric acid (HNO_3) and sulfuric acid (H_2SO_4) in order to further elucidate the above stated mechanism of precursor transformation into rutile.

When the nitric acid concentration was 130 g/L the XRD results showed that the product synthesized was pure rutile. When the nitric acid concentration was 70 g/L a mixed phase of rutile and anatase was formed. The presence of a mixed phase at 70 g/L nitric acid concentration can be explained as follows. The driving mechanism for titanate precursor transformation into rutile is driven solely on the basis of the molar ratio between the precursor and the acid. If the molar ratio between the acid protons (H^+) and precursor Ti^{4+} ions is too low a mixed phase of anatase and rutile is formed. This is because the titanate [TiO_6] octahedra rearrange via the two competiting mechanisms shown in Figure 38 (a) and (b). One leads to rutile particle formation and the other to anatase particle formation. When the synthesis was carried out with a nitric acid concentration of 130 g/L the product was pure rutile, which is reasonable since H^+ molar concentration is about the same as with a hydrochloric acid concentration of 70 g/L, which also leads to the formation of pure rutile. The experiments carried out using nitric acid confirmed that acid and its concentration drives the precursor transformation into either rutile or a mixed phase of both.

In order to compare TiO_2 materials produced with nitric acid and hydrochloric acid a SEM analysis was performed (Figure 43).

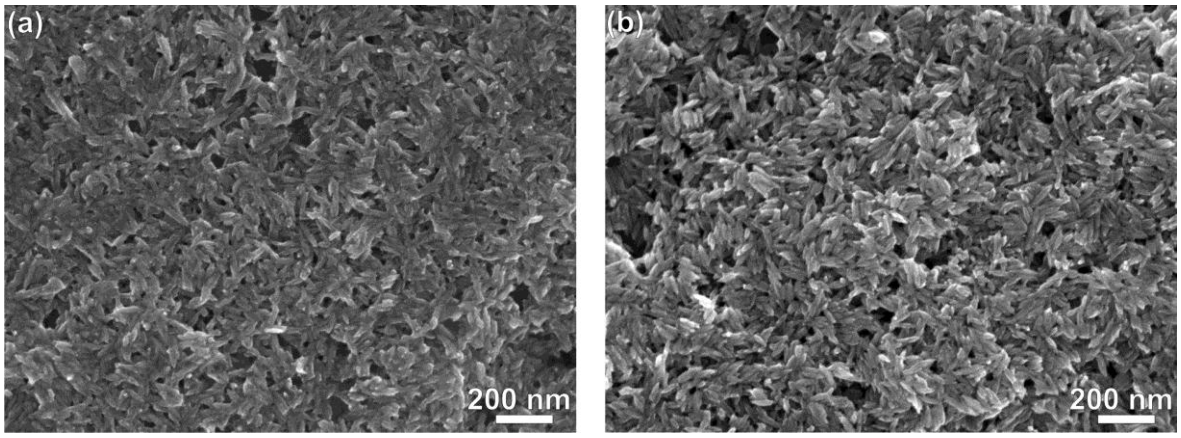

Figure 43: *SEM images of nanoparticles produced with nitric acid at different concentrations.* The nitric acid concentration was 70 g/L (a) and 130 g/L (b).

As seen from Figure 43 the produced nanoparticles exhibit very similar morphology and particle size to those produced with hydrochloric acid. This probably means that the nitrate anion behaves similarly to a chloride ion in the sense they both have an extra electron (they act as a Lewis base) which makes it possible to bind electrostatically to areas of lower electron density. Therefore, the nitrate anion could bind onto the surface of a growing rutile particle like the chloride anion does, which leads to anisotropic crystallite growth and particle morphology. This is a confirmation of the results already acquired, namely that acid concentration determines the final product crystal structure and particle size while the anion present determines the particle morphology.

Since sulfuric acid is a strong mineral acid it could also lead to rutile formation when added in large amounts. However, XRD analysis of the TiO_2 materials synthesized when sulfuric acid was used showed that only anatase is formed, regardless of the sulfuric acid concentration in the reaction medium. This means that a sulfate anion exhibits an effect that dominantly directs the transformation of the titanate precursor into anatase only. The reason for this observation is that the sulphate anions prevent the [TiO_6] octahedra from rearranging into linear chains which are specific for the rutile crystal structure [15]. Only zig-zag [TiO_6] octahedra chains form, as schematically presented in Figure 5. This leads to the formation of anatase particles.

It can be concluded that the ST1 sodium titanate approach to synthesizing TiO_2 nanoparticles clearly promotes the formation of TiO_2 nanoparticles with a rutile crystal structure. The nanoparticles produced by this method are named type B1 nanoparticles to distinguish them from TiO_2 types that were synthesized by other methods.

4.1.2.2.2 Gel-sol synthesis of TiO_2 nanoparticles using type ST2 sodium titanate

Since only the sodium titanate type was changed, it was reasonable to expect that the overall mechanism of TiO_2 particle formation would be similar to the one that occurs with rutile formation using the ST1 sodium titanate type. To elucidate the formation mechanism we conducted the synthesis reactions at varying reaction temperatures and TiO_2 concentrations.

Again, it was evident that the set precursor concentration (the amount of TiO_2) and the set reaction temperature play a less important role in the determination of the final TiO_2 nanoparticle characteristics. The effect of the change in reaction temperature (Figure 44), and the precursor (TiO_2) concentration (Figure 45) seems to have no or very little effect on the final material properties.

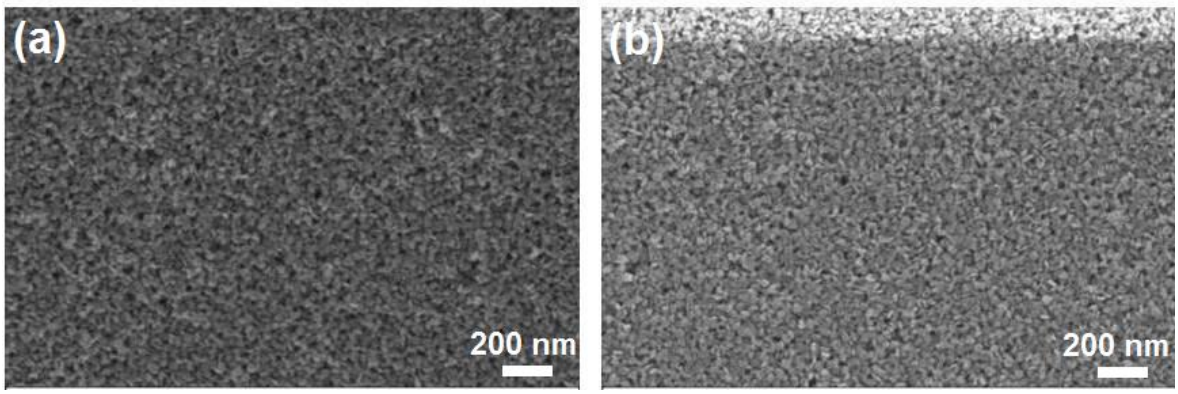

Figure 44: *Anatase nanoparticles produced using type ST2 sodium titanate by varying the reaction medium temperature.* (a) Anatase nanoparticles synthesized at 50 °C. (b) Anatase nanoparticles synthesized at 100 °C.

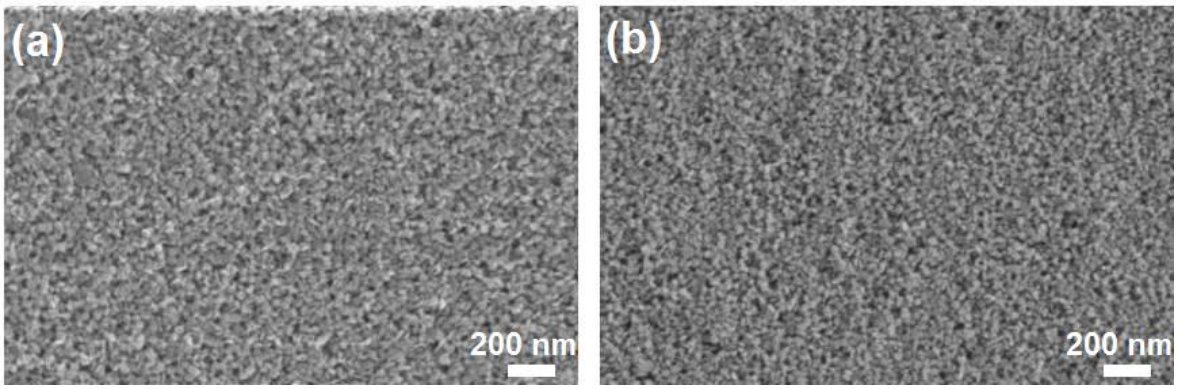

Figure 45: *Anatase nanoparticles produced using type ST2 sodium titanate by varying the precursor concentration.* (a) Anatase nanoparticles synthesized at TiO_2 concentration of 60 g/L. (b) Anatase nanoparticles synthesized at TiO_2 concentration of 180 g/L.

The synthesis conditions and the characteristics of the synthesized TiO_2 nanoparticles (particle size, morphology, crystal structure) using ST2 sodium titanate and different mineral acids are given in the Table 6.

Table 6: *Summary of the results for the gel-sol synthesis of TiO_2 nanoparticles using type ST2 sodium titanate as the precursor.* The results provided in Table 6 are based on synthesis reactions where the mineral acid concentration has been changed.

Mineral Acid / Ionic Salt	***Crystal Structure***	***Particle Size / nm***	***Particle Morphology***
HCl – 20 g/L	A	40 – 50	Spherical
HCl – 40 g/L	A	40 – 50	Spherical
HCl – 60 g/L	A	40 – 50	Spherical
HCl – 80 g/L	A	40 – 50	Spherical
HCl – 100 g/L	A	40 – 50	Spherical
HCl – 150 g/L	A	40 – 50	Spherical

When the hydrochloric acid concentration was varied, some differences in particle size were observable, but were only minor as seen in Figure 46.

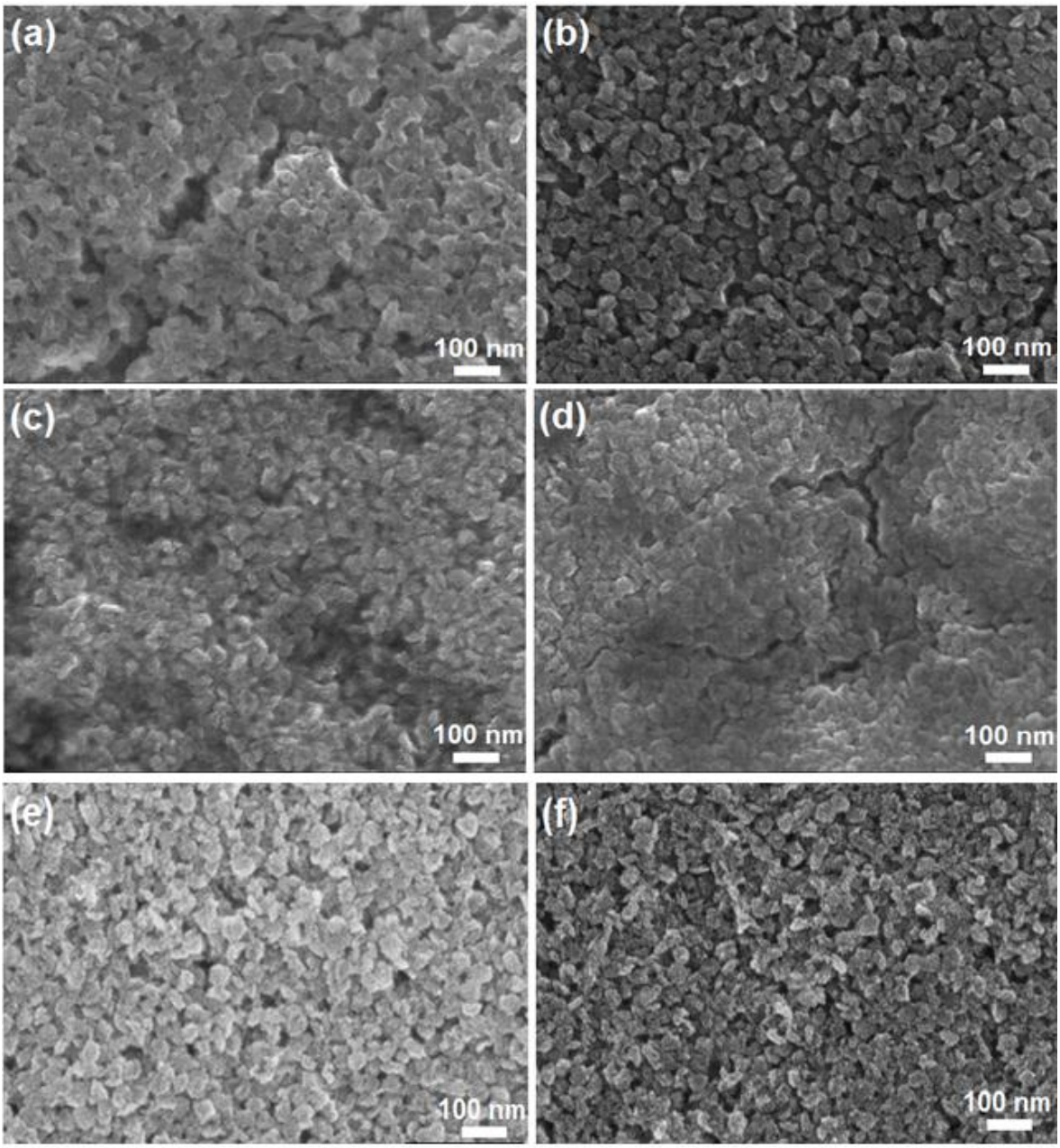

Figure 46: *SEM images of anatase nanoparticles that were synthesized using varying hydrochloric acid concentrations.* The HCl concentration was 30 g/L (a), 50 g/L (b), 60 g/L (c), 70 g/L (d), 100 g/L (e) and 150 g/L (f).

It seems that changing any of the three reaction parameters (TiO_2 concentration, HCl concentration, reaction temperature) does not significantly affect the basic nanoparticle properties. This could be because the main property-determining parameter in the gel-sol synthesis of TiO_2 nanoparticles using the ST2 sodium titanate is the sodium titanate itself. Namely, the sodium titanate ST2 type shows a similar crystal structure (determined with the XRD) as the final anatase material. Therefore, it seems possible that the use of HCl as the mineral acid in the gel-sol reaction influences the particle formation only by converting the ST2 sodium titanate into the final nanoparticulate material via peptization. This means that also other mineral acids, apart from HCl, could be successful in the gel-sol synthesis of anatase nanoparticles.

This was tested by performing the gel-sol reaction using sulfuric acid (H_2SO_4). The particles that were produced are shown in Figure 47.

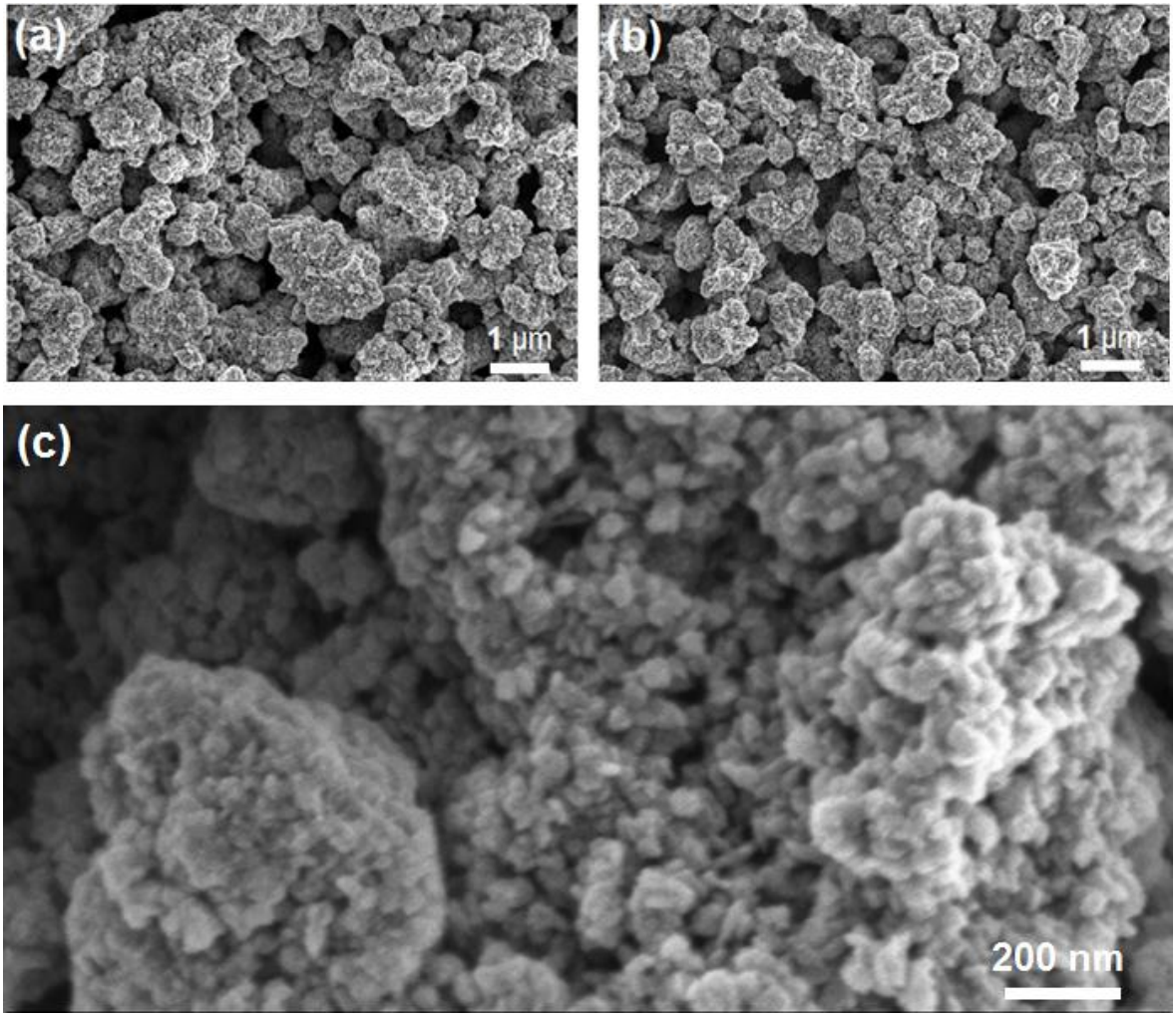

Figure 47: *SEM images of anatase nanoparticle agglomerates that were synthesized using varying sulfuric acid concentrations.* The sulfuric acid concentration was 50 g/L (a) and 100 g/L (b). At higher magnifications (c) individual anatase nanoparticles can be observed.

As can be seen from Figure 47, the material that is produced from type ST2 sodium titanate using sulfuric acid is different than when using hydrochloric acid. The main difference is that the nanoparticles are present in the form of large agglomerates when sulfuric acid is used. The formation of large agglomerates may be attributed to sulfuric acid and was observed in previous studies [63]. However, it seems that the individual anatase nanoparticles that were produced using sulfuric acid do not differ in size when compared with anatase nanoparticles that were synthesized using hydrochloric acid. We conclude that mineral acid may act only to disperse the anatase nanoparticles that are already present in type ST2 sodium titanate. This is different than with the gel-sol synthesis of TiO_2 nanoparticles using type ST1 sodium titanate, where mineral acids (HCl, HNO_3 and H_2SO_4) have shown a profound effect on the final nanoparticle characteristics.

It is therefore the sodium titanate type that influences the final material characteristics, not only the reaction parameters and the mineral acid type. Depending on the sodium titanate type, the gel-sol synthesis may produce various TiO_2 materials. The sodium titanate type seems to influence the reaction type that takes place during the gel-sol synthesis. Reactions that may occur are the gel-sol reactions (gel dissolution – $[TiO_6]$ octahedra rearrangement - particle formation) that were observed using the ST1 type

sodium titanate and peptization reactions that were observed using the ST2 type sodium titanate.

It is evident that the gel-sol synthesis of TiO_2 nanoparticles using type ST2 sodium titanate enables the production of anatase nanoparticles if an appropriate mineral acid is used. But the anatase nanoparticle size cannot be influenced, since it is determined in the course of precursor synthesis. Namely, type ST2 sodium titanate is produced from metatitanic acid, which itself is produced in the course of black liquor hydrolysis. As was shown in a previous section the metatitanic acid consists of small anatase nanoparticles the size of which is determined by the amount of anatase seeds added to the black liquor prior to its hydrolysis. Therefore, in order to produce anatase nanoparticles of varying sizes using the gel-sol synthesis approach and type ST2 sodium titanate, the metatitanic acid must first be engineered. This metatitanic acid can be engineered using anatase seed inoculation, while the following gel-sol synthesis using type ST2 sodium titanate enables only the production of a final acidic suspension containing well-dispersed anatase nanoparticles.

It was concluded that phase-pure anatase can be easily produced by performing the gel-sol reaction using ST2 sodium titanate as the precursor and hydrochloric acid as the mineral acid. The resulting nanoparticles are polycrystalline, consisting of very small, approximately 5 nm in size, crystallites that are aggregated to form the anatase nanoparticles, as shown in Figure 48. The anatase nanoparticles size is the same as the size of the anatase nanoparticles in the metatitanic acid from which the ST2 sodium titanate is produced.

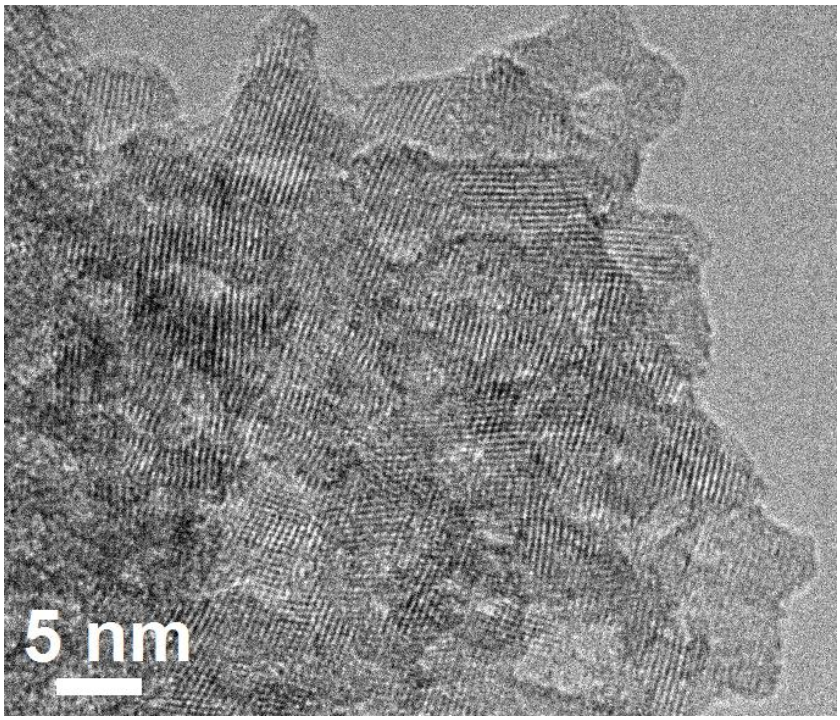

Figure 48: *HRTEM image of an individual anatase nanoparticle as produced by the gel-sol method using type ST2 sodium titanate and hydrochloric acid.*

The anatase nanoparticles produced using ST2 sodium titanate as the precursor in the gel-sol reaction are named type B2 nanoparticles throughout the thesis.

4.1.3 Hydrothermal synthesis of TiO_2 nanoparticles

The hydrothermal synthesis was performed in order to acquire a highly-crystalline material in anatase form. The starting material for the hydrothermal reaction was the acidic suspension of polycrystalline anatase nanoparticles (either type A or type B2).

Based on what is known about the mechanism of hydrothermal synthesis, it is essential that an appropriate pH value is set so that the material that is autoclaved may dissolve and subsequently crystallize into the final product. Neutral and basic conditions seem to be the most appropriate to form the anatase [85, 89, 96, 116]. The problem that arises when using the acidic suspension of TiO_2 nanoparticles as the starting material is the fact that by adjusting an appropriate neutral/basic pH value nanoparticles agglomerate. Therefore, the first thing that had to be solved in order to perform the hydrothermal synthesis was the prevention of TiO_2 nanoparticles agglomeration, which normally occurs when changing the pH value.

The problem was addressed by adding a suitable dispersant into the acidic TiO_2 suspension and raising the pH to the desired value. If the dispersing agent exhibits appropriate properties, it prevents nanoparticle agglomeration via a specific stabilization mechanism (electrostatic, steric or electrosteric stabilization). A vast array of commercially available dispersing agents was tested, ranging from organic to inorganic. The ability to prevent TiO_2 nanoparticle agglomeration was analyzed by DLS measurements. The most appropriate dispersing agent has proven to be sodium polyfosfate, $Na_5P_3O_{10}$, which was used in all the stabilization experiments carried out to prepare a suitable suspension form that was later on subjected to hydrothermal synthesis.

In order to prepare a well-dispersed nanoparticle suspension, a sufficient amount of the dispersing agent had to be added. The experiments showed that a suitable amount of the dispersing agent was 10 – 20 % (relative to the TiO_2 in suspension), which, although high, has proven to prevent drastic nanoparticle agglomeration as seen from the DLS measurements in Figure 49.

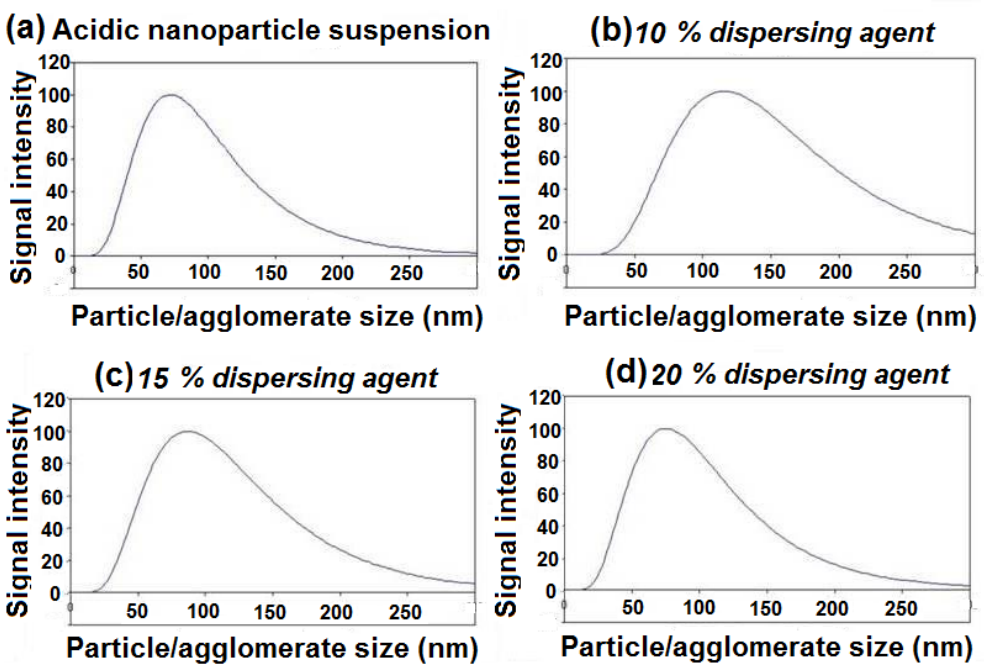

Figure 49: *DLS measurements of anatase nanoparticle suspensions after neutralization to basic pH value.* (a) The starting acidic anatase suspension. (b) Anatase suspension after neutralization with 10 % dispersing agent. (c) Anatase suspension after neutralization with 15 % dispersing agent. (d) Anatase suspension after neutralization with 20 % dispersing agent.

As can be seen from Figure 49 the dispersing agent (sodium polyfosfate, $Na_5P_3O_{10}$) acts well in preventing anatase nanoparticle agglomeration during neutralization. The agglomeration may be controlled by adjusting the amount of the dispersing agent. At a lower dispersing-agent amount the nanoparticle agglomeration is more considerable as may be seen from Figure 49 (b). But when the amount of the dispersing agent is increased, agglomeration becomes less evident. If enough of the dispersing agent is added the nanoparticle agglomeration may be averted as seen in Figure 49 (d).

Stabilization experiments were performed with anatase suspensions having varying TiO_2 concentrations. We observed that the degree of agglomeration is not dependent on TiO_2 concentration if the amount of dispersing agent was held constant. Based on these results it was decided that all the stabilization experiments will be carried out with 250 g/L of TiO_2. These suspensions were the precursor suspensions for the hydrothermal synthesis. First we carried out the experiments for the hydrothermal synthesis of suspensions having varying pH value. The other reaction parameters, hydrothermal synthesis temperature and the reaction time, were set to 240 °C and 10 h, respectively. The pH values during hydrothermal synthesis and the characteristics of the synthesized nanoparticles (particle size, morphology, crystal structure) are given in the Table 7.

Table 7: *Summary of the results for the hydrothermal synthesis of TiO_2 nanoparticles.* The results provided in Table 7 are based on synthesis reactions where the pH value of the suspensions was varied.

pH value	***Crystal Structure***	***Crystallinity***	***Particle size (Scherrer/TEM) / nm***	***Particle Morphology***
5	A	Crystals + amorphous phase	10	/
6	A	Crystals + amorphous phase	10	/
7	A	Crystals + amorphous phase	13	/
7.5	A	Crystals + amorphous phase	15	/
8	A	Crystals + amorphous phase	20	/
8.5	A	Crystals + amorphous phase	25	/
9	A	Monocrystalline	~ 30	Spherical
9.5	A	Monocrystalline	~ 30	Spherical
10	A	Monocrystalline	~ 30	Spherical
10.5	A	Monocrystalline	~ 30	Spherical
11	A	Monocrystalline	~ 30	Spherical
11.5	A	Monocrystalline	~ 30	Spherical
12	A	Monocrystalline	~ 30	Spherical

As can be seen from Table 7, the pH value is one of the most important parameters in hydrothermal synthesis, since it determines not only the final material crystal structure, but also affects the crystallinity. It should be noted that if the pH value is set to an inappropriate value, the formed particles are less crystalline, to some extent even amorphous. This is probably due to the fact, that the hydrothermal synthesis proceeds via a dissolution-crystallization mechanism, where the pH value considerably determines both, the dissolution process and also the crystallization process kinetics. On the other hand, the reaction time and the temperature also play a crucial role in the hydrothermal synthesis. Consequently, it is only reasonable to assume that a prolonged time and an elevated reaction temperature lead to the formation of a well-crystallised product even when the pH value is not set accordingly.

The experiments proved that a well-crystalline product may be already acquired at a reaction temperature as low as 130 ºC, however in this case the reaction time is prolonged to about 24 h. Given the fact that a relatively fast synthesis procedure was one of the main goals of our experiments, we have chosen to perform the hydrothermal method at a temperature of 240 ºC for which the reaction time is about 10 h. These reaction parameters were used throughout the hydrothermal synthesis experiments.

One more interesting observation is also the fact that the TiO_2 concentration seems to have little or no effect on the final nanoparticle size. This is why throughout the course of the hydrothermal synthesis, the TiO_2 concentration was set to approximately 250 g/L.

To sum up, we have succeeded in developing a simple hydrothermal synthesis route with which we have converted the polycrystalline TiO_2 nanoparticles as-prepared with the gel-sol reaction, into a highly crystalline anatase product as seen from SEM images and the inset XRD diffractograms in Figure 50.

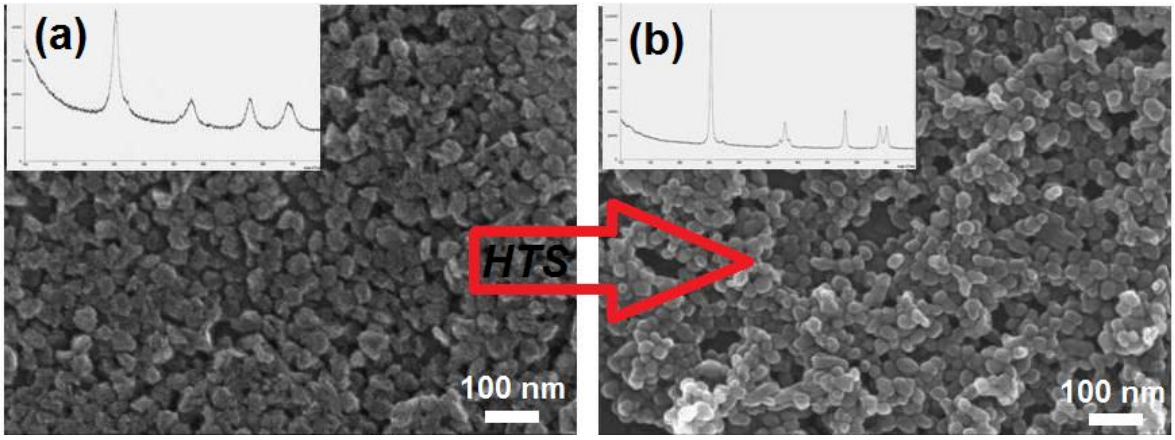

Figure 50: *SEM images with inset XRD diffractograms of TiO_2 nanoparticles prior to and after the hydrothermal synthesis.* (a) SEM image of the precursor TiO_2 nanoparticles used to perform the hydrothermal synthesis. The precursor TiO_2 particles are polycrystalline in nature. (b) SEM image of the monocrystalline TiO_2 nanoparticles as-prepared with the hydrothermal synthesis.

The inset XRD diffractograms in Figure 50 correspond to the anatase crystal structure which was confirmed using the ‘’Database of Raman spectroscopy, X-ray diffraction and chemistry data for minerals’’ [200]. The XRD diffractograms differ in peak width which is contributed to the difference in respective crystallite sizes. The HTS prepared anatase particles are monocrystalline and the XRD diffractogram peaks are consequently narrower than with the precursor (polycrystalline) anatase.

The obtained anatase nanoparticles were additionally observed by TEM. As can be seen from the HRTEM image (Figure 51), the TiO_2 nanoparticles are nearly spherical and are highly crystalline with no visible surface amorphous films.

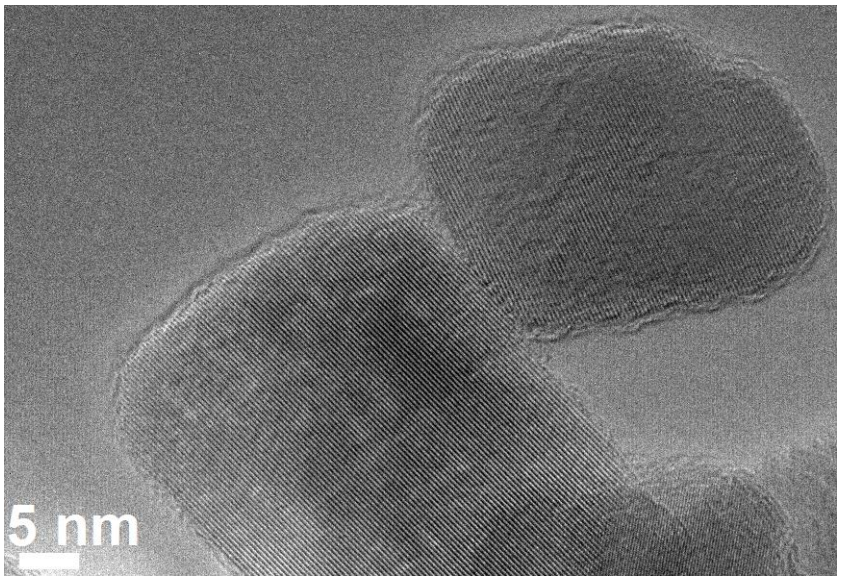

Figure 51: *HRTEM image of anatase nanoparticles as-prepared with the hydrothermal method.*

The monocrystalline anatase nanoparticles produced using the hydrothermal reaction are named type C nanoparticles throughout the thesis.

4.1.4 Synthesis methods summary

For the summary of the reaction synthesis methods used to prepare TiO_2 nanoparticles, the most important reaction parameters and the TiO_2 nanoparticle characteristics are given in Table 8.

Table 8: *Summary for the synthesis methods used to produce TiO_2 nanoparticles, the main reaction parameters and the most important nanoparticle characteristics.*

Synthesis method/ Precursor type	***Reaction temperature / °C***	***Reaction medium pH value***	***TiO_2 concentration range / g/L***	***Reaction time / h***	***Crystal structure***	***Crystallite size / nm***	***Crystallinity***
Sol-gel synthesis/ titanyl sulphate solution	< 100	< 1	24 – 130	< 3	***A*** ***A+R*** ***R***	5 **(Rutile)** Anisotropic morphology	Polycrystalline
Gel-sol synthesis/ metatitanic acid + $BaCl_2$(aq) ***Type A TiO_2 nanoparticles***	< 100	< 1	10 – 500	< 3	***A***	5 **(Anatase)** Spherical morphology	Polycrystalline
Gel-sol synthesis/type ST1 sodium titanate ***Type B1 TiO_2 nanoparticles***	< 100	< 1	10 – 200	< 3	***A*** ***A+R*** ***R***	5 – 10 nm in width and 60 – 140 nm in length **(Rutile)** Anisotropic morphology	Polycrystalline
Gel-sol synthesis/type ST2 sodium titanate ***Type B2 TiO_2 nanoparticles***	< 100	< 1	10 – 200	< 3	***A***	5 **(Anatase)** Spherical morphology	Polycrystalline
Hydrothermal synthesis/gel-sol derived anatase nanoparticles in neutral – basic suspensions ***Type C TiO_2 nanoparticles***	120 – 240	9 – 12	10 – 50	10 – 24 (dependent on the HTS temperature)	***A***	30 **(Anatase)** Spherical morphology	Monocrystalline

4.2 Photovoltaic applications of TiO_2 nanoparticles

4.2.1 Measurements of the photocatalytic activity of synthesized TiO_2 nanoparticles

The photocatalytic activity of TiO_2 nanoparticles was determined at the University of Nova Gorica (UNG). The photocatalytic activity of the TiO_2 nanoparticles had to be determined to choose the material that would be most appropriate to prepare the final photocatalytically active coatings.

The photocatalytic activity of TiO_2 nanoparticles was determined for the following types:

- type A TiO_2
- type B1 TiO_2
- type B2 TiO_2
- type C TiO_2

Types A and B2 do not differ much in the basic particle properties (crystallinity, morphology, particle size). Nevertheless, the type A TiO_2 was found to be easily engineered when it comes to particle size, giving it an advantage when it comes to material properties variability. Also, the type C anatase is very interesting as a possible high-performance photocatalyst, since it is in monocrystalline form. This is beneficial since exciton recombination reactions are hindered when compared to the polycrystalline type (A and B2) [165–168]. Although rutile is known to be a less potent photocatalyst than anatase, the rutile nanoparticles show promise with the photocatalysis application since they absorb UV radiation at a higher wavelength. From the two rutile types that we successfully synthesized, only type B1 was studied for its photocatalytic performance. The sol-gel synthesized rutile nanoparticles were excluded from the photocatalytic activity measurements. The decision was based on the fact that the gel-sol synthesis produces smaller rutile nanoparticles, which should be better photocatalysts because of their higher specific surface.

4.2.1.1 Measurement of photocatalytic activity of type A and B2 anatase nanoparticles

Type A and B2 anatase nanoparticles do not differ significantly in their characteristics. Furthermore, type A and B2 nanoparticles both originate from the same precursor (metatitanic acid) and the difference between the two types is only in the synthesis method with which we produce a well-dispersed nanoparticle suspension. Therefore, type A and B2 anatase nanoparticles were tested for their photocatalytic activity in parallel and compared for their respective results. The results of the photocatalytic activity of type A and B2 anatase nanoparticles are shown in Figure 52 and were determined by the quantitative method of the organic TPA (terephthalic acid) layer decomposition into HTPA (hydroxyterephthalic acid) [191]. The type A and B2 anatase suspensions were set to a 100 g/L concentration prior to performing the measurement.

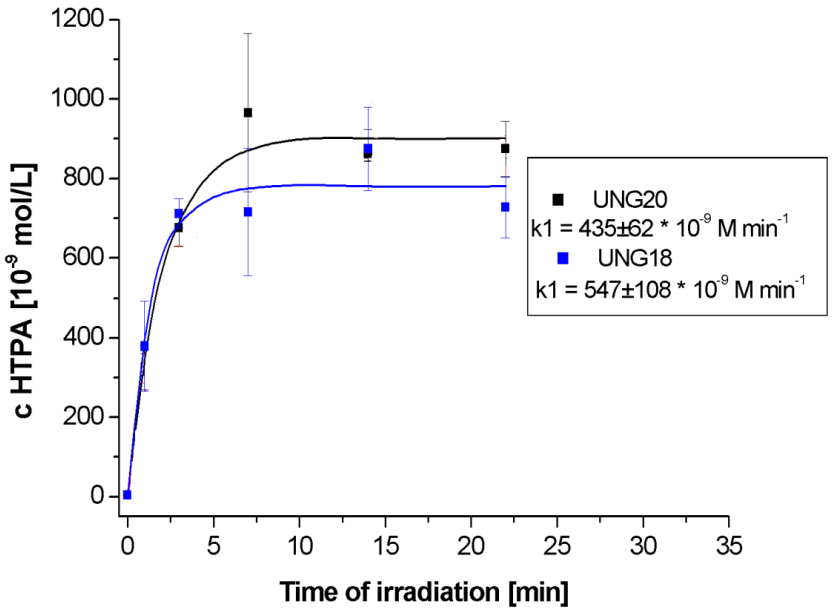

Figure 52: *Photocatalytic activity of type A (UNG 18) and type B2 (UNG 20) anatase nanoparticles as determined by the quantitative method of HTPA formation rate.*

As is seen from the observed HTPA formation rate (k1 value), the type A nanoparticles (UNG 18) show a slightly higher photocatalytic activity (higher k1 value) than the type B2 anatase nanoparticles. The difference in the photocatalytic activity is small, which is reasonable since the respective particle characteristics do not differ significantly if at all. It has to be stressed, that the two samples (UNG 18 and UNG 20) were prepared with the same metatitanic acid type and therefore do not differ in nanoparticle size. The difference between the two types is mainly in the final suspension's chemical composition.

4.2.1.2 Measurement of photocatalytic activity of type B1 rutile nanoparticles

Figure 53 shows photocatalytic activity measurements for type B1 rutile nanoparticles having different size particles. The type B1 rutile suspensions were set to 100 g/L concentration prior to performing the measurement.

The following type B1 rutile nanoparticles were analysed:

- *Susp 29* – synthesized at 70 g/L HCl concentration
- *Susp 30* – synthesized at 90 g/L HCl concentration
- *Susp 31* – synthesized at 110 g/L HCl concentration
- *Susp 32* – synthesized at 130 g/L HCl concentration
- *Susp 33* – synthesized at 150 g/L HCl concentration
- *Susp 34* – synthesized at 70 g/L HCl concentration and NaCl molar concentration 1.5 M

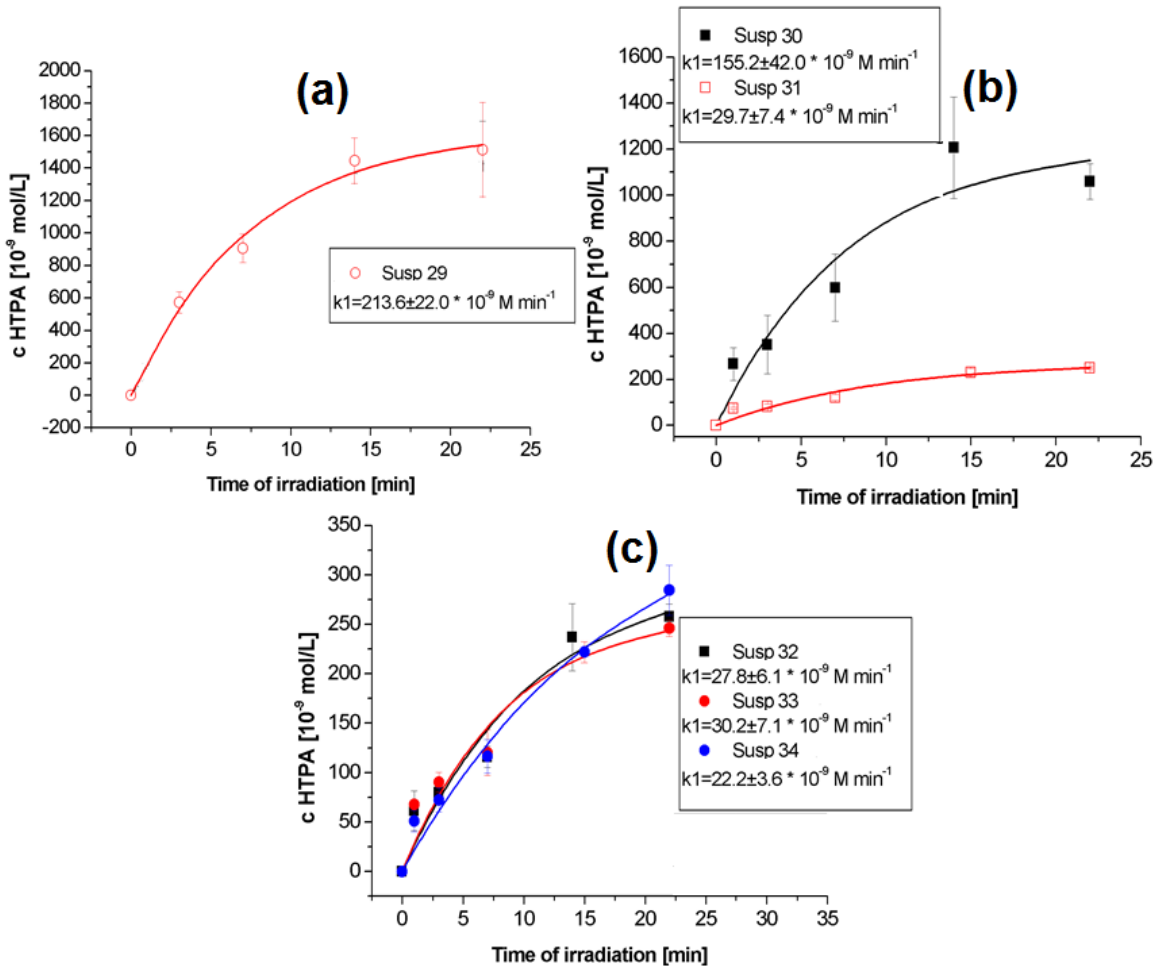

Figure 53: *Photocatalytic activity of type B1 rutile nanoparticles as determined by the quantitative method of HTPA formation rate.* (a) Photocatalytic activity of rutile nanoparticles *Susp 29*. (b) Photocatalytic activity of rutile nanoparticles *Susp 30* and *Susp 31*, respectively. (c) Photocatalytic activity of rutile nanoparticles *Susp 32*, *Susp 33* and *Susp 34*, respectively.

As can be seen from Figure 53 the rutile nanoparticles differ in their respective photocatalytic activities. The difference in photocatalytic activities could arise due to different rutile particle sizes. Consequently, the specific surface area can change considerably from one rutile particle size to another, which affects the overall photocatalytic performance.

But when compared to the photocatalytic activity of type A and B2 anatase nanoparticles, rutile nanoparticles show considerably lower activities. This is in accordance with previous studies and is based on the many differences in the physical characteristics between anatase and rutile.

4.2.1.3 Measurement of photocatalytic activity of type C anatase nanoparticles

Figure 54 shows the photocatalytic activity measurements for type C anatase nanoparticles prepared with the hydrothermal method. The TiO_2 nanoparticles in precursor suspensions were stabilized with 10, 15 and 20 % of $Na_5P_3O_{10}$ dispersant so as to prevent their agglomeration during pH value adjustment. The type C anatase suspensions were set to a 100 g/L concentration prior to performing the measurement.

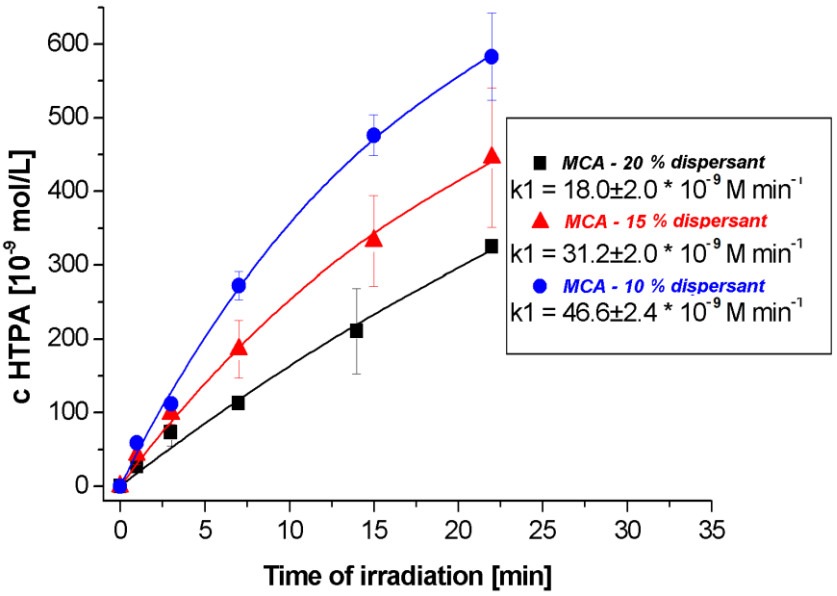

Figure 54: *Photocatalytic activity of type C anatase nanoparticles as determined by the quantitative method of HTPA formation rate.*

As can be seen from the photocatalysis measurements presented in Figure 54, the monocrystalline anatase nanoparticles seem to have a rather low photocatalytic activity when compared to types A and B2 anatase or even when compared to type B1 rutile.

There are several possible reasons. As was already stated, the performance of a TiO_2 photocatalyst is mainly determined by the processes of impurity adsorption and charge separation. Since a rather large amount of the dispersant was used, it is plausible that a great deal of TiO_2 adsorption sites may be occupied and thus the photocatalyst performs worse than expected. Even though the monocrystalline TiO_2 nanoparticles have been washed extensively after the hydrothermal reaction by centrifugation cycles, the dispersant cannot be removed entirely. This is confirmed with the observed differences in the photocatalytic activity of the monocrystalline nanoparticles that were stabilized with different amounts of the dispersing agent. It seems that the adsorption of the organic pollutant, the TPA, is hindered by the dispersant, which lowers the overall activity. If the dispersing agent could be removed entirely by centrifuging, then there would probably be none of the observed differences in photocatalytic activity.

Furthermore, as was also noted, there is still some discrepancy as to which TiO_2 properties are the most important in promoting (or hindering) the photocatalytic activity. The monocrystalline TiO_2 form could be more appropriate since the exciton recombination rate is lower [165]. Also, the bandgap value of the monocrystalline TiO_2 form is smaller than with a TiO_2 photocatalyst with very small crystallite sizes where a bandgap shift, ΔE_g, is observed [175, 176]. On the other hand, the charge carriers can migrate more easily onto the surface and access charge-trapping sites in smaller particles rather than in larger ones [166].

Overall, our results show that the rate of organic pollutant adsorption could be the photocatalytic efficiency-determining parameter, since the observed difference in activities of type A, B2 and type C anatase can hardly be attributed to charge-separation dynamics.

Of the TiO_2 nanoparticles that were tested the most active photocatalyst seems to be the type A and B2 anatase nanoparticles. Because there is really no significant difference in their respective characteristics since both types emanate from the same precursor (metatitanic acid), there was no preference to choose one type over the other. Nevertheless, we decided to prepare the final photocatalytically active coatings using type

A anatase nanoparticles. The type A anatase nanoparticles were prepared using different metatitanic acid types. The difference in metatitanic acid types is in the anatase nanoparticle size, which arises due to different anatase seeding volumes in the course of its synthesis. By using different size type A anatase nanoparticles in the final coatings, we tried to determine the optimal nanoparticle size that is best suited for the application.

4.2.2 Photocatalytic coatings for Si solar modules

The photocatalytic coatings were prepared at UNG using the A type anatase nanoparticles. The coatings were prepared using a wet chemical method [190]. The coating was applied onto glass substrates and as well as onto commercially available Si solar modules in order to test the possibility of retaining long-term efficiency due to the ability of the coating to photocatalytically decompose organic matter and to enable rinsing off of any inorganic particles. The glass substrates and the solar modules were tested under various weather conditions.

Figure 55: *Si solar modules and glass substrates that were used to determine the photocatalytic activity of the coatings.*

Since the surface of the glass substrate and Si modules is quite large and since the glass itself is tempered, only the contact angle measurements were performed to determine the initial photocatalytic activity of the coatings.

The photocatalytic activity of the coatings was determined on glass substrates first. The coatings on glass substrates were prepared using type A anatase nanoparticles that differ in their respective sizes.

The following coatings were prepared:

- NTi1, and both NTi2 and NTi3, were prepared with anatase nanoparticles synthesized with a seeding volume of 0.3 and 0.6 %, respectively. No additional thermal treatment of the coating was applied.
- NTi4, NTi5 and NTi6 were prepared with anatase nanoparticles synthesized with a seeding volume of 1.8 and 0.6 % and 0.3 %, respectively, and were used to test the effect of the particle size on the photocatalytic activity of the final coating. The three coating types were also thermally treated at 450 ºC (30 min) to achieve a good adhesion on the glass substrate.

Figure 56 shows that the samples NTi1 and NTi2 decompose the methyl stearate test pollutant rapidly, since the water contact angle fell after less than one hour of UVA

irradiation from the initial hydrophobic value, characteristic for the fatty deposit, to the final hydrophilic value, characteristic for clean and hydroxylated TiO_2. The sample coating NTi1 performed slightly better than the sample coating NTi2, which can be attributed to the fact that the layer thickness differs for the two samples. This could be due to the fact that the anatase nanoparticles differ in size since they were prepared using 0.3 and 0.6 % seeding volume, respectively. However, the difference in layer thickness was not examined. The slight difference in the photocatalytic activity of the NTi1 and NTi2 coatings could also be a direct result of the fact that anatase nanoparticles differ in size. The anatase nanoparticles used for the NTi1 coating are depicted in Figure 26 (d), the anatase nanoparticles used for NTi2 coating in Figure 26 (c). Our results indicate that the anatase nanoparticles depicted in Figure 26 (d) could be slightly more photocatalytically active than the anatase nanoparticles depicted in Figure 26 (c). However, raw anatase nanoparticles were not analysed for their photocatalytic activity and therefore the difference in the photocatalytic activity for the NTi1 and NTi2 coating cannot be adequately addressed. Sample coating NTi3 performed worse even though the coatings were additionally thermally treated in order to enhance the particle crystallinity and adhesion to the substrate. Such worsening in performance can be attributed to the fact that a thermal treatment was used. It is possible that during the treatment the nanoparticles present in the coating became larger due to sintering, which lowered their specific surface and consequently the photocatalytic activity of the coating as a whole. Since anatase nanoparticles are well crystallised at the beginning, the thermal treatment does not contribute to their crystallinity and thus does not enhance it.

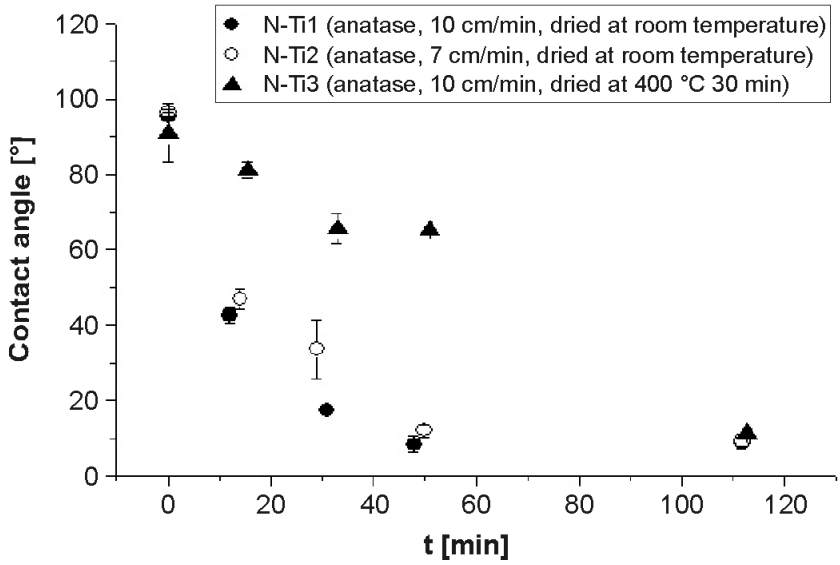

Figure 56: *Contact-angle measurements for self-cleaning coatings prepared from anatase nanoparticles presented in Figure 26 (c) using a soft-chemical method.* Water contact angles were measured after different times of irradiation of the coatings covered by methyl stearate layer.

As one can see (Figure 57) the photocatalytic activity of the anatase nanoparticles depends greatly on the synthesis procedure, i.e., on the seeding volume used for the secondary nucleation during the nanoparticle synthesis. Although the nanoparticles synthesized using the 1.8 % seeding volume (NTi4 coating) are smaller in size and thus have a greater specific surface, they performed worse in comparison to the nanoparticles that were synthesized using the 0.6 % seeding volume (NTi5 coating). This can be explained by the fact that the hydrolysis and polycondensation reactions during the synthesis are carried out more rapidly when using a greater seeding volume, which consequently influences the overall crystallinity of the final product. Since the

hydrolysis/polycondensation reactions were very fast when the 1.8 % seeding volume was used, it can be assumed that the product crystallinity is worse since the kinetics of the reaction do not allow the crystal structure to be fully developed during the synthesis. Therefore, smaller seeding volumes are necessary and provide a better nanoparticulate anatase, which is suitable for self-cleaning applications. However, it seems that a smaller seeding volume of 0.3 % produces a photocatalytically more active anatase than the 0.6 % seeding volume since the NTi6 coating (anatase prepared with 0.3 % seeding volume) performs better than the NTi5 coating (anatase prepared with 0.6 % seeding volume).

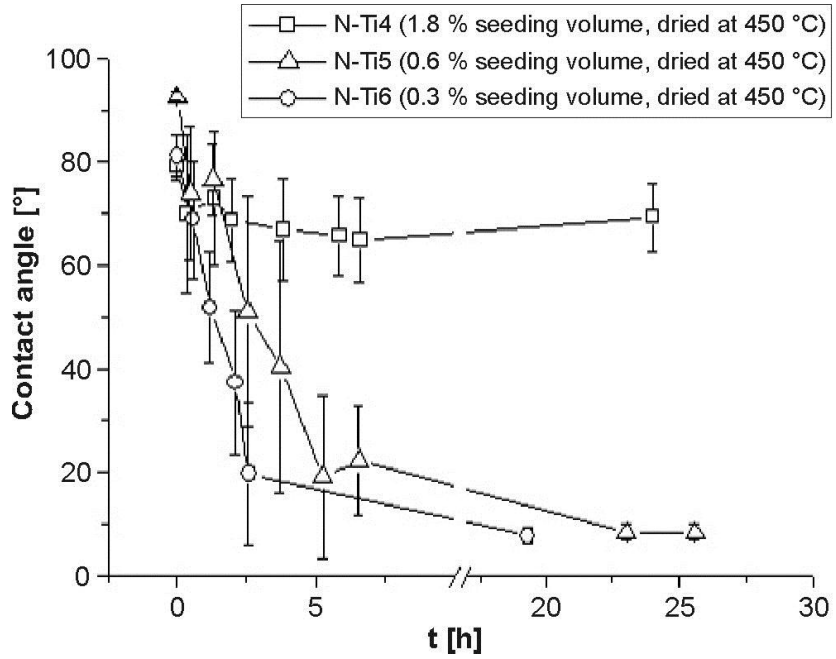

Figure 57: *Contact-angle measurements for different coatings prepared from anatase nanoparticles using a soft-chemical method.* The anatase nanoparticles were prepared using different seeding volumes during the synthesis and therefore differ in size. Water contact angles were measured after different times of irradiation of the coatings covered by the methyl stearate layer.

To prepare the final coatings only type A anatase nanoparticles prepared with 0.3 % seeding volume were used. The coatings were not additionally thermally treated.
A measurement of the photocatalytic activity of the coating on a glass substrate is shown in Figure 58.

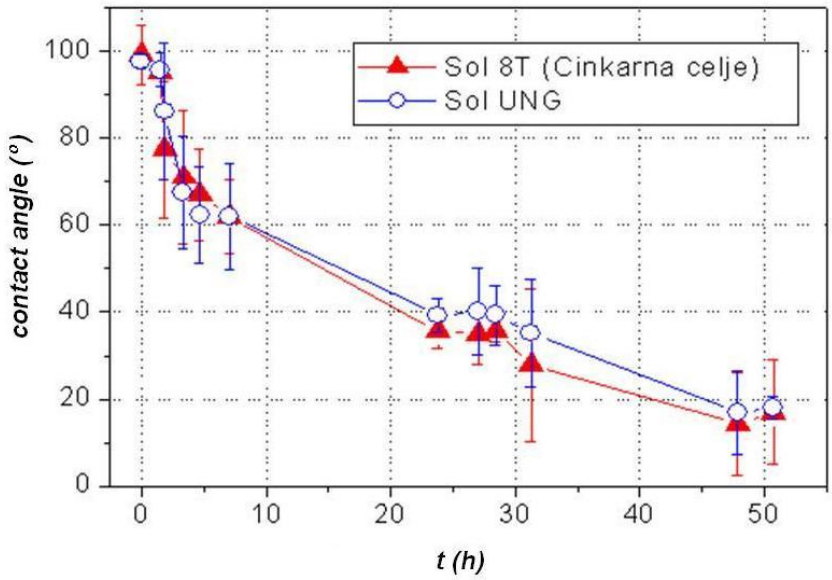

Figure 58: *Photocatalytic activity of the coating prepared with type A anatase nanoparticles (0.3 % seeding volume). The coating was not thermally treated.*

As can be seen from Figure 58, the coating prepared using the A anatase nanoparticles is effective in the decomposition of methyl stearate. It is as effective and even slightly more effective, than the coating prepared using TiO_2 nanoparticles synthesised with a reflux acidic method developed at UNG [190]. The latter coating was made for a comparison of the photocatalytic activity between the two TiO_2 types.

The superhydrophilic effect (PSH) of the coating was not quantitatively measured, but was nevertheless observed on the glass substrates. The PSH effect of the photocatalytic coatings is shown in Figure 59.

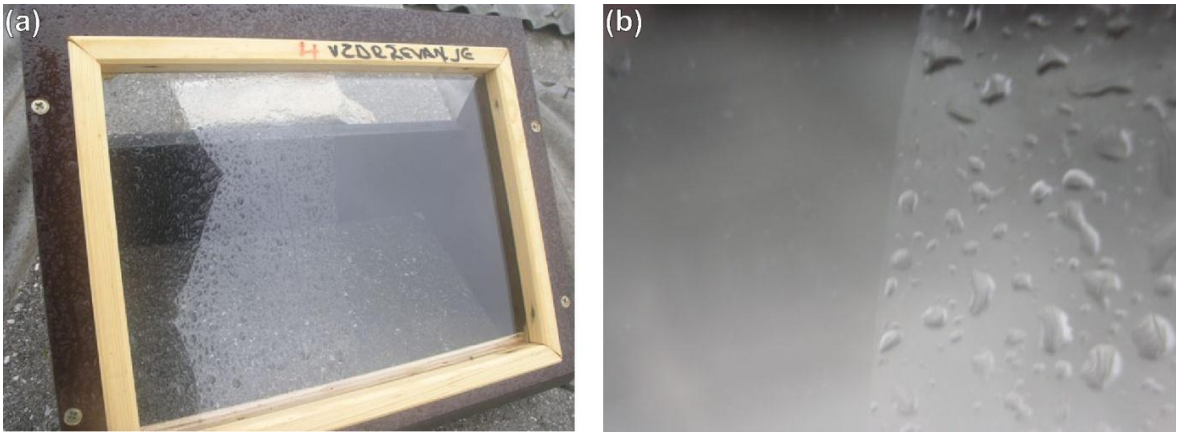

Figure 59: *Glass substrates treated with self-cleaning coating and placed in real-life environmental conditions (a).* The coatings exhibit the super-hydrophilic effect, which is depicted clearly in image (b), where a clear distinction between the treated (super-hydrophilic) and untreated (water droplets) surface is shown.

Since the TiO_2 coatings exhibited both the photocatalytic activity and the superhydrophilic effect (PSH), it is reasonable to expect that the coatings would remove possible organic and inorganic pollutants that could soil the substrate surfaces. This is why we followed the time dependence of the efficiency of the Si solar modules in order to determine whether the coating would help in sustaining the initial light-to-electricity conversion efficiencies over a long period of time. The short time response of the Si solar

modules (one with and one without the TiO_2 coating) under real weather conditions is shown in Figure 60.

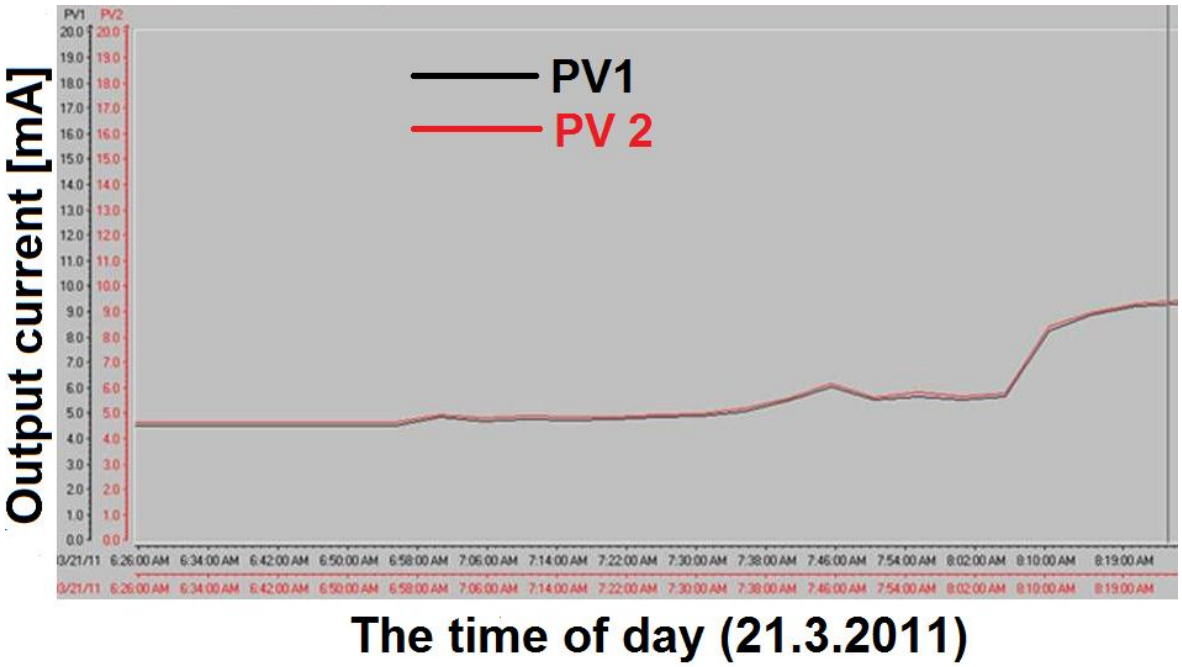

Figure 60: *PV module current output for the coated and the uncoated Si solar module on 21.3.2011*. The coated PV module is presented by the red curve (PV1), while the uncoated PV module is presented by the black curve (PV2).

As can be seen in Figure 60, there is no observable difference in the light-to-electricity conversion between the uncoated (PV1) and the TiO_2 coated (PV2) Si modules. Although the coated module could have a slightly lesser efficiency than the uncoated module due to TiO_2 UV light absorption, the latter effect seems to be hindered by the mere fact that the amount of UV light in the sunlight spectra is insignificant compared to the amount of the visible light spectra.

The measuring of the light-to-electricity conversion efficiency was also done over a longer period of time. After about two months, the difference in the electricity output for the two Si modules was as shown in Figure 61.

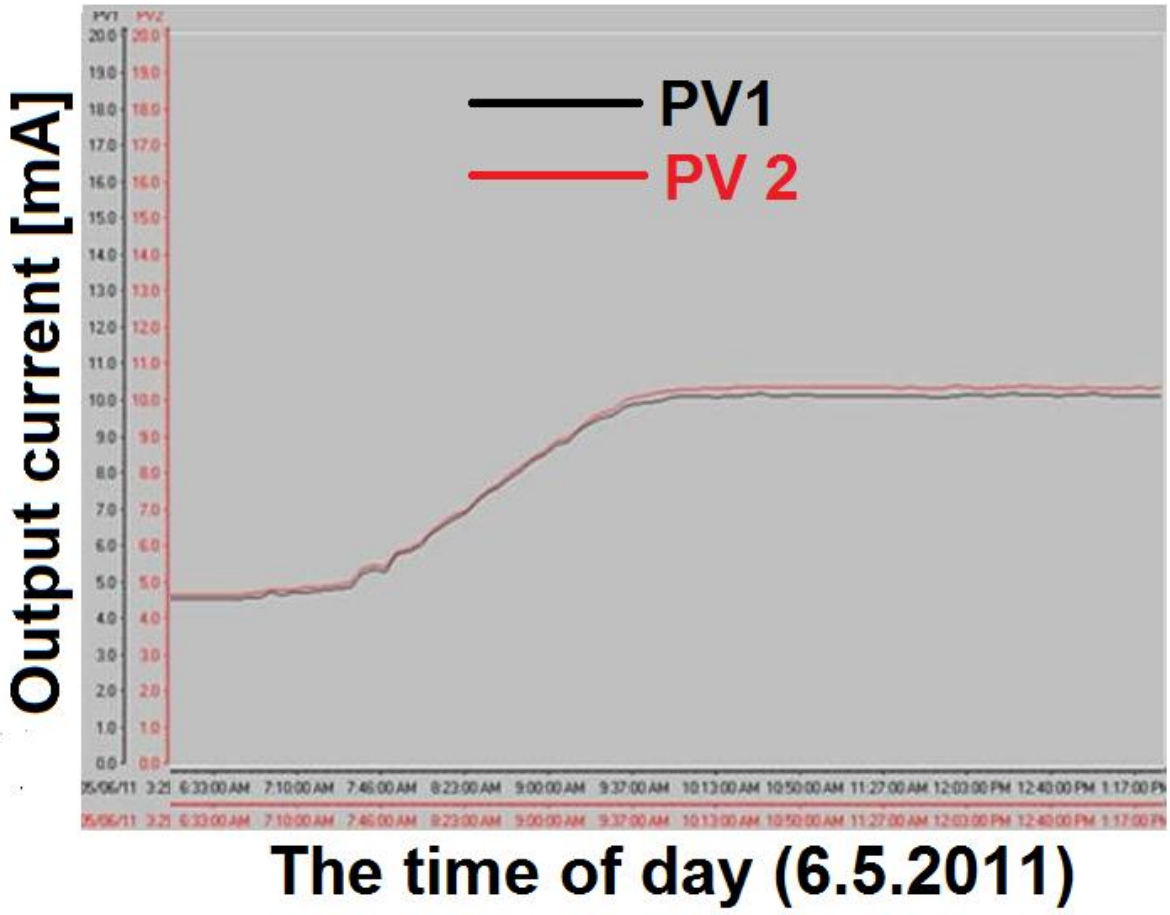

Figure 61: *PV module current output for the coated and the uncoated Si solar module on 6.5.2011*. The coated PV module is presented by the red curve (PV1), while the uncoated PV module is presented by the black curve (PV2).

It can be seen that the difference in electricity production output was still quite small, which was surprising since the testing environment was subjected to real-life changes in weather and to possible dusting and soiling.

The lack of a more significant difference in the electricity production output measurement between the modules could be due to too a small sensitivity of the measuring technique or, on the other hand, due to the coating itself, which could lose its initial PSH and photocatalytic activity.

The latter was tested by performing tests for photocatalytic performance measurements using the resazurin dye. The dye was stained onto the coated glass substrates which were subjected to the same conditions as the solar modules. If the TiO_2 coating was to lose its activity or was even mechanically washed away due to improper and inadequate adhesion, the resazurin dye would not decompose and no observable change in colour would occur (Figure 62).

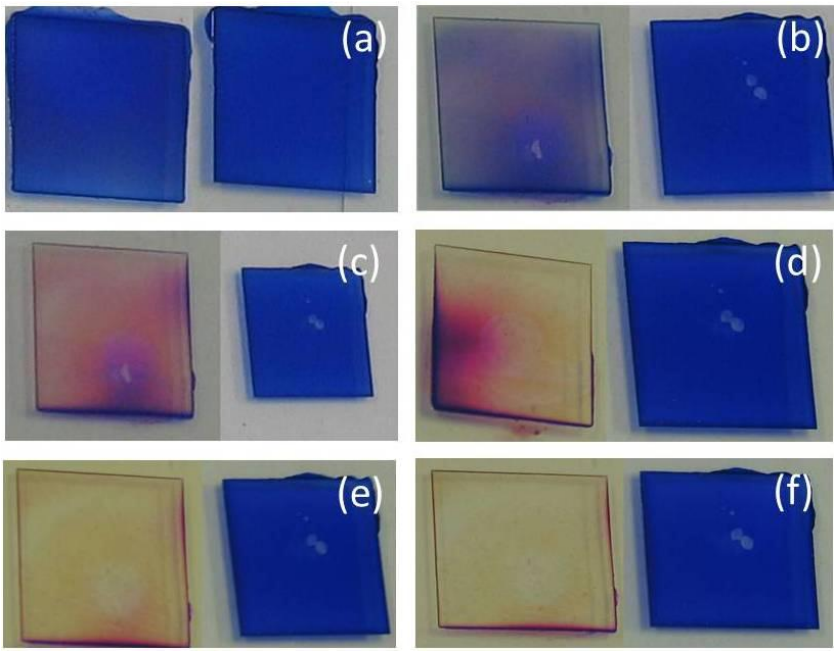

Figure 62: *The resazurin decomposition test after (a) 0 min, (b) 2.5 min, (c) 5 min, (d) 7.5 min, (e) 12.5 min and (f) 20 min.* As can be seen, the resazurin dye decomposes when UV illumination is applied, which clearly indicates that the TiO_2 layer remained active and mechanically stable.

As seen from Figure 62, the resazurin test confirmed that the TiO_2 coating was still present and photocatalytically active after two months of exposure to real-life weather conditions. The presence of the TiO_2 coating was additionally confirmed by SEM of the glass surface (Figure 63).

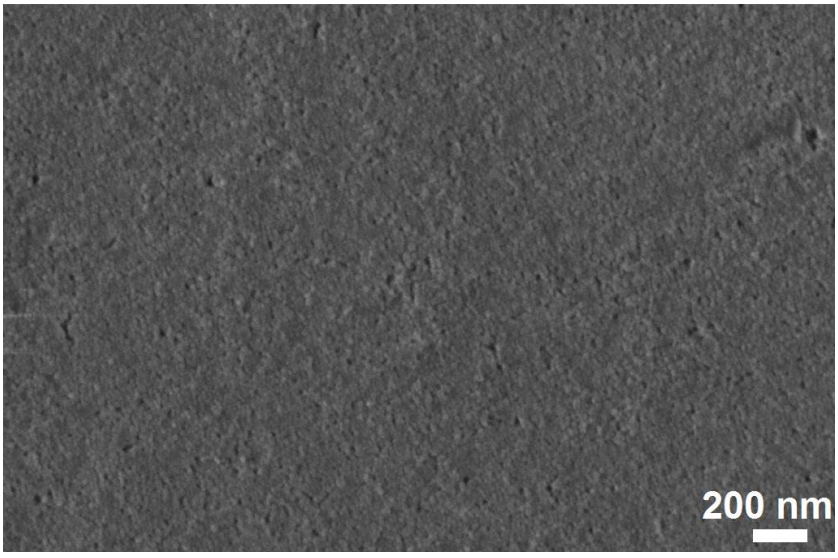

Figure 63: *SEM image of the photocatalytic coating on the glass substrate surface.*

Since the TiO_2 coating retained its photocatalytic activity the main reason for the similar efficiencies of the Si solar modules were attributed to the loss of the superhydrophilic effect (PSH) of the coating. Indeed, as can be seen from Figure 64, the PSH effect of the coating cannot be observed after a prolonged period of time, or, at best, it is only slightly observable.

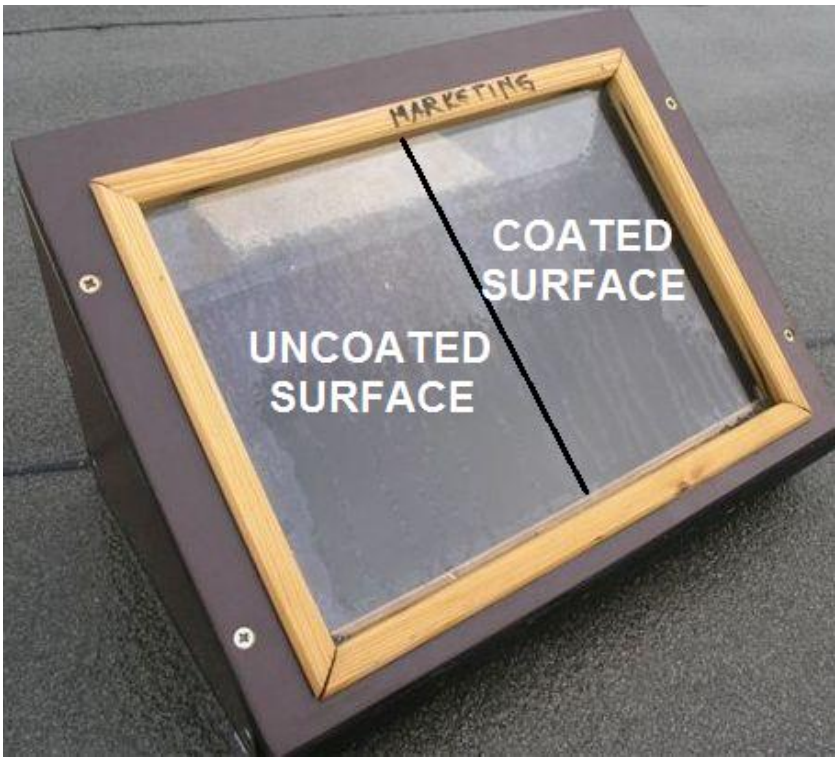

Figure 64: *Glass surface after two months exposure to real-life environmental conditions.* The PSH effect of the coated side is not observable. The coated and the uncoated side of the glass substrate look almost the same.

The reason for the loss of the PSH effect is unclear, but it could be due to the specific composition of the final coating. Especially silica (SiO_2), which is present in the coating, may affect the PSH. Therefore, we conclude that further tests have to be performed, i.e. by varying the initial coating composition and by performing long-term exposure to real-life weather conditions. These are currently under way and will hopefully prove the coating to be both photocatalytically active and able to retain the PSH, which could prove to be beneficial for the proposed Si modules' long-term electrical output increase.

4.2.3 TiO_2 photoanodes for dye-sensitized solar cells (DSSCs)

The DSSC were made using commercially available components (Solaronix). The TiO_2 paste is the only component that was not purchased and was the focus of our research. The goal of our activities was to develop a TiO_2 paste using TiO_2 nanoparticles that were synthesized during the course of the thesis.

The choice of the TiO_2 type that would be used for the TiO_2 paste preparation was made based on a literature review. The preferred TiO_2 crystal structure for DSSC is anatase since it has a larger bandgap and a higher conduction band edge energy, which overall leads to a higher Fermi level and photovoltage [203]. Anatase nanoparticles that were so far tested for DSSC have been synthesized using various methods. For instance, the sol-gel method was also used [141, 142]. But in this case a post-thermal treatment was necessary in order to obtain a monocrystalline TiO_2 product. Monocrystallinity of the TiO_2 nanoparticles seems to be a prerequisite in DSSCs. This can understood on the basis of the processes occurring during DSSC work action. One of the most important features of the DSSC TiO_2 photoanode is the transportation of electrons upon light absorption and

charge separation. The electrons can migrate through the TiO_2 film only if the nanoparticles are well-interconnected and have a suitable electronic structure. This means that defects in the nanoparticle structure, such as grain boundaries, should be absent [204].

Therefore, only type C monocrystalline anatase nanoparticles were used to prepare the TiO_2 paste. TiO_2 paste preparation was based on the Pechini method [146]. The Pechini method is suitable because of its many benefits, namely, it is based on relatively cheap materials, it provides easy handling and it allows the use of water-based TiO_2 slurries. Type C TiO_2 nanoparticles also resemble the P25 TiO_2 (Evonik, Germany). This is advantageous since P25 is known to be a standard material for DSSC paste preparation. The comparison between P25 and C type monocrystalline anatase nanoparticles is provided in Figure 65.

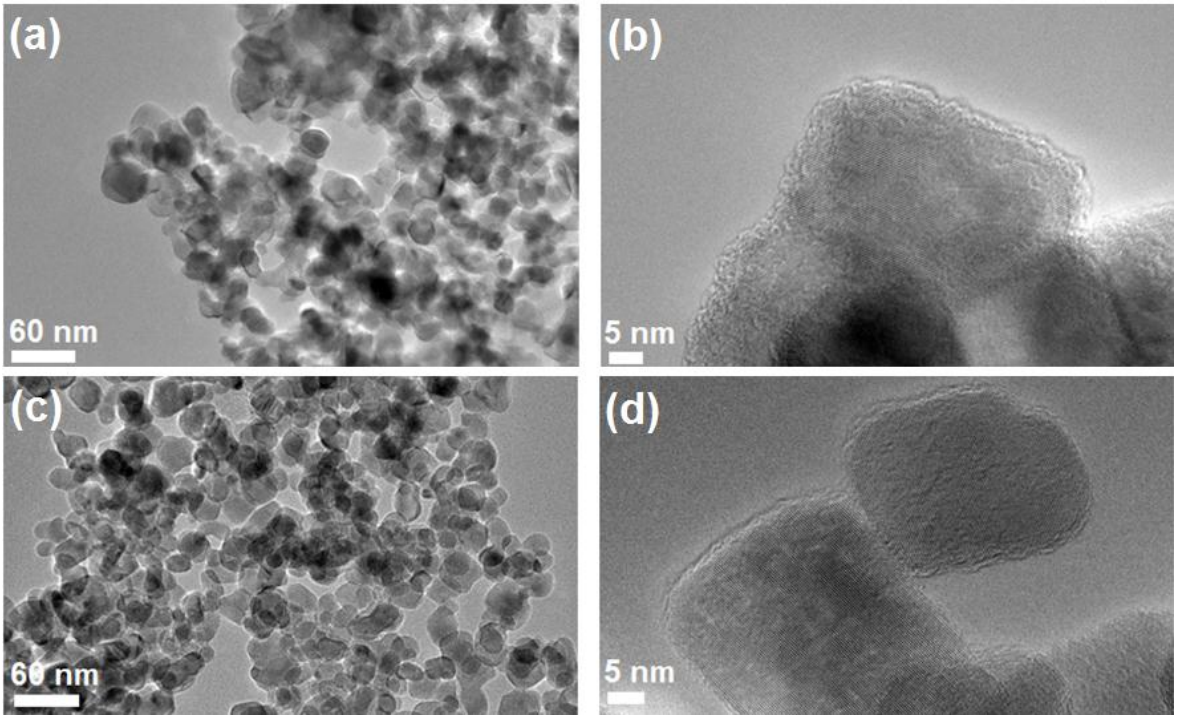

Figure 65: *TEM images of P25 and C type monocrystalline anatase nanoparticles.* (a) Low-magnification TEM image of P25 nanoparticles. (b) HRTEM image of P25 nanoparticles. (c) Low-magnification TEM image of C type anatase nanoparticles. (d) HRTEM image of C type anatase nanoparticles.

The TiO_2 pastes were made as described in the Materials and Methods section, with the polyester being prepared by varying the molar concentrations of metal alkoxide/titanyl sulphate : citric acid : ethylene glycol between 0.5 – 1.5x : 5x : 20x, where X represents a chosen molar amount of any of the components. The molar ratio of the metal alkoxide/titanyl sulphate and TiO_2 nanoparticles added was 1:7.

The results of the efficiencies for the final DSSCs using type C monocrystalline nanoparticles and P25 nanoparticles are given in Table 9. A commercially available TiO_2 paste (Solaronix) was also used in order to compare the efficiencies of the final DSSCs.

Table 9: *DSSC efficiencies for TiO_2 pastes prepared by the Pechini method.* The pastes were made using type C monocrystalline anatase nanoparticles and commercially available P25 nanoparticles. The TiO_2 paste was prepared using either titanyl sulphate (TS) or titanium tetraisopropoxide (TTIP).

Sample	***Metal alkoxide/titanyl sulphate : citric acid : ethylene glycol***	***Voc / V***	***Jsc / mA/cm^2***	***Fill factor / %***	***Efficiency / %***
DSSC 109	1x : 5x : 20x / TS	0.601931	1.94861	58.1118	0.6305
DSSC 110	1x : 5x : 20x / TS	0.612859	0.560472	63.3018	0.2184
DSSC 111	0,5x : 5x : 20x / TS	0.693819	1.138653	54.7069	0.4341
DSSC 112	1,5x : 5x : 20x / TS	0.658409	3.775499	60.7845	1.5175
DSSC 114 / **P25**	1x : 5x : 20x / TS	0.60591	0.618725	37.3003	0.1404
DSSC 115 / **P25**	0,5x : 5x : 20x / TS	0.678028	1.003736	54.1288	0.37
DSSC 116 / **P25**	1,5x : 5x : 20x / TS	0.605075	0.91175	49.7774	0.2758
DSSC 117 / **P25**	1x : 5x : 20x / TTIP	0.768716	5.320565	56.66	2.33
DSSC 120	1x : 5x : 20x / TTIP	0.703125	4.808253	64.03	2.17
DSSC 124	1x : 5x : 20x / TTIP	0.733496	2.225821	67.1039	1.1003
DSSC 125	1.5x : 5x : 20x / TTIP	0.71553	2.884117	67.4928	1.3988
DSSC 126	1.5x : 5x : 20x / TTIP	0.682484	2.959036	50.8717	1.0318
DSSC 127	1.5x : 5x : 20x / TTIP	0.699051	2.86989	50.3183	1.0138
DSSC 133	1.5x : 5x : 20x / TTIP	0.721223	4.408249	59.0094	1.8842
DSSC 134	1.5x : 5x : 20x / TTIP	0.701727	3.353797	54.354	1.2847
DSSC 135	1.5x : 5x : 20x / TTIP	0.71337	3.9367	58.4368	1.6482
DSSC 136	1x : 5x : 20x / TTIP	0.736609	2.70686	59.9795	1.2011
DSSC 137	1.5x : 5x : 20x / TTIP	0.649068	2.029338	63.5427	0.8406
DSSC 138	1.5x : 5x : 20x / TTIP	0.42756	0.350249	58.8158	0.0885
DSSC 139	1.5x : 5x : 20x / TTIP	0.748709	3.701257	59.7528	1.663
DSSC 140	1x : 5x : 20x / TTIP	0.755152	4.109703	56.841	1.7717
DSSC 142	1x : 5x : 20x / TTIP	0.781797	4.401761	62.1186	2.1469
Solaronix TiO_2paste	UNKNOWN COMPOSITION	0.652395	9.585902	59.16	3.72

Based on the results given in Table 9, we can make the following conclusions:

- the titanyl sulphate may be used as a substitute for metal alkoxide (titanium isopropoxide), but seems to perform worse. This may be due to its chemical composition (sulphuric acid present, high ion concentration).
- the composition of the polyester influences the final efficiency. This may be due to TiO_2 nanoparticle characteristics, namely the specific surface area. The metal alkoxide must be added in an optimal amount regarding the surface area of the TiO_2 nanoparticles in the paste. If small nanoparticles are used, then the amount of the added metal alkoxide must be higher and vice versa. Based on the results it seems that an increase in the alkoxide amount increases the overall DSSC efficiency.
- the difference in efficiencies between the type C and P25, a commercially available product known for its high degree of surface purity, is only slight. This may be a confirmation that the C type TiO_2 nanoparticles are appropriate for DSSC TiO_2 paste preparation.

The DSSC photoanodes prepared with the above mentioned TiO_2 pastes were also investigated with SEM to determine their porosity, photoanode thickness and particle agglomeration.

It was observed that the photoanodes differ significantly in some of their properties. A low magnification SEM analysis revealed that some photoanodes form a uniform layer, while some seem to exhibit cracking. The difference between the two cases is shown in Figure 66.

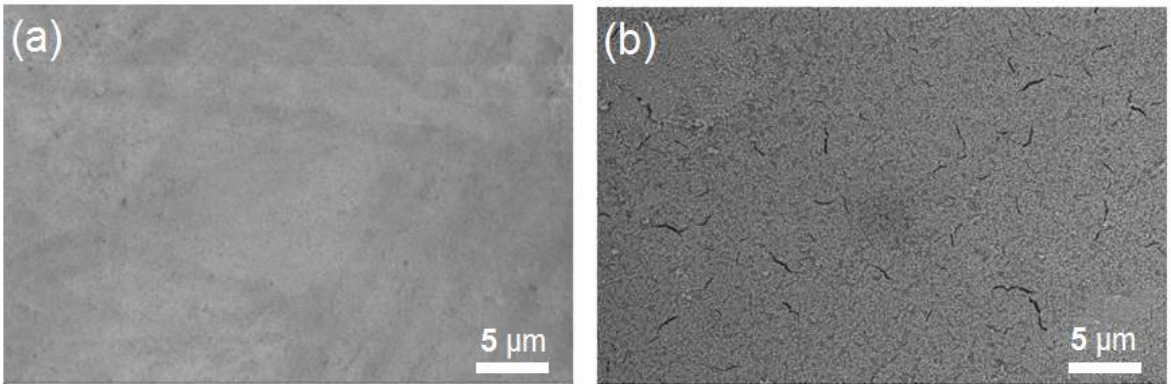

Figure 66: *SEM image of photoanode surface.* (a) Low-magnification SEM image of a photoanode surface which shows no cracking. (b) Low-magnification SEM image of a photoanode surface which shows surface cracking.

The cracking of some DSSC photoanodes could be a reason for the observed differences in DSSC efficiencies. The cracking may be the result of a specific TiO_2 paste composition. It is possible that the high water content (more than 50 % in the TiO_2 slurry) may disturb the process of film formation during the thermal treatment. This is why we could successfully prepare only relatively thin photoanodes. As is seen in Figure 67, the average photoanode film thickness that exhibited no cracking is of the order of 1 – 3 microns, which is less than optimal [203].

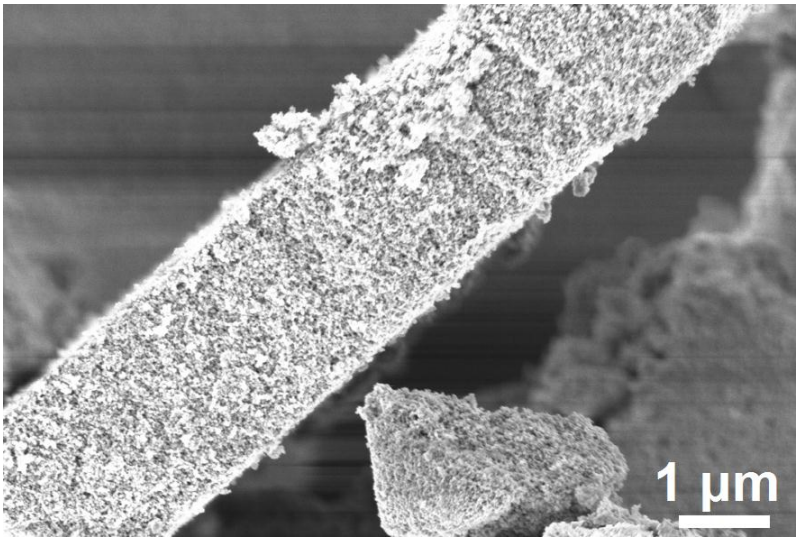

Figure 67: *SEM image of a typical photoanode prepared with the Pechini method.*

It seems that both, film cracking and low photoanode thickness could lower the final DSSC efficiencies considerably. However, the two problems should be addressed more thoroughly in the future. If they are appropriately solved, DSSC efficiencies using TiO_2 pastes based on type C anatase nanoparticles could be much higher.

5 Conclusions

The thesis is a summation of the work done in three different areas, namely TiO_2 nanoparticle synthesis and the development of two TiO_2-based applications in the field of photovoltaics.

The synthesis of TiO_2 nanoparticles was done using materials from the established Sulphate process of TiO_2 pigment production. The synthesis methods were focused on the development of water-based chemical methods with which we may not only suitably determine the material properties (particle size, crystal structure, morphology, crystallinity), but also avoid any post-reaction thermal treatment, which inherently leads to nanoparticle agglomeration, energy consummation and dusting. Out of the possible synthesis methods, three were chosen to be researched, namely the sol-gel method, the gel-sol method and the hydrothermal method. The synthesis type employed was mainly dependent on the material used as a precursor and on the basis of predefining the final TiO_2 properties. Three distinctive materials were used in order to develop nano-TiO_2, which are titanyl sulphate, metatitanic acid and sodium titanate. It has to be noted that the metatitanic acid was used to prepare the titanyl sulphate solution and the sodium titanate precursor.

Using the three material precursors and the above-mentioned synthesis methods, five different methods were implemented.

The **sol-gel method** in which titanyl sulphate was used as the starting material. The method was used successfully and enabled the production of polycrystalline nano-TiO_2 with the rutile crystal structure. Furthermore, the sol-gel method allows control over the particle size and morphology, which may be accomplished by controlling the supersaturation and by adding a small amount of rutile nanoparticles as seeds, respectively.

The **gel-sol method** has proven more successful, since three synthesis methods were successfully developed. It must be pointed out that the first synthesis approach is based on a simple ionic reaction between sulphate ions present in the metatitanic acid and a barium chloride solution, which may not be regarded as a classical gel-sol reaction, since none of the complex reactions of hydrolysis/polycondensation/deoxolation occur. Nevertheless, the metatitanic acid itself is the result of complex sol-gel reactions that take place during the course of its preparation, resulting in a highly viscous gel, which upon barium chloride addition is converted into a very stable nanoparticle suspension (sol phase). In this regard we discussed the synthesis method of a gel-sol type. One main feature of this synthesis method is the possibility to predefine the nanoparticle size. This may be done in the course of metatitanic acid preparation. Based on a specific amount of the anatase seeds added in the course of metatitanic acid preparation, the formed particles may vary in size. It was discovered that the seed inoculation volume is the most important size-determining parameter which allows the production of anatase nanoparticles ranging in size from 30 to 90 nm. This method allows the production of anatase nanoparticles only, since the material crystal structure is already predefined with metatitanic acid.

The other approach of gel-sol synthesis was based on using sodium titanate as the precursor. Two sodium titanate types were used. It was shown that the sodium titanate type importantly determines the final material properties, most significantly, the crystal

structure of TiO_2 nanoparticles. Therefore, both sodium titanate types were individually used to produce a phase-pure rutile and anatase nanoparticles. In the case of rutile nanoparticles, a simple method was also developed that allows size-tailoring. Therefore, rutile nanoparticles with anisotropic morphology were prepared ranging in size from 60 to 160 nm in length and 15 to 50 nm in width. Anatase nanoparticles, on the other hand, were prepared with spherical morphology with a narrow size distribution and an average particle size of about 40 – 50 nm. Anatase nanoparticles are the same as the ones produced by a direct ionic reaction using metatitanic acid. This is because the final anatase nanoparticles are predefined with the metatitanic acid type used in the following synthesis reactions.

All of the gel-sol-prepared TiO_2 nanoparticles are polycrystalline.

The **hydrothermal method** was used to prepare the so-called monocrystalline nano-TiO_2 form by employing a stable basic suspension of polycrystalline TiO_2 nanoparticles. In order to perform the hydrothermal synthesis we first had to stabilize the acidic nanoparticle suspension. This was done to avoid undesired nanoparticle agglomeration. For this purpose, various dispersants were tested, but sodium polyfosfate has shown to be the most convenient. After successful nanoparticle stabilization and neutralization to an appropriate pH value, the hydrothermal synthesis was performed using relatively low temperatures (240ºC) and relatively short reaction times (10h). The hydrothermal method enabled the production of a narrow-size monocrystalline anatase material, resembling the commercially available P25 TiO_2. The size of the anatase nanoparticles produced is about 30 nm and they have a spherical morphology.

The materials produced were critically evaluated in order to determine the best possible type for the photocatalytically-active coating preparation and DSSCs, respectively. For the preparation of photocatalytically-active coatings, we have chosen to use the polycrystalline anatase nanoparticles prepared by the gel-sol method using metatitanic acid as the precursor. For the DSSC photoanode preparation, monocrystalline anatase nanoparticles were employed.

The photocatalytically-active coatings were produced at the University of Nova Gorica and were tested in real-life conditions. The focus of the coatings' use was to determine any positive effects regarding the possibility of sustaining the light-to-electricity conversion efficiencies for commercially available Si solar modules. The sustainment of the light-to-electricity conversion efficiency could arise from the photocatalytic effect and as a result of the photo-induced superhydrophilicity (PSH) of the coating. The coatings exhibited both effects initially, while, after a few months of testing, the PSH seems to disappear completely. Nevertheless, the coatings show promise in providing a way for self-cleaning applications. The use of these coatings on Si solar modules is just one of the vast number of possible uses. Therefore, future research is essential.

The DSSC photoanodes were prepared using the Pechini method. Various monocrystalline TiO_2 types were tested, the difference between them being the amount of the dispersant used prior to hydrothermal synthesis. As a reference material, P25 TiO_2 was used in paste preparation. Also, commercially available TiO_2 pastes were tested. It was determined that the Pechini method is a suitable method for paste preparation, although some problems are still not solved, especially the photoanode thickness limitation, which probably arises due to specific TiO_2 paste composition (water content). In addition, it was proven that the monocrystalline TiO_2 prepared by the hydrothermal method is comparable to P25 in the final DSSC efficiency. The final DSSC efficiencies we achieved ranged from 0.5 to 2.3 %.

Overall, it can be concluded that TiO_2 nanoparticles may be produced using industrial-scale production materials which may be important for a possible scale-up production. Furthermore, the research on the two applications, the photocatalytic coatings and the

DSSCs, has shown that the materials produced are well-suited for both. Also, since the mechanisms of nanoparticle formation have also been devised and property-determining parameters successfully revealed, it is reasonable to assume that for any of the vast array of existing nano-TiO_2 based applications, a suitable tailor-made TiO_2 material could be engineered.

6 Acknowledgements

Firstly, I would like to thank my Ph.D. supervisors, Prof. Dr. Miran Čeh and Mag. Pavel Blagotinšek. Prof. Dr. Miran Čeh has provided me with constant guidance and fruitful discussions and has given me the necessary support and understanding during my graduate study. Mag. Pavel Blagotinšek has provided me with all the necessary and much needed support during my graduate study and has helped me decisively in all of my research efforts. His guidance, experience and leadership skills have helped me to adjust to my new career in Cinkarna and to quickly comprehend the truly important guidelines regarding the work that had to be carried out and has resulted in numerous results presented in this thesis.

I would also like to thank my other coworkers and colleagues at SRR. Every one of them has been helpful with my work and has also contributed in setting up what I regard as the best possible R&D department I have come to know.

I would like to thank Amadej Kujan and Dr. Andrej Lubej for the collaboration and fruitful discussions regarding the R&D activities centered on DSSCs.

I would like to thank Assist. Prof. Dr. Sašo Šturm, Prof. Dr. Miran Gaberšček, Assist. Prof. Dr. Goran Dražić, Assist. Prof. Paul McGuiness and also my SRR colleague Mag. Vladimir Vrečko for their many useful comments, suggestions and corrections that were used to make the final thesis a much better work than it was initially.

I would like to thank Dr. Zoran Samardžija for his excellent work on SEM of TiO_2 nanoparticles. The SEM images he provided were in great deal the reason why my work progressed more quickly and successfully.

I would like to thank Kristina Žagar, my fellow scientist and a dear friend. She has always been there to provide any help I needed regarding my research work and has also encouraged me whenever I experienced some rough times on a personal level.

I would like to thank Prof. Dr. Boris Orel and Dr. Ivo Jerman for inviting me to collaborate in many research activities that have also resulted in the publishing of some very important scientific papers.

I would like to thank Prof. Dr. Urška Lavrenčič Štangar and Marko Kete that have provided the measurements of the photocatalytic activities of various TiO_2 nanomaterials that are included in the thesis.

Finally, I would like to thank my family for their support, patience and encouragement. They were always there for me and have unselfishly given me everything a young up-and-coming individual needs to make the best of life.

This work was partially financed by the European Union, European Social Fund under grant P-MR-07/26 by the TIA of Republic of Slovenia.

7 References

1. Luque, A. (ed.); Hegedus, S. (ed.) *Handbook of photovoltaic science and engineering. Second edition* (John Wiley and sons, Ltd., UK, 2011).
2. Peter, L. M. Towards sustainable photovoltaics: the search for new materials. *Philosophical Transactions of the Royal Society A* **369**, 1840–1856 (2011)
3. O'Regan, B.; Gratzel, M. A low-cost, high-efficiency solar cell based on dye-sensitized colloidal TiO_2 films. *Nature* **353**, 737–740 *(*1991**)**.
4. Gratzel, M. Solar Energy Conversion by Dye-Sensitized Photovoltaic Cells. *Inorganic Chemistry* **44**, 6841–6851 (2005).
5. Nazeeruddin, M. K.; De Angelis, F.; Fantacci, S.; Selloni, A.; Viscardi, G.; Liska, P.; Ito, S.; Takeru, B.; Gratzel, M. Combined Experimental and DFT-TDDFT Computational Study of Photoelectrochemical Cell Ruthenium Sensitizers. *Journal Of The American Chemical Society* **127**, 16835–16847 (2005).
6. Simons, P. Y., Dachille, F. The structure of TiO_2 II, a high-pressure phase of TiO_2 *Acta Crystallographica* **23**, 334–336 (1967).
7. Latroche, M.; Brohan, L.; Marchand, R.; Tournoux, M.; New hollandite oxides: TiO_2(H) and $K_{0.06}TiO_2$. *Journal of Solid State Chemistry* **79**, 78–82 (1989).
8. Muscat, J.; Swamy, V.; Harrison, N. M. First-principles calculations on the phase stability of TiO_2. *Physical Review B* **65**, 224112 (2002).
9. Cheng, H.; Ma, J.; Zhao, Z.; Qi, L. Hydrothermal Preparation of Uniform Nanosize Rutile and Anatase Particles. *Chemistry of Materials* **7**, 663–671 (1995).
10. Carp, O.; Huisman, C. L.; Reller, A. Photoinduced reactivity of titanium dioxide. *Progress in Solid State Chemistry* **32**, 33–177 (2004).
11. Zhang, H.; Banfield, J. F.; Understanding Polymorphic Phase Transformation Behaviour during Growth of Nanocrystalline Aggregates: Insights from TiO_2. *Journal of Physical Chemistry B* **104**, 3481–3487 (2000).
12. Jalava, J. P.; Hiltunen, E.; Kähkönen, H.; Erkkilä, H.; Härmä, H.; Taavitsainen, V. M. Structural Investigation of Hydrous Titanium Dioxide Precipitates and their Formation by Small-Angle X-ray Scattering. *Industrial and Engineering Chemistry Research* **39**, 349–361 (2000).
13. Wang, W.; Gu, B.; Liang, L.; Hamilton, W. A.; Wesolowski, D. J. Synthesis of rutile (α-TiO_2) Nanocrystals with Controlled Size and Shape by Low-Temperature Hydrolysis: Effects of Solvent Composition. *Journal of Physical Chemistry B* **108**, 14789–14792 (2004).
14. Yan, M.; Chen, F.; Zhang, J.; Anpo, M. Preparation of Controllable Crystalline Titania and Study on the Photocatalytic Properties. *Journal of Physical Chemistry B* **109**, 8673–8678 (2005).
15. Shi, L. J.; Yang, R.; Li, M. Nanocrystalline TiO_2: Crystal Structure Controlled Synthesis via Low Temperature Hydrolysis Method and Surface Texture. *Chinese Journal of Inorganic Chemistry* **22**, 1196–1202 (2006).
16. Ranade, M. R.; Navrotsky, A.; Zhang, H. Z.; Bansfield, J. F.; Elder, S. H.; Zaban, A.; Borse, P. H.; Kulkarni, S. K.; Doran, G. S.; Whitfield, H. J. Energetics of nanocrystalline TiO_2. *Proceedings of the National Academy of Sciences of the United States of America* **99**, 6476–6481 (2002).

17. Linsebigler, A. L.; Guangquan, L.; Yates, J. T. Jr. Photocatalysis on TiO_2 Surfaces: Principles, Mechanisms, and Selected Results. *Chemical Reviews* **95**, 735–758 (1995).
18. Winkler, J. *Titanium dioxide* (Vincentz Verlag, Hannover, 2003).
19. Koelsch, M.; Cassaignon, S.; Guillemoles, J. F.; Jolivet, J. P. Comparison of optical and electrochemical properties of anatase and brookite TiO_2 synthesized by the sol-gel method. *Thin Solid Films* **312**, 403–4040 (2002).
20. Guozhong, C. *Nanostructures & Nanomaterials – Synthesis, properties and applications* (Imperial College Press, London, 2004).
21. Rulison, A. J.; Miquel, P. F.; Katz, J. L. Titania and silica powders produced in a counterflow diffusion flame. *Journal of Materials Research* **11**, 3083–3089 (1996).
22. Khalil, K. M. S.; Zaki, M. I.; El-Samahy, A. A. Texture and morphology of titania particles prepared by vapor-phase pyrolysis of titanium tetra-isopropoxide. *Journal of Analytical and Applied Pyrolysis* **42**, 123–133 (1997).
23. Murugavel, P.; Kalaiselvam, M.; Raju, A. R.; Rao, C. N. R. Sub-micrometre spherical particles of TiO_2, ZrO_2 and PZT by nebulized spray pyrolysis of metal-organic precursors. *Journal of Materials Chemistry* **7**, 1433–1438 (1997).
24. Nedeljkovic, J. M.; Saponjic, Z. V.; Rakocevic, Z.; Jokanovic, V.; Uskokovic, D. P. Ultrasonic spray pyrolysis of TiO_2 nanoparticles. *Nanostructured Materials* **9**, 125–128 (1997).
25. Yanagi, H.; Ohoka, Y.; Hishiki, T.; Ajito, K.; Fujishima, A. Characterization of dye-doped TiO_2 films prepared by spray-pyrolysis. *Applied Surface Science* **426**, 113–114 (1997).
26. Depero, L. E.; Sangaletti, L.; Allieri, B.; Pioselli, F.; Casale, C.; Notaro, M. Microstructural Properties of Ta-doped TiO_2 powders obtained by Laser Pyrolysis. *Materials Science Forum* **654**, 278–281 (1998).
27. Natarajan, C.; Fukunaga, N.; Nogami, G. Titanium dioxide thin film deposited by spray pyrolysis of aqueous solution. *Thin Solid Films* **322**, 6–8 (1998).
28. Saponjic, Z. M.; Rakocevic, Z.; Dimitrijevic, N. M.; Nedeljkovic, J. M.; Jokanovic, V.; Uskokovic, D. P. Tailor made synthesis of Q-TiO_2 powder by using quantum dots as building blocks. *Nanostructured Materials* **10**, 333–339 (1998).
29. Ahonen, P. P.; Kauppinen, E. I.; Joubert, J. C.; Deshanvres, J. L.; Van Tendeloo, G. Preparation of nanocrystalline titania powder via aerosol pyrolysis of titanium tetrabutoxide. *Journal of Materials Research* **14**, 3938–3948 (1999).
30. Chen, C. H.; Kelder, E. M.; Schoonman, J. Electrostatic sol-spray deposition (ESSD) and characterization of nanostructured TiO_2 thin films. *Thin Solid Films* **342**, 35–41 (1999).
31. Golego, N.; Studenikin, S. A.; Cocivera, M. Spray pyrolysis preparation of porous polycrystalline thin films of titanium dioxide containing Li and Nb. *Journal of Materials Research* **14**, 698–707 (1999).
32. Okuya, M.; Prokudina, N. A.; Mushika, K.; Kaneko S. TiO_2 thin films synthesized by the spray pyrolysis deposition (PSD) technique. *Journal of the European Ceramic Society* **19**, 903–906 (1999).
33. Oswald, M.; Hessel, V.; Riedel, R. Formation of ultra-thin ceramic TiO_2 films by the Langmuir-Blodgett technique – a two-dimensional sol-gel process at the air-water interface. *Thin Solid Films* **339**, 284–289 (1999).
34. Depero, L. E.; Marino, A.; Allieri, B.; Bontempi, E.; Sangaletti, L.; Casale, C.; Notaro, M. Morphology and microstructural properties of TiO_2 nanopowders

doped with trivalent Al and Ga cations. *Journal of Materials Research* **15**, 2080–2086 (2000).
35. Seifried, S.; Winterer, M.; Hahn, H. Nanocrystalline Titania Films and Particles by Chemical Vapor Synthesis. *Chemical Vapor Deposition* **6**, 239–244 (2000).
36. Ahonen, P. P.; Tapper, U.; Kauppinen, E. I.; Joubert, J. C.; Deschanvres, J. L. Aerosol synthesis of Ti-O powders via in-droplet hydrolysis of titanium alkoxide. *Materials Science and Engineering A* **315**, 113–121 (2001).
37. Ding, Z.; Hu, X.; Yue, P. L.; Lu, G. Q.; Greenfield, P. F. Synthesis of anatase TiO_2 supported on porous solids by chemical vapor deposition. *Catalysis Today* **68**, 173–182 (2001).
38. Li, Y.; Ishigaki, T. Synthesis of Crystalline Micron Spheres of Titanium Dioxide by Thermal Plasma Oxidation of Titanium Carbide. *Chemistry of Materials* **13**, 1577–1584 (2001).
39. Oh, S.-M.; Park, D.-W. Production of ultrafine titanium dioxide by DC plasma jet. *Thin Solid Films* **386**, 233–238 (2001).
40. Arnal, P.; Corriu, R. J. P.; Leclercq, D.; Mutin, P. H.; Vioux, A. Preparation of anatase, brookite and rutile at low temperature by non-hydrolytic sol–gel methods. *Journal of Materials Chemistry* **6**, 1925–1932 (1996).
41. Andrianainarivelo, M.; Corriu, R. J. P.; Leclercq, D.; Mutin, P. H.; Vioux, A. Non-hydrolytic sol–gel process: zirconium titanategels. *Journal of Materials Chemistry* **7**, 279–284 (1997).
42. Hay, J. H.; Raval, H. M. Preparation of Inorganic Oxides via a Non-Hydrolytic Sol-Gel Route. *Journal of Sol-Gel Science and Technology* **13**, 109–112 (1998).
43. Trentler, T. J.; Denler, T. E.; Bertone, J. F.; Agrawal, A.; Colvin, V. L. Synthesis of TiO_2 Nanocrystals by Nonhydrolytic Solution-Based Reactions. *Journal of the American Chemical Society* **121**, 1613–1614 (1999).
44. Lafond, V.; Mutin, P. H.; Vioux, A. Non-hydrolytic sol–gel routes based on alkyl halide elimination: toward better mixed oxide catalysts and new supports: Application to the preparation of a SiO_2-TiO_2 epoxidation catalyst. *Journal of Molecular Catalysis A: Chemical* **182**, 81–88 (2002).
45. Niederberger, M.; Bartl, M. H.; Stucky, G. D. Benzyl Alcohol and Titanium Tetrachloride − A Versatile Reaction System for the Nonaqueous and Low-Temperature Preparation of Crystalline and Luminescent Titania Nanoparticles. *Chemistry of Materials* **14**, 4364–4370 (2002).
46. Yang, J.; Li, D.; Wang, X.; Yang, X.; Lu, L. Synthesis and microstructural control of nanocrystalline titania powders via a stearic acid method. *Materials Science and Engineering A* **328**, 108–112 (2001).
47. Fox, M. A.; Dulay, M. T. Heterogeneous Photocatalysis. *Chemical Reviews* **93**, 341–357 (1993).
48. Livage, J.; Henry, M.; Sanchez, C. Sol-Gel Chemistry of Transition Metal Oxides. *Progress in Solid State Chemistry* **18**, 259–342 (1988).
49. Brinker, C. J.; Scherer, G. W. *Sol-Gel Science. The Physics and Chemistry of Sol-Gel Processing* (Academic Press, London, 1989).
50. Sugimoto, T.; Zhou, X.; Muramatsu, A. Synthesis of uniform anatase TiO_2 nanoparticles by gel-sol method. 3. Formation process and size control. *Journal of Colloid and Interface Science* **259**, 43–52 (2003).
51. Livage, J. Sol-Gel synthesis of heterogenous catalysts from aqueous solutions. *Catalysis Today* **41**, 3–19 (1998).
52. Zhang, H.; Finnegan, M.; Bansfield, J. F. Preparing Single-Phase Nanocrystalline Anatase from Amorphous Titania with Particle Sizes Tailored by Temperature. *Nano Letters* **1**, 81–85 (2001).

53. Ding, X.-Z.; Qi, Z.-Z.; He, Y.-Z. Effect of hydrolysis water on the preparation of nano-crystalline titania powders via a sol-gel process. *Journal of Materials Science Letters* **14**, 21–22 (1995).
54. Ding, X.-Z.; Liu, X.-H. Synthesis and microstructure control of nanocrystalline titania powders via a sol-gel process. *Materials Science and Engineering A* **224**, 210–215 (1997).
55. Bacsa, R. R.; Kiwi, J. Effect of rutile phase on the photocatalytic properties of nanocrystalline titania during the degradation of *p*-coumaric acid. *Applied Catalysis B Environmental* **16**, 19–29 (1998).
56. Madhusudan, R. K.; Guin, D.; Manomara, S. V. Selective synthesis of nanosized TiO_2 by hydrothermal route: Characterization, structure property relation, and photochemical application. *Journal of Materials Research* **19**, 2567–2575 (2004).
57. Gopal, M.; Moberly Chan, W. J.; De Jonghe, L. C. Room temperature synthesis of crystalline metal oxides. *Journal of Materials Science* **32**, 6001–6008 (1997).
58. Li, Y.; White, T. J.; Lim, S. H. Low-temperature synthesis and microstructural control of titania nano-particles. *Journal of Solid State Chemistry* **177**, 1372–1381 (2004).
59. Zhang, R.; Gao, L. Effect of peptization on phase transformation of TiO_2 nanoparticles. *Materials Research Bulletin* **36**, 1957–1965 (2001).
60. Zhu, H. Y.; Lan, X.; Gao, X. P.; Ringer, S. P.; Zheng, Z. F.; Song, D. Y.; Zhao, J. C. Phase Transition between Nanostructures of Titanate and Titanium Dioxides via Simple Wet-Chemical Reactions. *Journal of the American Chemical Society* **127**, 6730–6736 (2005).
61. Jolivet, J. P.; Casaignon, S.; Chaneac, C.; Chiche, D.; Trone, E. Design of oxide nanoparticles by aqueous chemistry. *Journal of Sol-Gel Science and Technology* **46**, 299–305 (2008).
62. Koelsch, M.; Cassaignon, S.; Jolivet, J. P. Synthesis of nanometric TiO_2 in aqueous solution by soft chemistry: obtaining of anatase, brookite and rutile with controlled shapes. *Materials Research Society Symposium Proceedings* **822**, S.5.3.1–S5.3.6 (2004).
63. Bischoff, B. L.; Anderson, M. A. Peptization Process in the Sol-Gel Preparation of Porous Anatase (TiO_2). *Chemistry of Materials* **7**, 1772–1778 (1995).
64. Pottier, A.; Chaneac, C.; Trone, E.; Mazerolles, L.; Jolivet, J. P. Synthesis of brookite TiO_2 nanoparticles by thermolysis of $TiCl_4$ in strongly acidic media. *Journal of Materials Chemistry* **11**, 1116–1121 (2001).
65. Oliver, P. M.; Watson, G. W.; Kelsey, E. T.; Parker, S. C. Atomistic simulation of the surface structure of theTiO_2 polymorphs rutileand anatase. *Journal of Materials Chemistry* **7**, 563–568 (**1997)**.
66. Zhang, Q.; Gao, L. Preparation of Oxide Nanocrystals with Tunable Morphologies by the Moderate Hydrothermal Method: Insights from Rutile TiO_2. *Langmuir* **19**, 967–971 (2003).
67. Huang, Q.; Gao, L. A Simple Route for the Synthesis of Rutile TiO_2 Nanorods. *Chemistry Letters* 32, 638–639 (2003).
68. Watson, S. S.; Beydoun, D.; Scott, J. A.; Arnal, R. The effect of preparation method on the photoactivity of crystalline titanium dioxide particles. *Chemical Engineering Journal* **95**, 213–220 (2003).
69. Klein, S. M.; Choi, J. H. Synthesis of rutile titania powders: Agglomeration, dissolution and reprecipitation phenomena. *Journal of Materials Research* **18**, 1457–1464 (2003).

70. Li, Y.; Fan, Y.; Chen, Y. A novel method for preparation of nanocrystalline rutile TiO_2 powders by liquid hydrolysis of $TiCl_4$. *Journal of Materials Chemistry* **12**, 1387–1390 (2002).
71. Scolan, E.; Sanchez, C. Synthesis and Characterization of Surface-Protected Nanocrystalline Titania Particles. *Chemistry of Materials* **10**, 3217–3223 (1998).
72. Chemseddine, A.; Moritz, T. Nanostructuring Titania: Control over Nanocrystal Structure, Size, Shape, and Organization. *European Journal of Inorganic Chemistry* **1999**, 235–245 (1999).
73. Yang, J.; Mei, S.; Ferreira, J. M. F. Hydrothermal Synthesis of Nanosized Titania Powders: Influence of Peptization and Peptizing Agents on the Crystalline Phases and Phase Transitions. *Journal of the American Ceramic Society* **83**, 1361–1368 (2000).
74. Yang, J.; Mei, S.; Ferreira, J. M. F. Hydrothermal Synthesis of Nanosized Titania Powders: Influence of Tetraalkyl Ammonium Hydroxides on Particle Characteristics. *Journal of the American Ceramic Society* **84**, 1696–1702 (2001).
75. Yang, J.; Mei, S.; Ferreira, J. M. F. Hydrothermal synthesis of TiO_2 nanopowders from tetraalkylammonium hydroxide peptized sols. *Materials Science and Engineering C* **15**, 183–185 (2001).
76. Kotov, N. A.; Meldrum, F. C.; Fendler, J. H. Monoparticulate Layers of Titanium Dioxide Nanocrystallites with Controllable Interparticle Distances. *Journal of Physical Chemistry* **98**, 8827–8830 (1994).
77. Rabenau, A. The Role of Hydrothermal Synthesis in Preparative Chemistry. *Angewandte Chemie International Edition in English* **24**, 1026–1040 (1985).
78. Oguri, Y.; Riman, R. E.; Bowen, H. K. Processing of anatase prepared from hydrothermally treated alkoxy-derived hydrous titania. *Journal of Materials Science* **23**, 2897–2904 (1988).
79. Adschiri, T.; Kanazawa, K.; Arai, K. Rapid and Continuous Hydrothermal Crystallization of Metal Oxide Particles in Supercritical Water. *Journal of the American Ceramic Society* **75**, 1019–1022 (1992).
80. Kondo, M.; Shinozaki, K.; Ooki, R.; Mizutani, N. Crystallization Behavior and Microstructure of Hydrothermally Treated Monodispersed Titanium Dioxide Particles. *Journal of the Ceramic Society of Japan* **102**, 742–746 (1994).
81. Kominami, H.; Matsuura, T.; Iwai, K.; Ohtani, B.; Nishimoto, S.; Kera, Y. Ultra-highly Active Titanium(IV) Oxide Photocatalyst Prepared by Hydrothermal Crystallization from Titanium(IV) Alkoxide in Organic Solvents. *Chemistry Letters* **8**, 693–694 (1995).
82. Ohtani, B.; Iwai, K.; Kominami, H.; Matsura, T.; Kera, Y.; Nishimoto, S. Titanium(IV) oxide photocatalyst of ultra-high activity for selective N-cyclization of an amino acid in aqueous suspensions. *Chemical Physics Letters* **242**, 315–319 (1995).
83. Bacsa, R. R.; Gratzel, M. Rutile Formation in Hydrothermally Crystallized Nanosized Titania. *Journal of the American Ceramic Society* **79**, 2185–2188 (1996).
84. Kominami, H.; Takada, Y.; Yamagiwa, H.; Kera, Y. Synthesis of thermally stable nanocrystalline anatase by high-temperature hydrolysis of titanium alkoxide with water dissolved in organic solvent from gas phase. *Journal of Materials Science Letters* **15**, 197–200 (1996).
85. Barbe, C. J.; Arendse, F.; Comte, P.; Jirousek, M.; Lenzmann, F.; Shklover, V.; Gratzel, M. Nanocrystalline Titanium Oxide Electrodes for Photovoltaic Applications. *Journal of the American Ceramic Society* **80**, 3157–3171 (1997).

86. Yanagisawa, K.; Yamamoto, Y.; Feng, Q.; Yamasaki, N. Formation mechanism of fine anatase crystals from amorphous titania under hydrothermal conditions. *Journal of Materials Research* **13**, 825–829 (1998).
87. Kominami, H.; Kato, J.; Murakami, S.; Kera, Y.; Inoue, M.; Inui, T.; Ohtani, B. Synthesis of titanium(IV) oxide of ultra-high photocatalytic activity: high-temperature hydrolysis of titanium alkoxides with water liberated homogeneously from solvent alcohols. *Journal of Molecular Catalysis A: Chemical* **144**, 165–171 (1999).
88. Ovenstone, J.; Yanagisawa, K. Effect of Hydrothermal Treatment of Amorphous Titania on the Phase Change from Anatase to Rutile during Calcination. *Chemistry of Materials* **11**, 2770–2774 (1999).
89. Penn, R. L.; Banfield, J. F. Morphology development and crystal growth in nanocrystalline aggregates under hydrothermal conditions: insights from titania. *Geochimica et Cosmochimica Acta* **63**, 1549–1557 (1999).
90. Wang, C.-C.; Ying, J. Y. Sol−Gel Synthesis and Hydrothermal Processing of Anatase and Rutile Titania Nanocrystals. *Chemistry of Materials* **11**, 3113–3120 (1999).
91. Wu, M.; Long, J.; Huang, A.; Luo, Y. Microemulsion-Mediated Hydrothermal Synthesis and Characterization of Nanosize Rutile and Anatase Particles. *Langmuir* **15**, 8822–8825 (1999).
92. Yanagisawa, K.; Ovenstone, J. Crystallization of Anatase from Amorphous Titania Using the Hydrothermal Technique: Effects of Starting Material and Temperature. *Journal of Physical Chemistry B* **103**, 7781–7787 (1999).
93. Aruna, S. T.; Tirosh, S.; Zaban, A. Nanosize rutile titania particle synthesis via a hydrothermal method without mineralizers. *Journal of Materials Chemistry* **10**, 2388–2391 (2000).
94. Kominami, H.; Kohno, M.; Kera, Y. Synthesis of brookite-type titanium oxide nano-crystals in organic media. *Journal of Materials Chemistry* **10**, 1151–1156 (2000).
95. Saadoun, L.; Ayllon, J. A.; Jimenez-Becerril, J.; Peral, J.; Domenech, X.; Rodriguez-Clemente, R. Synthesis and photocatalytic activity of mesoporous anatase prepared from tetrabutylammonium-titania composites. *Materials Research Bulletin* **35**, 193–202 (2000).
96. Zaban, A.; Aruna, S. T.; Tirosh, S.; Gregg, B. A.; Mastai, Y. The Effect of the Preparation Condition of TiO_2 Colloids on Their Surface Structures. *Journal of Physical Chemistry B* **104**, 4130–4133 (2000).
97. Zheng, Y.; Shi, E.; Cui, S.; Li, W.; Hu, X. Hydrothermal Preparation of Nanosized Brookite Powders. *Journal of the American Ceramic Society* **83**, 2634–2636 (2000)
98. Ovenstone, J. Preparation of novel titania photocatalysts with high activity. *Journal of Materials Science* **36**, 1325–1329 (2001).
99. Wang, C.; Deng, Z.-X.; Li, Y. The Synthesis of Nanocrystalline Anatase and Rutile Titania in Mixed Organic Media. *Inorganic Chemistry* **40**, 5210–5214 (2001).
100. Yin, H.; Wada, Y.; Kitamura, T.; Kambe, S.; Murasawa, S.; Mori, H.; Sakata, T.; Yanagida, S. Hydrothermal synthesis of nanosized anatase and rutile TiO_2 using amorphous phase TiO_2. *Journal of Materials Chemistry* **11**, 1694–1703 (2001).
101. Zheng, Y.; Shi, E.; Chen, Z.; Li, W.; Hu, X. Influence of solution concentration on the hydrothermal preparation of titania crystallites. *Journal of Materials Chemistry* **11**, 1547–1551 (2001).

102. Hayashi, H.; Torii, K. Hydrothermal synthesis of titania photocatalyst under subcritical and supercritical water conditions. *Journal of Materials Chemistry* **12**, 3671–3676 (2002).
103. Kang, M. Preparation of TiO_2 photocatalyst film and its catalytic performance for 1,1′-dimethyl-4,4′-bipyidium dichloride decomposition. *Applied Catalysis B: Environmental* **37**, 187–196 (2002).
104. Wang, C.; Deng, Z.-X.; Zhang, G.; Fan, S.; Li, Y. Synthesis of nanocrystalline TiO_2 in alcohols. *Powder Technology* **125**, 39–44 (2002).
105. Wu, C.; Lin, G.; Chen, D.; Wang, G.; He, D.; Feng, S.; Xu, R. Sol-Hydrothermal Synthesis and Hydrothermally Structural Evolution of Nanocrystal Titanium Dioxide. *Chemistry of Materials* **14**, 1974–1980 (2002).
106. Yin, H.; Wada, Y.; Kitamura, T.; Sumida, T.; Hasegawa, Y.; Yanagida, S. Novel synthesis of phase-pure nano-particulate anatase and rutile TiO_2 using $TiCl_4$ aqueous solutions. *Journal of Materials Chemistry* **12**, 378–383 (2002).
107. Chae, S. Y.; Park, M. K.; Lee, S. K.; Kim, T. Y.; Kim, S. K.; Lee, W. I. L. Preparation of Size-Controlled TiO_2 Nanoparticles and Derivation of Optically Transparent Photocatalytic Films. *Chemistry of Materials* **15**, 3326–3331 (2003).
108. Cozzoli, P. D.; Kornowski, A.; Weller, H. Low-Temperature Synthesis of Soluble and Processable Organic-Capped Anatase TiO_2 Nanorods. *Journal of the American Chemical Society* **125**, 14539–14548 (2003).
109. Jeon, S.; Braun, P. V. Hydrothermal Synthesis of Er-Doped Luminescent TiO_2 Nanoparticles. *Chemistry of Materials* **15**, 1256–1263 (2003).
110. Klein, S. M.; Choi, J. H.; Pine, D. J.; Lange, F. F. Synthesis of rutile titania powders: Agglomeration, dissolution, and reprecipitation phenomena. *Journal of Materials Research* **18**, 1457–1464 (2003).
111. Kolen'ko, Y. V.; Burukhin, A. A.; Churagulov, B. R.; Oleynikov, N. N. Synthesis of nanocrystalline TiO_2 powders from aqueous $TiOSO_4$ solutions under hydrothermal conditions. *Materials Letters* **57**, 1124–1129 (2003).
112. Park, L.-S.; Jang, S.-R.; Hong, J.-S.; Vittal, R.; Kim, K.-J. Preparation of Composite Anatase TiO_2 Nanostructure by Precipitation from Hydrolyzed $TiCl_4$ Solution Using Anodic Alumina Membrane. *Chemistry of Materials* **15**, 4633–4636 (2003).
113. Pottier, A.; Cassaignon, S.; Chaneac, C.; Villain, F.; Tronc, E.; Jolivet, J.-P. Size tailoring of TiO_2 anatase nanoparticles in aqueous medium and synthesis of nanocomposites. Characterization by Raman spectroscopy. *Journal of Materials Chemistry* **13**, 877–882 (2003).
114. Kominami, H.; Kato, J.; Kohno, M.; Kera, Y.; Ohtani, B. Photocatalytic Mineralization of Acetic Acid in Aerated Aqueous Suspension of Ultra-highly Active Titanium(IV) Oxide Prepared by Hydrothermal Crystallization in Toluene. *Chemistry Letters* **25** , 1051–1052 (1996).
115. Hsu, J.-P.; Nacu, A. On the Factors Influencing the Preparation of Nanosized Titania Sols. *Langmuir* **19**, 4448–4454 (2003).
116. Byrappa, K.; Adschiri, T. Hydrothermal technology for nanotechnology *Progress in Crystal Growth and Characterization of Materials* **53**, 117–166 (2007).
117. Fungo, F.; Otero, L.; Durantini, E. N.; Silber, J. J.; Sereno, L. E. Photosensitization of Thin SnO_2 Nanocrystalline Semiconductor Film Electrodes with Metallodiporphyrin. *Journal of Physical Chemistry B* **104**, 7644–7651 (2000).

118. Kay, A.; Gratzel, M. Artificial Photosynthesis. 1. Photosensitization of TiO_2 Solar Cells with Chlorophyll Derivatives and Related Natural Porphyrins. *Journal of Physical Chemistry* **97**, 6272–6277 (1993).
119. Kay, A.; Humphry-Baker, R.; Gratzel, M. Artificial Photosynthesis. 2. Investigations on the Mechanism of Photosensitization of Nanocrystalline TiO_2 Solar Cells by Chlorophyll Derivatives." *Journal of Physical Chemistry* **98**, 952–959 (1994).
120. Hagfeldt, A.; Bjorksten, U.; Lindquist, S. E. Photoelectrochemical studies of colloidal TiO_2 films: the charge separation process studied by means of action spectra in the UV region. *Solar Energy Materials And Solar Cells* **27**, 293–304 (1992).
121. Tsubomura, H.; Matsumura, M.; Nomura, Y.; Amamiya, T. Dye sensitised zinc oxide: aqueous electrolyte: platinum photocell. *Nature* **261**, 402–403 (1976).
122. Vlachopoulos, N.; Liska, P.; Augustynski, J.; Gratzel, M. Very efficient visible light energy harvesting adn conversion by spectral sensitization of high surface area polycrystalline titanium dioxide films. *Journal of the American Chemical Society* **110**, 1216–1220 (1988).
123. Hagfeldt, A.; Gratzel, M. Light-Induced Redox Reactions in Nanocrystalline Systems. *Chemical Reviews* **95**, 49–68 **(**1995).
124. Diebold, U. The surface science of titanium dioxide. *Surface Science Reports* **48**, 53–229 (2003).
125. Nazeeruddin, M. K.; Kay, A.; Rodicio, I.; Humphry-Baker, R.; Muller, E.; Liska, P.; Vlachopoulos, N.; Gratzel, M. Conversion of Light to Electricity by cis- X2Bis(2,2'-bipyridyl-4,4'-dicarboxylate)ruthenium(II) Charge-Transfer Sensitizers on Nanocrystalline TiO_2 Electrodes. *Journal of the American Chemical Society* **115**, 6382–6390 (1993).
126. Gratzel, M. Conversion of sunlight to electric power by nanocrystalline dye-sensitized solar cells. *Journal of Photochemistry and Photobiology A: Chemistry* **164**, 3 (2004).
127. Nazeeruddin, M. K.; Pechy, P.; Renouard, T.; Zakeeruddin, S. M.; Humphry- Baker, R.; Comte, P.; Liska, P.; Cevey, L.; Costa, E.; Shklover, V.; Spiccia, L.; Deacon, G. B.; Bignozzi, C. A.; Gratzel, M. Engineering of Efficient Panchromatic Sensitizers for Nanocrystalline TiO_2-Based Solar Cells. *Journal of the American Chemical Society* **123**, 1613–1624 (2001).
128. Ramamurthy, V.; Schanze, K. S. *Semiconductor Photochemistry and Photophysics* (Marcel Dekker, Inc., New York, 2003).
129. Zakeeruddin, S. M.; Liska, P.; Gratzel, M. A Quasi-Solid-State Dye-Sensitized Solar Cell Based on a Sol-Gel Nanocomposite Electrolyte Containing Ionic Liquid. *Chemistry Of Materials* **15**, 1825–1829 (2003).
130. Nusbaumer, H.; Moser, J. E.; Zakeeruddin, S. M.; Nazeeruddin, M. K.; Gratzel, M. Co(II)(dbbip)2(2+) Complex Rivals Tri-iodide/Iodide Redox Mediator in Dye-Sensitized Photovoltaic Cells. *Journal of Physical Chemistry B* **105**, 10461–10464 (2001).
131. Oskam, G.; Bergeron, B. V.; Meyer, G.; Searson, P. C. Pseudohalogens for Dye-Sensitized TiO_2 Photoelectrochemical Cells. *Journal of Physical Chemistry B* **105**, 6867–6873 (2001).
132. Matsumoto, M.; Miyazaki, H.; Matsuhiro, K.; Kumashiro, Y.; Takaoka, Y. A dye-sensitized TiO_2 photoelectrochemical cell constructed with polymer solid electrolyte. *Solid State Ionics* **89**, 263–267 (1996).
133. Nogueira, A. F.; De Paoli, M. A.; Montanari, I.; Monkhouse, R.; Nelson, J.; Durrant, J. R. Electron Transfer Dynamics in Dye Sensitized Nanocrystalline

Solar Cells Using a Polymer Electrolyte. *Journal of Physical Chemistry B* **105**, 7517–7524 (2001).

134. Cao, F.; Oskam, G.; Searson, P. C. A Solid State, Dye Sensitized Photoelectrochemical Cell. *Journal of Physical Chemistry* **99**, 17071–17073 (1995).
135. Cao, F.; Oskam, G.; Meyer, G.; Searson, P. C. Electron Transport in Porous Nanocrystalline TiO_2 Photoelectrochemical Cells. *Journal of Physical Chemistry* **100**, 17021 (1996).
136. Rensmo, H.; Keis, K.; Lindstrom, H.; Sodergren, S.; Solbrand, A.; Hagfeldt, A.; Lindquist, S. E. High Light-to-Energy Conversion Efficiencies for Solar Cells Based on Nanostructured ZnO Electrodes. *Journal of Physical Chemistry B* **101**, 2598–2601 (1997).
137. Bedja, I.; Hotchandani, S.; Kamat, P. V. Preparation and Photoelectrochemical Characterization of Thin SnO_2 Nanocrystalline Semiconductor Films and Their Sensitization with Bis(2,2'-bipyridine)(2,2'-bipyridine-4,4'-dicarboxylic acid)ruthenium(II) Complex. *Journal of Physical Chemistry* **98**, 4133–4140 (1994).
138. Bjorksten, U.; Moser, J. E.; Gratzel, M. Photoelectrochemical Studies on Nanocrystalline Hematite Films. *Chemistry of Materials* **6**, 858–863 (1994).
139. Sayama, K.; Sugihara, H.; Arakawa, H. Photoelectrochemical Properties of a Porous Nb_2O_5 Electrode Sensitized by a Ruthenium Dye. *Chemistry of Materials* **10**, 3825–3832 (1998).
140. Hodes, G.; Howell, I. D. J.; Peter, L. M. Nanocrystalline Photoelectrochemical Cells: A New Concept in Photovoltaic Cells. *Journal of the Electrochemical Society* **139**, 3136–3140 (1992).
141. Li, Y. X.; Hagen, J.; Schaffrath, W.; Otschik, P.; Haarer, D. Titanium dioxide films for photovoltaic cells derived from a sol-gel process. *Solar Energy Materials and Solar Cells* **56**, 167–174 (1999).
142. Fan, Q.; McQuillin, B.; Bradley, D. D. C.; Whitelegg, S.; Seddon, A. B. A solid state solar cell using sol-gel processed material and a polymer. *Chemical Physics Letters* **347**, 325–330 (2001).
143. Burnside, S. D.; Shklover, V.; Barbe, C.; Comte, P.; Arendse, F.; Brooks, K.; Gratzel, M. Self-Organization of TiO_2 Nanoparticles in Thin Films. *Chemistry of Materials* **10**, 2419–2425 (1998).
144. Kavan, L.; O'Regan, B.; Kay, A.; Gratzel, M. Preparation of TiO_2 (anatase) films on electrodes by anodic oxidative hydrolysis of $TiCl_3$. *Journal of Electroanalytical Chemistry* **346**, 291–307 (1993).
145. Ito S., Chen P., Comte P., Nazeeruddin M. K., Liska P., Pechy P., Gräetzel M. Fabrication of Screen-Printing Pastes From TiO_2 Powders for Dye-Sensitised Solar Cells. *Progress in Photovoltaics: Research and Applications* **15**, 603–612 (2007).
146. Hočevar, M.; Krašovec, U. O.; Berginc, M.; Dražič, G.; Hauptman, N.; Topič, M. Development of TiO_2 pastes modified with Pechini sol–gel method for high efficiency dye-sensitized solar cell. *Journal of Sol-Gel Science and Technology* **48**, 156–162 (2008).
147. Shklover, V.; Ovchinnikov, Y. E.; Braginsky, L. S.; Zakeeruddin, S. M.; Gräetzel, M. Structure of Organic/Inorganic Interface in Assembled Materials Comprising Molecular Components. Crystal Structure of the Sensitizer Bis[(4,4'-carboxy-2,2'-bipyridine)(thiocyanato)]ruthenium(II). *Chemistry of Materials* **10**, 2533–2541 (1998).

148. Fujishima, A.; Honda, K. Electrochemical Photolysis of Water at a Semiconductor Electrode. *Nature* **238**, 37–38 (1972).
149. Hoffmann, M. R.; Martin, S. T.; Choi, W.; Bahnemann, D. W. Environmental Applications of Semiconductor Photocatalysis. *Chemical Reviews* **95**, 69–96 (1995)
150. Ohtani, B.; Nishimoto, S. Effect of surface adsorptions of aliphatic alcohols and silver ion on the photocatalytic activity of titania suspended in aqueous solutions. *Journal of Physical Chemistry* **97**, 920–926 (1993).
151. Davis, A. P.; Huang, C. P. A kinetic model describing photocatalytic oxidation using illuminated semiconductors. *Chemosphere* **26**, 1119–1136 (1993).
152. Nozik, A. J.; Memming, R. Physical Chemistry of Semiconductor−Liquid Interfaces. *Journal of Physical Chemistry* **100**, 13061–13078 (1996).
153. Gerischer, H.; Heller, A. The role of oxygen in photooxidation of organic molecules on semiconductor particles. *Journal of Physical Chemistry* **95**, 5261–5267 (1991).
154. Mills, G.; Hoffmann, M. R. Photocatalytic degradation of pentachlorophenol on titanium dioxide particles: identification of intermediates and mechanism of reaction. *Environmental Science and Technology* **2**, 1681–1689 (1993).
155. Tsai, S.-J.; Cheng, S. Effect of TiO_2 crystalline structure in photocatalytic degradation of phenolic contaminants. *Catalysis Today* **33**, 227–137 (1997).
156. Ollis, D. F.; Hsiao, C.-Y.; Budiman, L.; Lee, C.-L. Heterogeneous photoassisted catalysis: Conversions of perchloroethylene, dichloroethane, chloroacetic acids, and chlorobenzenes. *Journal of Catalysis* **88**, 89–96 (1984).
157. Turchi, C. S.; Ollis, D. F. Photocatalytic degradation of organic water contaminants: Mechanisms involving hydroxyl radical attack. *Journal of Catalysis* **122**, 178–192 (1990).
158. Terzian, R.; Serpone, N.; Draper, R. B.; Fox, M. A.; Pelizzetti, E. Pulse radiolytic studies of the reaction of pentahalophenols with OH radicals: formation of pentahalophenoxyl, dihydroxypentahalocyclohexadienyl, and semiquinone radicals. *Langmuir* **7**, 3081–3089 (1991).
159. Jaeger, C. D.; Bard, A. J. Spin trapping and electron spin resonance detection of radical intermediates in the photodecomposition of water at titanium dioxide particulate systems. *Journal of Physical Chemistry* **83**, 3146–3152 (1979).
160. Anpo, M.; Shima, T.; Kubokawa, Y. ESR and Photoluminiscence Evidence for the Photocatalytic Formation of Hydroxyl Radicals on Small TiO_2 Particles. *Chemistry Letters* **12**, 1799–1802 (1985).
161. Rothenberger, G.; Moser, J.; Gratzel, M.; Serpone, N.; Sharma, D. K. Charge carrier trapping and recombination dynamics in small semiconductor particles. *Journal of the American Chemical Society* **107**, 8054–8059 (1985).
162. Sclafani, A.; Palmisano, L.; Schiavello, M. Influence of the preparation methods of titanium dioxide on the photocatalytic degradation of phenol in aqueous dispersion. *Journal of Physical Chemistry* **94**, 829–832 (1990).
163. Liu, X.; Liang, C.; Wang, H.; Yang, X.; Lu, L.; Wang, X. Usage of ultrafine anatase/$TiO_2 \cdot nH_2O$ powder: photocatalysis and microstructure control for nanocrystalline TiO_2. *Materials Science and Engineering A* **326**, 235–239 (2002).
164. Micic, O. I.; Zhang, Y.; Cromack, K. R.; Trifunac, A. D.; Thurnauer, M. C. Photoinduced hole transfer from titanium dioxide to methanol molecules in

aqueous solution studied by electron paramagnetic resonance. *Journal of Physical Chemistry* **97**, 13284–13288 (1993).

165. Almquist, C. B.; Biswas, P. Role of Synthesis Method and Particle Size of Nanostructured TiO_2 on Its Photoactivity. *Journal of Catalysis* **212**, 145–156 (2002).
166. Kim, S. J.; Lee, E. G.; Park, S. D.; Jeon, C. J.; Cho, Y. H.; Rhee, C. K.; Kim, W. W. Photocatalytic Effects of Rutile Phase TiO_2 Ultrafine Powder with High Specific Surface Area Obtained by a Homogeneous Precipitation Process at Low Temperatures. *Journal of Sol-Gel Science and Technology* **22**, 63–74 (2001).
167. Tanaka, K.; Capule, M. F. V.; Hisanaga, T. Effect of crystallinity of TiO_2 on its photocatalytic action. *Chemical Physics Letters* **187**, 73–76 (1991).
168. Cao, L.; Huang, A.; Spiess, F.-J.; Suib, S. L. Gas-Phase Oxidation of 1-Butene Using Nanoscale TiO_2 Photocatalysts. *Journal of Catalysis* **188**, 48–57 (1999).
169. Wang, C.-C.; Zhang, Z.; Ying, Y. Photocatalytic decomposition of halogenated organics over nanocrystalline titania. *Nanostructured Materials* **9**, 583–586 (1997).
170. Nishimoto, S.; Ohtani, B.; Kajiwara, H.; Kagiya, T. Photoinduced oxygen formation and silver-metal deposition in aqueous solutions of various silver salts by suspended titanium dioxide powder. *Journal of the Chemical Society, Faraday Transactions 1: Physical Chemistry in Condensed Phases* **79**, 2685–2694 (1983).
171. Harvey, P. R.; Rudham, R. Photocatalytic oxidation of iodide ions by titanium dioxide. *Journal of the Chemical Society, Faraday Transactions 1: Physical Chemistry in Condensed Phases* **84**, 4181–4190 (1988).
172. Ku, Y.; Leu, R.-M.; Lee, K.-C. Decomposition of 2-chlorophenol in aqueous solution by UV irradiation with the presence of titanium dioxide. *Water Research* **30**, 2569–2578 (1996).
173. Ohtani, B.; Handa, J.; Nishimoto, S.; Kagiya, T. Highly active semiconductor photocatalyst: Extra-fine crystallite of brookite TiO_2 for redox reaction in aqueous propan-2-ol and / or silver sulfate solution. *Chemical Physics Letters* **120**, 292–294 (1985).
174. Hurum, D. C.; Agrios, A. G.; Gray, K. A.; Rajh, T.; Thurnauer, M. C. Explaining the Enhanced Photocatalytic Activity of Degussa P25 Mixed-Phase TiO_2 Using EPR. *Journal of Physical Chemistry B* **107**, 4545–4549 (2003).
175. Wang, Y.; Herron, N. Nanometer-sized semiconductor clusters: materials synthesis, quantum size effects, and photophysical properties. *Journal of Physical Chemistry* **95**, 525–532 (1991).
176. Reddy, K. M.; Manorama, S. V.; Reddy, A. R. Bandgap studies on anatase titanium dioxide nanoparticles. *Materials Chemistry and Physics* **78**, 239–246 (2002).
177. Ohno, T.; Tokieda, K.; Higashida, S.; Matsumura, M. Synergism between rutile and anatase TiO_2 particles in photocatalytic oxidation of naphthalene. *Applied Catalysis A: General* **244**, 383–391 (2003).
178. Lopez, T.; Gomez, R.; Sanchez, E.; Tzompantzi, F.; Vera, L. Photocatalytic Activity in the 2,4-Dinitroaniline Decomposition Over TiO_2 Sol-Gel Derived Catalysts. *Journal of Sol-Gel Science and Technology* **22**, 99–107 (2001).
179. Bickley, R. I.; Gonzalez-Carreno, T.; Lees, J. T.; Palmisano, L.; Tilley, R. J. D. A structural investigation of titanium dioxide photocatalysts. *Journal of Solid State Chemistry* **92**, 178–190 (1991).

180. Yamaguchi, Y.; Yamazaki, M.; Yoshihara, S.; Shirakashi, T. Photocatalytic ZnO films prepared by anodizing. *Journal of Electroanalytical Chemistry* **442**, 1–3 (1998).
181. Li, D.; Haneda, H. Morphologies of zinc oxide particles and their effects on photocatalysis. *Chemosphere* **51**, 129–137 (2003).
182. Selloni, A.; Vitadini, A.; Gratzel, M. The adsorption of small molecules on the TiO_2 anatase (101) surface by first-principles molecular dynamics. *Surface Science* **402–404**, 219–222 (1998).
183. Vittadini, A.; Selloni, A.; Rotzinger, F. P.; Gratzel, M. Structure and Energetics of Water Adsorbed at TiO_2 Anatase \(101\) and \(001\) Surfaces. *Physical Review Letters* **81**, 2954–2957 (1998).
184. Hashimoto, K.; Irie, H.; Fujishima, A. TiO_2 Photocatalysis: A Historical Overview and Future Prospects. *Japanese Journal of Applied Physics* **44**, 8269–8285 (2005).
185. Wang, R.; Hashimoto, K.; Fujishima, A.; Chikuni, M.; Kojima, E.; Kitamura, A.; Shimohigoshi, M.; Watanabe, T. Light-induced amphiphilic surfaces. *Nature* **388**, 431–432 (1997).
186. Wang, R.; Hashimoto, K.; Fujishima, A.; Chikuni, M.; Kojima, E.; Kitamura, A.; Shimohigoshi, M.; Watanabe, T. Photogeneration of Highly Amphiphilic TiO_2 Surfaces. *Advanced Materials* **10**, 135–138 (1998).
187. Sakai, N.; Fujishima, A.; Watanabe, T.; Hashimoto, K. Quantitative Evaluation of the Photoinduced Hydrophilic Conversion Properties of TiO_2 Thin Film Surfaces by the Reciprocal of Contact Angle. *Journal of Physical Chemistry B* **107**, 1028–1035 (2003).
188. Sathyamoorthy, S.; Moggridge, D. G.; Hounslow, M. J. Controlling Particle Size During Anatase Precipitation. *Particle Technology and Fluidization* **47**, 2012–2024 (2001).
189. Sathyamoorthy, S.; Moggridge, D. G.; Hounslow, M. J. Particle Formation during Anatase Precipitation of Seeded Titanyl Sulfate Solution, *Crystal Growth & Design* **2**, 123–129 (2001).
190. Černigoj, U.; Lavrenčič, Š. U. Preparation of TiO2/SiO2 sols and use thereof for deposition of self-cleaning anti-fogging coatings. International patent application number PCT/SI2009/000052. International patent publication number WO 2010/053459 A1, 2009.
191. Černigoj, U.; Kete, M.; Lavrenčič, Š. U. Development of a fluorescence-based method for evaluation of self-cleaning properties of photocatalytic layers. *Catalysis Today* **151**, 46–52 (2010).
192. Černigoj, U.; Kete, M., Lavrenčič, Š. U.; Ducman, V. Testing of Photocatalytic Activity of Self-Cleaning Surfaces. *Advances in Science and Technology* **68**, 126–134 (2010).
193. Mullin, J. W. *Cystallization – third edition* (Butterworth-Heinemann Ltd, Oxford, 1993).
194. Godec, A.; Maver, U.; Bele, M.; Planinšek, O.; Srčič, S.; Gaberščček, M.; Jamnik, J. Vitrification from solution in restricted space: Formation and stabilization of amorphous nifedipine in a nanoporous silica xerogel carrier. *International Journal of Pharmaceuticals* **343**, 131–140 (2007).
195. Becher, R.; Döring, W. Kinetische Behandlung der Keimbildung in übersättigten Dämpfen. *Annalen der Physik* **416**, 719–752 (1935).
196. Parfitt, G. D. Surface chemistry of oxides. *Pure and Applied Chemistry* **48**, 415–418 (1976).

197. Parfitt, G. D.; Ramsbotham, J.; Rochester, C. H. An electrophoretic investigation of the effect of chloride and of silanol groups on the properties of the surface of rutile. *Journal of Colloid and Interface Science* **41**, 437–444 (1972).
198. Evans, T. W.; Sarofim, A. F.; Margolis, G. Models of secondary nucleation attributable to crystal-crystallizer and crystal-crystal collisions. *AlChE Journal*. **20**, 959–966 (1974).
199. Denk, E. G.; Botsaris, G.D. Mechanism of contact nucleation. *Journal of Crystal Growth* **15**, 57–60 (1972).
200. Database of Raman spectroscopy, X-ray diffraction and chemistry data for minerals. http://rruff.info/ (Dostop: januar 2012).
200. Sugimoto, T. Underlying mechanisms in size control of uniform nanoparticles. *Journal of Colloid and Interface Science* **309**, 106–118 (2007).
201. Park, J.; Privman, V.; Matijević, E. Model of formation of monodispersed colloids. *Journal of Physical Chemistry B* **105**, 11630–11635 (2001).
202. Hagfeldt, A.; Boschloo, G.; Sun, L.; Kloo, L.; Pettersson, H. Dye-Sensitized Solar Cells. *Chemical Reviews* **110**, 6595–6663 (2010).
203. Roy, P., Kim, D.; Lee, K.; Spiecker, E.; Schmuki, P. TiO_2 nanotubes and their application in dye-sensitized solar cells. *Nanoscale* **2**, 45–59 (2010).

Index of Figures

Index of Tables

Appendix

List of publications related to this dissertation

Original scientific article

1. Jerman, I.; Mihelčič, M.; Verhovšek, D.; Kovač, J.; Orel, B. Polyhedral oligomeric silsesquioxane trisilanols as pigment surface modifiers for fluoropolymer based Thickness Sensitive Spectrally Selective (TSSS) paint coatings. *Solar Energy Materials and Solar Cells*. **95**, 423–431 (2011).

Expertise article

1. Veronovski, N.; Verhovšek, D.; Godnjavec, J. Protection from the sun : surface treated rutile TiO_2 nanoparticles are effective UV absorbers. *European Coatings Journal* **3**, 90–95 (2011).

Published scientific conference contribution abstracts

1. Verhovšek, D.; Žagar, K.; Čeh, M. The synthesis and characterization of rutile titanium oxide nanoparticles. V: GROGGER, Werner (ur.), HOFER, Ferdinand (ur.), PÖLT, Peter (ur.). *Microscopy Conference, MC 2009, Materials Science* **3**, 127–128 (Verlag der Technischen Universität, Graz, 2009).

2. Veronovski, N.; Verhovšek, D.; Bele, M.; Zorko, M. Površinska obdelava rutilnih TiO_2 nanodelcev = TiO_2 rutile nanoparticles surface modification. V: *Slovenski kemijski dnevi* (FKKT, Maribor, 2010).

3. Verhovšek, D. Anatase nanoparticles synthesis and photocatalytic coatings preparation for self-cleaning applications. V: *Easy-to-clean / Self-cleaning coatings III*. 119–131 (Vincentz Network, Hannover, 2011).

4. Verhovšek, D.; Veronovski, N.; Selišnik, A.; Čeh, M. Hydrothermal synthesis of TiO_2 nanoparticles and development of sol-gel modified pastes applicable for flexible dye-sensitized solar cells. V: *Thin film & advanced solutions*. 244–245 (Aix en Provence, 2011).

Published scientific conference contribution

1. Makovec, D.; Sajko, M.; Verhovšek, D.; Mertelj, A.; Drofenik, M. Superparamagnetic photocatalytic nanocomposite particles for application in the decomposition of pollutants

in water. V: *ECIS, 23rd Conference of the European Colloidal and Interface Society, 3rd COST D43 Action Workshop.* Abstracts [S. l.] (European Colloid and Interface Society, Antalya, 2009).

2. Primc, D.; Sajko, M.; Verhovšek, D.; Drofenik, M.; Makovec, D. Hidrotermalna sinteza anatasnih fotokatalitskih nanodelcev. V: VALANT, Matjaž (ur.), PIRNAT, Urša (ur.). *Slovenska konferenca o materialih in tehnologijah za trajnostni razvoj. Knjiga povzetkov. Zbornik.* (Založba Univerze, Ajdovščina, 2009).

3. Makovec, D.; Sajko, M.; Verhovšek, D.; Čampelj, S.; Drofenik, M. Superparamagnetni fotokatalitski nanokompozitni delci za razgradnjo onesnažil v vodi. V: VALANT, Matjaž (ur.), PIRNAT, Urša (ur.). *Slovenska konferenca o materialih in tehnologijah za trajnostni razvoj. Knjiga povzetkov. Zbornik.* (Založba Univerze, Ajdovščina, 2009).

4. Kete, M.; Verhovšek, D.; Černigoj, U.; Lavrenčič Štangar, U. Preparation and photocatalytic activity tests of self-cleaning surfaces by fluorescence measurements. V: *Third International Conference on Semiconductor Photochemistry, Book of abstracts* p. 130 (University of Strathclyde, Glasgow, 2010).

5. Makovec, D.; Verhovšek, D.; Sajko, M.; Drofenik, M. Superparamagnetic photocatalytic nanocomposite particles for application in the decomposition of pollutants in water. V: *SOLAR 10, International Conference on Nano/Molecular Photochemistry and Nanomaterials for Green Energy Development, Going NanoGreen in a big way in Cairo : program and abstracts* 39–40 (Cairo, 2010).

6. Verhovšek, D.; Čeh, M. Sinteza nanodelcev TiO_2 s kristalno strukturo rutila = The synthesis of rutile nanoparticles. V: GLAVIČ, Peter (ur.), BRODNJAK-VONČINA, Darinka (ur.). *Slovenski kemijski dnevi, Zbornik povzetkov referatov s posvetovanja* p. 31 (FKKT, Maribor, 2010).

7. Veronovski, N.; Verhovšek, D.; Bele, M.; Zorko, M. Površinska obdelava rutilnih TiO_2 nanodelcev = TiO_2 rutile nanoparticles surface modification. V: GLAVIČ, Peter (ur.), BRODNJAK-VONČINA, Darinka (ur.). *Slovenski kemijski dnevi, Zbornik povzetkov referatov s posvetovanja* p. 34 (FKKT, Maribor, 2010).

8. Verhovšek, D.; Čeh, M. TiO_2 nanoparticles and their various technological applications. V: *SLONANO, Book of abstracts* p. 70 (Ljubljana, 2011).

9. Dergan, A.; Arčon, D.; Umek, P.; Lubej, A.; Verhovšek, D. EPR study of interfacial charge transfer in titanium dioxide nanoparticles. V: *SLONANO, Book of abstracts* p. 101 (Ljubljana, 2011).

10. Verhovšek, D.; Dražič, G.; Horvat, B.; Čeh, M. Hidrotermalna sinteza TiO_2 nanodelcev in njihova uporaba v pastah za fotoelektrokemijske sončne celice = Hydrothermal synthesis of TiO_2 nanoparticles used for paste preparation for photoelectrochemical solar cells. V: KRAVANJA, Zdravko (ur.), BRODNJAK-VONČINA, Darinka (ur.), BOGATAJ, Miloš (ur.). *Slovenski kemijski dnevi, Zbornik povzetkov referatov s posvetovanja* p. 73 (FKKT, Maribor, 2011).

11. Verhovšek, D.; Čeh, M. TiO_2 nanoparticle engineering in Cinkarna Celje, Inc. V: ŽAGAR, Kristina (ur.), LENART, Alenka (ur.), PEČKO, Darja (ur.). *6th Young Researcher's Day, Program and abstract book* p. 14 (Jožef Stefan Institute, Department of Nanostructured Materials, Ljubljana, 2012).

Final report on research results

1. Veronovski, N.; Verhovšek, D.; Zorko, M., Erjavec, B.; Genorio, B.; Jerman, I.; Bele, M.; Gaberščček, M. *Zagotavljanje stabilnosti suspenzij nano TiO_2 ter razvoj ustreznih metod za površinsko obdelavo nano delcev TiO_2. Poročilo industrijsko razvojne raziskave* (Delovno poročilo KI, 2607) (Kemijski inštitut, Ljubljana, 2011).

Expert's detailed report

1. Makovec, D.; Primc, D.; Čampelj, S.; Verhovšek, D. *Analiza nanodelcev TiO_2 tujih proizvajalcev : 2. fazno poročilo*, (IJS delovno poročilo, 2008).

2. Makovec, D.; Primc, D.; Čampelj, S.; Verhovšek, D.; Sajko, M. *Hidrotermalna sinteza fotokatalitskih nanodelcev : 2. fazno poročilo*, (IJS delovno poročilo, 2008).

3. Žigon, S.; Makovec, D.; Gyergyek, S.; Anželak, B.; Primc, D.; Čampelj, S.; Selišnik, A.; Verhovšek, D. *Razvoj fotokatalitskih superparamagnetnih nanokompozitov za postopke zmanjševanja emisij škodljivih snovi v okolje*, (IJS delovno poročilo, 2011).

Patent registration

1. Veronovski, N.; Verhovšek, D.; Selišnik, A. *Oplaščevanje rutilnih nanodelcev TiO_2 v suspenziji s hidratiziranim SiO_2 in Al_2O_3. Patentna prijava P-201000397* (Urad RS za intelektualno lastnino, Ljubljana, 2010).
2. Verhovšek, D.; Veronovski, N.; Selišnik, A.; Čeh, M.; Samardžija, Z. *Postopek za pridobivanje nanodelcev anatasa visoke specifične površine in sferične morfologije. Patentna prijava P-201000342* (Urad RS za intelektualno lastnino, Ljubljana, 2010).

Patents

1. Makovec, D.; Verhovšek, D.; Sajko, M. *Fotokatalitski nanosi TiO_2 na superparamagnetnih nosilcih ter postopek njihove izdelave. Patent : SI 23210 (A)* (Urad RS za intelektualno lastnino, Ljubljana, 2011).
2. Verhovšek, D.; Gominšek, T.; Čeh, M.; Blagotinšek, P.; Šturm, S.; Žagar, K. *Nanodelci anatasa in postopek sinteze za pridobivanje nanodelcev anatasa. Patent : SI 23219 (A)* (Urad RS za intelektualno lastnino, Ljubljana, 2011).

3. Verhovšek, D.; Rožman, T.; Čeh, M.; Blagotinšek, P.; Šturm, S.; Žagar, K. *Nanodelci rutila in postopek sinteze za pridobivanje nanodelcev rutila. Patent : SI 23218 (A)* (Urad RS za intelektualno lastnino, Ljubljana, 2011).